Oxygenates in Iron Fischer-Tropsch Synthesis: is Copper a selectivity promoter?

Pete Cairns

Submitted to the University of Cape Town
in fulfilment of the requirements
for the degree of
Doctor of Philosophy

September 2008

The most exciting phrase to hear in science,
the one that heralds the most discoveries,
is not "Eureka!" (I found it!) but,
"That's funny..."

-Isaac Asimov

“Rabbit’s clever,” said Pooh thoughtfully,
“Yes,” said Piglet, “Rabbit’s clever.”
“And he has Brain.”
“Yes,” said Piglet, “Rabbit has Brain.”
There was a long silence.
“I suppose,” said Pooh, “that that’s why he never understands anything.”

-A.A. Milne
The house at Pooh corner

ACKNOWLEDGEMENTS

Before acknowledging the people who have helped along the way I'd like to apologise and thank the people that I forget to mention for your love, guidance, prayers, input and support, thank you.

This wasn't an easy task and I think I might have been lucky not to have succumbed to insanity. It is for this reason that I'd like to thank those that helped me stay sane.

A special word of thanks must go Michael Claeys without whose input, patience and help I'd still be trying to get the reactors to work and the GC-MS to make sense. You kept the project interesting by asking me tough questions that I usually didn't know the answer to. To Mark Dry and Eric van Steen, thanks for always being available for questions and being willing to share your knowledge in a way that I could understand.

Jack, Walter, Klaus, Itai, Elvera, Cathrin, Mark, Lebo, Helman, Jurie, Jako, Marc, Shaun, Elma, the Chinese guy, Steve (I'll master that doosra yet), Rein, Peter, Jochim, Helen, Suzanna, Susan, Meg, Catherine, Heidi, and everyone in the catalysis group and chemical engineering department, thanks for the help, input and fun times. To the two possums Virginia and Analie, STOP breaking things! Mohammed, in your cold dark little room, thanks for helping me try find that copper. Giles, for the beer.

To the scientists at Sasol: Stanley, Siyanda, Esna, Lodya and Frans, for your help in deciphering the XRD and MAS raw results into something that meant something to someone.

Mom, Dad, Patrick, Grace, Tara, Biff and the rest of the family, thanks for the support and the accommodation when I was homeless, also to Margaux Cairns, welcome to the family, I hope you enjoy it.

To those who I've stayed with, both as a paying customer, and as a lodger taking up valuable room that could have been used by someone who wasn't grumpy; Ian, Graeme, Peter, Adrian, Peta, Bruce, Lindsay, Fuzz, Godwin, Finx (although to be fair I think you stayed with me), Nick, Caryn, KC, Taryn, and especially John (who had me at my most cheerful, I wish you lots of love and happiness in your life with Alex) thanks. Let's hope the list doesn't grow too much longer.

To everyone at the parish of St Thomas, thanks for the prayers and support, they got me through the dark times. Rose, Kerry, Jane, Michele, Richard, Myrna, Murray and Gina, you can stop praying for my reactor now, it worked long enough for me to get some data out of it.

To Sasol, UCT, THRIP and the NRF thank you for the financial assistance without which this crazy rollercoaster would never have started.

To Taryn, I love you, thanks for putting up with "locked in his room Pete" for far too long, let's go on holiday!

Finally, I'd like to dedicate this to all of you, from then till now and further on. Without you I'd just be me and that really wouldn't be too exciting would it?

Pete
Johannesburg
August,2008

SYNOPSIS

The Fischer-Tropsch synthesis is regarded as a stepwise polymerisation reaction between adsorbed hydrogen, carbon monoxide and monomers formed from them. Commercially, a supported precipitated iron catalyst promoted with small amounts of potassium and copper is one of the catalysts used in this reaction. Precipitated iron catalysts are chemically promoted with potassium in order to enhance the product selectivity, while copper is added as a reduction promoter which increases the reduction rate and decreases the reduction temperature of the iron catalyst. The effect of copper on the product selectivity however, remains unclear.

This study falls into three distinct categories: firstly the preparation of co-precipitated iron-copper catalysts of varying copper loading and the characterisation of the calcined, reduced and spent catalysts; secondly Fischer-Tropsch synthesis in both fixed-bed and Berty reactors to investigate the effects on product selectivity in regard to copper, and finally the co-feeding of C_8 oxygenates, over a pure iron, and an iron catalyst promoted with 50 wt% copper, to investigate the mechanism and pathways of interaction.

Co-precipitated iron-copper catalysts were prepared from their nitrates and subsequently promoted with potassium. Characterisation of these catalysts showed that the addition of copper formed small (x-ray amorphous) iron crystallites that decreased in size with copper loading. It was also found that the added potassium had a higher affinity for the iron than the copper. Upon reduction the iron crystallites agglomerated to a constant size while the size of the copper crystallites increased with copper loading. Examination of the spent catalysts showed constant ratios of Hägg carbide to magnetite but a decrease in the size of the iron carbide crystallites with increased copper promotion.

Examination of the hydrocarbon product showed that copper has no effect on the overall activity, or exit partial pressures. It could play a role in increasing methane selectivity and decreasing chain growth probability. The hydrocarbon product is slightly affected by copper promotion with increased paraffin formation. This is believed to be due to a slight shift of primary product selectivity as well as effects of

secondary hydrogenation. Promotion with high concentrations of copper also led to an enhanced alcohol formation and an overall increase in the oxygenate selectivity. It is further shown that these effects are not due to uneven potassium promotion and that the iron and copper need to be co-precipitated in order to achieve maximum oxygenate promotion.

Co-feeding of 1-octanol and octanal showed strong interaction between the two oxygenates and higher conversions of the fed component over the catalyst containing copper. Octanoic acid was also seen when the C_8 alcohol and aldehyde were fed. Inversely, the feeding of octanoic acid produced both 1-octanol (promoted on the iron-copper catalyst) and octanal, suggesting a common intermediate between these three components. Nonan-2-one was also detected upon co-feeding of all three oxygenates, suggesting that this intermediate is also responsible in forming the n+1 methyl-ketone. The reverse reaction between the methyl-ketone and the n-1 oxygenates was not seen upon octan-2-one feeding; however the ketone was hydrogenated to 2-octanol. Once again copper promoted this reaction.

The route between the aldehyde and the acid was also clearly demonstrated but the hydrogenation of both the acid and the aldehyde to form the corresponding primary alcohol were preferred reactions, especially on the copper-iron catalyst.

Additional results showed the esterification reactions of octanol and octanoic acid to form octylacetate and methyl caprylate. It is also thought that the formation of octanoic acid octyl ester from the reaction of octanoic acid with 1-octanol was seen.

The results of this work therefore provide important information on the formation rates, and the interaction of, oxygenates in Fischer-Tropsch synthesis.

TABLE OF CONTENTS

LIST OF FIGURES

LIST OF TABLES

NOMENCLATURE

Notation		Unit
A_i	Response area of component *i* in chromatogram	
CHx	Internal standard: cyclohexane or neohexane	
$đ_{c\text{-}XRD}$	Average crystallite diameter from XRD analysis	nm
d_p	Particle diameter	m
$f_{FID,i}$	FID response factor of component *i*	
$f_{TCD,i}$	TCD response factor of component *i*	
G^R	Gibbs heat of reaction	kJ/mol
H^F	Heat of formation	kJ/mol
H^R	Heat of reaction	kJ/mol
k	Debye-Scherrer shape factor	
K_a	Equilibrium constant	
K_{pwgs}	Equilibrium constant of the Water-gas shift reaction	
m/z	Mass to charge ratio – MS ions	
N_c	Number of carbon atoms in a molecule	
n	Number of carbon atoms in a molecule	
n_i	Molar flow rate of component *i*	mol/min
p_g	Chain growth probability	
p[X]	Partial pressure of component X	bar
R	Ideal gas constant	J/mol.K
W_n	Mass fraction of a product consisting of carbon number n	wt%

Greek letters		
α	Chain growth probability	
β	Line broadening at FWHM	radians
λ	Wavelength	m

Abbreviations	
AAS	Atomic Absorption Specroscopy
amu	Atomic Mass Units

ASF	Anderson-Schulz-Flory
BET	Brunauer-Emmett-Teller
EDX	Energy Dispersive X-ray
Eq	Equilibrium
FWHM	Full Width at Half Maximum intensity

Abbreviations	
FID	Flame Ionisation Detector
FT	Fischer-Tropsch
GC	Gas Chromatograph
HCNs	Hydrocarbons
MS	Mass Spectrometer
MSD	Mass Selective Detector
NIST	National Institute of Standards and Technology
NTP	Normal Temperature and Pressure (0 °C, 1.013 bar)
Obs	Observed
rpm	Revolutions per minute
SEM	Scanning Electron Microscope
spm	Superparamagnetic
SV	Space Velocity
TCD	Thermal Conductivity Detector
TEM	Transmission Electron Microscope
TPD	Temperature Programmed Desorption
TPR	Temperature Programmed Reduction
VOC	Volatile Organic Compounds
XRD	X-ray Diffraction

Chapter 1

Introduction and review of literature

1.1 Fischer-Tropsch synthesis

In 1923 two German scientists, Franz Fischer and Hans Tropsch, discovered that hydrogen and carbon monoxide produced an oily liquid in the presence of alkalised iron turnings in a tubular reactor at 400 to 450 ˚C and pressures of 100 to 150 bar (*Storch et al.*, *1951*). The product, termed 'synthol', contained mainly oxygen containing products. However Fischer and Tropsch found that at lower pressures, around 7 bar, the product consisted of mainly olefinic and paraffinic hydrocarbons. This was the start of what was to become known as Fischer-Tropsch synthesis.

1.1.1 The Fischer-Tropsch reaction

Fischer-Tropsch synthesis is the exothermic catalytic hydrogenation of carbon monoxide (CO) with hydrogen (H_2) to form a range of organic products. This reaction also produces water as its main co-product, and can be summarised as:

$$\text{FTS:} \quad nCO + 2nH_2 \Rightarrow -(CH_2)_n- + nH_2O \qquad (1.1)$$

where ΔH^R (250 ˚C) = –158 kJ/mol for n = 1

The main products of the Fischer-Tropsch reaction are linear paraffins and olefins (compositions of cuts of industrial Fischer-Tropsch products are shown below in Table 1.1 (results taken from Jager (1997)). These are used in the manufacture of high quality

sulphur free diesel, gasoline and as speciality chemicals. Oxygenates are also formed in this reaction, including alcohols, aldehydes, ketones and acids. Most of these are used in fuel or sold as valuable speciality chemicals. Some of the longer chain oxygenates are broken down or removed before further product workup due to their corrosive properties (*Teng et al.*, *2005*).

Table 1.1 Typical product composition for low and high temperature Fischer-Tropsch reactors using iron catalysts (*Jager*, *1997*)

	Tubular Fixed-bed reactor		**Sasol Slurry Phase Distillate reactor**		**High Temperature Fischer-Tropsch**	
	C_5–C_{12}	**C_{13}–C_{18}**	**C_5–C_{12}**	**C_{13}–C_{18}**	**C_5–C_{10}**	**C_{11}–C_{14}**
Paraffins (wt%)	53	65	29	44	13	15
Olefins (wt%)	40	28	64	50	70	60
Aromatics (wt%)	0	0	0	0	5	15
Oxygenates (wt%)	7	7	7	6	12	10

The product spectrum and average carbon number obtained is determined mainly by the process temperature, pressure and catalyst used. Typically the low temperature (220 – 250 °C) process is used mainly for the production of long chain paraffins from diesel to hard waxes (*Dry*, *1982*), while high temperature (320 – 350 °C) process produces lighter products including associated petroleum gas (APG), petrol and chemicals (*Dry*, *2004*). Operating pressures typically range between 15 and 40 bar (*Steynberg*, *2004*). While Fischer-Tropsch synthesis is a heterogeneous catalytic reaction activated by the transition metals, mainly iron (Fe), cobalt (Co), nickel (Ni), and ruthenium (Ru) (*Dry*, *1981*), commercially only cobalt and iron catalysts are used for this process.

1.1.2 Competing reactions and CO_2 formation

Over iron catalysts the Water-Gas Shift reaction (Eq 1.2) is active, and has been found that above about 300 °C the water and carbon dioxide generally exit the reactor together in equilibrium (*Dry*, *1996*).

$$\text{WGS: } CO + H_2O \Leftrightarrow CO_2 + H_2 \qquad (1.2)$$

Where ΔH^R (250 ˚C) = –39.5 kJ/mol

The other competing reaction of interest is the Boudouard reaction. It is of concern as the disproportionation of CO can lead to the formation of carbon on the catalyst surface which leads to blocking of the active sites and thus deactivation of the catalyst (*Dry*, *2004*).

$$\text{Boudouard:} \quad 2CO \Leftrightarrow C + CO_2 \tag{1.3}$$

Where ΔH^R (270 ˚C) = –172.4 kJ/mol

The carbon formed can also be incorporated into the catalysts itself, i.e. with iron catalysts iron carbides are typically formed and are believed to be the active catalytic component in the working catalysts (*Dry*, *1981*).

Both reactions above can lead to the formation of carbon dioxide which will result in low carbon efficiency of the reaction. It can be assumed that the co-feeding of carbon dioxide will minimise its subsequent formation and the loss of valuable carbon monoxide through the limitation of the thermodynamic equilibrium.

1.2 Proposed Fischer-Tropsch mechanisms

"… the description of a mechanism for a reaction as complex as the Fischer-Tropsch synthesis is fraught with pitfalls. Unlike many reactions, the Fischer-Tropsch synthesis converts two of the simplest compounds, H_2 and CO, into a complex array of products, consisting predominantly of alkenes and alkanes but also a variety of minor compounds including a range of oxygenate compounds." Davis (2001).

The products from the Fischer-Tropsch synthesis are believed to be formed through a surface polymerisation reaction where adsorbed reactants initiate chain growth, grow, and desorb as different products. These desorbed products can subsequently readsorb and undergo further reactions. Many reaction pathways have been proposed but only four will be discussed here: they are the alkyl or carbide mechanism (*Fischer and Tropsch*, *1926* and *Craxford and Rideal*, *1939*), the Enol mechanism (*Storch et al.*, *1951*), the CO-insertion mechanism (*Pichler and Schulz*, *1970*) and the alkenyl mechanism (*Maitlis et al.*, *1999*).

1.2.1 Formation of hydrocarbon and oxygenated products

Figure 1.1 and the following explanation have been adapted from Mabaso (2005). The figure shows a summary of the four proposed mechanisms and reaction pathways. The alky mechanism developed from the carbide mechanism, (*Fischer and Tropsch*, *1926* and *Craxford and Rideal*, *1939*) is presently widely accepted as the growth mechanism in the Fischer-Tropsch synthesis (*Claeys and van Steen*, *2004*). In this mechanism a CH species is formed from the dissociative adsorption of CO and the subsequent hydrogenation of the resulting carbon species (1 to 4). The subsequent hydrogenation of the adsorbed CH through surface hydrogen yields CH_2 (5), and CH_3 (6) surface species (*Erley et al.*, *1983*, *Wang and Ekerdt*, *1984* and *Kaminsky et al.*, *1986*). The CO-insertion mechanism, proposed by Pichler and Schulz (*Pichler and Schulz*, *1970*), has identical steps leading to the formation of the adsorbed CH_x species. In essence the two mechanisms have the same chain growth initiator, the surface methyl species (CH_3 – 6), but different chain propagation monomers. Insertion of the surface CH_2 (5) species into a metal-alkyl bond (7) to form a surface alkyl species (10) is regarded as the process of chain growth in the alkyl mechanism, while insertion of the chemisorbed CO (1) in the case of the insertion mechanism will lead to the formation of a surface acyl species (8) which can be hydrogenated to form species (9). This surface species has also been proposed by Subramanyam and Rao (1970a). Chain termination of either oxygen containing species (8) or (9) will lead to the formation of oxygenates (*Anderson and Ekerdt*, *1985* and *Dry*, *1990*). Oxygen elimination of the surface species (9) through the formation of water leads to the formation of the alkyl species (10), identical to the species formed via the alkyl mechanism. Chain termination of this alkyl species occurs either through H-addition yielding n-paraffins or via β-H-elimination yielding α-olefins. It should be noted that the alkyl mechanism fails to explain the formation of oxygenate species.

To explain the formation of oxygenate species, Johnston and Joyner (1993) suggested a common intermediate to both oxygenate and hydrocarbon synthesis, possibly an adsorbed ethylidyne species. They suggested that this intermediate could form oxygenates through parallel reactions – CO insertion (as described above) on π-bonded olefins and OH attack on σ-bonded species Figure 1.2. Here the adsorbed ethylidyne

species (21) is attacked by an adsorbed OH species (22) to form the adsorbed oxygenate species (9).

In the alkenyl mechanism described by Maitlis *et al.* (1999), the vinyl surface species $CH{=}CH_2$ (11), formed through the coupling of methlidyne (CH) (4) and methylene (5), is considered the chain growth initiator and the CH_2 surface species the chain growth propagation monomer. Product desorption involves the addition of hydrogen to an alkenyl (13) species yielding α-olefins.

The alkenyl mechanism however, fails to explain the primary formation of n-paraffins, or the formation of oxygenates. Furthermore there is no experimental evidence for the isomerisation reaction of the allyl species (12) to form the vinyl species (13).

The final mechanism discussed is the Enol mechanism proposed by Storch *et al*. (1951). Here the chemisorbed CO (1) is hydrogenated to form an enolic surface species (14) which is both the chain initiator and monomer. Chain growth occurs via a condensation reaction between two enol species. Chain termination of species (14) will yield α-olefins and oxygenates while the further hydrogenation of the species will result in (15) which can be converted to methyl species (6), the chain initiator of the alky and CO-insertion mechanisms. However there is no experimental evidence for the existence of the enol species on the catalyst surface and the precise electronic mechanism for the self-condensation of two electrophilic hydroxycarbene intermediates has not been shown (*Hindermann et al., 1993*). While it is considered unlikely that each type of FT metal has its own unique mechanism, it seems feasible that different mechanisms take place on the catalyst surface at the same time (*Dry in Ertl et al., 1997*).

The formation of water is prevalent in Fischer-Tropsch synthesis while carbon dioxide is also formed depending on the catalyst used. The mechanism for water formation would most likely be through the reaction of surface oxygen (19) with adsorbed hydrogen (20). CO_2 on the other hand is formed via the reaction of chemisorbed CO (1) and surface oxygen (19).

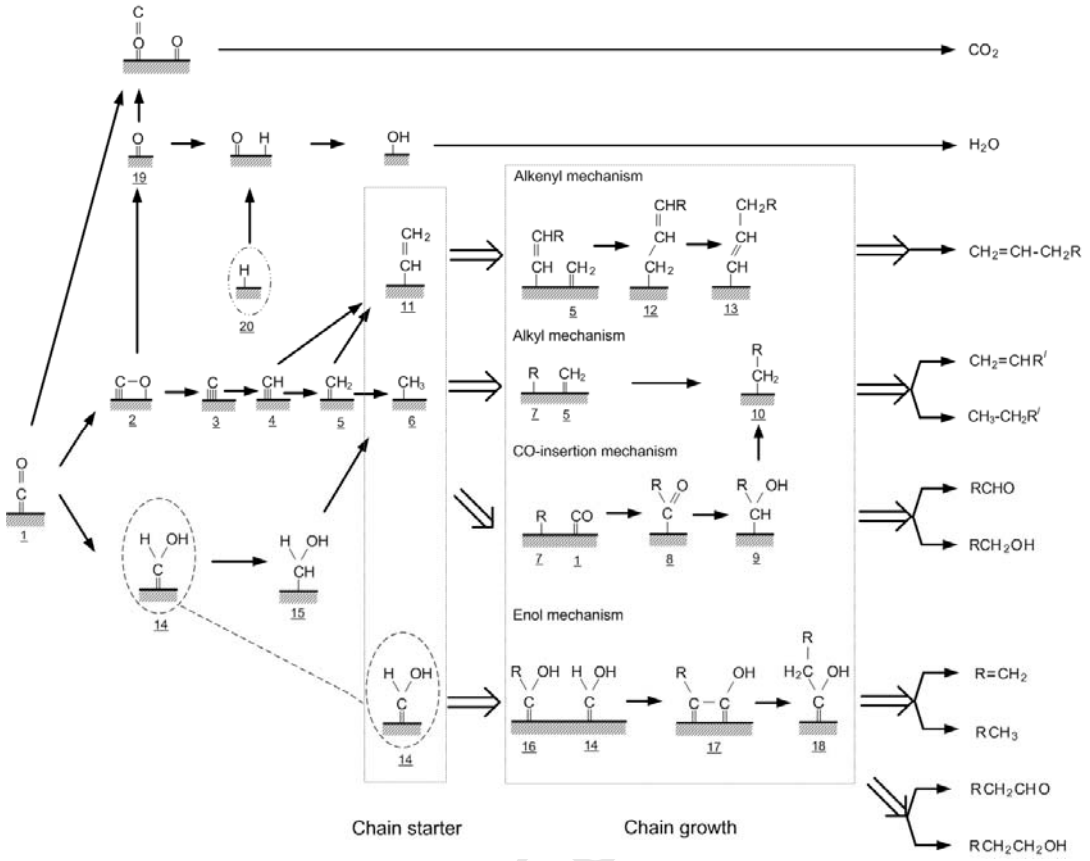

Figure 1.1 Overview of Fischer-Tropsch reaction pathways (adopted from Mabaso (2005))

Figure 1.2 Pathway of formation of surface oxygenates from Johnston and Joyner (1993)

1.3 Fischer-Tropsch product spectrum

Even though different mechanisms for the Fischer-Tropsch synthesis have been proposed, all of them assume that the growth of the surface species has a stepwise mechanism sequence. This means there will either be chain growth of an adsorbed species on the catalyst surface or it will desorb from the catalyst surface as product (*Dry*, *1981* and *2003*) (see Figure 1.3). The probability of the species on the surface growing by one carbon number (C_{n-1} to C_n) as opposed to desorbing is described as the chain growth probability ($p_{g\ n-1}$).

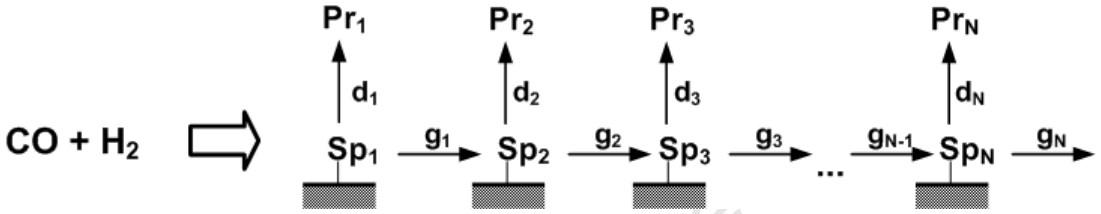

Figure 1.3 Kinetic scheme of chain growth and product desorption (*Claeys*, *1997*)

If p_g (α) is independent of carbon number it can be found from the Anderson-Schulz-Flory (ASF) plot:

$$\frac{W_n}{n} = n \log \alpha + \text{constant} \qquad (1.4)$$

Where W_n is the mass fraction of the product species with carbon number n and α is the independent chain growth probability. This implies that the Fischer-Tropsch synthesis is not selective towards any particular carbon number product range of product except methane where a 100 % selectivity would be true for a chain growth probability equal to zero. Figure 1.4 shows the change in product weight fraction as the chain growth probability increases. It can be clearly seen that as the chain growth probability increases, so the molecular weight of the product increases.

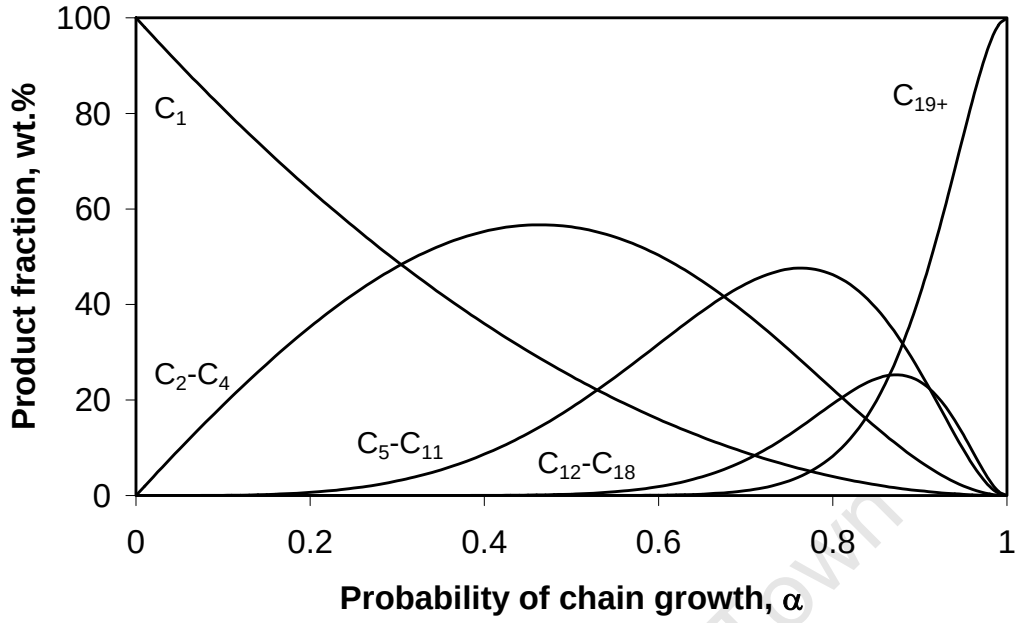

Figure 1.4 Plots of various theoretical product distributions as a function of chain growth probability assuming ideal ASF kinetics (*Dry*, *1981*)

1.3.1 Deviation from ideal distributions

When the product mass fraction is plotted against carbon number an ideal Anderson-Schulz-Flory plot will result in a straight line. For Fischer-Tropsch synthesis this is not always the case. Invariably the product is often large for C_1, at a minimum for C_2 then reaches a maximum at C_3 or C_4 and then decreases monotonically (*Anderson*, *1984*). This deviation is usually ascribed to the ease of methane formation (no chain growth is required) or active sites that only form methane while the high reactivity of ethene which can be reincorporated to longer chain products (*Dry*, *1981*) may explain the dip in the C_2 product fraction (*Schulz and Claeys, 1999b*).

In the carbon number range from C_3 to C_{10} typically linear plots are observed, however after this sometimes a (left) curved ASF plot becomes apparent. There has been much debate around the reason for this, and it has been ascribed to either being due to a primary or secondary effect (*Claeys and van Steen, 2008*).

Huff and Satterfield (1984) proposed that the reaction happened on two different catalyst sites with different chain growth probabilities, while others have suggested that

two separate chain growth mechanisms could account for this shift (*Tau et al.*, *1990* and *Patzlaff et al.*, *1999*).

A secondary route for change in chain growth probability has to do with the reversibility of olefin desorption. Figure 1.5 shows how primarily formed alpha olefins can re-adsorb onto the catalyst surface and undergo isomerisation to an olefin with an internal double bond, be reincorporated for further chain growth or hydrogenate to the corresponding paraffin. An increase in the re-incorporation due to carbon number dependent effects of diffusion (*Iglesia et al.*, *1993*) or solubility (*Schulz and Claeys*, *1999a and 1999b* and *Claeys and Schulz*, *2004*) would lead to deviations from ASF kinetics. If this is correct, the reincorporation of oxygenates may also be a possibility as they have been reported to be more reactive than olefins (*Davis*, *1993*).

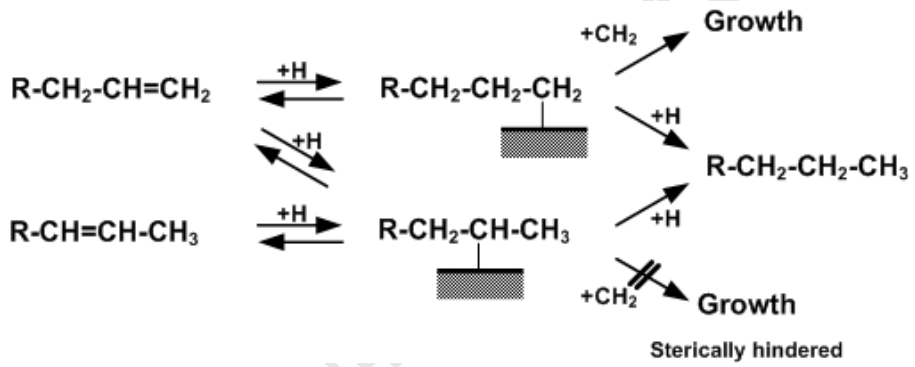

Figure 1.5 Secondary reactions of α-olefins (*Claeys*, *1997*)

1.4 Iron catalysts and Fischer-Tropsch synthesis

Commercially, the preparation of iron catalysts varies depending on the process temperatures at which the catalyst will be operated. Low temperature catalysts are prepared by precipitation while the catalysts used in high temperature synthesis are generally prepared by fusing magnetite together in the presence of promoters (*Dry*, *2002*). The main reason for fusing the catalyst for high temperature reaction is to ensure that the catalyst has the mechanical strength to withstand conditions in the reactor where it is fluidised. Both catalysts are made with chemical and structural promoters but due to the high temperatures used for reduction of the high temperature catalyst no reduction promoter is present.

1.4.1 Chemical promoters

Iron, unlike cobalt and ruthenium, requires chemical promoters in the form of strong bases (typically group I metals and especially K_2O) which are key in both activity and selectivity of the catalysts (*Dry and Oosthuien*, *1968*, *Dry et al.*, *1970*, *Subramanyam and Rao*, *1970b*, *Dry*, *1981*, *Arakawa and Bell*, *1983, Li et al.*, *2002* and *Luo et al.*, *2003*). The potassium promotion leads to an increase in the strength of the CO chemisorbed to reduced iron, a decrease in the turnover frequency for total CO consumption, an increase in the average molecular weight of the product, an increase in the olefin to paraffin ratio and an increase in the water-gas-shift activity (*Arakawa and Bell*, *1983*). Other effects of increased potassium loading include an increase in the acid and alcohol selectivities (*Dry*, *1981*) and a decrease in methane selectivity (*Dry and Oosthuizen*, *1968*). The increase of olefin and oxygenates content in potassium promoted catalysts is mainly believed to be due to effects of inhibiting secondary reactions of these valuable products as for example evidenced via co-feeding experiment using promoted and un-promoted iron catalysts (*Schulz and Claeys, 1999a*). Too high a potassium loading however can lead to catalyst deactivation through blocking of active sites by potassium (*van Steen and Claeys*, *2008*) or carbon deposition on the surface of the catalyst (*Arakawa and Bell*, *1983*).

By increasing the CO bond strength on the surface of the catalyst, potassium decreases the rate at which adsorbed products can be hydrogenated, thus producing a more primary Fischer-Tropsch product. The addition of potassium also serves to neutralise some of the added support promoters like alumina and silica, thus decreasing unwanted secondary reactions such as olefin isomerisation (*Claeys*, *1997* and *Claeys and van Steen*, *2004*).

1.4.2 Reduction promoters

Typically calcined iron catalysts are prepared/conditioned for synthesis by activation either in hydrogen or carbon monoxide or mixtures thereof. In hydrogen the iron oxide undergoes a two-step reduction: the first phase change is from hematite (Fe_2O_3) to magnetite (Fe_3O_4) while the second is the formation of metallic iron (Fe) from magnetite (*Bukur et al.*, *1995*). Under carbon monoxide activation the route of activation is the reduction of hematite to magnetite; the magnetite is then subsequently reduced and carbided predominantly to Hägg carbide (Fe_5C_2) (*Bukur et al.*, *1995* and *Li et al.*, *2001*). In both cases the reduction of the magnetite is slow.

Commercially precipitated catalysts are promoted with copper to enhance the rate of iron reduction (*Dry*, *1981*). The addition of copper has been found to enhance the rate of reduction and thus enable it to be carried out at lower temperatures in both a hydrogen rich and carbon monoxide rich atmosphere, therefore minimising effects of crystallite sintering and corresponding loss of catalyst activity (*Storch et al.*, *1951*, *Anderson*, *1984, O'Brien et al.*, *1997* and *Li et al.*, *2001*).

Under hydrogen reduction the promotional effect of copper on the reduction of the iron oxides has been attributed to the initial facile reduction of copper, which is then able to assist in hydrogen dissociation, and thus provide a source of atomic hydrogen to assist in the reduction of the iron to metallic iron (*Jin and Datye*, *2000* and *Li et al.*, *2001*), a type of hydrogen spillover.

The effect of copper on the reduction of iron in carbon monoxide has been attributed to the activation of the CO on the surface of the reduced copper and interaction with the metal oxide to form CO_2 and metallic iron. The addition of potassium to an iron-copper matrix enhances the rate of carburisation under carbon monoxide even more due to the potassium promoting the activation of CO while copper aids in oxygen removal via CO_2 formation (*Li et al.*, *2001*).

While copper clearly enhances catalyst reduction, there is still no understanding on the effect of copper on product selectivity. O'Brien *et al*. (1997) reported that copper addition did not affect the Fischer-Tropsch selectivity, while Li *et al*. (2001) suggested that copper increases the methane and paraffin content, but that this effect was damped out by the addition of potassium.

1.4.3 Phase changes during synthesis

Under Fischer-Tropsch synthesis conditions the metallic iron phase is not stable (*Dry*, *1981*) and undergoes phase changes via oxidation and carburisation (*Anderson*, *1984*). Dry, (1981) discusses the phase changes that occur in a fluidised bed reactor at around 600 K. The initial metallic iron is rapidly converted to a mixture of magnetite and iron carbides (consisting of an unstable pseudo cementite phase (Fe_3C) and Hägg carbide (Fe_5C_2)). After several days another carbide phase, Eckstrom Adcock (Fe_7C_3) appears. This additional carbide phase however does not seem to affect the activity of the catalyst. Such changes of catalyst composition from metallic iron to carbide phases have also been observed by Storch *et al*. (1951), Mansker *et al*., (1999), Schulz *et al*., (1999), and Li *et al*., (2001).

The effect of potassium on the phase changes in the iron catalyst has been studied and it has been shown that catalysts with K_2O carburize more rapidly than those that do not contain K_2O (Pichler and Merkel (1949) as referenced in Dry, (1981)). Dry also reports (1981), that an increase in K_2O loading increases the rate of carburization. The addition of copper to the iron catalyst has also been shown to increase the rate of catalyst carburisation from Fe_3O_4 to FeC_x (Li *et al*., 2001). In light of this information the presence of copper possibly effects the phase changes, and the rate of phase change, within the catalyst system.

1.5 Oxygenates in Fischer-Tropsch synthesis

Oxygenated hydrocarbons (or oxygenates) are commonly thought to be primary Fischer-Tropsch products and are produced in quantities higher than expected in thermodynamic calculations (*Dry*, *1981*). Oxygenates formed during Fischer-Tropsch synthesis mainly include primary and secondary alcohols, aldehydes, acids and methyl-ketones, but also esters (*Schulz and Zein el Deen, 1977a*). The primary nature of alcohols, the predominantly formed oxygenates, along with the olefins can be seen in Table 1.2 which shows that the residence time inside the reactor decreases the selectivities of these products. This implies that the products can re-adsorb and be re-

incorporated into the paraffinic product. It can also be seen that the addition of potassium to the iron catalyst increases these products, thus suggesting the primary nature of the product.

Table 1.2 Effect of process conditions on product selectivities (taken from (*Claeys*, *1997*))

	Parameter			
	Temperature	Pressure	Residence time	Potassium
Methane selectivity	+	–	+	–
Chain growth	–	+	~	+
Olefin selectivity	~	~	–	+
Alcohol selectivity	–[1]	+	–	+
Carbon deposition	+	~	~	+

Generally little is known about the formation routes of oxygenates, in particular the acids and methyl-ketones. Mechanistically, both the CO-insertion mechanism and the Enol mechanism show oxygenates as primary products. The formation of oxygenates in the alkyl mechanism can be explained through the insertion of an OH group (section 1.2). The desorption of the oxygen containing surface species (8) and (9) in Figure 1.1 can easily explain the formation of 1-alcohols and aldehydes, while the addition of OH or alkyl species to the acyl species (8) may account for the formation of acids and ketones as proposed by Schulz (1977b). Dry noticed a correlation between acid formation rates and CO_2 partial pressure, which may also suggest that CO_2 is mechanistically involved in the acid formation.

It has further been noted that 1-alcohols and aldehydes can be formed via olefin hydroformylation, an observation which ultimately led to the development of the 'oxosynthesis' by Roelen (*Roelen, 1938* and *Pichler and Roelen, 1957*). This secondary reaction can however not explain the formation of C_1 and C_2 oxygenates so that primary oxygenate formation routes must exist in addition to secondary ones.

[1] This result at first glance seems to be in disagreement with that reported by (*Jager*, *1997*) in Table 1.1. However, direct comparison of Jager's results at the different temperatures is not readily possible as the process variables and the mass fractions reported are different.

1.5.1 Interaction

Dry (1981) analysed the exiting molar ratios of oxygenates (namely ethanol, acetaldehyde, acetone and acetic acid) from the product of a fluidised iron bed and found that the exit ratios were in equilibrium at high temperatures. Dry goes on to claim: "Whenever ethanol, acetaldehyde or ethyl acetate was injected individually into the feed gas all three components were always found in the exhaust gas. At the higher temperatures acetone also was always present". These tests confirm the ability of the oxygenates not only to re-adsorb and be re-incorporated, but also to interact readily with other oxygenate species.

Dry (2004) also postulates that the formation of acetone, and thus methyl-ketones, is a secondary reaction formed through a ketonisation reaction between two carboxylic acids. The reaction:

$$2\text{acetic acid} \Leftrightarrow \text{acetone} + CO_2 + H_2 \qquad (1.5)$$

was found to be close to equilibrium at 600K. Additionally he stated that the adding of acetic acid or ethanol to the feed at 340 °C increased the yield of acetone in the product.

The interaction pathways of primary and secondary alcohols, aldehydes, ketones and carboxylic acids is described by McMurry (1996) and the schemes are shown in Figure 1.6 for primary alcohols, aldehydes and carboxylic acids and Figure 1.7 for secondary alcohols and ketones. The interaction pathway from the alcohol is through an oxidizing reaction while from the acid or ketone is via reduction. The exact mechanistic pathways for the formation of oxygenates are however not known.

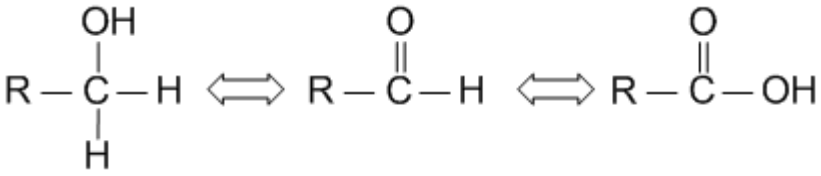

Figure 1.6 Scheme showing the interaction pathways between primary alcohols, aldehydes and carboxylic acids (*McMurry*, *1996*)

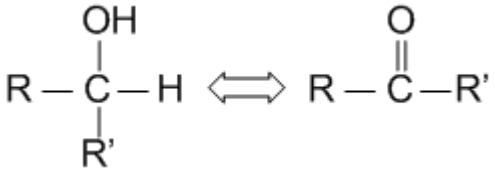

Figure 1.7 Scheme showing the interaction pathways between secondary alcohols and ketones (*McMurry*, *1996*)

1.5.2 Co-feeding

Much co-feeding work has been conducted on Fischer-Tropsch catalysts to study reaction pathways of oxygenates. For the most part is has focused on the C_{1-3} alcohols, acetaldehyde and olefins. Emmett and co-workers fed ^{14}C labelled alcohols with synthesis gas over iron catalysts (*Emmett et al. as referenced in Anderson*, *1984*). They found that ethyl, n-propyl and isobutyl alcohols initiated chain growth while isopropyl alcohol was incorporated to only a slight extent. Methanol was found to initiate as well as to be incorporated into existing chains. Snel and Espinoza (1989) co-fed acetaldehyde to a synthesis gas feed for iron catalysed Fischer-Tropsch. They found that the aldehyde suppressed the Fischer-Tropsch reaction, probably due to the high concentrations of the co-fed component. This result is interesting in light of the work conducted by Johnston and Joyner (1993) where co-fed acetaldehyde over a rhodium catalyst acted as a chain growth initiator and was incorporated into the hydrocarbon product and did not seem to change the product spectrum.

A rapid interaction via hydrogenation and dehydrogenation was reported to exist for 1-alcohols and aldehydes as well as methyl-ketones and the corresponding 2-alcohols, in a review article by Eidus (1967), who also noted that oxygenates can – in analogy to olefins – undergo secondary reactions such as hydrogenation to the corresponding paraffins and incorporation. Work by Tau *et al.* (1987) investigated other oxygenated products formed through ^{14}C labelled ethanol co-feeding. Their results again showed that there was interaction between the alcohol and aldehyde, where the alcohol was dehydrogenated to the aldehyde to form an equilibrium ratio. Other products that were found to have been formed included methyl acetate, ethyl acetate, some longer chained alcohols and acetals. These products were thought to have been formed from acetaldehyde and not directly from the alcohol. Some hydrocarbon product (5 to 15%)

was also found to have ^{14}C present suggesting ethanol was a chain growth initiator. In addition Tau *et al.* (1988) reported in a later publication that 1-propanol incorporation can lead to linear products while 2-propanol addition can lead to branched compounds, reactions that were previously also reported by Kummer *et al.* (1951, 1953).

Pijolat and Perrichon (1985) investigated the production of alcohols and hydrocarbons from syn-gas on a supported iron catalyst. Included in their experimentation was the feeding of 1-butene with the synthesis gas. They found a marked increase ("five-fold") in the production of n-pentanol. Other effects included the increase of the C_5 fraction, an increase in 1-hexanol and some minor peaks they attributed to 2-pentanol and 2-hexanol. They concluded that the existence of a CO insertion type mechanism must occur for the reaction pathway to the alcohol.

Wang and Davis (1999) fed alcohols over prepared iron oxide and iron carbide catalysts with no synthesis gas present. 1-Octanol was converted to octanal over both catalysts and the aldehyde underwent a secondary reaction to form a 15-number symmetrical ketone. 2-Octanol was found to dehydrogenate to octan-2-one while tertiary alcohols were dehydrated mainly to olefins. They suggested that this result showed that the dehydration of alcohols to olefins in the Fischer-Tropsch synthesis was a minor reaction pathway.

Generally it appears that, although a number of co-feeding experiment have been reported in literature, the reactions the oxygenates undergo depend strongly on the reaction conditions and the catalyst used.

1.6 Higher alcohol synthesis

The formation of higher alcohols from synthesis gas has received a lot of interest since the oil crisis in the 1980's (*Hindermann et al., 1993*). While ethanol has value as a pure component the use of other long chain alcohols was limited to solvents, surfactants, plasticizers and base lubricants. However, addition of these alcohols to poor fuels greatly increases their octane number and so selective formation of these alcohols in the fuel industry is beneficial.

1.6.1 Methanol catalysts

Methanol is commercially produced using copper-zinc-alumina catalysts at operating temperatures around 220 to 290 °C and pressures ranging from 40 to 60 bar, these catalysts generally have a 98% or higher selectivity (*Xiaoding et al., 1987*). Methanol is formed via the reaction of carbon monoxide and hydrogen; however, carbon dioxide invariably needs to be present as well. This has led to much debate on the reaction pathway of methanol (from CO or CO_2).

Figure 1.8 shows proposed mechanisms for methanol formation from mixtures of hydrogen and carbon monoxide as well as hydrogen and carbon dioxide (with and without carbon monoxide) (*Chichen et al., 1986a, 1986b, 1987*). In the formation of methanol from carbon monoxide, [1*], the carbon monoxide is activated by the copper metal and the dissociated hydrogen is introduced in a step wise manner. It has been found that these reaction steps occur on the copper metal composition of the catalyst.

The formation of methanol in the presence of carbon dioxide takes a different pathway that includes an oxygen covered copper surface [3*], this adsorbed oxygen is thought to have adsorption sites on the zinc as well as the copper (*Spencer, 1999*). These adsorbed oxygen atoms promote the adsorption of the CO_2 (the main source of carbon is methanol synthesis). The adsorbed oxygen is also an intermediate in the water-gas-shift reaction [5* and 6*]. The formation of methanol then follows a stepwise activated hydrogen [2*] insertion [4*].

Traditional copper based methanol catalysts have been modified with alkali to produce higher alcohol synthesis catalysts these include the addition of potassium, rubidium and caesium (*Smith & Anderson, 1983; Vedage et al., 1985; Smith et al., 1989; Nunan et al., 1989; Forzatti et al., 1991; Campos-Martín 1996*; *Herman, 2000* and Nowicki, *2005*).

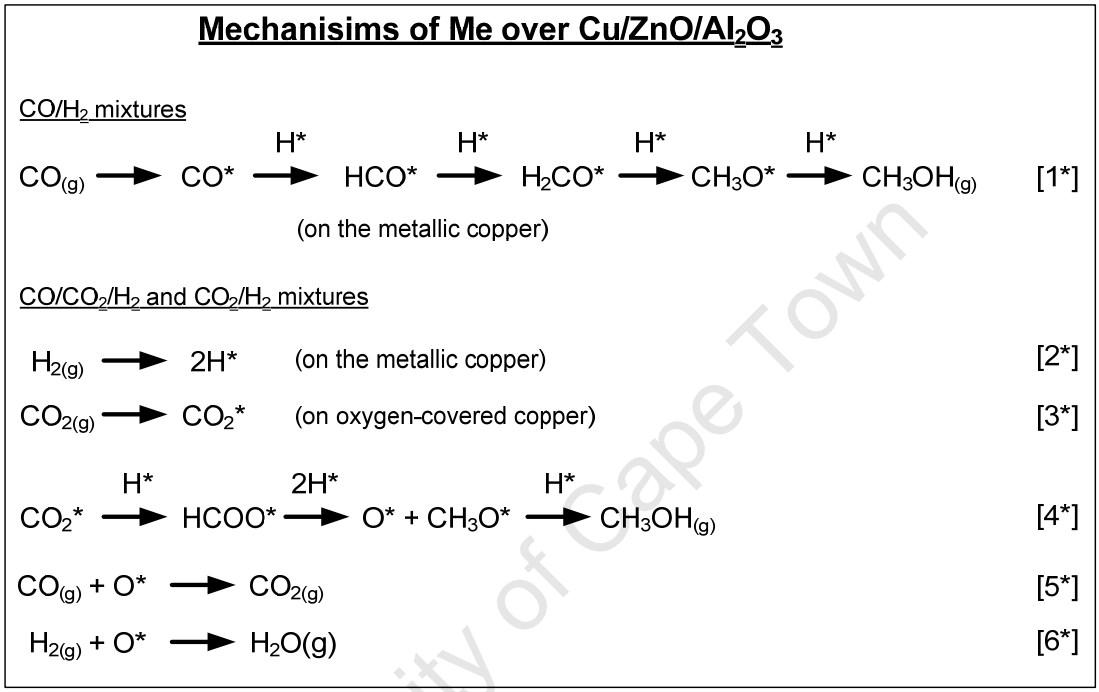

Figure 1.8 Mechanisms for the formation of methanol over $Cu/ZnO/Al_2O_3$ catalysts for different gas mixtures.

1.6.2 Rhodium based catalysts

Rhodium has been found to be active with a variety of supports for the production of a range of C_2 oxygenates including, acetic acid, acetaldehyde, and ethanol on metal oxide supports including SiO_2, Al_2O_3 and La_2O_3 (*Bhasin et al. 1978; Wilson et al., 1981; Underwood and Bell 1987; Kieffer et al., 1988; Lisitsyn et al., 1990; Hindermann et al., 1993*). The addition of promoters such as iron, manganese, lanthanum, vanadium, and samarium, can change the selectivity of the catalysts significantly (*Bhasin et al. 1978; Wilson et al., 1981; Underwood and Bell 1988; Luo et al. 2001*).

Of immense interest however is the effect of rhodium particle size on the product selectivity. Arakawa *et al*. (1984) discovered that a decreasing particle size (and

increased Rh dispersion) lead to an increase in methanol and ethanol selectivity. As the particle sizes increased to the selectivity to acetaldehyde and acetic acid increased. An optimal Rh particle size for oxygenate selectivity was found in the region of 2 to 3.5 nm. Other work in the area of particle size selectivity (*Underwood and Bell 1987; Hanaoka et al. 2000; Tago et al., 2000; Ojeda et al. 2004* and *Chen et al., 2006*) have confirmed size sensitivity of rhodium to product selectivity.

1.6.3 Modified Fischer-Tropsch catalysts with copper

Work on higher linear alcohol synthesis was initially conducted on iron Fischer-Tropsch catalysts that had been modified by alkali addition or nitriding (*Hindermann et al.*, *1993*). Patents by Ruhrchemie, (1955a, 1955b and 1956) claim an alcohol content of up to 45% in the reaction products boiling between 100 and 180 °C over an iron-copper catalyst. Razzaghi *et al*. (*Razzaghi et al.*, *1984*) also found a high oxygenate selectivity (22%) with silica supported iron-copper catalysts.

IFP has conducted work over alkalised cobalt-copper catalysts (1978 and 1981) and their results suggest that higher linear alcohol synthesis is possible over this catalyst system. Hindermann *et al.* (1993) in reviewing the formation of alcohols from CO hydrogenation suggest that as a result of the recent IFP work on cobalt-copper systems there is room to re-investigate iron-copper catalyst systems.

Recently patents by Sasol have claimed that co-precipitated copper-iron catalysts lead to an increase in the yields of olefins and oxygenates (*Visagie et al.*, *2001*, *van Zyl et al.*, *2004a* and *van Zyl et al.*, *2004b*). They claim this is through copper aiding the formation of a ferrihydrite precursor. They also claim that this precursor, although not present in the working catalyst anymore, somehow affects the catalyst selectivity.

Chapter 2

Scope of this work

The Fischer-Tropsch synthesis is regarded as a stepwise polymerisation reaction between adsorbed hydrogen, carbon monoxide and their monomers formed from them. Commercially, a supported precipitated iron catalyst promoted with small amounts of potassium and copper is one of the catalysts used in this reaction. Much work has been done into the effect of potassium promotion on product selectivities and that of copper on the reduction rate and temperature of reduction on the iron catalyst. The effect of copper on the product selectivity however, remains unclear. Copper, which on its own is an effective catalyst for methanol synthesis, may aid formation of oxygenates if added in significant quantities to Fischer-Tropsch-type catalysts.

Copper-iron catalysts have been prepared in this work via the co-precipitation of their nitrates for a series of copper loadings in order to examine the effect of copper on the product selectivity. No additional support material was added so as to minimise any additional effects. Potassium was loaded to the catalysts in order to maximize formation of olefins and oxygenates; its loading was kept constant on a metal basis as it was assumed that the potassium would evenly distribute over the metal surfaces and not have a preferred affinity for either the iron or copper. The calcined, reduced and spent catalysts were extensively characterised using techniques including XRD, MAS, SEM and TEM.

The catalysts were tested in both a fixed-bed and Berty reactor under Fischer-Tropsch conditions: 300 °C, 18 or 21 bar(a) and a fresh feed of hydrogen, carbon monoxide and carbon dioxide in a ration of 4:1:1. The temperature, which is on the low end of the temperature range for high temperature Fischer-Tropsch synthesis, was chosen so as to decrease secondary effects, thereby increasing the selectivity towards a more primary

product, including olefins and oxygenates. The pressures kept the inlet partial pressures constant for both reactor set-ups, and high enough to ensure Fischer-Tropsch conditions were met satisfactorily. The feed ratios were chosen so as to closely mimic industrial reactors and carbon dioxide was fed not only as it is present in industrial recycle streams, but also to force back carbon deposition.

Previously oxygenate interaction has been examined closely in the low carbon number products. However, the carboxylic acids are generally ignored due to the difficulty in extracting them quantitatively. This work proposes a new method for the quantification of the oxygenates in the liquid carbon fraction, including GC-MS analysis techniques.

C_8 oxygenates (1-octanol, octanal, octan-2-one, and octanoic acid) were co-fed with syn-gas using a saturator over a pure iron catalyst and a catalyst containing 50 wt% copper. The re-adsorption and interaction pathways of these oxygenates were monitored in the liquid carbon fraction, and the effect copper had on these interactions was investigated.

Chapter 3

Experimental methods

3.1 Preparation of co-precipitated iron-copper catalysts

Iron-copper catalysts were prepared by the discontinuous co-precipitation of hot aqueous 1 Molar solutions of $Fe(NO_3)_3 \cdot 9H_2O$ and $Cu(NO_3)_2 \cdot 3H_2O$ with a 5 wt% aqueous ammonia solution using the method described by Claeys (1997). Iron and copper nitrate solutions were mixed together in different ratios in order to obtain iron-copper catalysts as described in Table 3.1. Both a pure iron and a pure copper catalyst were included in this series as benchmark cases for the study.

Table 3.1 Weight loadings and ratios of prepared iron-copper catalysts.

Catalyst (Cu wt%)[a]	Iron (g)[b]	Copper (g)[b]
0	100	0
2	100	2
9	100	10
23	100	30
50	100	100
77	30	100
100	0	100

[a] Basis: Fully reduced catalyst

[b] Basis: Pure metal

3.1.1 Method of co-precipitation

Solutions of 1 molar aqueous iron nitrate ($Fe(NO_3)_3 \cdot 9H_2O$, Sigma) and copper nitrate ($Cu(NO_3)_2 \cdot 2½H_2O$, Sigma) were mixed to the desired volume ratios in a 2 *l* beaker and brought to the boil. A separate 2 *l* beaker of 5 wt% ammonium hydroxide solution (diluted from 25% ammonia solution, Saarchem) was also brought to the boil. The volume of ammonia solution needed was determined in pre-tests using a 'cold' precipitation of nitrates and ammonia to achieve a pH of 7 (Appendix A).

Once boiling, the ammonia solution was quickly added to the nitrate solution which was being stirred at a rate of 25000 rpm using an IKA T 25 basic ULTRA-TURRAX® disperser with a S25N-25G dispersion element. The pH was measured using a ThermoOrion 410Aplus pH meter with a 91065NWP electrode (Thermo electron corporation, USA), which was calibrated using buffer solutions of known pH before each use. When needed, additional ammonia was added to the solution to achieve a final pH of 7. This solution was then stirred for 15 minutes on a warm hotplate. The precipitate was filtered and washed with boiling deionised water until the solution was nitrate free. The filter cake was dried for 18 hours in an oven in air at 120 °C.

The dried precipitate was crushed to a size fraction below 125 μm and calcined at 400 °C for 3 hours in air, in a glass fluidised bed reactor, (SV = 900 ml/g_{Fe}/h (NTP) at a heating rate of 10 °C per minute).

3.1.2 Impregnation with potassium

Impregnation with potassium was done using a 1 molar aqueous solution of KNO_3 (99%, Sigma) in a rotary evaporator (Büchi Rotavapour R-205) to obtain an overall potassium loading of 5 g potassium per 100 g metal (iron and copper). The oil bath was set at 65 ºC, rotation at 50 rpm and the pressure was decreased from 760 mbar to 50 mbar by 5 mbar every 10 seconds. The evaporator was left at 50 mbar until the catalyst was dry.

Potassium loading was kept constant on a metal basis as it was assumed that the potassium would evenly distribute over the metal surfaces and not have a high affinity for either the iron or copper. To test this assumption on Fischer-Tropsch experiments a pure iron catalyst with 10 g potassium per 100 g iron was prepared, as this would be

similar in potassium loading to the 50 wt% copper catalyst if the potassium was only located on the iron.

Impregnated catalysts were calcined again at 400 °C for 3 hours in air, in a glass fluidised bed reactor, (SV = 900 ml/g_{Fe}/h (NTP) at a heating rate of 10 °C per minute) to remove all traces of nitrates.

3.2 Characterisation of co-precipitated catalysts

3.2.1 Atomic absorption spectroscopy, AAS

A Varian SpectrAA-30 spectrometer attached to a DS-15 station was used to determine the concentrations of iron, copper and potassium on the calcined catalysts. A mixture of 8 ml 30% hydrochloric acid and 2 ml 40% hydrofluoric acid was added to 0.1 g of catalyst sample and brought to the boil in a 250 ml Erlenmeyer flask. Once boiling, 10 ml 60% nitric acid was added and the resulting solution was reduced to approximately 2 ml in volume. 5 ml of concentrated perchloric acid was added and the resulting solution was reduced again to 2 ml.

The sample was quantitatively transferred to a 100 ml volumetric flask and made up to a volume of 100 ml with distilled water. The liquid sample was then filtered and the filtrate was analysed for iron, copper and potassium.

3.2.2 Scanning electron microscopy and energy dispersive X-ray analysis, SEM-EDX

A scanning electron microscope (LEO S444 SEM, La:Ka, UK) equipped with a Four Quadrant Back Scatter Detector and an energy dispersive Fissons Kevex X-ray spectrometer (EDXA) with sigma analysis software was used to determine the concentrations of iron, copper and potassium on the calcined catalysts.

Sample preparation involved sprinkling the sample on an aluminium stub coated with glue containing graphite. Here, graphite is used to conduct electrons, thereby preventing charge build up. The samples are then coated with carbon which does not

interfere with the elemental analysis. Single spot analysis was done on different parts of the samples to determine the metal concentrations.

3.2.3 X-ray diffraction spectroscopy, XRD

Analysis of the crystalline phases as well as the average crystallite size of calcined, reduced[2] and spent[2] catalysts were determined by means of X-ray analysis. X-ray diffraction measurements were done on a Phillips X-ray diffractometer with Cu-Kα radiation of wavelength 1.540 Å at 40 kV and 25 mA. The scan range was $0° < 2\theta < 90°$. All diffraction patterns were recorded in the step-scan mode with a step size of 0.01 degrees and a scan rate of 1 °/min. The diffractograms were analysed using X'Pert Highscore plus software and the diffraction peaks of crystalline phases were compared with those of standard compounds reported in the JCPDS[3] data file. The average crystallite sizes, $đ_{c\text{-}XRD}$ were calculated from the peak width at half-height using the Debye-Scherrer equation:

$$đ_{c\text{-}XRD} = \frac{k\lambda}{\beta\cos\theta} \tag{3.1}$$

Where, λ is the X-ray wavelength, k is the shape factor (k = 0.9), θ is the diffraction angle in degrees and β is the line broadening of FWHM[4] in radians. The units for $đ_{c\text{-}XRD}$ are in manometres. In cases where there was peak overlap the X'Pert software was used to deconvolute the peaks.

3.2.4 Mössbauer Spectroscopy, MAS

Analysis of the crystalline phases as well as the average crystallite size of calcined, reduced[2] and spent[2] catalysts were determined by means of Mössbauer spectroscopy. The experiments are performed using constant acceleration spectrometers equipped with ^{57}Co/Rh sources. The data were recorded at room temperature over a velocity range of ± 12 mm/s. The spectra were analysed by means of a least squares program "Normos" that models them as a combination of quadruple doublets and sextets based on a

[2] Passivated in CO_2 as per the method described by Baker and Rodriguez (1994).

[3] Joint Committee for Powder Diffraction Standards

[4] Full Width at Half Maximum intensity

Lorentzian line-shape profile. The individual absorption features were then identified on the basis of their isomer shift (δ), quadrupole splitting (ΔE_Q) and magnetic hyperfine field (B_{hf}) values. The relative amount of each phase was determined from the area of the absorption peaks. Metallic iron (α-Fe) was used to calibrate the velocity scale and the isomeric shift values of all the species are reported relative to it.

3.2.5 Brunauer-Emmett-Teller method, BET

The specific surface areas of the calcined catalysts were determined via N_2 adsorption/desorption according to the BET method using a Micromeritics ASAP 2000 analyser (Micromeritics Instruments Corp., USA).

3.2.6 Temperature programmed reduction, TPR

The reduction behaviour of both the potassium-impregnated and non-impregnated calcined catalysts was investigated by means of temperature programmed hydrogen reduction. Temperature programmed reduction was carried out in a U-type quartz reactor on a Micromeritics AutoChem2910 (Micromeritics Instrument Corp., USA). Catalysts were treated under a 4.9 vol% H_2 in Ar gas flow at a flow rate of 50 ml(NTP)/min, from 100 to 950 °C with a constant heating rate of 10 °C/min. In all cases a constant loading of 0.0379 g catalyst was used. This was done as opposed to using a constant iron loading, as with the high copper loaded catalysts the hydrogen consumption was too much for the system to be able to record accurately.

The instrument was also used to determine the degree of reduction of a catalyst as present after hydrogen pre-treatment prior to a Fischer-Tropsch experiment. For this the catalyst samples were exposed to *in situ* Fischer-Tropsch synthesis pre-treatment conditions i.e., heating under hydrogen at a rate of 1 ºC/min to 100 ºC holding for 1 hour, then 1 ºC/min to 400 ºC and holding for 16 hours, at ambient pressure and a WHSV = 4000 ml(NTP)/g_{Fe}/h and thereafter reduction in 4.9 vol% H_2 in Ar gas flow ramping from 100 to 950 °C.

For both methods the hydrogen consumption was measured using a thermal conductivity detector, which was calibrated at regular intervals using samples with known reduction behaviour (e.g. Ag_2O). The samples were heated within a regulated

furnace and the temperature was measured by a thermocouple placed 2 mm above the sample.

3.2.7 Transmission electron microscopy, TEM

Calcined, reduced[5] and spent[5] samples were analysed using a LEO 912 (Leo, now Zeiss GERMANY) Transmission Electron Microscope operating at 120 kV. The samples were ultrasonically suspended in methanol and a drop of each sample was transferred onto a carbon coated copper grid. Samples were left to dry at room temperature before analysis.

3.3 Fischer-Tropsch synthesis

Fischer-Tropsch synthesis was conducted in two separate reactor systems. Firstly, testing of catalysts and examination of initial catalyst behaviour was done on a fixed-bed apparatus. Secondly, a Berty reactor was used in order to collect oil and water samples for GC analysis of the catalyst series and for co-feeding of C_8 oxygenates on the 0 and 50 wt% Cu catalysts. The latter reactor is particularly suited for the co-feeding studies as it can be considered gradientless with respect to the partial pressure of reactants (hydrogen, carbon monoxides) and products (such as water and carbon dioxide), all of which can impact on the kinetics of product formation and consumption.

Not shown in the results, was the repeat of certain of these reactions in both the fixed-bed and Berty reactor. This was done to verify experimental repeatability. In most cases the repeat experiments were exceedingly accurate and suggested a good repeatability for the system. In cases where the results did not agree, experimental deviations such as gas leakages, temperature control problems or power failures were identified.

[5] Passivated in CO_2 as per the method described by Baker and Rodriguez (1994).

3.3.1.1 Experiments in a Fixed-bed reactor

All eight catalysts were tested in a fixed-bed apparatus, additionally an iron catalyst with twice the potassium loading and a mixture of 50 wt% (by metal) potassium promoted iron and copper oxides was also tested in the fixed-bed reactor to examine the difference in selectivities between potassium loadings and co-precipitated and manual mixtures of copper and iron.

3.3.1.2 Experimental set-up

The physical set-up of the apparatus for the Fischer-Tropsch synthesis experiments is shown in Figure 3.1. It consists of a U-tube micro fixed-bed reactor, (E-6). Gases are supplied from cylinders (Air Products, H_2 5.0, CO 5.0, CO_2 4.5, Ar 5.0, N_2 5.0) and fed via mass flow controllers (Brooks 5850S, Brooks Instruments, The Netherlands). During operation, the synthesis gas is fed to the system via mass flow controllers (F-1 – 3); a 4-way valve (4WV) is used to change flow from bypass to reactor.

A pressure-controlled argon-stream was fed after the reactor to maintain and control the total pressure of the system. A N_2/cyclohexane mixture (0.15 vol% cyclohexane[6] in N_2), used as an internal standard for sample analysis, was fed to the system via mass flow controller F-4 directly to the product line at atmospheric pressure just before the product ampoule sampler (E-8) (see also section 3.3.1.5). Liquid hydrocarbon products in Fischer-Tropsch experiments are collected in a wax trap (E-7) set to 190 °C, in order to ensure efficient wax collection. The temperatures of all other lines after the reactor were kept at 210 °C.

[6] Cyclohexane is not formed in Fischer-Tropsch synthesis and can be easily separated in the gas-chromatographic procedures applied.

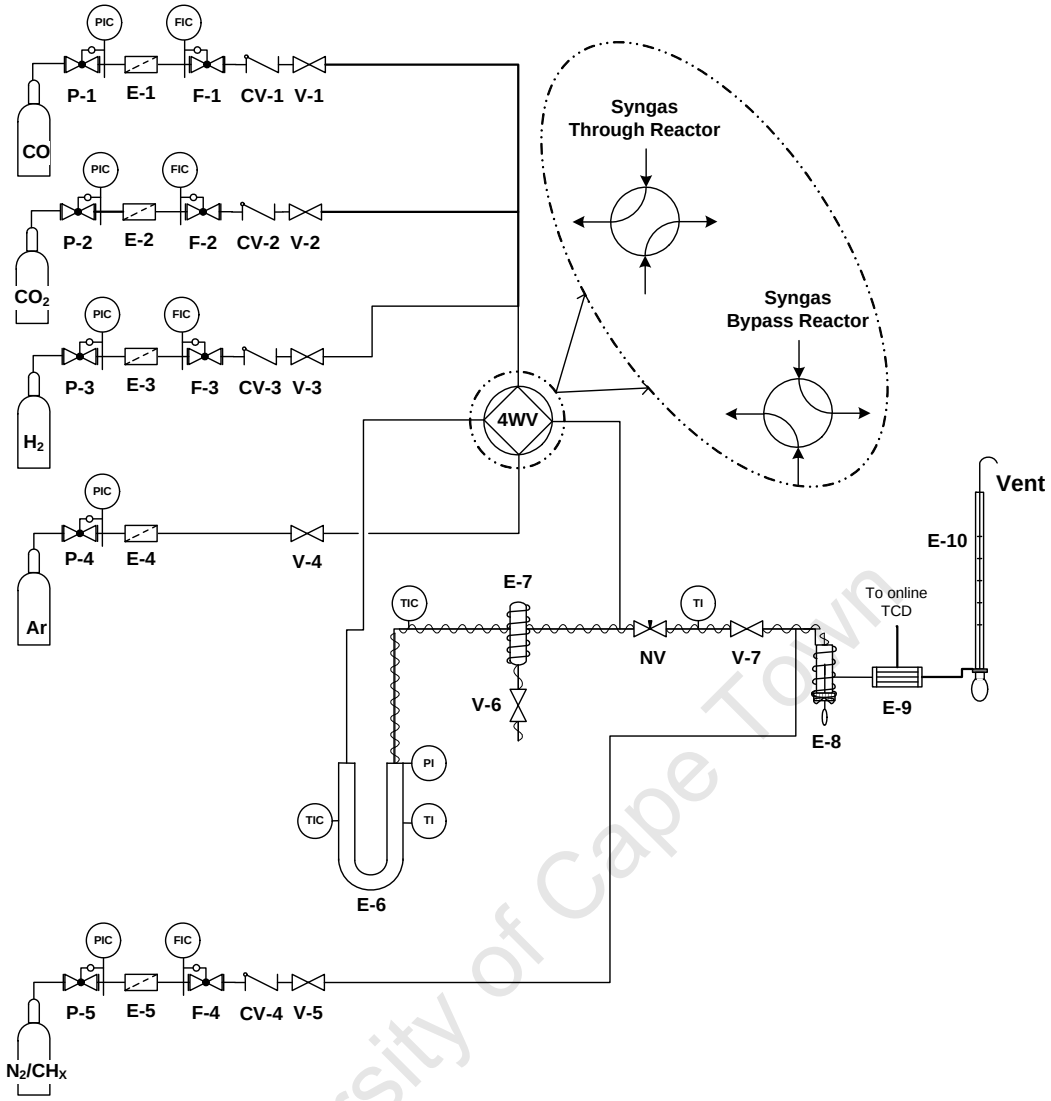

Figure 3.1 Experimental set-up for Fischer-Tropsch synthesis using a fixed-bed reactor

P-1 – 5: Pressure regulators; E-1 – 5: Line filters; E-6: Reactor; E-7: Wax trap; E-8: Ampoule breaker; E-9: Condenser; E-10: Bubble flow-meter; CV-1 – 4: Check valves; V-1 – 7: One-way valves; 4WV: Four-way valve; NV: Needle valve; PIC: Pressure indicator and control; FIC: Flow indicator and control; TIC: Temperature indicator and control; PI: Pressure indicator; TI: Temperature indicator.

3.3.1.3 Reactor loading

The reactor used was a U-tube fixed-bed reactor (Figure 3.2) made from stainless steel (O.D. 1/4 inch, I.D. 3 mm). The catalyst, diluted with silicone carbide (Aldrich - 212 – 250 μm) at a ratio of 1.4g catalyst to 1g silicone carbide, was packed inside the reactor; on the inlet side of the reactor more silicone carbide was added with glass wool plugs between the catalyst bed and at the top of the reactor. The outlet was plugged with glass wool only. This was done to prevent the catalyst bed from moving during the

experiment and the pressurising and de-pressurising of the system, as well as to ensure good mixing and heating of the feed gases prior to reaching the catalyst bed. The reactor was then placed in a temperature controlled electric furnace comprising an aluminium block housing. A thermocouple was placed in an axial thermowell outside the reactor, centrally between the limbs of the U-tube (and in contact with the reactor wall), for the purpose of controlling and monitoring the temperature.

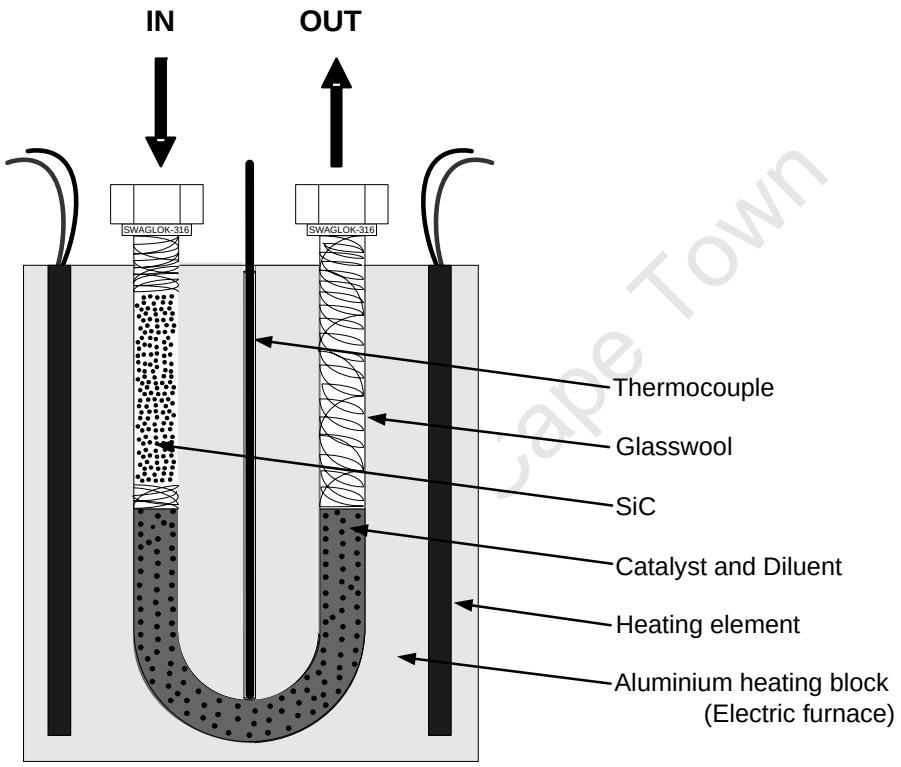

Figure 3.2 Configuration of U-tube reactor (not to scale)

Prior to the conducting of Fischer-Tropsch synthesis experiments, the temperature profile of the packed bed was determined under typical reaction conditions of temperature and flow rate. For these experiments an external thermocouple was positioned at different points along the full length of the packed bed in order to determine a complete bed temperature profile. The axial temperature profile was measured and found to be within +/- 0.1 °C of the average bed temperature over a bed length of approximately 10 cm. This became the length at which the total volume of the catalyst and diluent to fill the isothermal space was estimated at approximately 1.5 cm^3.

Diluting the catalyst with silicon carbide, which has a fairly high thermal conductivity, served to lower the amount of heat released per catalyst bed volume in the strongly exothermic Fischer-Tropsch reaction. The particle sizes of the diluent (212 – 250 μm) and the catalyst (53 – 125 μm) were chosen to allow for ideal plug flow behaviour with negligible wall effects as $\frac{ID_{Reactor}}{d_p} > 10$ (*Ertl et al.*, *1997*), yet large enough to ensure that the pressure drop across the bed was smaller than 0.1 bar at the reaction conditions. Furthermore with catalyst particles smaller than 300 μm no hampering effect due to intra-particle diffusion of the reactants is to be expected (*Claeys*, *1997* and *Claeys and Schulz*, *2004*). The inertness of the silicon carbide was tested and confirmed in a blank experiment.

The iron loading of all catalysts was kept constant for all experimental runs. This meant the overall catalyst mass varied with different copper to iron ratios. 0.69 g of iron was chosen as the base loading and the catalysts were loaded with a constant loading of 0.5 g of silicon carbide. To ensure a good mixing of diluent and catalyst, the mixtures were wet with iso-propanol and loaded before they dried and segregated again. Any remainder of iso-propanol was driven off under argon before the experimental run.

Special precaution was taken to make sure that the catalyst bed was placed equidistant from both the inlet and outlet of the reactor tube, i.e. positioned within the isothermal zone of the reactor tube.

After Fischer-Tropsch synthesis, the catalyst was passivated in flowing carbon dioxide at room temperature for one hour as described by Baker and Rodriguez (1994). The carbon dioxide forms a small oxide layer around the catalyst particle and keeps the bulk of the catalyst in the phase that was present during synthesis. This catalyst is then recovered for bulk characterisation purposes. In the case of the fixed-bed runs however the volume of catalyst recovered was insufficient to conduct characterisation tests on the spent catalyst.

3.3.1.4 Experimental procedure for synthesis runs

All catalyst samples were activated *in situ* at atmospheric pressure prior to reaction by reduction in hydrogen (see Table 3.2). After activation the reactor was switched to bypass (Figure 3.1 insert) and cooled under argon to the reaction temperature of 300 °C.

Once at reaction temperature the reactor system was pressure tested under argon at 20 bar (absolute) for 1 hour. After a successful pressure test the system was pressurised to 18 bar (absolute) via the pressure controlled argon-stream and controlled by opening the needle valve (NV) to allow the total flow of synthesis gas plus 20 ml/min of argon to exit the reactor system. The synthesis gases were introduced as detailed in Table 3.2. Correct and stable flow rates were confirmed by chromatographic online analysis of synthesis gas (H_2, CO and CO_2) relative to the reference gas (N_2) over several consecutive bypass analyses.

Table 3.2 Reduction and reaction conditions for fixed-bed tests

Reduction conditions	
Activation gas	Hydrogen
SV	4000 ml(NTP)/g_{Fe}/h
Temperature	at 1 °C/min to 100 °C, 60 min isothermal at 1 °C/min to 400 °C, 960 min isothermal
Pressure	Atmospheric
Reaction conditions	
Reaction gases	Hydrogen, carbon monoxide, carbon dioxide
SV	3900 ml(NTP)/g_{Fe}/h
H_2:CO:CO_2 ratio	4:1:1 (vol:vol:vol)
Reference gas	0.15 vol% Cyclohexane in nitrogen
Reference gas flow rate	15 ml(NTP)/min
Temperature	300 °C
Pressure	18 bar (absolute)

The system was then switched from bypass to reactor flow (Figure 3.1 insert). This point defines the start of the experiment. Progress of the reaction is then followed by regular sampling in a combination of online (TCD) and offline (FID, via ampoule sampling) analytical techniques (see section 3.4.1).

3.3.1.5 Sampling procedure

The total composition of the combined stream of product and reference gas was sampled in its reference state using heated glass ampoules as prescribed by Schulz and Nehren (1986). In this technique the capillary end of an evacuated ampoule is broken in

the sampling device; this draws a total vapour phase sample into the ampoule, after which the capillary is partially withdrawn and sealed with a butane flame. This is illustrated in Figure 3.3.

These ampoules are later crushed within an ampoule-breaking device (see Appendix B for diagram), releasing the sample contents into an offline chromatograph for analysis of organic compounds. Inorganic gases as well as methane were analysed by means of online chromatography. The experimental set-up is designed to measure fast initial changes of catalyst activity and selectivity of synthesis gas conversion.

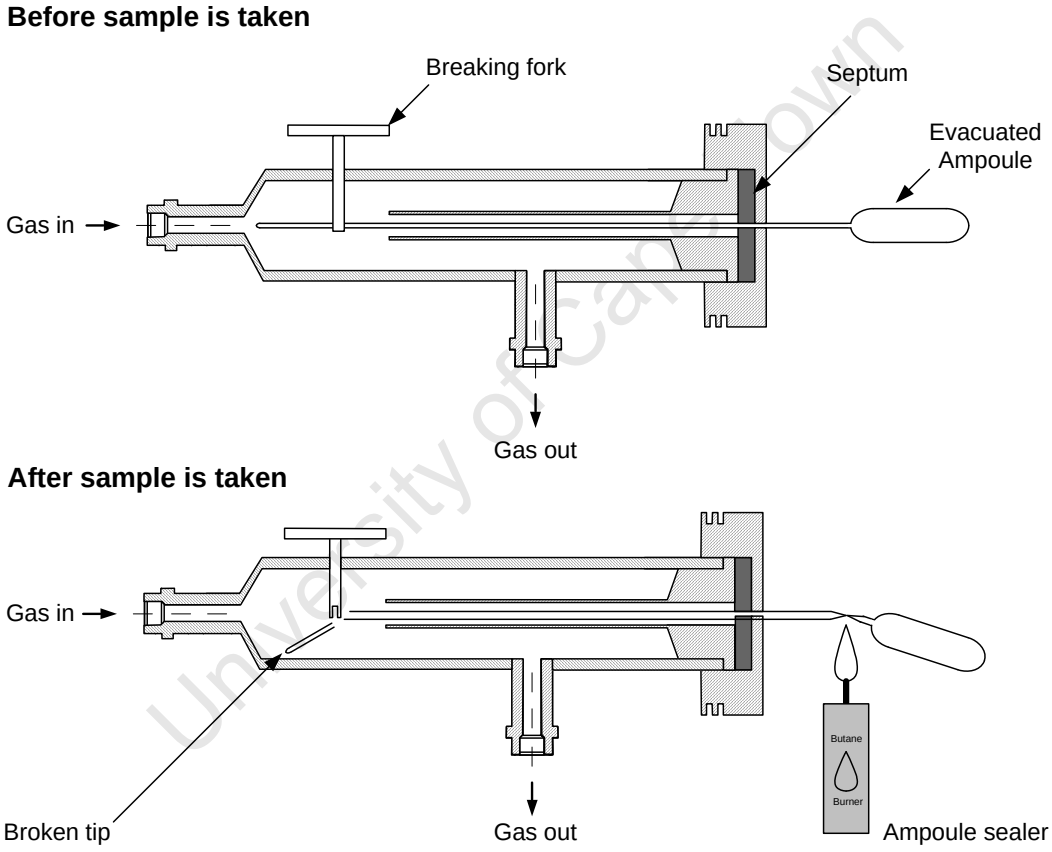

Figure 3.3 Ampoule sampling procedural set-up

3.3.2 Experiments in a Berty reactor

All eight catalysts were tested in a Berty reactor in order to collect water and oil samples for analysis.

The linear C_8 alcohol, aldehyde, ketone and acid were also co-fed using a saturator specifically designed for oxygenate feeding. Feeding experiments were conducted on the 0 wt% Cu and 50 wt% Cu catalysts using a Berty reactor as it can be considered gradientless with respect to partial pressure of reactants (hydrogen, carbon monoxides) and products (such as water and carbon dioxide), which all can impact on the kinetics of product formation and consumption (see Appendix C).

3.3.2.1 Experimental set-up

The physical set-up of the equipment for the Fischer-Tropsch synthesis experiments using the Berty reactor is shown in Figure 3.4. It consists of a Berty reactor (Autoclave Engineering), (E-7). Gases are supplied from cylinders (Air Products, H_2 5.0, CO 5.0, CO_2 4.5, Ar 5.0) and fed via mass flow controllers (Brooks 5850S, Brooks Instruments, The Netherlands). During operation, the synthesis gas is fed to the system via mass flow controllers (F-1 – 3); a 3-way valve (3WV-1) is used to send the flow of carbon monoxide and carbon dioxide through the saturator or straight to the reactor. A back-pressure regulator, (BPV-1) is used to maintain and control the total pressure of the system. An Ar/neo-hexane mixture (0.05 % neo-hexane[7] in Ar), used as an internal standard for sample analysis, is fed to the system via mass flow controller F-4 directly to the reactor feed (see also section 3.3.1.5), so as not to run the internal standard through the reactor all the time. It was possible to substitute this with pure argon by closing valve, V-4 and opening valve, V-5. It should be noted that the Berty reactor could not be by-passed (as in the case of the fixed-bed reactor); the reference gas was therefore fed with the reactants and the total pressure was raised accordingly to account for the added inert gas and to ensure the same partial pressures as in the experiments in the fixed-bed reactor (see also Table 3.5). Feed samples could be taken at the ampoule sampling point E-6, and product samples at E-9. Heavy liquid hydrocarbon products in Fischer-Tropsch experiments are collected in a wax trap, (E-8).

[7] 2,2 di-methyl butane (Note that this compound is not formed in Fischer-Tropsch synthesis and can be easily separated in the gas-chromatographic procedures applied. It was abstained to use cyclo-hexane as reference component, which was used in the fixed-bed reactor tests, as this may have undergone ring-opening reactions when fed to the reactor, whereas the paraffinic neo-hexane can be regarded inert. It is therefore ideally suited as an internal reference component in this set-up.)

The temperature of the wax trap is set to 190 °C, in order to ensure efficient collection of heavy reaction products. The temperatures of all lines after the reactor to the condenser are kept at 210 °C. The condenser (E-10) is set at 5 °C in order to ensure efficient collection of reaction water and liquid hydrocarbon product for offline GC analysis.

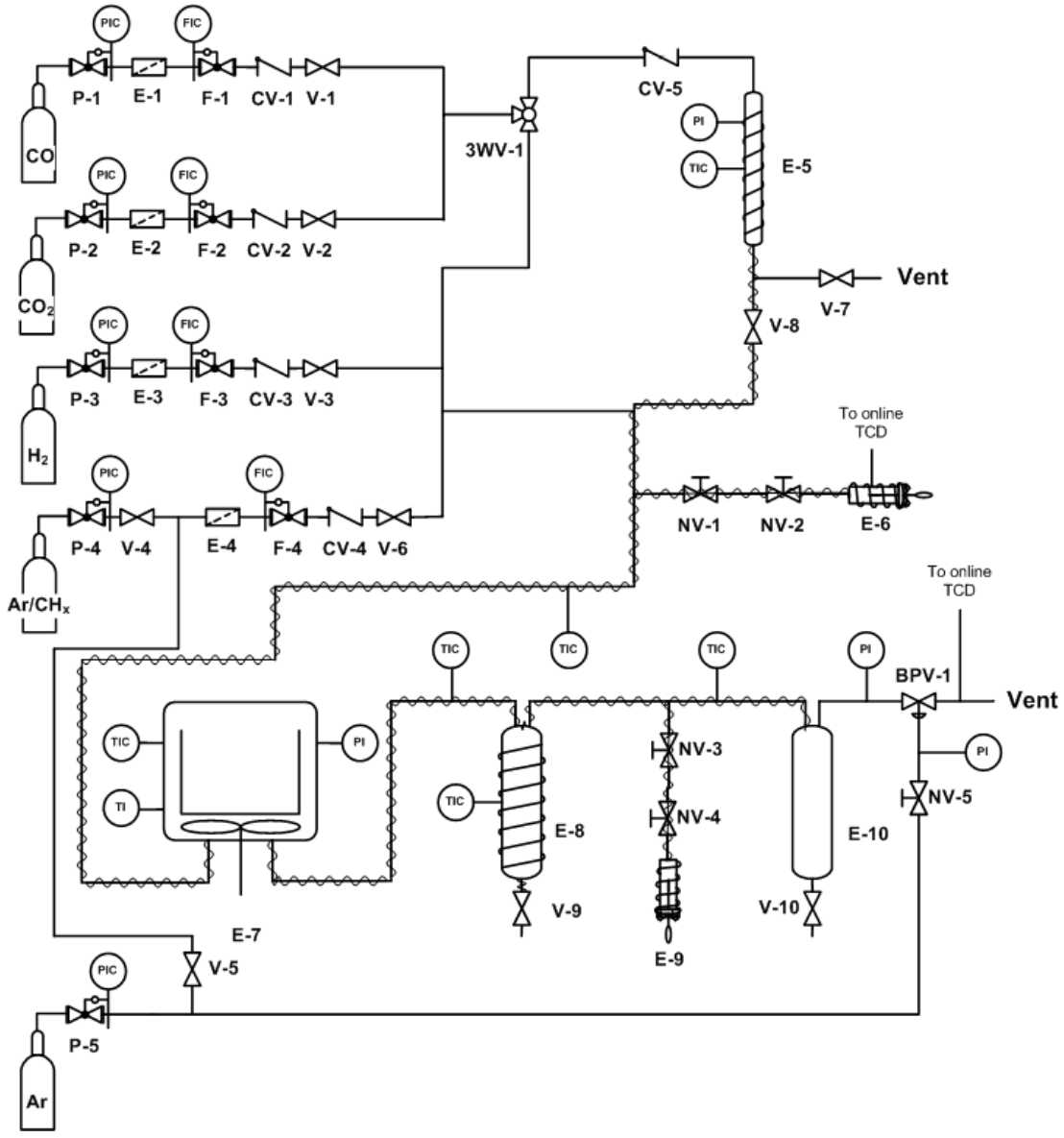

Figure 3.4 Experimental set-up for Fischer-Tropsch synthesis using a Berty reactor.

P-1 – 5: Pressure regulators; E-1 – 4: Line filters; E-5: Saturator; E-6: Bypass ampoule breaker; E-7: Reactor with stirrer; E-8: Wax trap; E-9: Tail gas ampoule breaker; E-10: Condenser; CV-1 – 5: Check valves; V-1 – 10: One way valves; 3WV-1: Three way valve; NV-1 – 5: Needle valve; BPV-1: Back-pressure regulator; PIC: Pressure indicator and control; FIC: Flow indicator and control; TIC:

Temperature indicator and control; PI: Pressure indicator; TI: Temperature indicator. Note: Pressure release valves are not shown

3.3.2.2 Reactor loading

The reactor used was a Berty reactor (Autoclave Engineering, Figure 3.5) made from stainless steel (I.D. 122.5 mm). The catalyst was packed inside an inner stainless steel insert (O.D. 111 mm, I.D. 33 mm), between 2 wire-mesh grids. Glass wool and then glass beads (O.D. 7 mm) were placed on top of the grid. This was done to prevent the catalyst bed from moving during the experiment and during pressurising and de-pressurising of the system as well as to ensure good mixing and heating of the feed gases prior to reaching the catalyst bed. The tube was then placed in a temperature controlled Berty reactor. A thermocouple was placed in the reactor above the catalyst bed for the purpose of monitoring the temperature.

The reactor was sealed with 8 bolts tightened alternatively from 60 to 220 nm. An external heating jacket was placed around the sealed reactor with a thermocouple placed between the jacket and the reactor wall for the purposes of monitoring and controlling the reactor temperature.

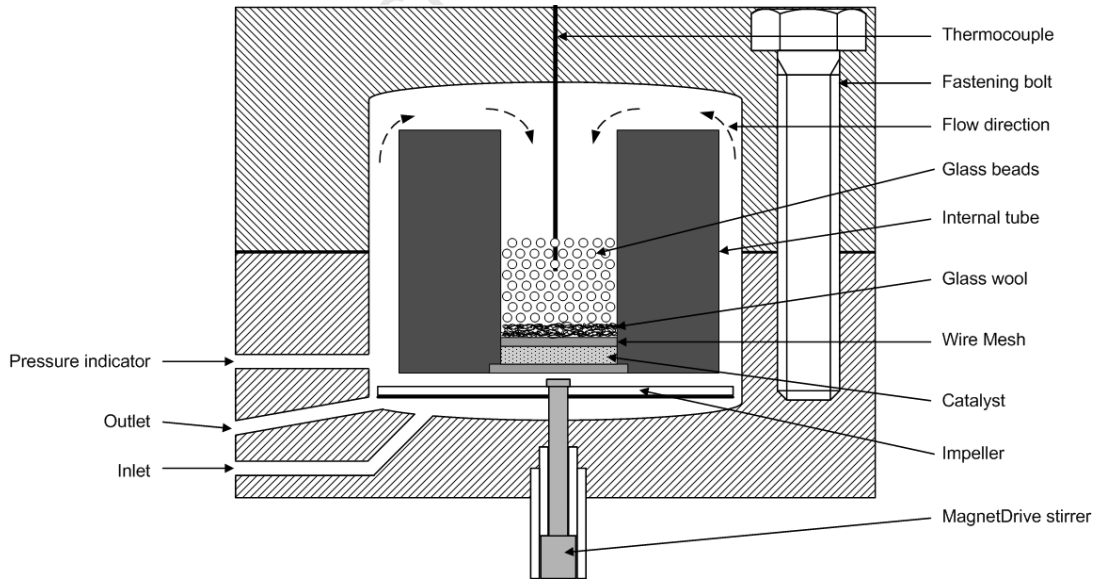

Figure 3.5 Configuration of Berty reactor (not to scale)

The size of the glass beads (O.D. 7 mm) was chosen to allow for ideal plug flow behaviour with negligible wall effects as $\frac{ID_{Reactor}}{d_p} > 10$ (*Ertl et al.*, *1997*), yet large enough to ensure that the pressure drop across the bed was smaller than 0.1 bar at the reaction conditions. Furthermore, with catalyst particles smaller than 300 μm no hampering effect due to intra-particle diffusion of the reactants is to be expected (*Claeys*, *1997* and *Claeys and Schulz*, *2004*). The impeller speed was set to 1700 rpm, which should ensure full CSTR behaviour of the reactor as evidenced in step function tests on the system with inert material (SiC) simulating the catalyst (Appendix C).

The amount of iron loaded was kept constant for all experimental runs; this meant the overall catalyst mass differed with different copper to iron ratios. 2.40 g of iron was chosen as the base loading. After Fischer-Tropsch synthesis, the catalyst was passivated in flowing carbon dioxide at room temperature for one hour, as described by Baker and Rodriguez (1994). The carbon dioxide forms a small oxide layer around the catalyst particle and keeps the bulk of the catalyst in the phase that was present during synthesis. This catalyst is then recovered for bulk characterisation purposes.

3.3.2.3 Saturator

All co-fed components are introduced to the reactor via a saturator. The saturator is a jacketed ½ inch stainless steel tube (I.D. 10 mm). The temperature of the saturator is controlled by a water bath which pumps a water/antifreeze mixture through the jacket. The saturator is 20 cm long and filled with ca. 15 ml Chromosorb (Chromosorb P, 60-80 mesh, pore volume 1.2 ml/g, sigma), a porous material often used in chromatography. Prior to a run the saturator is filled with 10 ml of the component which is to be co-fed. The synthesis gas has been split into hydrogen and argon, and carbon monoxide and carbon dioxide, the latter two passing through the saturator (Figure 3.4). As the synthesis gas flow rates in these experiments are fixed, the flow rate of the co-fed component is controlled by the temperature setting of the water bath. For co-feeding a vapour pressure of the co-fed component of 10 to 100 times that present in the reactor during steady state synthesis was sought. The feeding rate was chosen large enough to see clear effects on the oxygenates reactions, but low enough so that their presence should not impact on the overall synthesis gas conversion.

Vapour pressures used to estimate the feed flow rates of the co-fed components were calculated using data from Daubert *et al*. (1999) (

Table 3.3), and the simultaneous solving of the vapour pressure,

$$p^* = \exp\left(A + \frac{B}{T} + C \bullet \ln T + D \bullet T^E\right) \tag{3.2}$$

(where p* is vapour pressure in Pascals and T is the temperature in degrees Kelvin) and molar flow rate equations:

$$n_i = \frac{p^*}{p_{total}} \bullet \frac{\left(V_{CO} + V_{CO_2}\right)_{in}}{V_A} \tag{3.3}$$

Table 3.3 Thermodynamic constants for calculating vapour pressure data taken from Daubert *et al.* (1999).

Feeding component	A	B	C	D	E
1-Octanol	1.562×10^{2}	-1.430×10^{4}	-1.859×10	1.332×10^{-17}	6.000
Octanal	1.532×10^{2}	-1.105×10^{4}	-1.993×10	1.276×10^{-5}	2.000
Octanoic acid	2.602×10^{2}	-1.878×10^{4}	-3.609×10	2.568×10^{-2}	1.000
Octan-2-one	1.187×10^{2}	-1.130×10^{4}	-1.342×10	1.045×10^{-17}	6.000

Table 3.4 details the targeted vapour pressures and required temperature settings as calculated by their thermodynamic properties and ten times the standard vapour pressures as calculated after 24 hours time online.

Table 3.4 Target vapour pressures and the corresponding saturator temperatures for oxygenate co-feeding.

Feeding component	Desired vapour pressure (mbar)	Saturator temperature (°C)
Octanol	15.6	91.0
Octanal	2.2	55.6
Octanoic acid	6.0	111.3
Octan-2-one	1.5	34.1

3.3.2.4 Experimental procedure for synthesis runs

All catalyst samples were activated *ex situ* in a glass fluidized bed reactor (due to the difficulty of running definite temperature controlled programs in a Berty reactor), prior to reaction, at atmospheric pressure, by reduction in hydrogen, see Table 3.5. After activation the fluidized bed reactor was switched to pure argon and cooled to room temperature. Once cool the catalyst was transferred to the Berty reactor tube under argon and covered with n-heptane in order to avoid contact with air and potential re-oxidation of the reduced samples. The reactor tube was then placed inside the reactor and the reactor was sealed.

For the co-feeding experiments the saturator was loaded with the co-fed component, sealed and pressurised with a 1:1 mixture of carbon monoxide and carbon dioxide to 25 bar (absolute), at this point.

The reactor temperature was set at 150 °C and kept there for 4 hours under flowing argon in order to remove all traces of heptane from the system. Ampoule samples were taken in order to establish that the heptane had left the system.

The system was then pressurised to 21 bar (absolute) using the back-pressure regulator and the reactor temperature was set to 300 °C. Once the temperature and pressure were stable the system was pressure tested for 1 hour. After a successful pressure test the stirrer was set to a rate of 1700 rpm, and the synthesis gases were introduced as detailed in Table 3.5. The setting of the gas flows defines the start of the experiment.

Progress of the reaction was then followed by sampling of the reactor in 24 hour periods (the reactor was switched from pure argon to the argon/neo-hexane mixture at least 1 hour prior to sample taking to ensure the system was well mixed), in a combination of online (TCD) and offline (FID, ampoules, oil and water) analytical techniques (see section 3.4.1). As the reactor is well mixed fast changes in the system cannot be measured so more regular sampling would not have added transient information as obtained in the fixed-bed studies.

For co-feeding experiments, after 48 hours time on-stream the saturator temperature was set according to the required feeding temperature (Table 3.4) and the carbon monoxide and carbon dioxide were switched to flow through the saturator (3WV-1). Valve V-6 was opened and the system pressure was carefully equilibrated (note: it was imperative that the pressure inside the saturator was higher than the reactor pressure so as to

eliminate the chance of product back flow). After another 48 hours valve V-6 was closed and the carbon monoxide and carbon dioxide were switched to flow directly to the reactor again (3WV-1).

Sampling on the reactor during co-feeding was done more regularly, as the feeding only lasted for 48 hours; as many data points as possible were required to fully understand any trends present. A first oil and water sample (from E-10) was drained and discarded 10 hours after co-feeding began (to eliminate any high initial concentration effects). Further samples were scheduled for 24, 36 and 48 hours after feeding commenced. Both feed and product ampoule samples were taken in order to quantify the flow of components to the reactor as well as the products formed. At the end of the co-feeding (approximately 10 hours) the oil and water sample (from E-10) was drained again and discarded as some traces of the co-fed component were still visible in the captured product.

Table 3.5 Reduction and reaction conditions for Berty tests

Reduction conditions (conducted in external fluidized-bed reactor)	
Activation gas	Hydrogen
SV	4000 ml(NTP)/g_{Fe}/h
Temperature	at 1 °C/min to 100 °C, 60 min isothermal
	at 1 °C/min to 400 °C, 960 min isothermal
Pressure	Atmospheric
Reaction conditions	
Reaction gases	Hydrogen, carbon monoxide, carbon dioxide
SV	3900 ml(NTP)/g_{Fe}/h
H_2:CO:CO_2 ratio	4:1:1
Reference gas	0.05 % Neo-hexane in argon
Reference gas flow rate	26 ml(NTP)/min
Temperature	300 °C
Pressure	21 bar (absolute)[8]

3.3.2.5 Sampling procedure

The total composition of the combined stream of product and reference gas was sampled in its reference state, using heated glass ampoules as prescribed by Schulz and

[8] Pressure here higher than the 18 bar(a) described in the fixed-bed experiments due to the presence of argon in the reactor feed.

Nehren (1986). In this technique the capillary end of an evacuated ampoule is broken in the sampling device; this draws a total vapour phase sample into the ampoule after which the capillary is partially withdrawn and sealed with a butane flame. This is illustrated in Figure 3.3. These ampoules are later crushed within an ampoule breaking device (see Appendix B), releasing the sample contents into an offline chromatograph for analysis of organic compounds. Inorganic gases as well as methane were analysed by means of online chromatography. The reaction oil and water were collected in the condenser and separated by means of a separating funnel. The oil was injected in to an offline gas chromatograph while the water phase was mixed with 1-4 Dioxane and injected into another offline chromatograph for analysis of water soluble polar compounds in this phase.

3.4 Product analysis

3.4.1 Gas phase analysis

Different sampling techniques and chromatographs were used for the analysis of the results for the fixed-bed and Berty experiments.

3.4.1.1 Analysis of gas-phase results in a Fixed-bed reactor

Nitrogen was used as an internal standard for the online analysis where H_2, N_2, CO, CH_4 and CO_2 were analysed using a GC (Hewlett Packard 5890) equipped with a thermal conductivity detector (TCD); the conditions of this analysis method are detailed in Table 3.6.

Cyclohexane, CHx, which is not a product of Fischer-Tropsch synthesis at the conditions applied, was used as an internal standard for the offline analysis of organic compounds using a gas chromatograph (Agilent Technologies 6890N) equipped with a flame ionisation detector (FID), the conditions of which are detailed in

Table 3.7; see Figure 3.6 for a typical gas phase FID chromatogram.

Table 3.6 Conditions for gas-chromatographic analyses of inorganic gases and methane

Gas chromatograph	**Hewlett Packard 5890 (online)**
Detector	Single filament, modulated flow, thermal conductivity detector (TCD)
	$T_{Detector}$ = 200 °C
Column	Packed stainless steel, 10′ x 1/8″
Stationary phase	CarbosieveII, 100/120 (Supelco)
Carrier gas	Argon
Flow rate	30 ml(NTP)/min
Injector	Splitless
Analysis temperature	140 °C

Table 3.7 Conditions for gas-chromatographic analyses of organic products

Gas chromatograph	**Agilent Technologies 6890N (offline)** (adapted to ampoule technique)
Detector	Flame ionisation detector (FID)
	$T_{Detector}$ = 250 °C
Column	RTx-1 (Restek)
	Fused silica capillary column, 100 m x 0.25 mm
Stationary phase	0.5 μm dimethyl siloxane (crosslinked)
Carrier gas	Helium
Column-head pressure	2 bar
Injector	Split injector
	$T_{Injector}$ = 250 °C
	Split ratio 1:50
Temperature program	-60 °C, 10 min isothermal
	at 50 °C/min to -30 °C, 0 min isothermal
	at 2.5 °C/min to 250 °C, 30 min isothermal
Ampoule-breaker temperature	220 °C

3.4.1.2 Analysis of gas-phase results in a Berty reactor

Argon was used as an internal standard for the offline analysis of H_2, Ar, CO, CH_4 and CO_2, which were analysed using a three channel micro gas chromatograph (Varian CP-4900) equipped with three thermal conductivity detectors (TCD), three injectors and three columns, using hydrogen or argon as carrier gases; the conditions for the gas-chromatographic procedures using this GC are detailed in Table 3.8.

Neo-hexane, CHx, which is not a product of Fischer-Tropsch synthesis at the conditions applied, was used as an internal standard for the offline analysis of organic compounds using a gas chromatograph (Agilent Technologies 6890N) equipped with a flame ionisation detector (FID) and a mass spectrometer (MS, Agilent Technologies 5973N) employing a temperature programme. To allow for simultaneous analysis using both detectors two identical columns were used in the set-up, which were connected to the injector via a 2-hole ferrule. The conditions used are detailed in Table 3.9; see Figure 3.6 for a typical gas phase FID chromatogram. The set-up could be used for ampoule samples as well as direct liquid sample injection. The latter technique was used for analysis of long chain oxygenates, in particular those in the C_8 carbon number range,

which are of interest in the co-feeding studies conducted in this work. The technique is described further in section 3.4.2.1.

Table 3.8 Conditions for gas-chromatographic analyses of inorganic gases and methane

Gas chromatograph	**Varian CP-4900 Micro gas chromatograph (online)** (three-channel system)
Detector	Thermal conductivity detectors (TCD) $T_{Detector}$ = 110 °C
Module A	
Column	Molecular sieve 5A PLOT, 20 m
Carrier gas	Hydrogen
Column-head pressure	150 kPa
Analysis temperature	80 °C
Gases detected	Argon, nitrogen, methane, carbon monoxide
Module B	
Column	PoraPLOT Q, 10 m
Carrier gas	Hydrogen
Column-head pressure	100 kPa
Analysis temperature	60 °C
Gases detected	Carbon dioxide
Module C	
Column	Molecular sieve 5 PLOT, 10 m
Carrier gas	Argon
Column-head pressure	150 kPa
Analysis temperature	80 °C
Gases detected	Hydrogen, (methane and carbon monoxide)

Table 3.9 Conditions for gas-chromatographic analyses of organic gases

Gas chromatograph	**Agilent Technologies 6890N (offline)** (adapted to ampoule technique)
FID	
Detector	Flame ionisation detector (FID)
	$T_{Detector}$ = 250 °C
MS	
Detector	Mass selective detector (MSD), model 5973N
	$T_{Transfer\ line}$ = 280 °C
Scanning range	2 – 400 amu @ 3.64 scans/sec
Source	Electron impact (70 eV)
	T_{Source} = 230 °C
GC set-up	
Column	RTx-1 (Restek)
	Fused silica capillary column, 60 m x 0.25 mm
Stationary phase	0.5 μm dimethyl siloxane (crosslinked)
Carrier gas	Helium
Column head-pressure	2 bar
Injector	Split injector
	$T_{Injector}$ = 250 °C
	Split ratio 1:18
Temperature program	-60 °C, 10 min isothermal
	at 50 °C/min to -30 °C, 0 min isothermal
	at 2.5 °C/min to 250 °C, 30 min isothermal
Ampoule-breaker temperature	220 °C

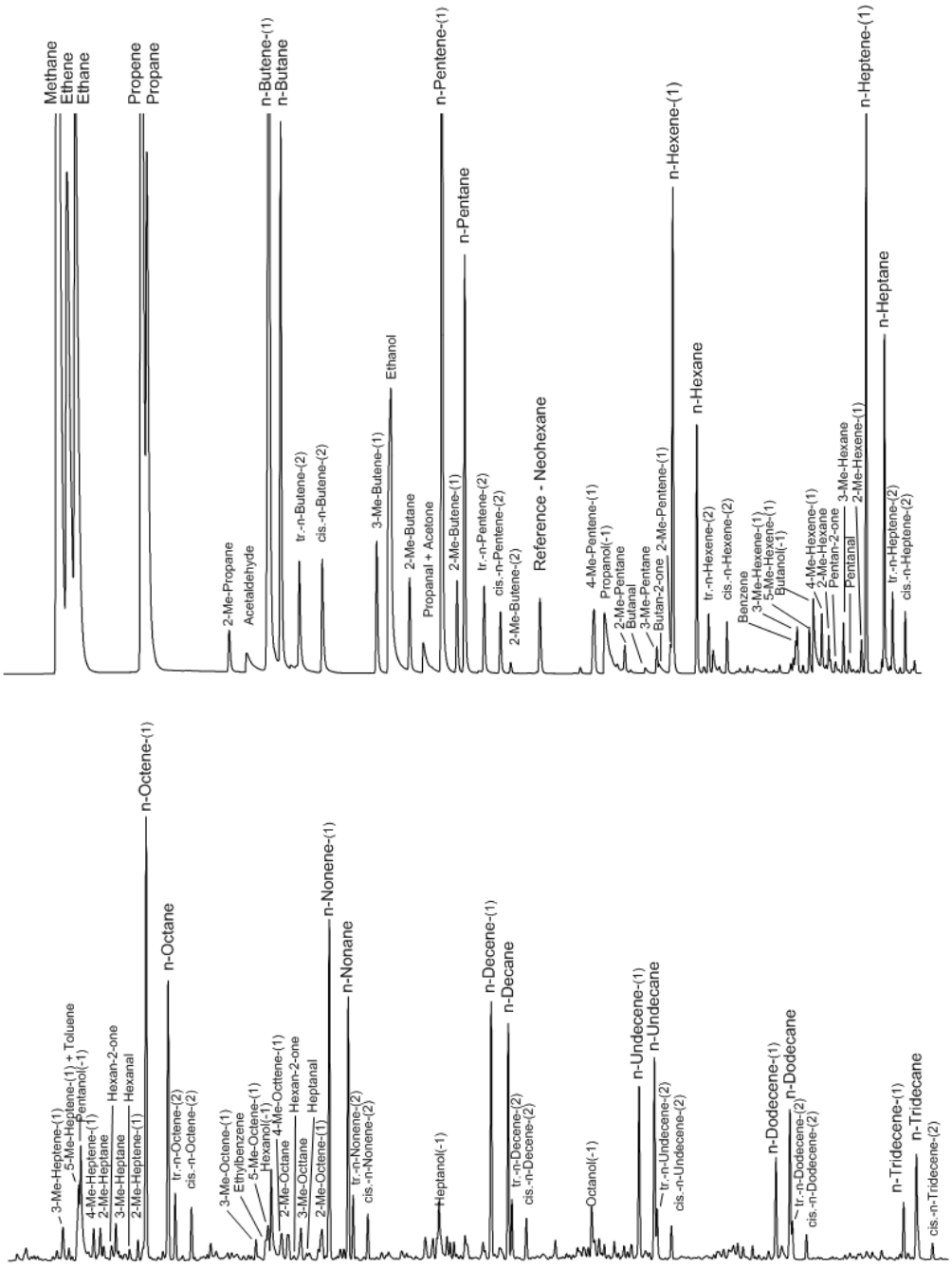

Figure 3.6 A typical gas phase chromatogram obtained from FID analysis (not all peaks labelled). Note: Where Cyclohexane is the reference gas the peak appears between 3-Me-Hexene-(1) and 5-Me-Hexene-(1).

3.4.1.3 Errors, calibration and chromatograms

Relative errors (repeatability of these analysis techniques) are typically ±3 % for TCD analyses and ±1 % for FID analyses. The internal standards, which were accurately fed to the product stream and subsequent samples, were used for calculation of flow rates of inorganic and organic components and subsequent conversions, yields, and selectivities.

The TCD set-up was calibrated on a weekly basis using a calibration gas mixture with a known composition. The peak areas (A_i) obtained from the TCD analysis of the calibration gas were then used to calculate the relative calibration factors (f_{TCD}), normalised for argon or nitrogen depending on the reference gas, for each species:

$$\left(\frac{n_i}{n_{Ar}}\right) = f_{TCD,i}\left(\frac{A_i}{A_{Ar}}\right) \tag{3.4}$$

Typical calibration factors were: f_{TCD,H_2}= 0.0874 ±0.044; $f_{TCD,CO}$= 1.0142 ±0.0148; f_{TCD,CH_4}= 0.1310 ±0.0170; f_{TCD,CO_2}= 0.9571 ±0.0011.

The response of an FID detector is strictly carbon specific; however, oxygen-containing components give a weaker response. In order to account for this, theoretical mass specific response factors have been used following an incremental approach suggested by Kaiser (1969). Here the response of all carbon atoms which are not bonded to an oxygen atom is 1, the response of carbon atoms with a single bond to an oxygen atom is 0.55 and those carbons with C=O double bonds are considered to give no response. The resulting factor for a component is then calculated by:

$$f_{FID,i} = \frac{N_C}{N_{C\ (no\ O)} + 0.55N_{C\ (with\ O)}} \tag{3.5}$$

Where N_C is the total number of carbon atoms in a molecule, $N_{C\ (no\ O)}$ is the number of carbon atoms not connected to an oxygen atom and $N_{C\ (with\ O)}$ is the number of carbon atoms connected to an oxygen atom with a single bond.

3.4.2 Liquid phase analysis

There are two major problems associated with analysis of the gas phase. The first is that the analysis of the organic acids is affected in someway by the injection method (see Appendix D). This is probably due to adsorption and/or reaction of the acids on the metallic surfaces of the ampoule sample introduction device. The second is that some

of the oxygenated compounds (because they are present in such small concentrations) cannot be successfully isolated from the other hydrocarbon products.

During Fischer-Tropsch synthesis oil and water is collected from the Berty reactor in the cold catch-pot. These are separated and analysed independently. In both cases it is possible to selectively extract the acids as well as achieve better analysis regarding the oxygenates. As the oxygenates are generally more soluble in one phase than the other, some understanding of the product composition can be reached.

3.4.2.1 Oil phase

A 1 µl of the oil sample was injected into the gas chromatograph described above (Agilent Technologies 6890N), which is equipped with a flame ionisation detector (FID) and a mass spectrometer (MS); conditions used in the analysis of the product oil are described in Table 3.10, also see Figure 3.7 and Figure 3.8 for typical FID and MS chromatograms.

The response of the FID is the same as for components in the gas phase analysis and is detailed in section 3.4.1.3.

It is possible to selectively extract relatively unique ions for each oxygenate class from the TIC chromatograms. By identifying particular ions that are unique to a particular type of compound, compounds that are not necessarily identifiable in the FID chromatogram can be accounted for through the MS. Examples of these products include alcohols, aldehydes, ketones, carboxylic acids and other longer chain oxygenates. Examples of such extracted ion chromatograms (extracted from a chromatogram similar to that of Figure 3.8) are shown in Figure 3.9 (1-alcohols, m/z = 31), Figure 3.10 (aldehydes, m/z = 44), Figure 3.11 (ketones, m/z = 58) and Figure 3.12 (carboxylic acids, m/z = 60). It should be noted that not all the compounds in a specific class are identified with the specific ion; however, it is generally the lighter components (C_4, C_5) that don't have the same specific ion as the rest of the series. The peaks were identified with spiking tests as well as using the NIST[9] library to compare extracted ions from MS chromatograms via MSD ChemStation (Agilent Technologies).

[9] NIST (National Institute of Standards and Technology) mass spectral search program V2.0 for the NIST/EPA/NIH mass spectral library.

The response of the ion specific components on the MS is usually non-linear and had to be calibrated though the injection of different mixtures of components (in this case linear oxygenates) and a standard Fischer-Tropsch hydrocarbon product with a large response area, that could be easily identified in the gas phase FID and was present in the oil phase. As the C_8 oxygenates were to be co-fed and they elute from the GC around the C_{10} hydrocarbon products, n-decene-(1), with m/z = 55 as a characteristic fragment in the MS spectrum, was chosen as the standard tie component.

By plotting the molar ratios of the oxygenate and the hydrocarbon against the area ratios of the oxygenate specific m/z and m/z = 55:

$$\left(\frac{x_i}{x_{C_{10}^=}}\right) \text{ vs } \left(\frac{A_i}{A_{C_{10}^=}}\right) \tag{3.6}$$

and fitting a 2nd order polynomial, the non-linear response of the MS can be determined.

$$\left(\frac{n_i}{n_{C_{10}^=}}\right) = A_{MS,i}\left(\frac{A_i}{A_{C_{10}^=}}\right)^2 + B_{MS,i}\left(\frac{A_i}{A_{C_{10}^=}}\right) \tag{3.7}$$

Where $A_{MS,i}$ and $B_{MS,i}$ are the relative calibration factors normalised for n-decene-(1) (m/z = 55). Typical response factors are listed in Table 3.11 and the calibration curves and compound histograms can be found in Appendix E.

Table 3.10 Conditions for gas-chromatographic analyses of oil product

Gas chromatograph	**Agilent Technologies 6890N (offline)**
FID	
Detector	Flame ionisation detector (FID)
	$T_{Detector}$ = 250 °C
MS	
Detector	Mass selective detector (MSD), model 5973N
	$T_{Transfer\ line}$ = 280 °C
Scanning range	2 – 400 amu @ 3.64 scans/sec
Source	Electron impact (70 eV)
	T_{Source} = 230 °C
GC set-up	
Column	RTx-1 (Restek)
	Fused silica capillary column, 60 m x 0.25 mm
Stationary phase	0.5 μm dimethyl siloxane (crosslinked)
Carrier gas	Helium
Column-head pressure	1.82 bar
Injector	Split injector
	$T_{Injector}$ = 250 °C
	Split ratio 1:30
Temperature program	70 °C, 2 min isothermal
	at 5 °C/min to 250 °C, 30 min isothermal

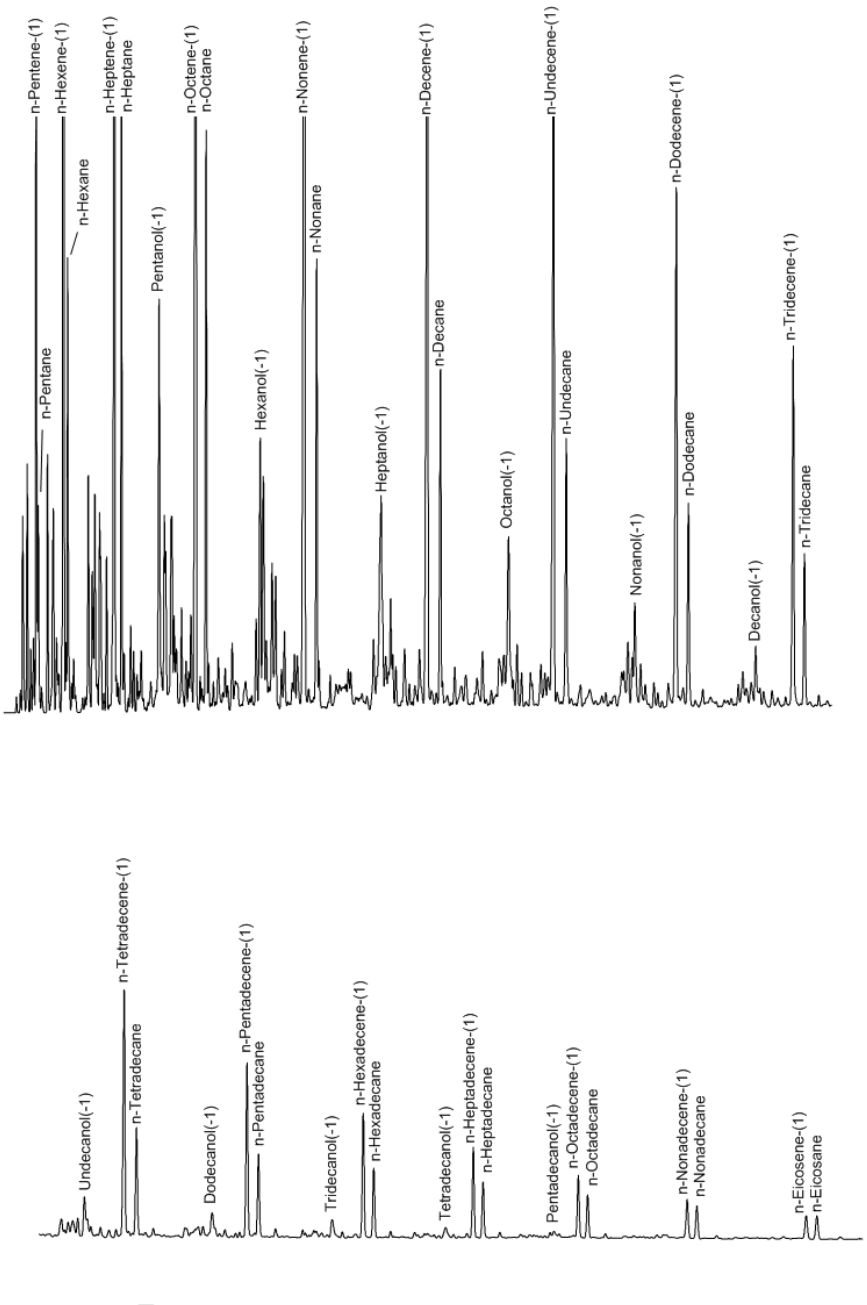

Figure 3.7 A typical oil chromatogram obtained from FID analysis (only major peaks labelled)

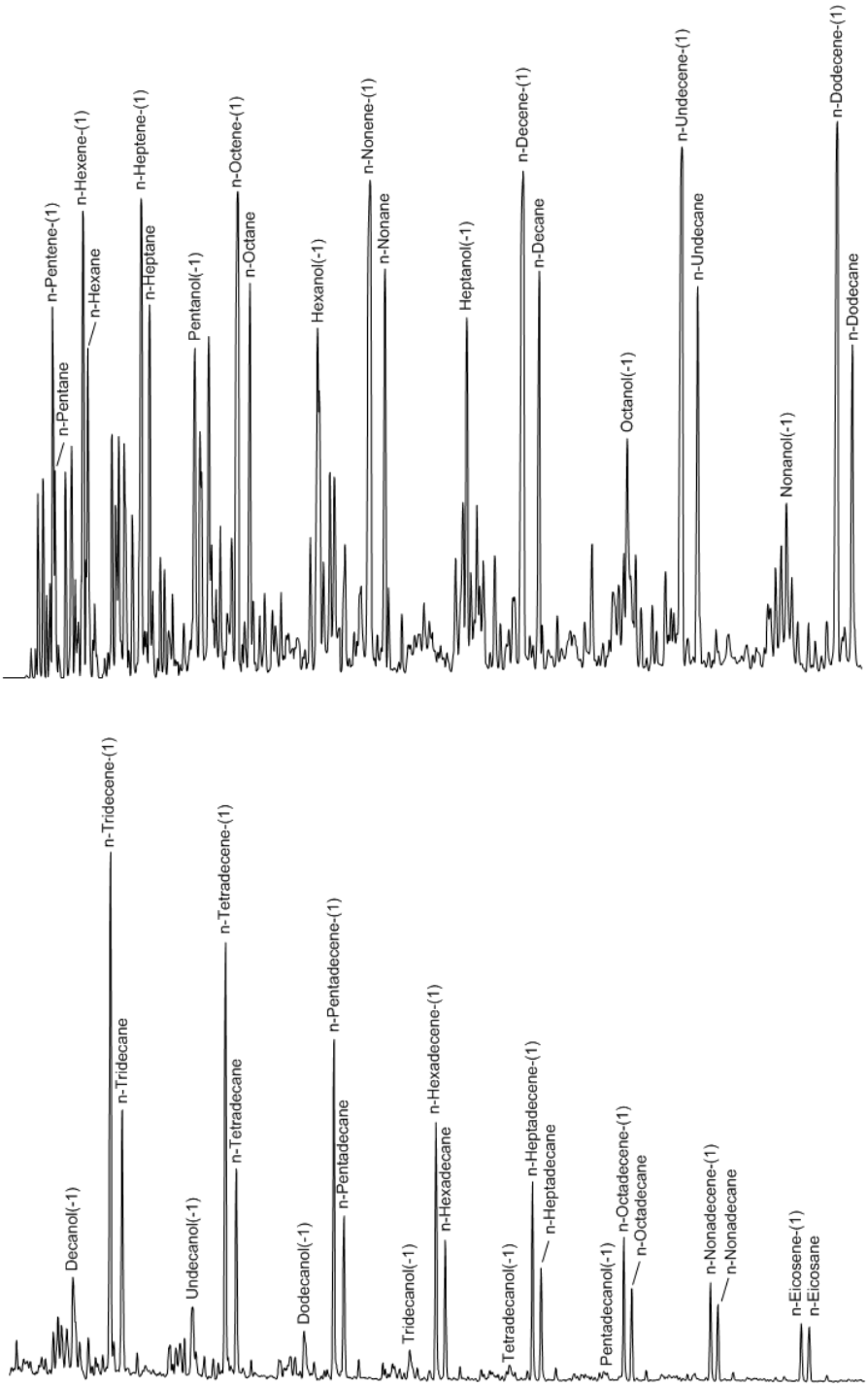

Figure 3.8 A typical oil chromatogram obtained from MS analysis (only major peaks labelled)

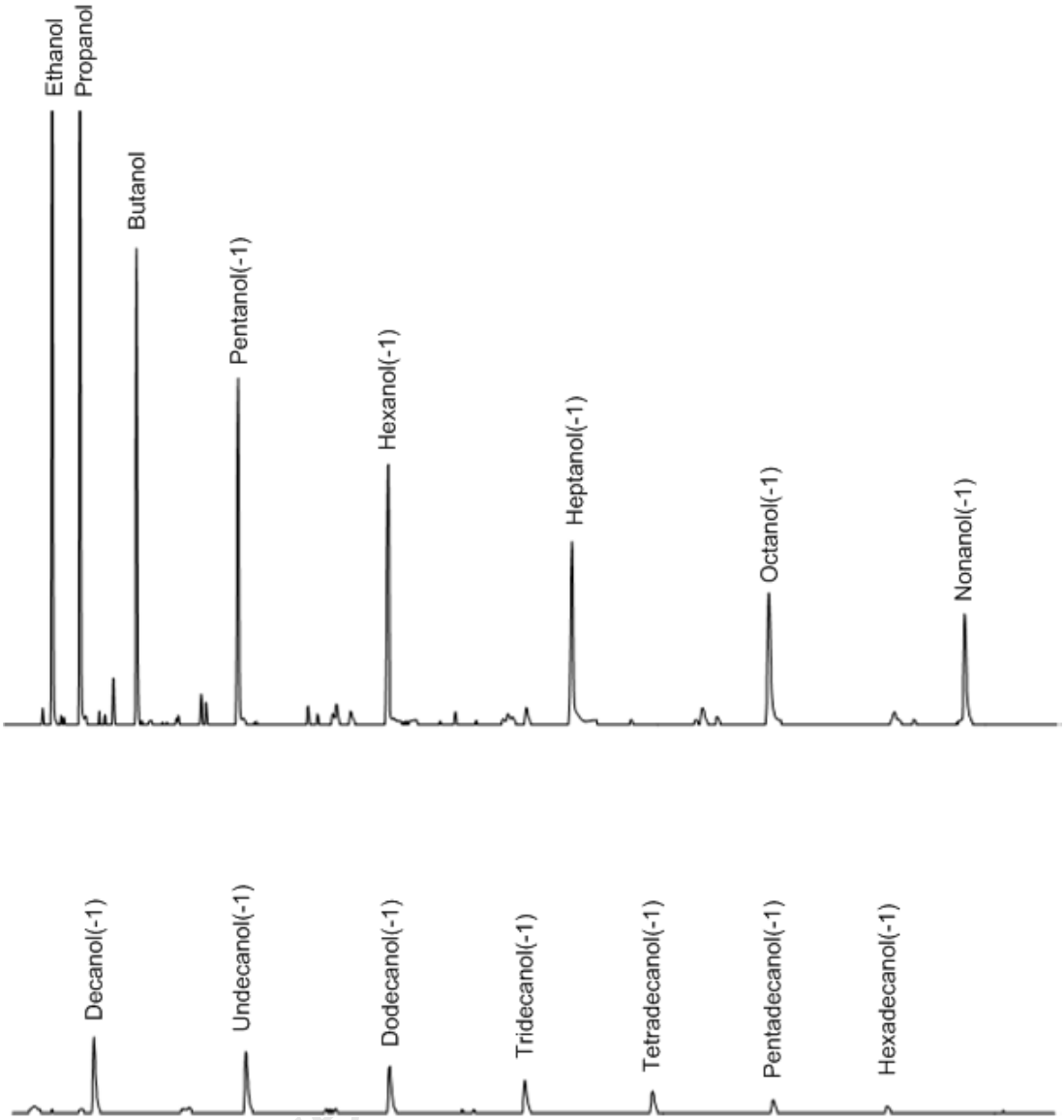

Figure 3.9 A typical oil chromatogram with m/z = 31 extracted

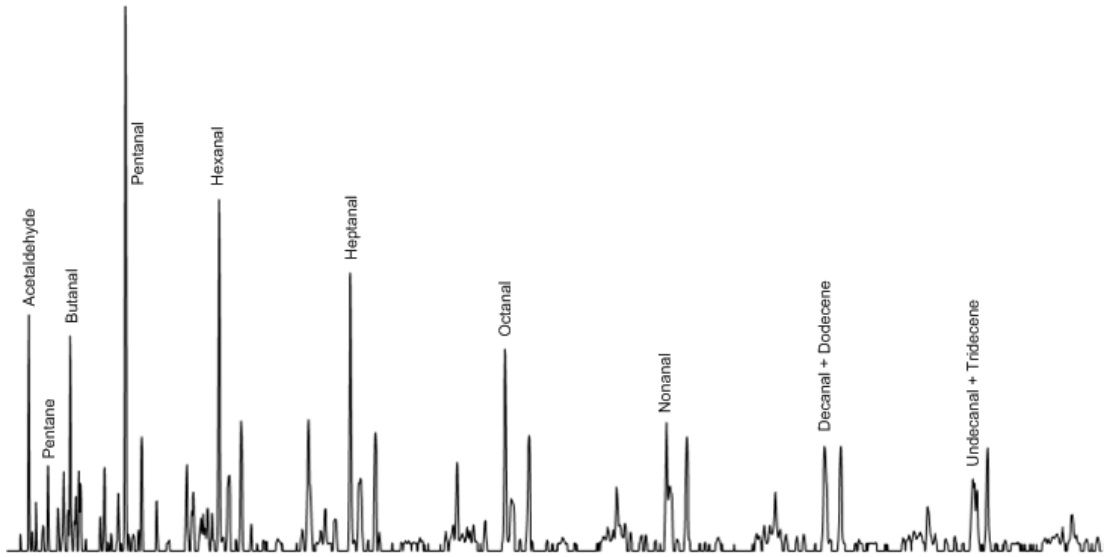

Figure 3.10 A typical oil chromatogram with m/z = 44 extracted (Note: Propanal does not have the m/z = 44 ion)

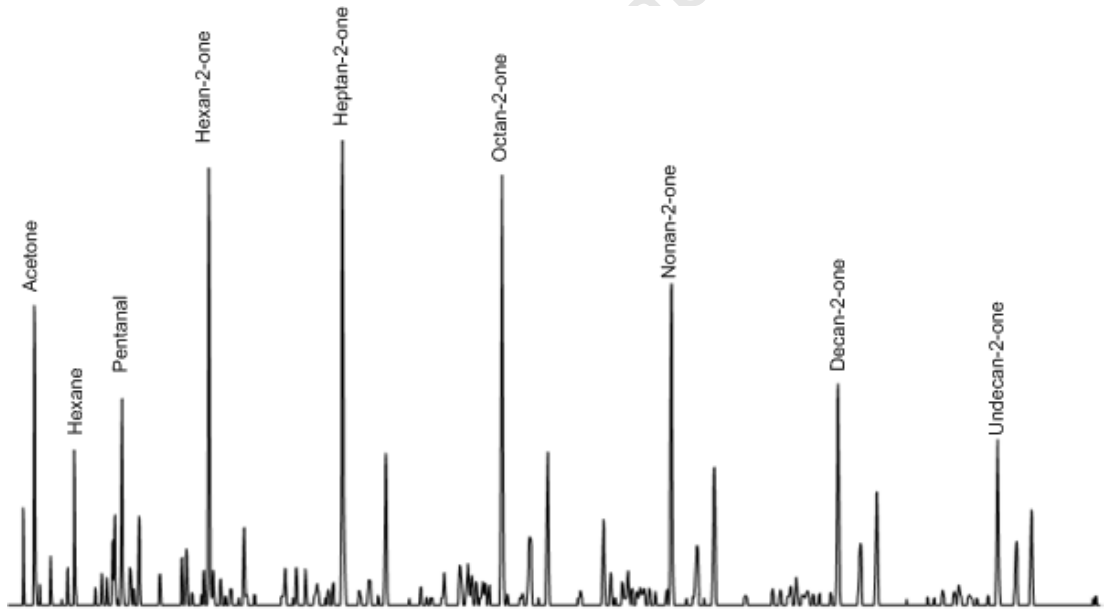

Figure 3.11 A typical oil chromatogram with m/z = 58 extracted (Note: Butan-2-one and Pentan-2-one do not have the m/z = 58 ion)

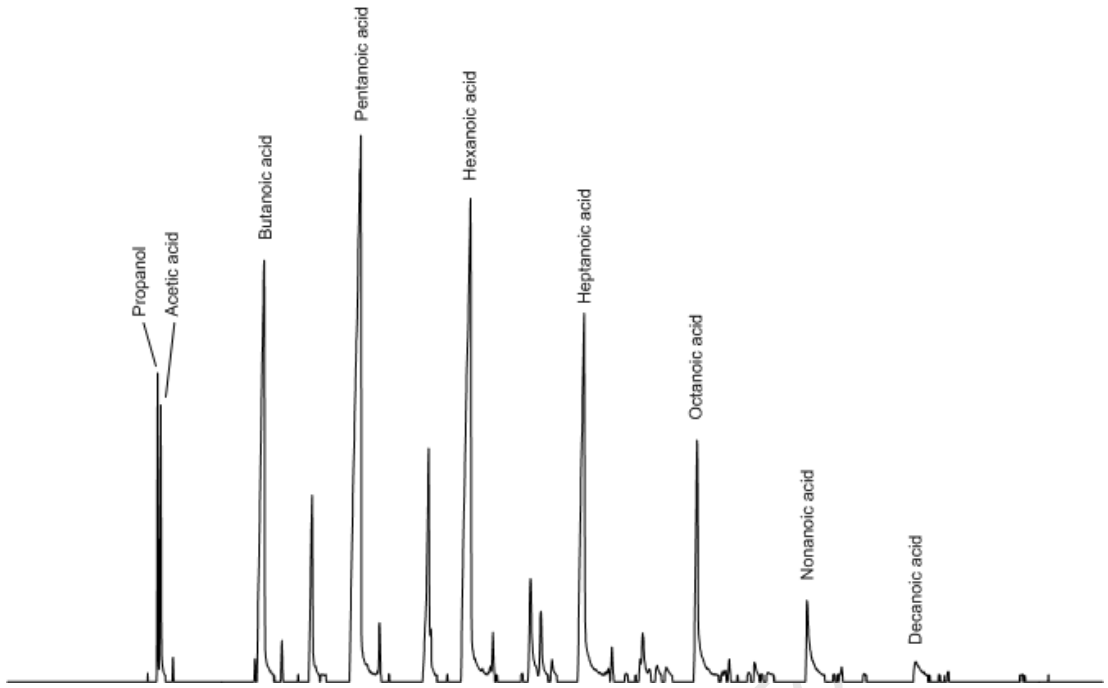

Figure 3.12 A typical oil chromatogram with m/z = 60 extracted (Note: Propanoic acid does not have the m/z = 60 ion)

Table 3.11 Calibrated molar response factors for 1-octanol (m/z = 31), octanal (m/z = 44), octan-2-one (m/z = 58) and octanoic acid (m/z = 60), using decene (m/z = 55) as a tie component

Compound	ion	Ratio	x^2	x	c	R^2
Octanol	31	31/55	14.665	0.274	0.0105	0.97
Octanal	44	44/55	6.148	0.658	-0.0114	0.98
Octanone	58	58/55	0.101	0.099	-0.0005	1.00
Octanoic acid	60	60/55	0.413	0.036	-0.0004	0.96

3.4.2.2 Water phase

One ml of the water sample was mixed with 10 µl of 1-4 Dioxane (Sigma) for use as an external standard. One µl of this solution was injected into a gas chromatograph (Varian 3400) equipped with a flame ionisation detector (FID) employing a temperature-program; conditions of the gas-chromatographic procedure are detailed in Table 3.12. Also see Figure 3.13 for a typical FID chromatogram. Peaks were identified via spiking of known components into the water phase.

Analysis of the water phase allows easy identification of the lighter oxygenate compounds in the product. As most of them are highly soluble in water the majority of

the compound will be in this phase as opposed to the oil phase. It should however be noted that some light oxygenates were also found present in the oil phase analyses (see chromatograms above) The advantage of water analysis over the gas sampling method is that the light oxygenates are easily separated and do not need to be separated from the hydrocarbon product in any way. Most importantly this method allows easy identification of the carboxylic acids that are otherwise not identifiable in the gas phase due to interactions with the ampoule method as mentioned above.

The response factors of Kaiser (1969) could have been used for these calculations (as done previously for the gas phase analysis) but due to the high concentration of water in the samples it was decided to use a manual calibration. As the response from the FID is linear the GC can be calibrated using one calibration solution. A water solution containing known amounts of the oxygenates of interest was made up and injected into the GC. The peak areas (A_i) obtained from the FID analysis of the calibration solution were used to calculate the relative calibration factors normalised for 1-4 dioxane (f_{FID}) for each species:

$$\left(\frac{n_i}{n_{Dioxane}}\right) = f_{FID,i}\left(\frac{A_i}{A_{Dioxane}}\right) \tag{3.8}$$

Typical response factors are listed in Table 3.13.

Table 3.12 Conditions for gas-chromatographic analyses of organic products in the water phase

Gas chromatograph	**Varian 3400 (offline)**
Detector	Flame ionisation detector (FID)
	$T_{Detector}$ = 250 °C
Column	ID-BP20 (SGE)
	Capillary column, 60 m x 0.25 mm
Stationary phase	Polyethylene glycol
Carrier gas	Hydrogen
Column-head pressure	2 bar
Injector	Splitless
	$T_{Injector}$ = 250 °C
Temperature program	40 °C, 8 min isothermal
	at 15 °C/min to 200 °C, 20 min isothermal

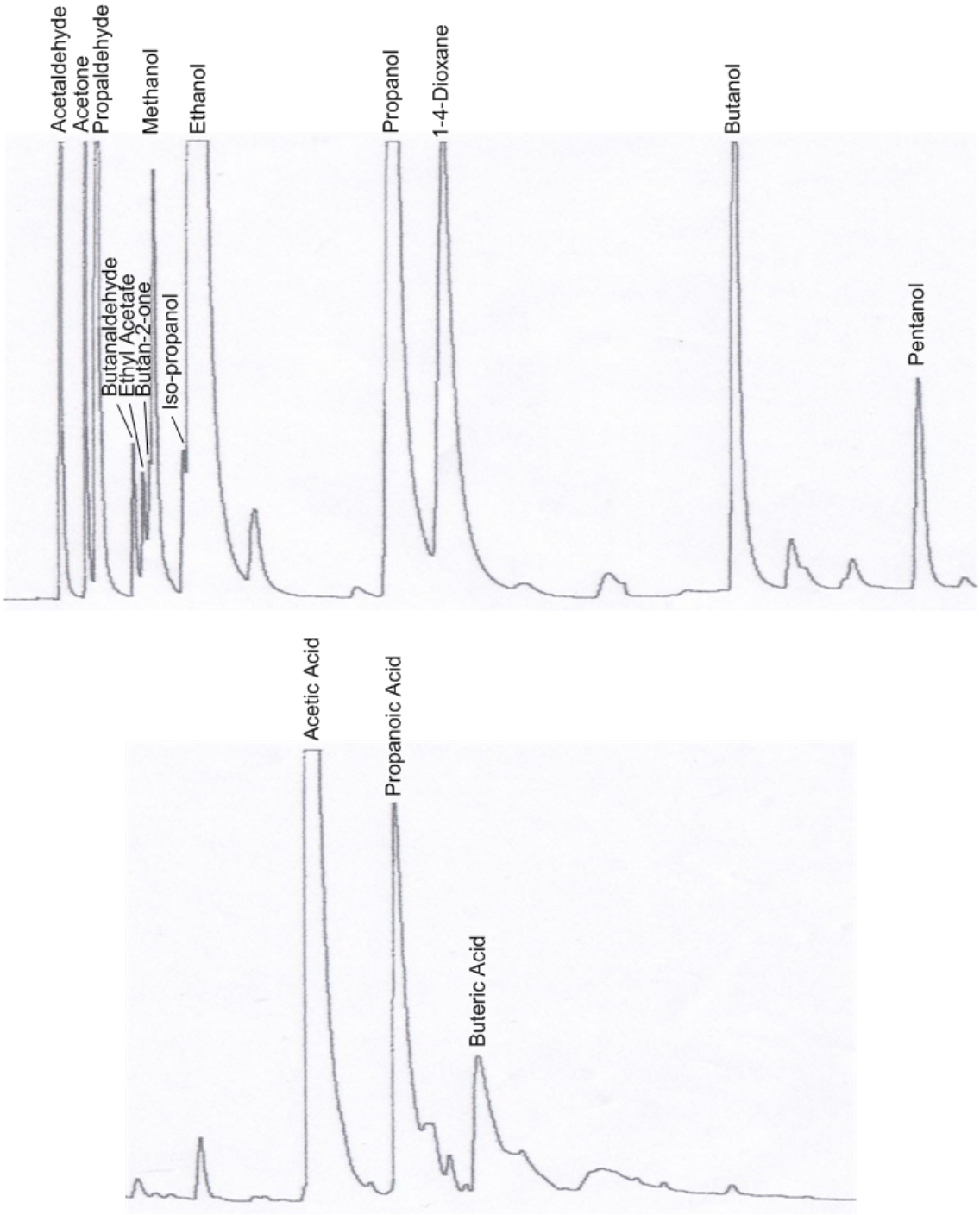

Figure 3.13 A typical chromatogram of the water product phase obtained from an FID

Table 3.13 Response factors of oxygenated compounds in water phase FID analysis

Compound	Response factor
Methanol	2.08
Ethanol	1.29
Propanol	0.96
Butanol	0.62
Pentanol	0.49
Iso-Propanol	1.55
Acetaldehyde	2.45
Propanaldehyde	1.07
Butanaldehyde	2.87
Acetic acid	2.31
Propanoic acid	1.26
Buteric acid	1.70
Acetone	1.51
Butan-2-one	1.47

3.4.3 Data work-up – gas phase

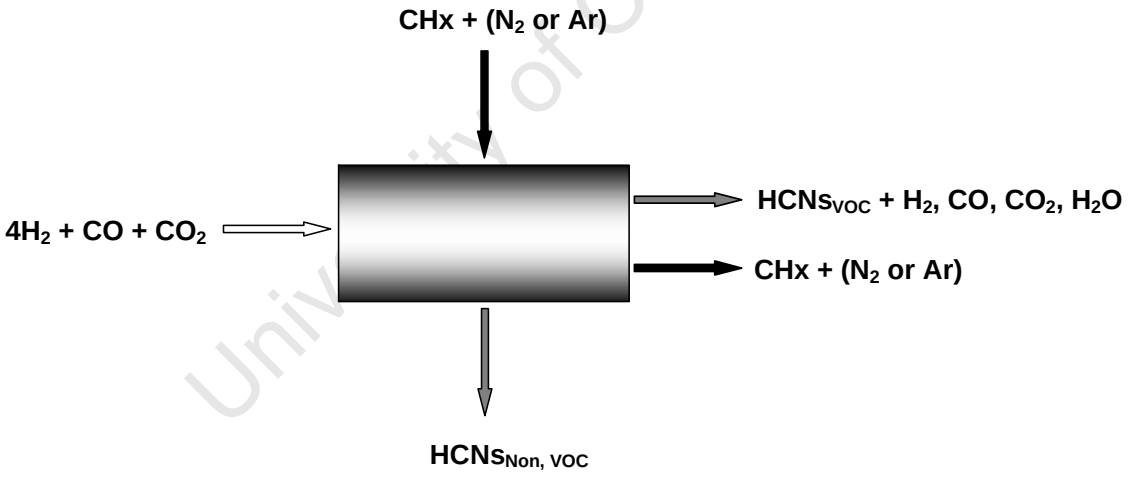

Figure 3.14 Ingoing and outgoing reactant, product and reference components required for mass balance around a Fischer-Tropsch reactor (VOC: Volatile organic compounds; HCNs: Hydrocarbons; CHx: Reference organic compound – cyclohexane or neo-hexane)

Before or during reaction bypass or feed samples of the reactants, H_2, CO and CO_2 are analysed. This then represents the quantity of reactants fed to the reactor. During Fischer-Tropsch synthesis, TCD and ampoule samples are taken and analysed. Each peak area for each species present is thus obtained and used to calculate the molar flow

rate of that particular species. The molar flow rates of the inorganic compounds or methane, n_i, obtained from TCD analysis are given by:

$$n_i = f_{TCD,i}\left(\frac{A_i}{A_{Ref\ gas}}\right) n_{Ref\ gas} \tag{3.9}$$

with

$$n_{Ref\ gas} = \frac{x_{Ref\ gas} \cdot V_{Ref}(NTP)}{V_A} \tag{3.10}$$

where $x_{Ref\ gas}$ is the molar concentration of nitrogen or argon in the reference gas; $V_{Ref}(NTP)$ is the volumetric gas flow rate of the reference gas and V_A is Avogadro's volume.

The molar flow rate of an organic compound, n_i, can be derived from results of FID analysis as follows:

$$n_i = \left(\frac{N_{CHx}}{N_i}\right) \cdot \left(\frac{f_i \cdot A_i}{f_{CHx} \cdot A_{CHx}}\right) n_{CHx} \tag{3.11}$$

with N_{CHx}, the carbon number of the reference compound (cyclohexane or neo-hexane), and n_{CHx} the molar flow rate of the reference compound (cyclohexane or neo-hexane), thus:

$$n_{CHx} = \frac{x_{CHx} \cdot V_{Ref}(NTP)}{V_A} \tag{3.12}$$

The molar flow rates of the individual products on a carbon basis can be expressed as:

$$(n_i)_c = N_{CHx}\left(\frac{f_i \cdot A_i}{f_{CHx} \cdot A_{CHx}}\right) n_{CHx} \tag{3.13}$$

Conversion of a reactant can be calculated as being:

$$X_i = 1 - \frac{(n_i)_{out}}{(n_i)_{in}} \tag{3.14}$$

The yield, $(Y_i)_c$ and selectivity, $(S_i)_c$ of a product on a carbon basis is:

$$(Y_i)_c = \frac{(n_i)_{out}}{(n_{CO})_{in} + (n_{CO_2})_{in}} \tag{3.15}$$

$$(S_i)_c = \frac{(n_i)_{out}}{(n_{CO})_{in} - (n_{CO})_{out} + (n_{CO_2})_{in} - (n_{CO_2})_{out}} \tag{3.16}$$

Alternatively, a selectivity/carbon content within the fraction of components which are found in ampoule samples, or which are volatile at reaction conditions respectively, can be defined as:

$$(S_i)_{\text{c-voc}} = \frac{(n_i)_{\text{c}}}{\sum(n_i)_{\text{c-voc}}} \tag{3.17}$$

This can be modified for carbon number specific selectivities. For instance the selectivity (or molar content) of linear olefins in linear hydrocarbon product for carbon number x, would be:

$$(S_{lin\ olefins})_{c_x} = \frac{(n_{lin\ olefins})_{c_x}}{\sum(n_{lin\ paraffin})_{c_x} + \sum(n_{lin\ olefins})_{c_x}} \tag{3.18}$$

The partial pressure of a reactant or a product at the reactor exit can be calculated as follows:

$$(p_i)_{\text{out}} = (x_i)_{\text{out}} \cdot P_{\text{total}} \tag{3.19}$$

with P_{total} the overall reaction pressure and $x_{i,\text{out}}$ the molar concentration of a component i at the reactor exit, where:

$$(x_i)_{\text{out}} = \frac{(n_i)_{\text{out}}}{(n_{H_2})_{\text{out}} + (n_{CO})_{\text{out}} + (n_{CO_2})_{\text{out}} + (n_{H_2O})_{\text{out}} + \sum(n_i)_{\text{voc}}} \tag{3.20}$$

The molar flow rate of exiting water can be derived from an oxygen balance as:

$$(n_{H_2O})_{\text{out}} = (n_{CO})_{\text{in}} + 2(n_{CO_2})_{\text{in}} - (n_{CO})_{\text{out}} - 2(n_{CO_2})_{\text{out}} - \sum(n_i)_{\text{ox-voc}} \tag{3.21}$$

with $(n_i)_{\text{ox-voc}}$ the molar flow of oxygen containing volatile products.

3.4.4 Data work-up – liquid phase

During Fischer-Tropsch synthesis oil and water are collected from the Berty reactor in the cold catch-pot. These are separated and analysed independently.

3.4.4.1 Oil phase

The molar flow rate of n-decene-(1) was decided upon as being the tie component between the oil and gas phase analysis. Thus the flow rate of an organic compound, n_i, can be derived from the results of FID analysis as follows:

$$n_i = \left(\frac{N_{C_{10}^=}}{N_i}\right) \cdot \left(\frac{f_i \cdot A_i}{f_{C_{10}^=} \cdot A_{C_{10}^=}}\right) n_{C_{10}^=} \tag{3.22}$$

With $n_{C_{10}^=}$ the molar flow rate of n-decene-(1) derived from the corresponding ampoule sample (see equation 3.11).

For MS analysis the flow rate of an organic compound, n_i, can be derived from the m/z specific chromatogram as follows:

$$n_i = A_{MS,i}\left(\frac{A_i}{A_{C_{10}^=}}\right)^2 + B_{MS,i}\left(\frac{A_i}{A_{C_{10}^=}}\right) n_{C_{10}^=} \tag{3.23}$$

With $n_{C_{10}^=}$ the molar flow rate of n-decene-(1) derived from the corresponding ampoule sample (see equation 3.11) and $A_{MS,i}$ and $B_{MS,i}$ are the relative calibration factors normalised for n-decene-(1) (m/z = 55).

Yields, selectivities and other results are calculated in the same way as for the gas phase.

3.4.4.2 Water phase

The molar concentrations of the components in the water phase were calculated by making up a solution of known quantities of the identified soluble organic products. From this solution the response factor of each particular compound was determined in relation to the 1,4-dioxane peak that was used as an internal standard.

$$f_i = \left(\frac{A_{1.4\text{-Dioxane}}}{A_i}\right) \cdot \left(\frac{n_i}{n_{1.4\text{-Dioxane}}}\right) \tag{3.24}$$

As the volume of 1,4-dioxane added to the solution is known, the moles of the soluble organic products in the sample vial and thus the collected water sample can be determined.

$$n_i = n_{1.4\text{-Dioxane}} \cdot f_i \cdot \left(\frac{A_i}{A_{1.4\text{-Dioxane}}} \right) \tag{3.25}$$

3.5 Thermodynamics of oxygenate reactions

As the Fischer-Tropsch synthesis is a very complex system, understanding of the interaction of products is best understood using thermodynamics. Thermodynamic calculations were conducted using data from Daubert *et al.* (1999). The results of these calculations enable one to determine which reactions are thermodynamically feasible in the reaction regime and also enable one to predict possible reaction pathways depending on which side of the thermodynamic equilibrium the product concentrations fall. These results however, in no way lead to the determination of the kinetic feasibility of these reactions. The data used for the major components described in this work are listed in Table 3.14; additional thermodynamic data can be found in Appendix F.

Table 3.14 Thermodynamic properties adapted from (*Daubert*, *1999*)

Compound	$\Delta H^F_{25\,°C}$	$\Delta G^F_{25\,°C}$	a	b	c	d
Ethanol	-234.4	-167.9	17.5	0.132	-0.22×10^{-4}	-1.59×10^{-8}
Acetaldehyde	-166.2	-128.9	19.9	0.209	-1.04×10^{-4}	2.00×10^{-8}
1-Butanol	-274.6	-150.3	-17.3	0.520	-3.69×10^{-4}	11.3×10^{-8}
Butanal	-207.0	-116.3	20.6	0.297	-0.79×10^{-4}	-1.33×10^{-8}
Butan-2-one	-238.4	-146.1	22.2	0.313	-1.47×10^{-4}	2.64×10^{-8}
Butanoic acid	-475.8	-360.0	13.8	0.405	-2.22×10^{-4}	3.80×10^{-8}
1-Octanol	-355.5	-115.5	-42.6	1.006	-7.34×10^{-4}	21.9×10^{-8}
Octanal	-290.2	-83.8	-7.3	0.789	-4.42×10^{-4}	8.72×10^{-8}
Octan-2-one	-321.6	-113.8	6.5	0.737	-3.95×10^{-4}	6.63×10^{-8}
Octanoic acid	-556.0	-325.0	-0.5	0.847	-5.55×10^{-4}	1.52E-07
Nonan-2-one	-340.7	-104.1	3.6	0.836	-4.43×10^{-4}	6.75×10^{-8}

The process used to calculate the equilibrium constant for a certain chemical reaction is as follows:

The heat of reaction for the reaction:

$$\Delta H^R_{25\,°C} = \Sigma\Delta H^F_{25\,°C}\,(\text{Products}) - \Sigma\Delta H^F_{25\,°C}\,(\text{Reactants}) \tag{3.26}$$

The Gibbs free energy for the reaction:

$$\Delta G^R_{25\,°C} = \Sigma\Delta G^F_{25\,°C}\,(\text{Products}) - \Sigma\Delta G^F_{25\,°C}\,(\text{Reactants}) \tag{3.27}$$

C_p constants for the reaction:

$$\Delta a^R_{25\,°C} = \Sigma a_{25\,°C}\,(\text{Products}) - \Sigma a_{25\,°C}\,(\text{Reactants}) \tag{3.28}$$

From this data the Gibbs free energy of reaction at the reaction temperature of 300 °C can be calculated:

$$\Delta G^R_{300\,°C} = 573.15\left(\left(\frac{\Delta G^R_{25\,°C}}{298.15}\right)1000 + \frac{W+V+X+Y+Z}{1000}\right) \tag{3.29}$$

Where:

$$V = 1000 \times U \times \left(\frac{1}{573.15} - \frac{1}{298.15}\right) \tag{3.30}$$

$$U = \Delta H^R_{25\,°C} - \left(\Delta a^R_{25\,°C} \times 298.15 + \frac{\Delta b^R_{25\,°C}}{2} \times 298.15^2 + \frac{\Delta c^R_{25\,°C}}{3} \times 298.15^3 + \frac{\Delta d^R_{25\,°C}}{4} \times 298.15^4\right) \tag{3.31}$$

$$W = \Delta a^{R}_{25\,^{\circ}C} \times \ln\left(\frac{573.15}{298.15}\right) \tag{3.32}$$

$$X = \frac{\Delta b^{R}_{25\,^{\circ}C}}{2} \times 573.15 \times 298.15 \tag{3.33}$$

$$Y = \frac{\Delta c^{R}_{25\,^{\circ}C}}{6} \times 573.15^{2} \times 298.15^{2} \tag{3.34}$$

and

$$Z = \frac{\Delta d^{R}_{25\,^{\circ}C}}{12} \times 573.15^{3} \times 298.15^{3} \tag{3.35}$$

From the Gibbs free energy of reaction the equilibrium constant can be found as follows:

$$K_a = \exp\left(\frac{\Delta G^{R}_{300\,^{\circ}C} \times 1000}{R \times 573.15}\right) \tag{3.36}$$

Where R is the ideal gas constant in this case equal to 8.314 J/(mol.K).

Calculated equilibrium constants and Gibbs free energies of reaction for reactions of possible interest at 300 °C are listed in Table 3.15. It can be seen that the reactions of interest considered here are all thermodynamically feasible.

Table 3.15 Equilibrium constant and Gibbs free energies of reaction at 300 °C for reactions of interest

Reaction	K_a	$\Delta G^{R}_{300\,^{\circ}C}$ (kJ/mol)
Acetaldehyde + H_2 ⇔ Ethanol	10.84	-11.36
1-Butanol ⇔ Butan-2-one + H_2	284	-26.92
Butanal ⇔ Butan-2-one	381	-28.32
Butanal + H_2 ⇔ 1-Butanol	1.34	-1.40
Octanoic acid + H_2 ⇔ Octan-2-one + H_2O	207.64	-25.43
1-Octanol ⇔ Octan-2-one + H_2	489.38	-29.51
Octanal ⇔ Octan-2-one	414.78	-28.72
1-Octanol + H_2O ⇔ Octanoic acid +2H_2	2.36	-4.09
Octanal + H_2O ⇔ Octanoic acid + H_2	2.00	-3.30
Octanal + H_2 ⇔ 1-Octanol	0.85	0.79

Using the equilibrium constant the equilibrium ratio of reactants to products can be found. For the following reaction:

$$aA + bB \Leftrightarrow cC + dD \tag{3.37}$$

The equilibrium constant can be found from the partial pressures of the reactants and products:

$$K_a = \frac{p[C]^c \bullet p[D]^d}{p[A]^a \bullet p[B]^b} \tag{3.38}$$

From this the equilibrium ratio of a product and reactant can be found by:

$$\frac{p[B]^b}{p[D]^d} = K_a \left(\frac{p[A]^a}{p[C]^c}\right) \tag{3.39}$$

The expected equilibrium ratio can then be compared to the actual product ratio giving information as to the interaction of the Fischer-Tropsch products.

Chapter 4

Results and discussion

4.1 Characterisation of calcined iron-copper catalysts

Calcined, potassium impregnated catalysts were characterised using different characterisation techniques. These techniques were used to confirm the elemental composition and phases present in the co-precipitated catalysts. In certain cases un-promoted catalysts were compared to promoted catalysts in order to determine the effect of potassium on the catalysts.

4.1.1 Atomic absorption spectroscopy, AAS

Theoretical and actual iron, copper and potassium loadings for each calcined catalyst as determined by AAS are shown in Table 4.1. While in most cases the copper to iron ratios were close to that expected, the 50 wt% Cu catalyst shows a large loss of copper. This is probably due to the formation of the water-soluble copper tetra-amine complex $[Cu(NH_3)_4^{2+}]$ during precipitation which, as they are soluble in water, are then washed out in the washing step. The other noteworthy aspect is that the potassium loading on all catalysts was lower than that expected. While this could be attributed partially to an error in the detection of potassium, it appears that the desired potassium loading (of 100 g Fe : 5 g K) was not reached using this impregnation method. The reason for this loss of potassium could be due to the formation of a white potassium salt precipitate on the side of the vessel. However the relative comparable potassium loading is still good and it was decided that this was acceptable.

Table 4.1 Theoretical and actual iron, copper and potassium loadings and mass ratios as determined by AAS for the calcined catalyst series

Catalyst (Cu wt%)[a]	Fe : Cu : K Theory	Fe : Cu : K AAS
0	100 : 0 : 5	100 : 0 : 1.7
2	100 : 2 : 5.1	100 : 3.6 : 1.9
9	100 : 10 : 5.5	100 : 9.8 : 2.1
23	100 : 30 : 6.5	100 : 30 : 2.6
50	100 : 100 : 10	100 : 74 : 4.4
77	30 : 100 : 6.5	31 : 100 : 2.6
100	0 : 100 : 5	0 : 100 : 3.5

[a] Basis: Fully reduced catalyst

4.1.2 Scanning electron microscopy and energy dispersive X-ray analysis, SEM-EDX

Theoretical and actual iron, copper and potassium loadings for each calcined catalyst as determined by SEM-EDX are shown in Table 4.2. The results agree well with the above AAS results.

Table 4.2 Theoretical and actual iron, copper and potassium loadings and mass ratios as determined by SEM-EDX for the calcined catalyst series

Catalyst (Cu wt%)[a]	Fe : Cu : K Theory	Fe : Cu : K SEM-EDX
0	100 : 0 : 5	100 : 0 : 1.2
2	100 : 2 : 5.1	100 : 5.1 : 2.4
9	100 : 10 : 5.5	100 : 10 : 2.8
23	100 : 30 : 6.5	100 : 32 : 2.6
50	100 : 100 : 10	100 : 85 : 5.8
77	30 : 100 : 6.5	25 : 100 : 2.6
100	0 : 100 : 5	0 : 100 : 2.0

[a] Basis: Fully reduced catalyst

4.1.3 X-ray diffraction spectroscopy, XRD

The results of X-ray diffraction spectroscopy (XRD) on the calcined potassium promoted samples are shown in Figure 4.1 with varying intensity scales (see Appendix G for diffractograms of same scale). For the first catalyst in the series (0 wt% Cu) it can clearly be seen that the iron is present as hematite (α-Fe_2O_3). With the addition of copper these hematite peaks start to broaden. At 9 wt% Cu the hematite peaks not only seem to broaden but could be on top of another broadening peak. This peak broadening could be due either to small crystallites of hematite or small crystallites of another compound such as ferrihydrite (FeO(OH)), as the crystallite size of ferrihydrite is extremely small. However it does appear as if the broad peaks are inline with the response of hematite as opposed to ferrihydrite. Due to the peak broadening, crystallite sizes of iron phases become difficult to determine for catalysts with copper loadings larger than 9 wt%.

As the copper loading increases on the catalysts, the copper oxide (CuO) peak becomes discernable. In the samples of 50 wt% Cu catalyst and higher the peaks are readily discernable and their size can be calculated.

Individual peaks that were discernable were used to calculate the specific crystallite sizes using the Scherrer equation: these are detailed in Table 4.3. It can be seen that as the catalysts move towards the amorphous phases the crystallites become smaller.

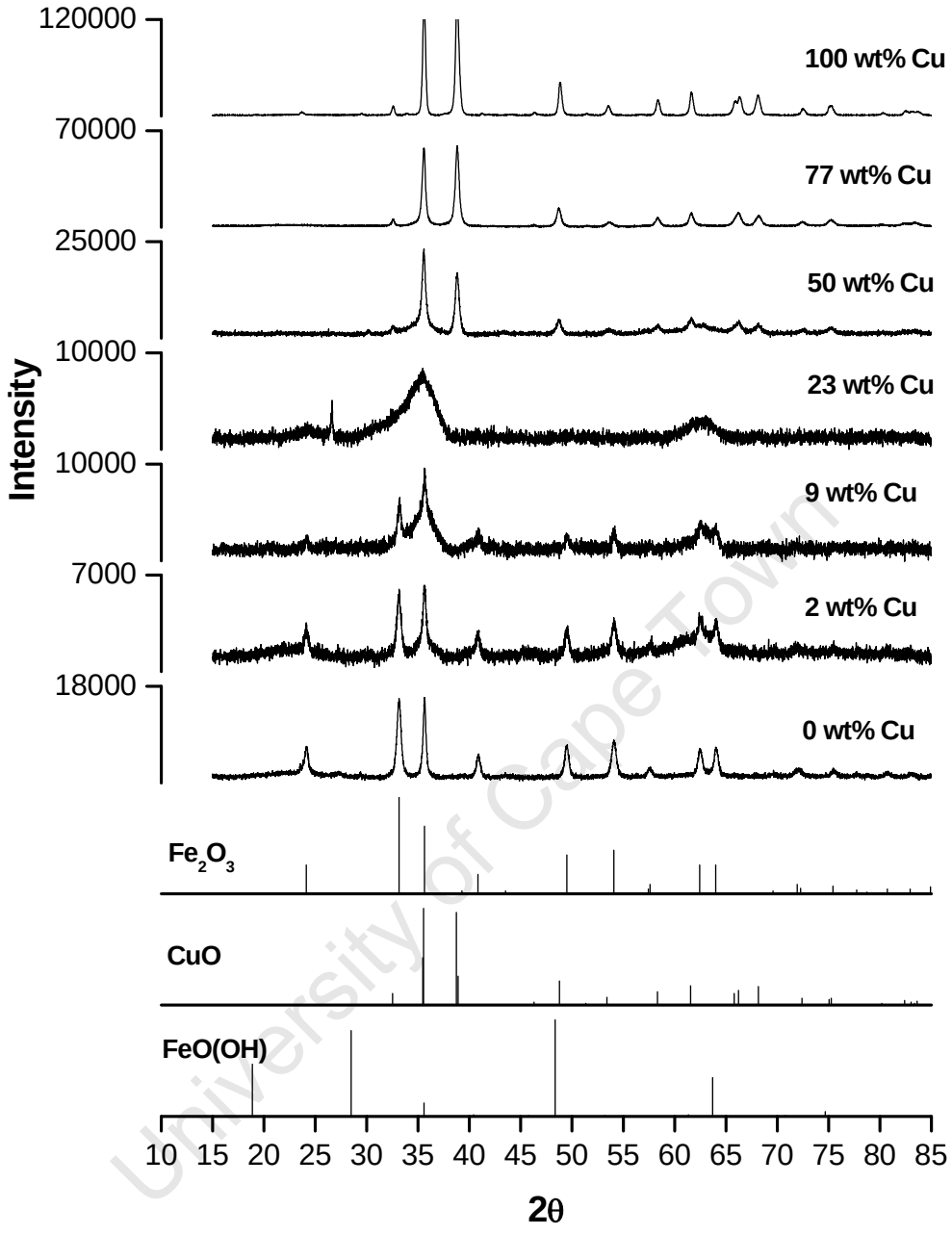

Figure 4.1 XRD diffractograms of calcined catalyst series

Table 4.3 Summary of phases identified using XRD as well as calculated crystallite sizes for the calcined catalysts from XRD analysis using the Scherrer equation

Catalyst (Cu wt%)[a]	Summary of phases identified using XRD		Calcined d Fe_2O_3 (nm)	Calcined d CuO (nm)
0	α- Fe_2O_3		24	-
2	α- Fe_2O_3		11	n/a[b]
9	α- Fe_2O_3	CuO	9	3
23		CuO	n/a[b]	3
50	α- Fe_2O_3	CuO	n/a[b]	17
77		CuO	n/a[b]	20
100		CuO	-	26

[a] Basis: Fully reduced catalyst

[b] n/a - Peak not detectable/integratable due to amorphous nature of sample

4.1.4 Mössbauer Spectroscopy, MAS

The spectra of room temperature MAS results from the calcined catalyst series are shown in Figure 4.2 while the corresponding hyperfine parameters are summarised in Table 4.4.

The MAS spectrum of the catalyst sample with 0 wt% Cu was fitted with a sextet (6 line) and quadrupole doublet (2 line). The parameters of the sextet, $\delta = 0.37$ mm/s, $\Delta = -0.21$ mm/s and $B_{hf} = 50.8$ T, are consistent with those of hematite (α- Fe_2O_3) and contributes to about 76% of the total iron bearing phases. This result is in agreement with those seen on the XRD studies discussed in section 4.1.3 above. However, about 24% of the iron bearing phase was superparamagnetic Fe(III) as manifested by the quadrupole doublet (with parameters ($\delta = 0.33$ mm/s and $\Delta = -0.21$ mm/s).

Most often during MAS analysis quadrupole doublets with parameters consistent with Fe^{3+} are encountered and are fitted with broad lines. The broadening of the lines can be due to a superposition of several components, indicative of the distribution of crystallite size or due to the presence of small crystallites which exhibit superparamagnetic (spm) behaviour at room temperature. The collapse of the magnetically split component (sextet) into paramagnetic doublets or singlets at temperatures below the Curie temperature (magnetic ordering temperature) of the bulk material is termed superparamagnetism. This is caused by the fast relaxation of the magnetic vector due to

thermal excitation at room temperature as a result of the presence of small crystallites. The exact nature of these crystallites, however, is unknown (they could be small hematite or ferrihydride crystallites) and can only be determined by cryogenic MAS analysis.

For the 2 wt% Cu catalyst the parameters match those of hematite and a quadrupole doublet with parameters consistent with those of an Fe^{3+} species. Once again the nature of this Fe^{3+} species is unclear and is the reason for the amorphous nature in the copper promoted iron catalyst XRD diffractograms. This trend, of an increasing Fe^{3+} species with copper loading, is seen and once again agrees well with the results seen from XRD analysis where an amorphous iron phase is seen.

Note that the catalyst sample containing 100 wt% Cu could not be analysed using MAS due to the absence of iron, which is essential for this technique.

Table 4.4 Hyperfine splitting parameters of the calcined catalysts series

Catalyst (Cu wt%)[a]	δ^b mm/s	Δ^b mm/s	$B_{hf}{}^c$ T	Identified Iron phase	% Relative Area	Phases identified by XRD
0	0.37	-0.21	50.8	α- Fe_2O_3	76	α- Fe_2O_3
	0.33	0.70	-	spm[d] Fe^{3+}	24	
2	0.37	-0.18	50.1	α- Fe_2O_3	10	α- Fe_2O_3
	0.33	0.70	-	spm Fe^{3+}	90	
9	0.37	-0.18	50.3	α- Fe_2O_3	3	α- Fe_2O_3
	0.34	0.71	-	spm Fe^{3+}	97	CuO
23	0.34	0.76	-	spm Fe^{3+}	100	CuO
50	0.34	0.77	-	spm Fe^{3+}	100	CuO α- Fe_2O_3
77	0.33	0.74	-	spm Fe^{3+}	100	CuO
100	-	-	-	-	-	CuO

[a] Basis: Fully reduced catalyst

[b] Error: ± 0.02 mm/s

[c] Error: ± 0.5 T

[d] spm: Superparamagnetic

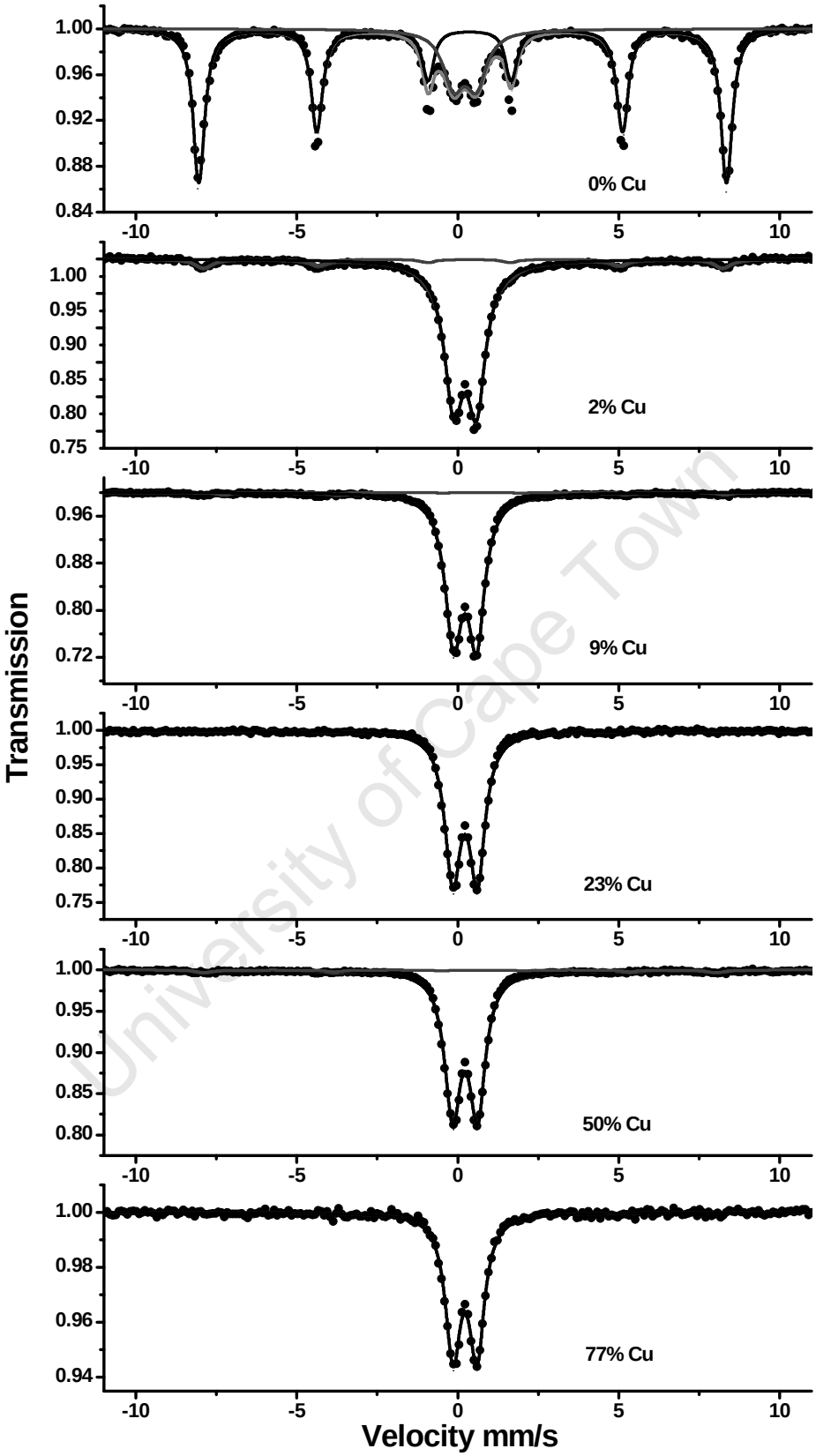

Figure 4.2 MAS spectra of calcined catalyst series

4.1.5 Brunauer-Emmett-Teller method, BET

Table 4.5 shows the BET surface areas of the calcined catalysts. The BET surface areas per gram of total catalyst mass show a sharp increase with the introduction of copper for the calcined samples; this agrees well with the XRD and MAS results, and the decrease in the iron crystallite size with the introduction of copper. At 77 wt% Cu the surface area suddenly decreases; this is probably due to an increase in the amount of large copper crystallites that have low surface areas.

Table 4.5 Calculated BET surface areas for the calcined catalysts

Catalyst (Cu wt%)[a]	Area (m^2/g_{cat})
0	53
2	114
9	95
23	107
50	106
77	52
100	2.6

[a] Basis: Fully reduced catalyst

4.1.6 Temperature programmed reduction, TPR

The study of the reduction behaviour of the different catalysts was done by means of temperature programmed reduction in a 5% hydrogen in argon-stream. The recorded hydrogen consumption for the seven catalysts is shown in Figure 4.3. In all cases 0.0379 g of potassium promoted catalyst was loaded.

Examination of the 0 wt% Cu catalyst shows a typical two peak reduction for iron where the first peak corresponds to the reduction of hematite (Fe_2O_3) to magnetite (Fe_3O_4) and the second, magnetite to metallic iron (Fe) (*Bukur et al.*, *1995* and *Jin and Datye*, *2000*).

The next catalyst in the series (2 wt% Cu) shows a large shift of the reduction peaks to lower temperatures (of about 100 °C) and better definition of the first reduction peak

than in the previous sample. The second peak also starts and ends at lower temperatures. In this case the initial peak corresponds both to the reduction of hematite to magnetite and that of the small amount of copper oxide (CuO) to the copper metal (Cu). The addition of copper to decrease the reduction temperature of iron is well known (*Storch et al., 1951, Dry, 1981,* and *Anderson 1984*) and this result serves as confirmation that the iron-copper system behaves as expected. The promotional effect of copper on the reduction of the iron oxides has been attributed to the reduced copper being able to dissociate hydrogen (H_2) and thus provide a source of atomic hydrogen (H) to assist in the reduction of the iron (*Jin and Datye*, *2000*). The shift of the first and second reduction peaks to lower temperatures holds for the rest of the catalyst series.

On the 100 wt% Cu catalyst there seems to be a two step reduction mechanism with the main reduction peak starting at a higher temperature than that of the iron-copper mixtures. This result is unexpected, as copper oxide is expected to begin reducing at a similar temperature to the first peak in the copper-iron catalysts. Comparison of the temperature programmed reduction responses on non-potassium promoted catalysts with the promoted catalysts (as shown in Figure 4.4) suggests that this is probably due to the addition of potassium. It is generally accepted that the adsorption of alkali additives to catalyst surfaces results in electron transfer from the alkali to the catalyst (metal) surface. It is thought that this would increase the electron density of the metal bulk and could strengthen the copper-oxygen bond, making the copper harder to reduce. This interaction is also (if only slightly) discernable on the pure iron catalyst.

From these results a reduction temperature of 400 °C was chosen. This temperature fits well into the reduction curves of all the catalysts and should ensure that full reduction would be seen over a sufficient time period. It should be noted that the reduction temperature does not need to be higher than the last reduction peak as this method uses a ramping temperature in order to show the stepwise phase changes of the catalysts. The higher temperature only increases the rate of the reduction but reduction should occur at any temperature in which phase changes are seen in the catalyst.

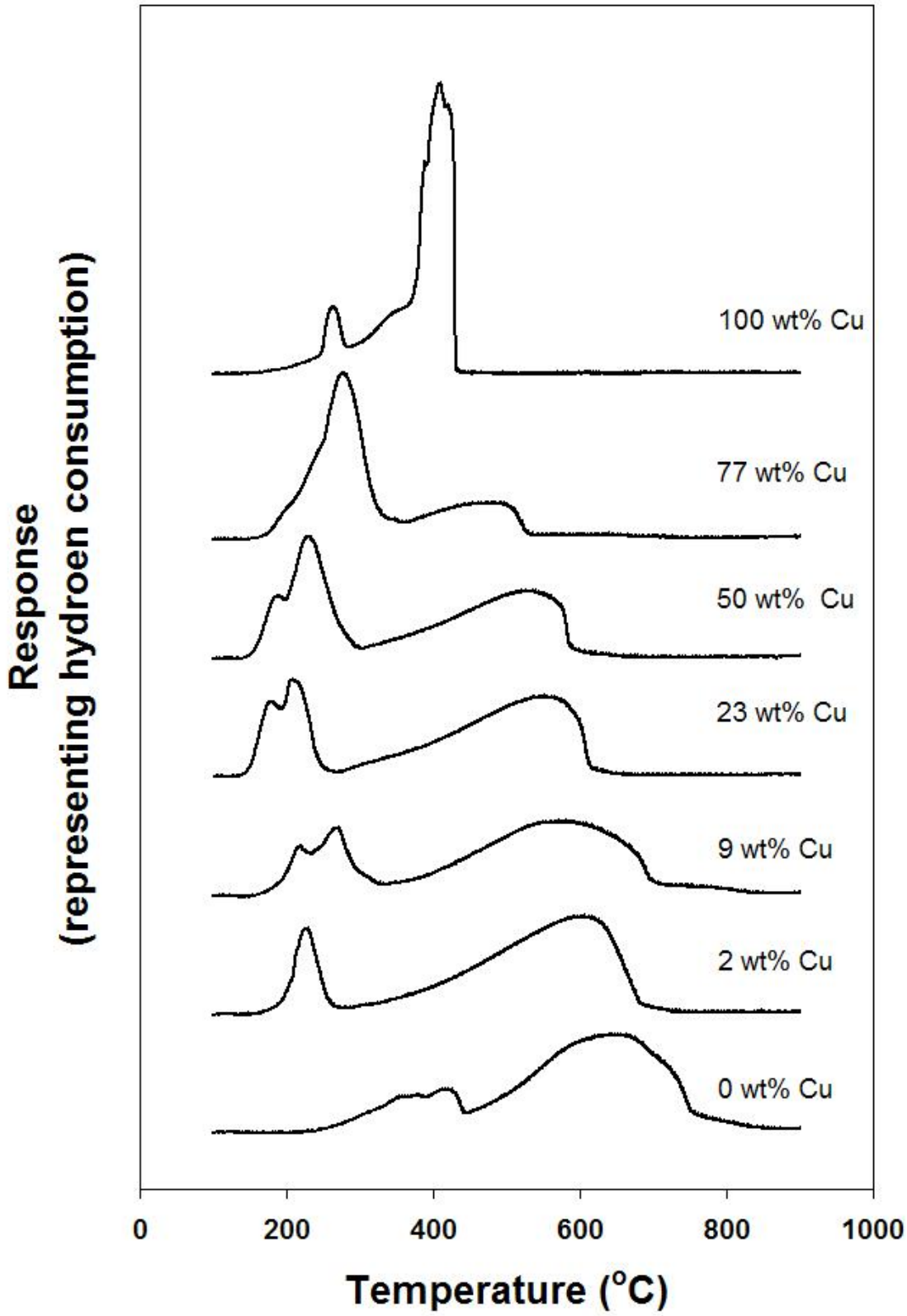

Figure 4.3 H_2-TPR profiles of calcined and potassium promoted catalyst series

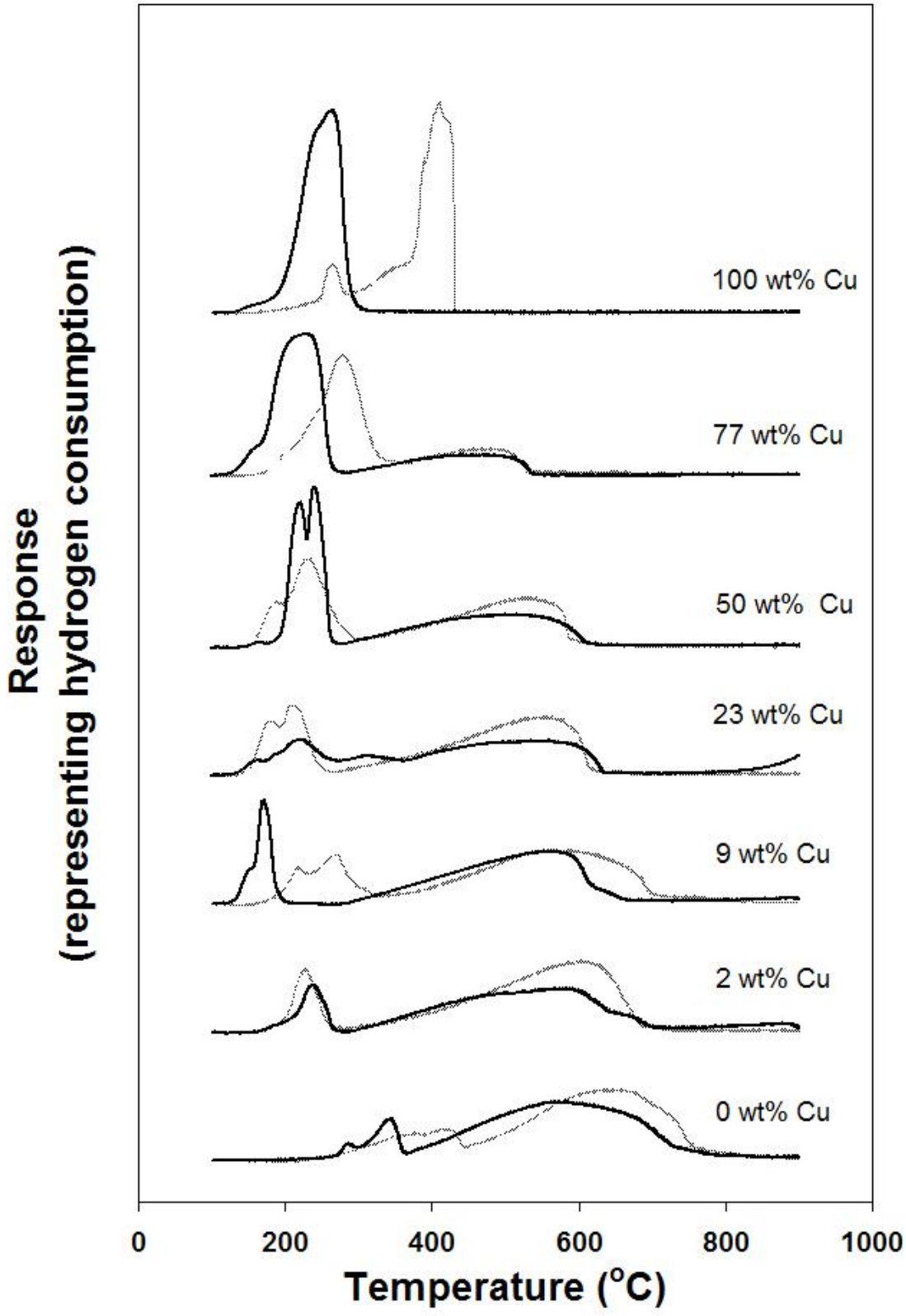

Figure 4.4 H_2-TPR profiles of calcined and potassium free catalyst series (black) compared to calcined and potassium promoted catalysts (grey)

4.1.7 Transmission electron microscopy, TEM

The TEM micrographs of the calcined potassium promoted catalysts are shown in Figure 4.5. The reduction in the size of the iron crystallites with the addition of copper is clear when comparing the 0 and 2 wt% Cu catalysts, as due to the small amount of copper present it can be assumed that the majority of the crystallites seen are iron. With this in mind it appears that copper only seems to become apparent in the 50 wt% Cu sample, and then as large crystallites in comparison to the iron. Attempts were made to obtain a crystallite size profile from the TEM imaging but difficulties in isolating "good" images and establishing the exact nature of the particles, using energy filtering for element identification, proved to be impossible with the equipment available.

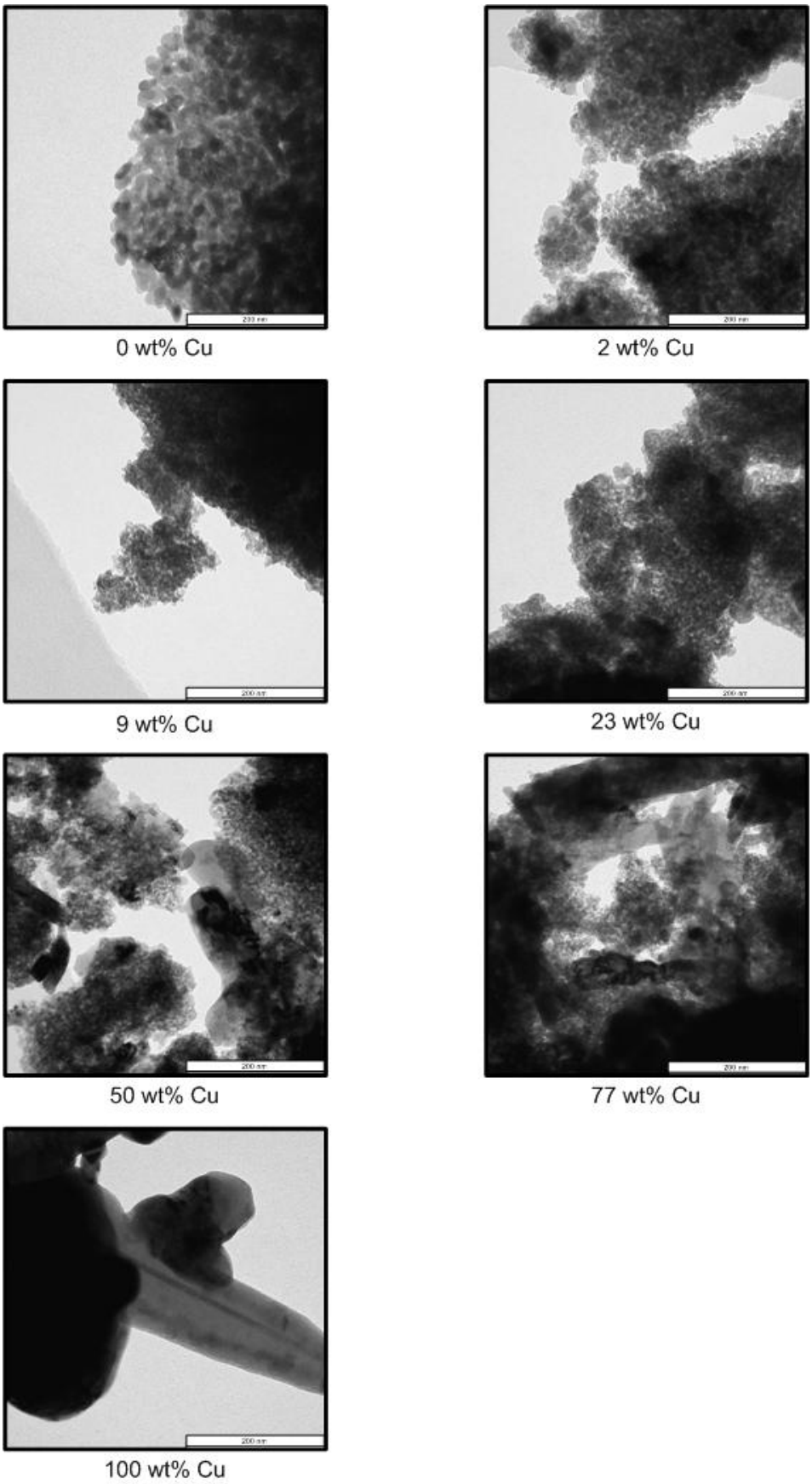

Figure 4.5 TEM micrographs of the calcined catalyst series (scale shown = 200 nm)

4.1.8 Summary of results on calcined catalysts

Iron catalysts with varying copper loadings were successfully prepared via the co-precipitation of their nitrates. After calcination in air at 400 °C, a trend of small iron crystallites (possibly hematite but this could not be fully confirmed) was seen with the addition of copper. The exact reason for the formation of the smaller iron crystallites is not known, but it is postulated that this is through a seeding effect, where the addition of copper leads to a faster (or earlier) precipitation of the iron and so larger clusters of the metal are not formed. It can be assumed that the relatively large crystallites of copper are formed via the sintering of smaller crystallites during calcination.

Additionally the addition of copper to the catalysts reduced the initial reduction temperature of the iron by 100 °C. However the assumption of the loaded potassium spreading evenly across both metal surfaces does not seem to be correct as evidenced in the TPR of the pure copper sample. It appears that all the potassium loaded onto the iron-copper catalysts had a higher affinity for the iron rather than the copper.

4.2 Characterisation of reduced iron-copper catalysts

Catalysts were reduced under typical Fischer-Tropsch synthesis pre-treatment conditions, i.e. heating under hydrogen at a rate of 1 ºC/min to 100 ºC, holding for 1 hour, then 1 ºC/min to 400 ºC and holding for 16 hours, at ambient pressure and a space velocity of 4000 ml(NTP)/g_{Fe}/h. For all characterisation methods except TPR the reduced catalysts were then cooled under argon and passivated with carbon dioxide for 30 minutes at room temperature as described by Baker and Rodriguez (1994).

4.2.1 Atomic absorption spectroscopy, AAS

Theoretical and actual iron, copper and potassium loadings for each reduced and passivated catalyst as determined by means of AAS are shown in Table 4.6. Comparison of this result to the calcined samples (Table 4.1) shows no change in the iron to copper ratios for the catalyst series with reduction. The exception is however the

2 wt% Cu catalyst, where it appears the copper loading has increased. This is probably due to an error in the analysis in detecting the extremely low copper loading. Comparison to the potassium loading seems to give credit to this theory as the potassium loading is also variable in comparison to the calcined samples.

Table 4.6 Theoretical and actual iron, copper and potassium loadings and mass ratios as determined by AAS for the reduced and passivated catalyst series

Catalyst (Cu wt%)[a]	Fe:Cu:K Theory	Fe:Cu:K AAS
0	100 : 0 : 5	100 : 0 : 1.7
2	100 : 2 : 5.1	100 : 5.7 : 3.0
9	100 : 10 : 5.5	100 : 9.1 : 3.6
23	100 : 30 : 6.5	100 : 30 : 3.5
50	100 : 100 : 10	100 : 74 : 4.5
77	30 : 100 : 6.5	31 : 100 : 2.3
100	0 : 100 : 5	0 : 100 : 1.3

[a] Basis: Fully reduced catalyst

4.2.2 Scanning electron microscopy and energy dispersive X-ray analysis, SEM-EDX

Theoretical and actual iron, copper and potassium loadings for each reduced and passivated catalyst as determined by SEM-EDX and are shown in Table 4.7. Comparison to the calcined catalysts in Table 4.2, as with AAS shows good agreement in the catalyst compositions with reduction, except for the 2 wt% Cu catalyst and in some cases the potassium loading. It is thought that the same problem could be seen here, where the low loadings on the catalyst lead to some analytical error. However, for the most part, as expected, reduction can be seen not to change the composition of the catalysts.

Table 4.7 Theoretical and actual iron, copper and potassium loadings and mass ratios as determined by SEM-EDX for the reduced and passivated catalyst series

Catalyst (Cu wt%)[a]	Fe : Cu : K Theory	Fe : Cu : K SEM-EDX
0	100 : 0 : 5	100 : 0 : 1.0
2	100 : 2 : 5.1	100 : 3.8 : 2.0
9	100 : 10 : 5.5	100 : 12 : 1.1
23	100 : 30 : 6.5	100 : 31 : 2.0
50	100 : 100 : 10	100 : 87 : 3.4
77	30 : 100 : 6.5	35 : 100 : 0.5
100	0 : 100 : 5	0 : 100 : 1.0

[a] Basis: Fully reduced catalyst

4.2.3 X-ray diffraction spectroscopy, XRD

After reduction of the catalysts the metallic iron and copper phases can be clearly seen, Figure 4.6. It does appear, however, that there is some existence of copper oxide (CuO) in the high copper containing samples. This is probably not due to incomplete reduction (as the copper is thought to reduce before or with the hematite (section 4.1.7)), but could be due to the oxidising of the copper in the samples once they have been in contact with air or carbon dioxide.

Interestingly, the sizes of the iron crystallites in the reduced catalysts are very similar, while those of the copper crystallites increase with copper loading (Table 4.8). As the Hüttig temperature of copper is around 325 ºC while that of iron is 460 ºC, which is above the reduction temperature of 400 ºC, the agglomeration of copper is to be expected and crystal growth is not surprising. However, the growth to a constant crystallite size of iron suggests that the surface energy of the resulting crystallites is close to that of a bulk phase, so that further sintering is very slow, and small particles that are touching will agglomerate to this crystallite size.

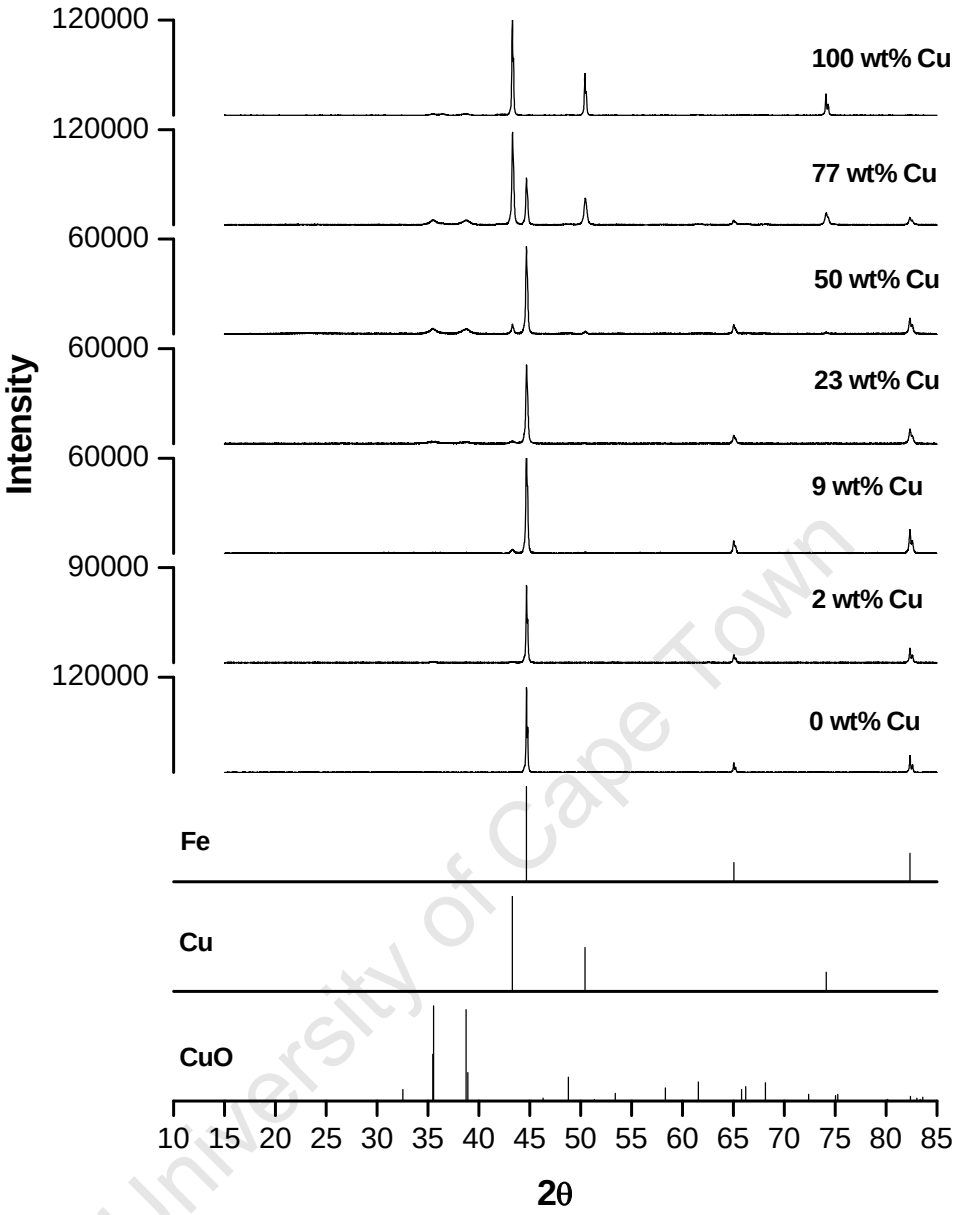

Figure 4.6 XRD spectra of reduced and passivated catalyst series

Table 4.8 Calculated crystallite sizes for reduced and passivated catalysts from XRD analysis

Catalyst (Cu wt%)[a]	Summary of phases identified using XRD		Reduced d Fe (nm)	Reduced d Cu (nm)
0	α-Fe		32	-
2	α-Fe	Cu	35	n/a[b]
9	α-Fe	Cu	35	25
23	α-Fe	Cu	30	25
50	α-Fe	Cu	33	30
77	α-Fe	Cu	35	34
100		Cu	-	45

[a] Basis: Fully reduced catalyst

[b] n/a - Peak too small to be detectable

The surface areas of the metals were calculated using the crystallite size determined from XRD and an assumption that the reduced metal particles are spherical in shape, these areas are detailed in Table 4.9. While the surface areas of iron per gram of iron (based on AAS results) are constant, those of copper increase with copper loading, which might facilitate interaction of the copper and the iron surfaces. The surface area of the copper crystallites per gram copper decreases with an increase of the copper loading on the catalysts. This is expected due to the increase in the copper crystallite size.

Table 4.9 Calculated surface areas for reduced catalysts from XRD analysis

Catalyst (Cu wt%)[a]	Fe Area Reduced (m^2/gFe)	Cu Area Reduced (m^2/gFe)	Cu Area Reduced (m^2/gCu)
0	24	-	-
2	22	n/a[b]	n/a[b]
9	22	2.7	27
23	25	8.1	27
50	23	22	22
77	22	66	20
100	-	-	15

[a] Basis: Fully reduced catalyst

[b] n/a - Peak too small to be detectable

4.2.4 Mössbauer Spectroscopy, MAS

Figure 4.7 shows the MAS spectra of the reduced catalyst series while the hyperfine splitting parameters are summarised in Table 4.10. The MAS spectrum fitted to the 0 wt% Cu sample is ascribed to metallic iron (94% overall iron-bearing composition) and superparamagnetic metallic iron (α-Fe) constituting about 6 area% of the total iron content. The presence of superparamagnetic α-Fe suggests there is a small amount of metallic iron still in the form of small crystallites, not identified in XRD.

The rest of the catalyst series shows the presence of magnetite (Fe_3O_4) along with metallic iron. This oxide phase is most likely due to the passivation of the catalyst with CO_2 where possible oxidation of some of the bulk phase has occurred, and not due to poor reduction of the catalyst (see section 4.2.5). The results also suggest the possible existence of superparamagnetic α-Fe in the 77 wt% Cu sample. This too could be due to small iron crystallites. However the small relative volume of this phase identified in the 0 and 77 wt% Cu catalysts suggest that these small crystallites in their small volumes could be present below the detection limits of the MAS in the other catalysts. Once again the catalyst sample containing 100 wt% Cu could not be analysed using MAS due to the absence of iron, which is essential for this technique.

Table 4.10 Hyperfine splitting parameters of the reduced and passivated catalyst series

Catalyst (Cu wt%)[a]	δ^b mm/s	Δ^b mm/s	B_{hf}^c T	Identified Iron phase	% Relative Area	Phases identified by XRD
0	0.00	0.00	33.1	α- Fe	94	α- Fe
	0.00	0	-	spm[d] α-Fe	6	
2	0.29	0.02	48.4	Fe_3O_4	8	α- Fe
	0.64	-0.03	45.3			Fe_3O_4
	0.00	0.00	33.1	α-Fe	92	
9	0.28	-0.03	48.4	Fe_3O_4	3	α- Fe
	0.65	0.00	45.3			Fe_3O_4
	0.00	0.00	33.1	α-Fe	97	
23	0.28	-0.20	49.0	Fe_3O_4	9	α- Fe
	0.64	0.09	45.5			Fe_3O_4
	0.00	0.00	33.1	α-Fe	91	Cu
						CuO
50	0.28	-0.03	48.9	Fe_3O_4	9	α- Fe
	0.65	0.06	45.4			Fe_3O_4
	0.00	0.00	33.1	α-Fe	90	Cu
						CuO
77	0.28	-0.02	49.0	Fe_3O_4	6	α- Fe
	0.65	0.11	45.5			Cu
	0.00	0.00	33.1	α- Fe	91	CuO
	0.00	0	-	spm[d] α-Fe	3	
100	-	-	-	-	-	Cu
						CuO

[a] Basis: Fully reduced catalyst

[b] Error: ± 0.02 mm/s

[c] Error: ± 0.5 T

[d] spm: Superparamagnetic

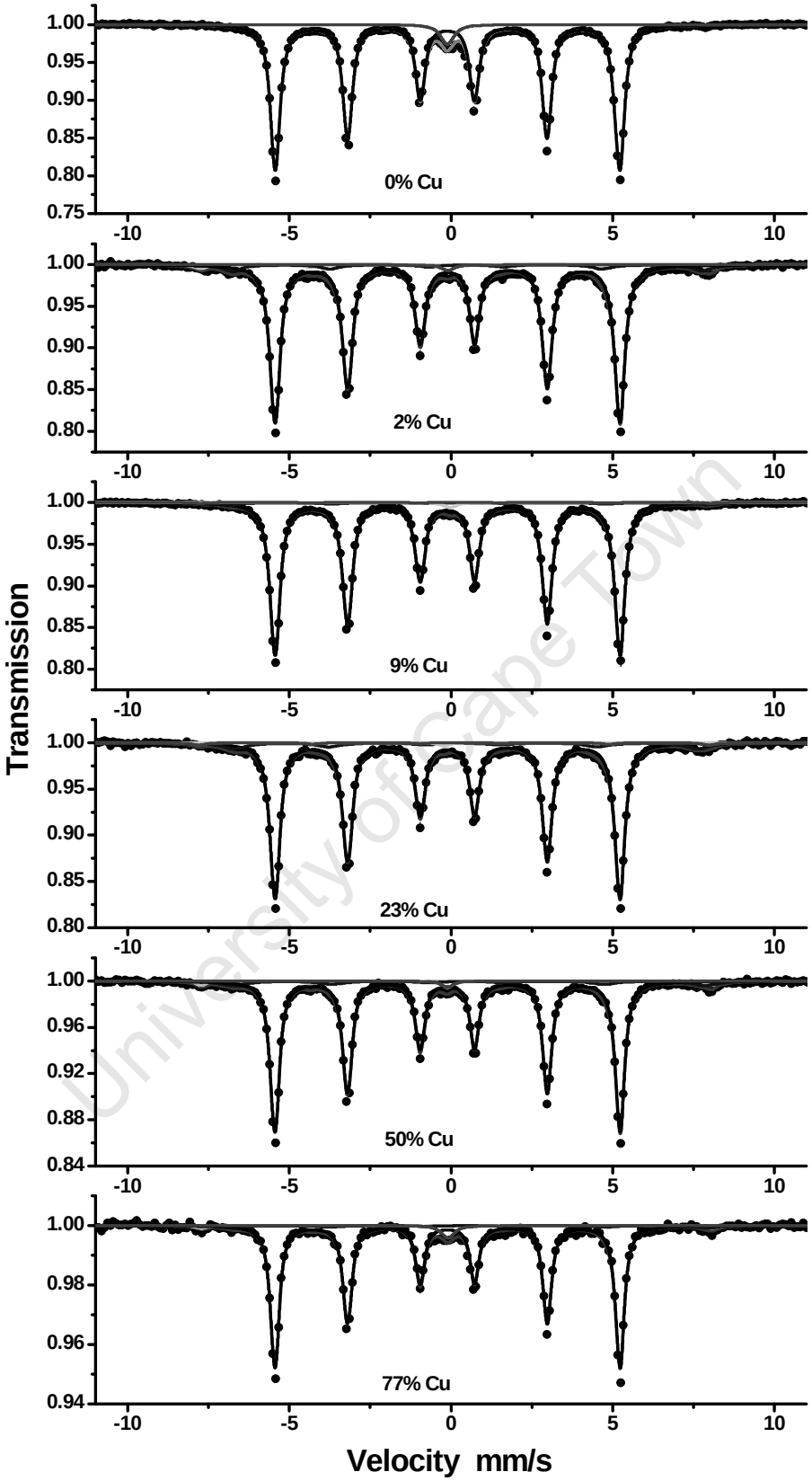

Figure 4.7 MAS spectra of reduced and passivated catalyst series

4.2.5 Brunauer-Emmett-Teller method, BET

The BET results for the reduced catalyst are not available due to a repeatability problem in the analysis. It appears that the passivated catalysts (both reduced and spent) interacted with the analytical method to create meaningless results. *In situ* reduction in the BET apparatus was attempted but this also failed due to an inadequate flow path.

4.2.6 Temperature programmed reduction, TPR

The degree of reduction of the catalyst series was measured, first by reducing the catalysts under the standard reduction conditions and then exposing them to H_2-TPR. The results are shown in Figure 4.8, and it can be seen that all results display a flat line representing no hydrogen consumption. This indicates that the reduction is complete under the reduction conditions which were applied.

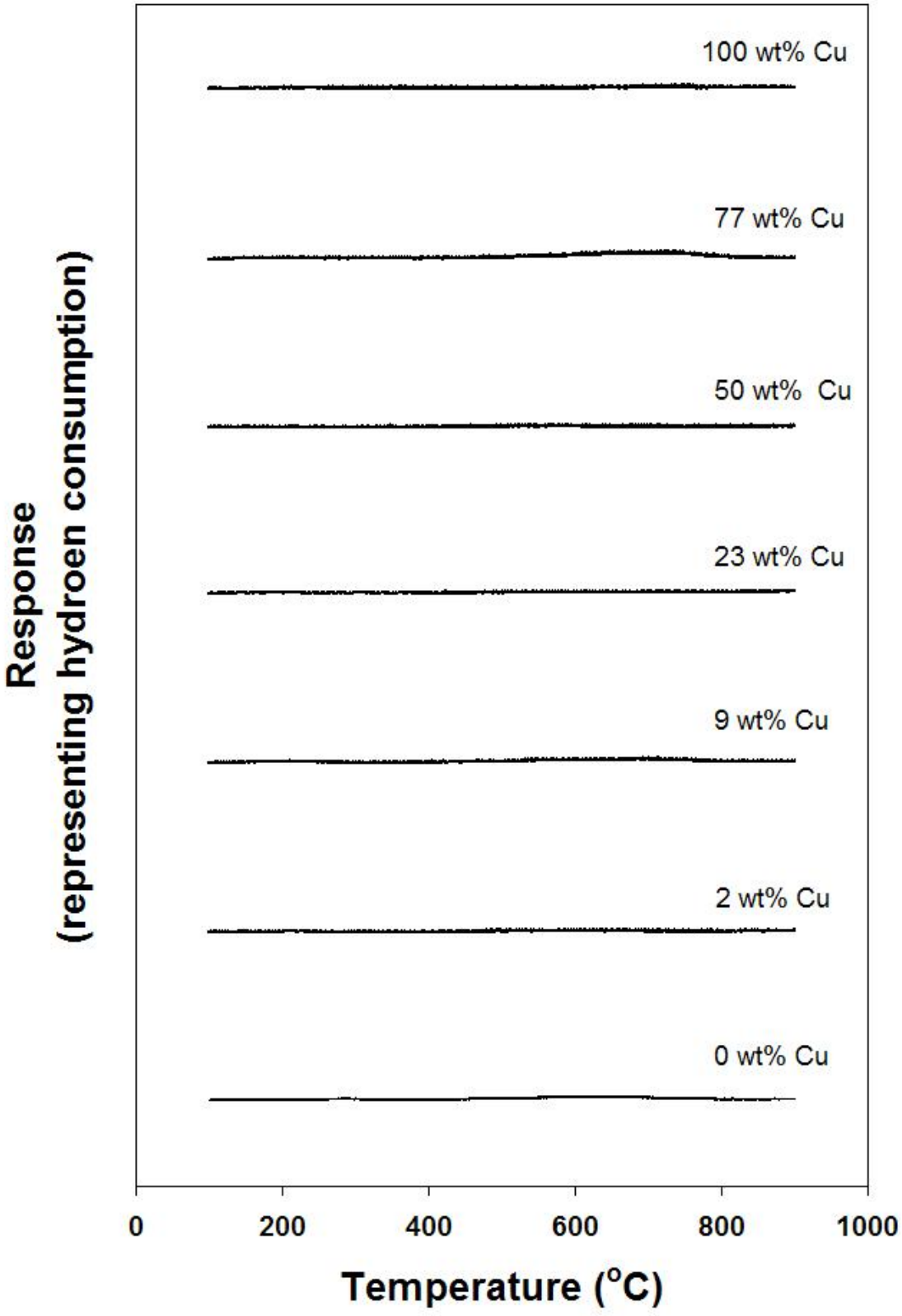

Figure 4.8 H_2-TPR of reduced catalysts for degree of reduction calculations

4.2.7 Transmission electron microscopy, TEM

Figure 4.9 shows the TEM micrographs of the reduced and passivated catalysts. The TEM images for these catalysts proved difficult to obtain, as in some cases they were contaminated by an unknown substance (possibly glass wool) that made analysis of the catalysts problematic.

For the catalysts with loadings up to 50 wt% Cu the majority of the crystallites in the images are most likely mainly of iron; these crystallites look extremely similar in size and shape and seem to be in the region of 40 to 70 nm; this result agrees well with the XRD iron crystallite sizes mentioned in section 4.2.3. At higher copper loadings the images are not very clear and also seem to have some sort of fine crystallite 'hairs'. The dark nature of the samples is probably due to the large copper crystallites which inhibit the movement of the electrons through the microscope.

What the crystalline 'hairs' may be can only be speculated at as their composition is unknown. But inspection of the 100 wt% Cu sample, while extremely dark due to the large copper crystallites, shows a plated effect on the lighter areas similar to the 'hairs' seen on the 50 and 77 wt% Cu catalysts. It is thought that these 'hairs' could be caused by spreading of the copper metal at the high reduction temperatures which also bring the copper metal into greater contact with the iron, thus accelerating the hydrogen spillover effect discussed with the catalyst reduction in section 4.1.6.

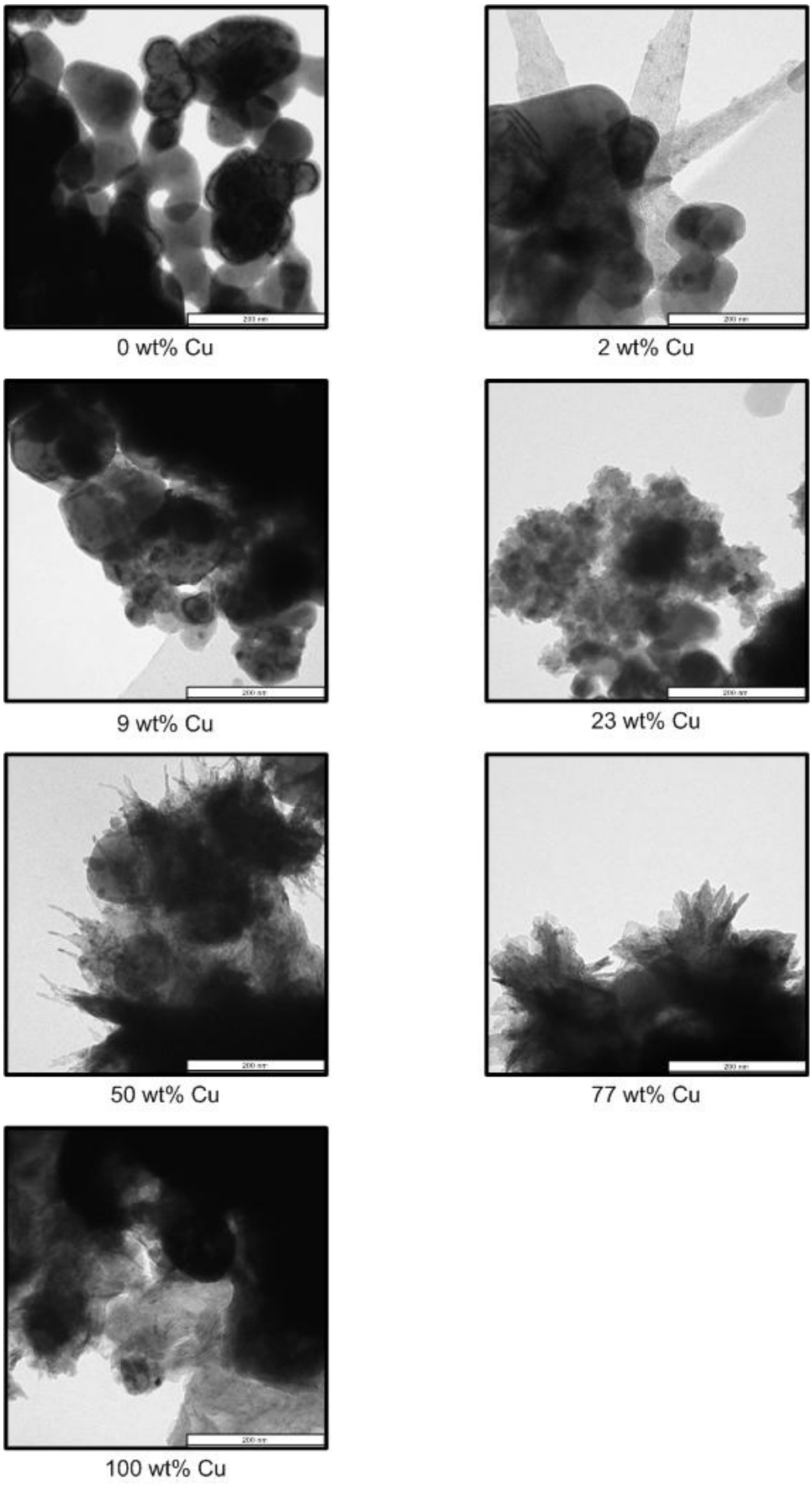

Figure 4.9 TEM micrographs of reduced and passivated catalyst series (scale shown = 200 nm)

4.2.8 Summary of results on reduced catalysts

There appears to be no change in either iron or copper metal loadings with reduction of the catalysts. But there is an effect on the crystallite sizes of both copper and iron upon reduction. The copper crystallites size increases with copper loading, while the iron crystallites all seem to reach a steady size in the region of 50 nm. The MAS results suggest the existence of smaller metallic iron but this seems to be in a very small amount.

The catalysts all appear to be fully reduced under these conditions. Thus there should be no effect by the degree of reduction or reduced crystallite sizes on the catalyst performance data; these effects can therefore be excluded.

4.3 Characterisation of spent and passivated iron-copper catalysts

Catalysts that were run in the Berty reactor under Fischer-Tropsch synthesis at 300 ºC at a space velocity of 3900 ml(NTP)/g_{Fe}/h, with a composition of 4:1:1 H_2:CO:CO_2 and a pressure of 21 bar(a) were cooled under argon and passivated with carbon dioxide for 30 minutes as described by Baker and Rodriguez (1994).

4.3.1 Atomic absorption spectroscopy, AAS

Atomic absorption spectroscopy was conducted on the samples, but for unknown reasons the result of the metal compositions were not repeatable; they are therefore not reported here.

4.3.2 Scanning electron microscopy and energy dispersive X-ray analysis, SEM-EDX

Theoretical and actual iron, copper and potassium loadings for each spent and passivated catalyst as determined by SEM-EDX are shown in Table 4.11. Comparison

with previous SEM-EDX results in Table 4.2 and Table 4.7 suggest some copper leaching during reaction. This result was confirmed by the presence of copper in the analysis of a small quantity of green oil/water captured in the ampoule sampling device (set to a lower temperature for this purpose) during the fixed-bed reactor runs.

The levels of potassium are also comparatively low for some samples, but as discussed previously, it is hard to determine if this is a true reflection of the potassium loading or an error in the analytical analysis due to the low concentration of potassium.

Table 4.11 Theoretical and actual iron, copper and potassium loadings and mass ratios as determined by SEM-EDX of the spent and passivated catalyst series

Catalyst (Cu wt%)[a]	Fe : Cu : K Theory	Fe : Cu : K SEM-EDX
0	100 : 0 : 5	100 : 0 : 1.1
2	100 : 2 : 5.1	100 : 2.4 : 1.2
9	100 : 10 : 5.5	100 : 6.5 : 1.3
23	100 : 30 : 6.5	100 : 24 : 1.0
50	100 : 100 : 10	100 : 78 : 1.3
77	30 : 100 : 6.5	38 : 100 : 1.6
100	0 : 100 : 5	0 : 100 : 1.6

[a] Basis: Fully reduced catalyst

4.3.3 X-ray diffraction spectroscopy, XRD

The results of X-ray diffraction spectroscopy (XRD) on the spent and passivated samples are shown in Figure 4.10. For the most part it seems that the iron has been carbided to Hägg carbide (Fe_5C_2) or oxidised to magnetite. These results are expected for iron catalysts under Fischer-Tropsch synthesis conditions (*Anderson*, *1984*, *Dry*, *1981*, *Storch et al.*, *1951*, *Mansker et al.*, *1999*, *Schulz et al.*, *1999*, *Schulz et al.*, *2002* and *Li et al.*, *2002*). The copper however has stayed in its metallic form for all catalysts.

Table 4.12 shows the crystallite sizes for Hägg carbide, magnetite and copper metal as calculated from the XRD spectra using the Scherrer equation. Here as with the calcined catalyst the iron carbides seem to decrease in size with copper loading during synthesis. While in the reduced samples iron crystallite sizes between 30 and 35 nm were

obtained, the size of Hägg carbide crystallites in the catalysts with low copper loading is much larger than the size increase of 4% to be expected simply due to density differences of metallic iron and Hägg carbide. Only in the iron catalyst which contains the largest amount of copper (77 wt% Cu) are much smaller crystallites of Hägg carbide present. Although unclear how, it is evident that copper must play a role on the resulting Hägg carbide crystallite size. Li *et al*. (2002) showed that iron-copper catalysts activated with carbon monoxide or syn-gas resulted in smaller iron carbide crystallites by supplying activate CO to the bulk iron oxide. These smaller crystallites coincided with larger iron carbide content in the catalyst which is not seen in these experiments (Section 4.3.4).

Not enough peaks of magnetite could be isolated successfully to quantify the trend, but it seems from the two points available that there is a decrease in the magnetite crystallite size in the same manner as the carbide. Finally, the copper crystallites seem to have increased in size from their reduced state, suggesting that the copper is slowly agglomerating over time.

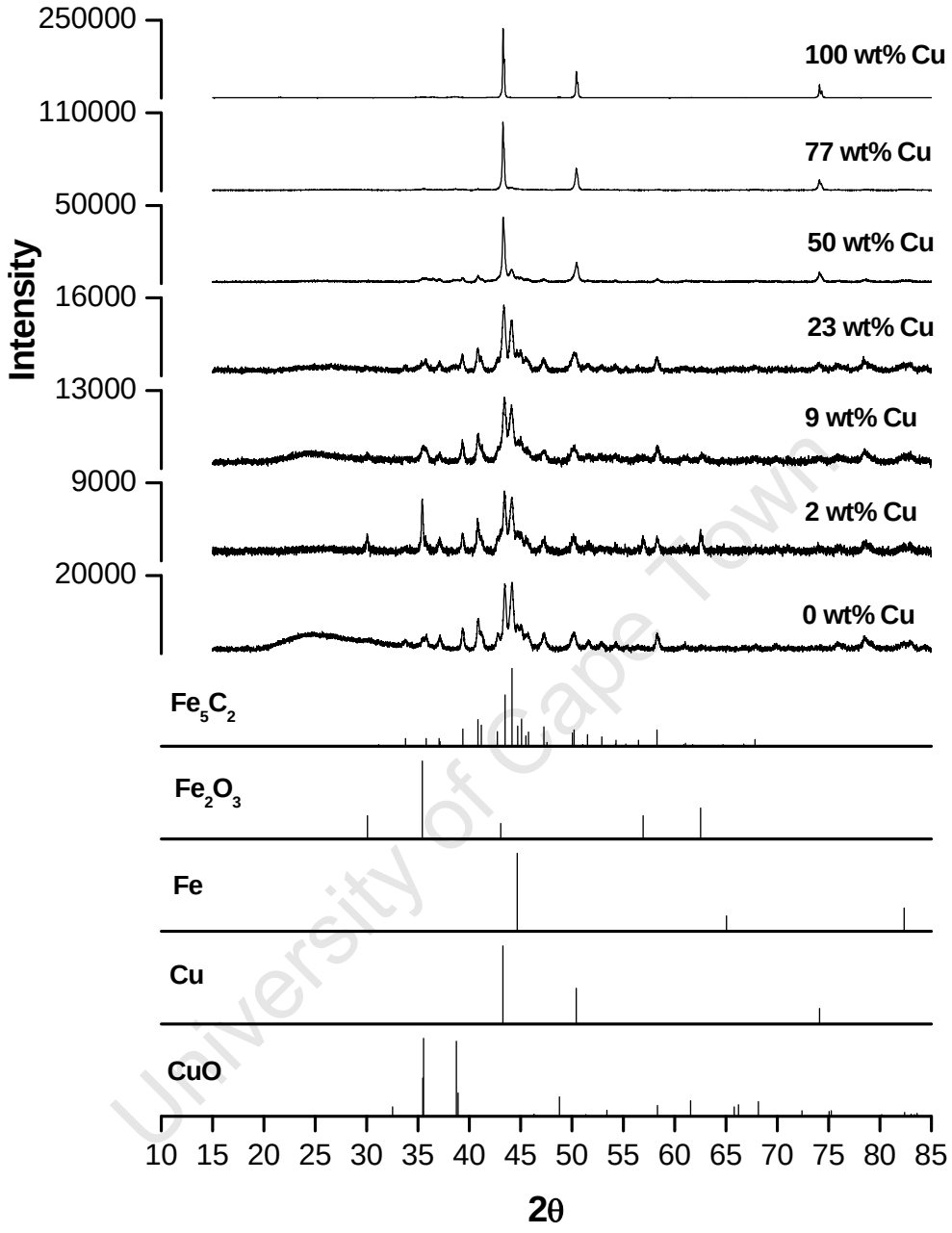

Figure 4.10 XRD spectra of spent and passivated catalyst series

Table 4.12 Calculated crystallite sizes for spent and passivated catalysts from XRD analysis

Catalyst (Cu wt%)[a]	Spent d Fe_5C_2 (nm)	Reduced d Fe_3O_4 (nm)	Reduced d Cu (nm)
0	53	n/a[b]	-
2	48	>50[c]	n/a[b]
9	41	20	n/a[b]
23	35	n/a[b]	31
50	31	n/a[b]	38
77	9	n/a[b]	>50[c]
100	-	-	>50[c]

[a] Basis: Fully reduced catalyst

[b] n/a - Peak too small to be detectable

[c] >50 - Crystallite size greater than value that can be determined accurately with Scherrer equation

4.3.4 Mössbauer Spectroscopy, MAS

Figure 4.11 shows the MAS spectra of the spent and passivated catalyst series; the hyperfine splitting parameters are summarised in Table 4.13.

All the iron-containing catalyst samples that were analysed consisted of mainly Hägg carbide (Fe_5C_2), and small amounts of magnetite and superparamagnetic Fe^{3+}. All the catalysts have comparable iron phase compositions and this does not seem to be affected by the presence of copper. The nature of the superparamagnetic Fe^{3+} cannot be conclusively identified at these temperatures. Once again the catalyst sample containing 100 wt% Cu could not be analysed using MAS due to the absence of iron, which is essential for this technique.

Table 4.13 Hyperfine splitting parameters of for spent and passivated catalyst series

Catalyst (Cu wt%)[a]	δ^b mm/s	Δ^b mm/s	$B_{hf}{}^c$ T	Identified Iron phase	% Relative Area	Phases identified by XRD
0	0.32	0.06	49.0	Fe_3O_4	4	Fe_3O_4 Fe_5C_2
	0.68	-0.06	45.6			
	0.26	0.09	21.7	Fe_5C_2	92	
	0.15	-0.08	18.5			
	0.22	-0.03	10.7			
	0.14	0.99	-	spm[d] Fe^{3+}	4	
2	0.28	-0.00	49.1	Fe_3O_4	14	Fe_3O_4 Fe_5C_2 α- Fe
	0.68	-0.06	45.9			
	0.25	0.09	21.7	Fe_5C_2	83	
	0.16	-0.07	18.5			
	0.23	-0.02	10.7			
	0.13	1.01	-	spm Fe^{3+}	3	
9	0.32	-0.04	48.9	Fe_3O_4	7	Fe_3O_4 Fe_5C_2 α- Fe
	0.65	-0.13	45.4			
	0.26	0.09	21.8	Fe_5C_2	89	
	0.17	0.06	18.5			
	0.21	0.12	11.1			
	0.28	1.17	-	spm Fe^{3+}	4	
23	0.37	-0.21	49.0	Fe_3O_4	4	Fe_5C_2 α- Fe CuO
	0.65	-0.25	46.0			
	0.26	0.11	21.6	Fe_5C_2	92	
	0.17	0.07	18.4			
	0.21	0.12	11.0			
	0.26	1.03	-	spm Fe^{3+}	4	
50	0.26	0.09	21.8	Fe_5C_2	94	Cu Fe_5C_2 CuO
	0.17	0.07	18.4			
	0.20	0.12	10.9			
	0.33	0.93	-	spm Fe^{3+}	6	
77	0.37	0.05	49.6	Fe_3O_4	4	Cu CuO Cu_2O
	0.65	-0.04	45.2			
	0.25	0.09	21.7	Fe_5C_2	93	
	0.16	0.07	18.5			
	0.22	0.14	10.9			
	0.35	1.05	-	spm Fe^{3+}	3	
100	-	-	-	-	-	Cu CuO

[a] Basis: Fully reduced catalyst

[b] Error: ± 0.02 mm/s

[c] Error: ± 0.5 T

[d] spm: Superparamagnetic

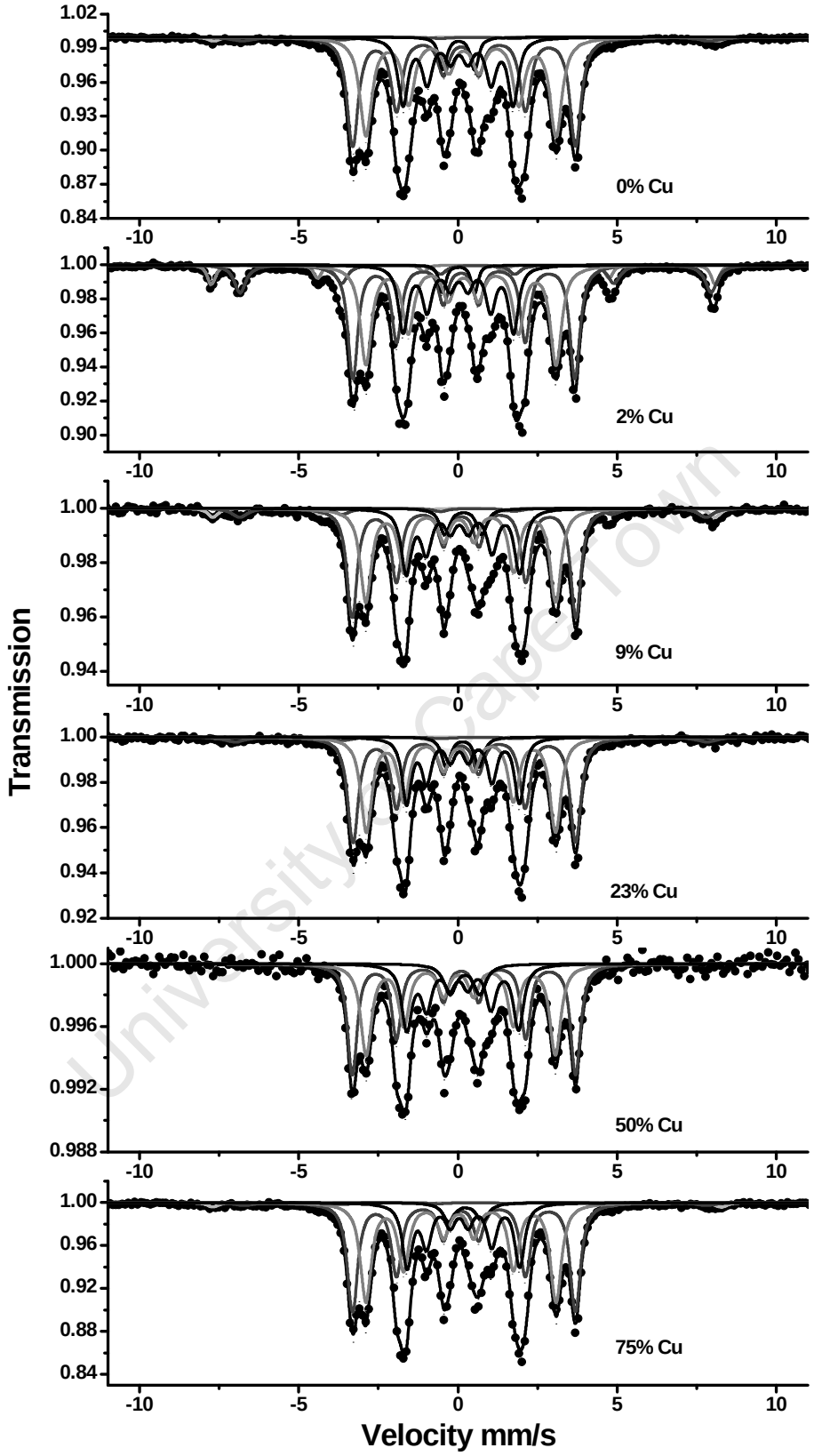

Figure 4.11 MAS spectra of spent and passivated catalyst series

4.3.5 Brunauer-Emmett-Teller method, BET

The BET results for the spent catalyst are not available due to a repeatability problem in the analysis. It appears that the passivated catalysts (both reduced and spent) interacted with the analytical method to create meaningless results.

4.3.6 Transmission electron microscopy, TEM

Figure 4.12 shows the TEM micrographs of the spent and passivated catalysts. For all the catalysts, the images are extremely dark. This is could be caused by a number of factors, including larger crystallites, wax on the surface of the catalysts and carbon deposition on the catalysts. For the iron-containing catalysts the results seen below are not clear, but could seem to show a constant crystallite size. However the 100 wt% Cu catalyst seems to have a lot of small, perhaps amorphous, particles present on the TEM as opposed to the large crystallites predicted with XRD analysis. Inspection of other micrographs suggests that these small particles are surrounding larger crystallites, as seen in the bottom of the micrograph. This imaging could agree with the theory postulated earlier that the crystallites are continuously growing through agglomeration, and these particles are in the process of agglomerating.

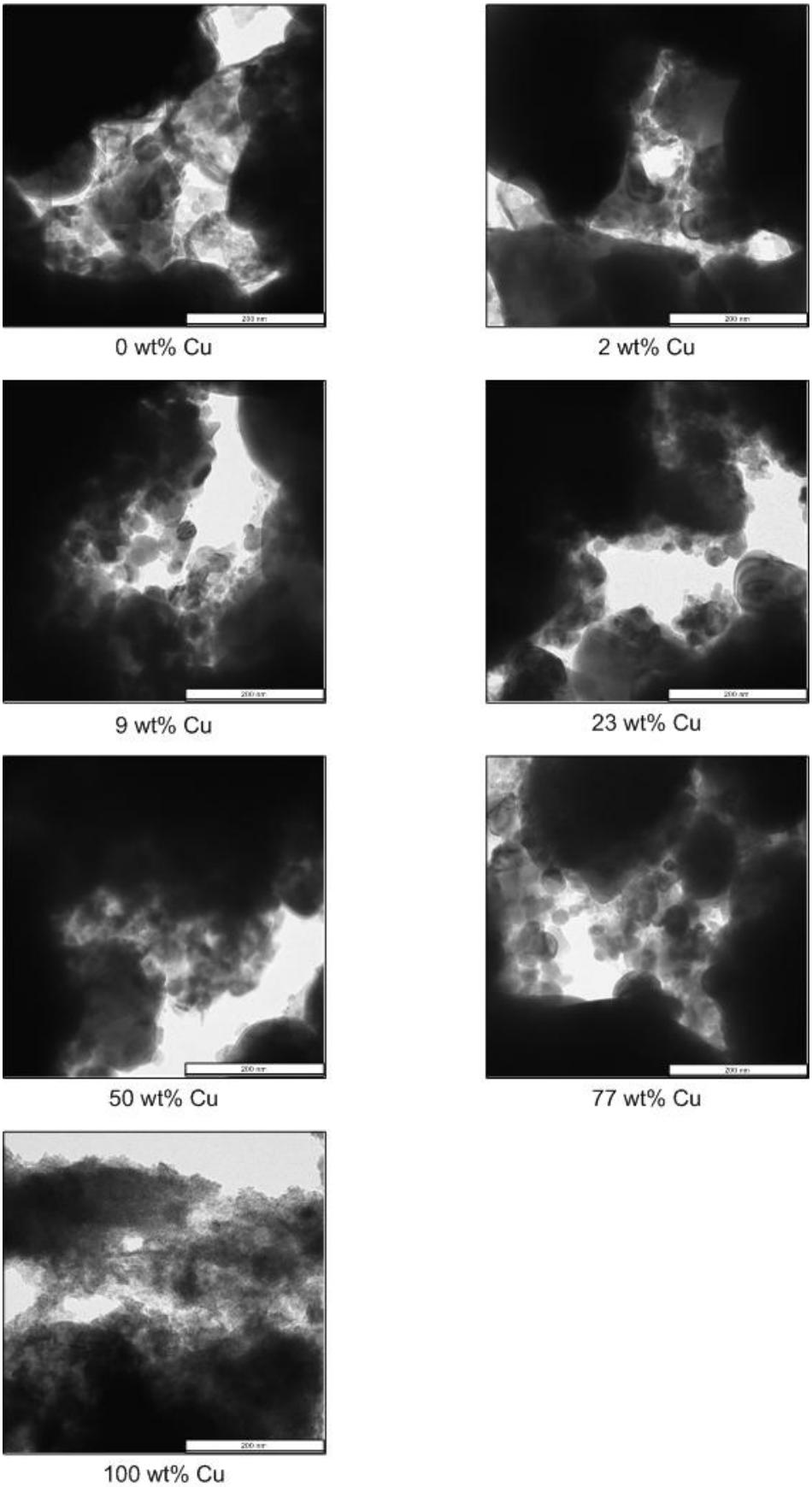

Figure 4.12 TEM micrographs of spent and passivated catalyst series (scale shown = 200 nm)

4.3.7 Summary of results on spent catalysts

During synthesis the metallic iron changes to a combination of mainly Hägg carbide and some magnetite, as expected during normal Fischer-Tropsch synthesis (the ratio of these two phases seems constant and is not affected by the catalyst copper loading). The copper phase is seen to be the same as after reduction (pure metallic phase). It does appear that some copper is leached out of the catalyst during synthesis, but this does not affect either the iron or copper phase compositions.

As with the calcined catalysts the crystallite sizes of the iron phases seem to decrease with copper loading while the copper crystallite sizes increase.

4.4 Fischer-Tropsch synthesis – Fixed bed

As mentioned previously Fischer-Tropsch synthesis was conducted in two separate reactor systems.

A fixed-bed apparatus was used for testing the catalyst series and examining the initial catalyst behaviour. The tests were conducted using a catalyst loading of 0.69 g of iron per sample. Prior to Fischer-Tropsch synthesis, catalysts were activated under hydrogen following the same reduction procedure as mentioned previously: heating under hydrogen at a rate of 1 ºC/min to 100 ºC holding for 1 hour, then 1 ºC/min to 400 ºC and holding for 16 hours, at ambient pressure and a space velocity of 4000 ml(NTP)/g_{Fe}/h. All tests were conducted for a minimum of 96 hours at a reaction temperature of 300 °C, a pressure of 18 bar(a) and a hydrogen to carbon monoxide to carbon dioxide ratio of 4:1:1. Run details and additional results are listed in Appendix H.

4.4.1 Catalyst activity

Catalyst activity, expressed as carbon conversion (sum of carbon monoxide and carbon dioxide conversion) was monitored as a function of time. This carbon conversion equals the yield of hydrocarbons formed. The initial activity of the catalyst (first 2 hours) is shown in Figure 4.13, while extended time on-stream activity is shown in

Figure 4.14. The pure copper catalyst showed little to no activity (0 to 2 % conversion, possibly within the error of the analysis techniques employed) over all time periods and seems not to be active under these conditions. No products were detectable through GC analysis using both TCD and FID techniques. Not even the formation of methanol was detectable. There will therefore be no further results discussed regarding this catalyst.

During the initial time period not all the catalysts behave in the same manner. While some reach a high activity (around 50%) within 10 minutes of being exposed to synthesis gas, others start off at 10 or 20% and seem to increase slowly. This low initial activity does not, however, seem to be related to the copper loading or any other physical aspect of the catalyst.

After 24 hours or 1 day on-stream all the catalysts begin to show a conversion of between 30 and 50% while after 96 hours time on-stream all the catalysts exhibit comparable activity (around 40%) and steady state behaviour. For this reason product selectivity around 96 hours can be directly compared to determine the effect of copper.

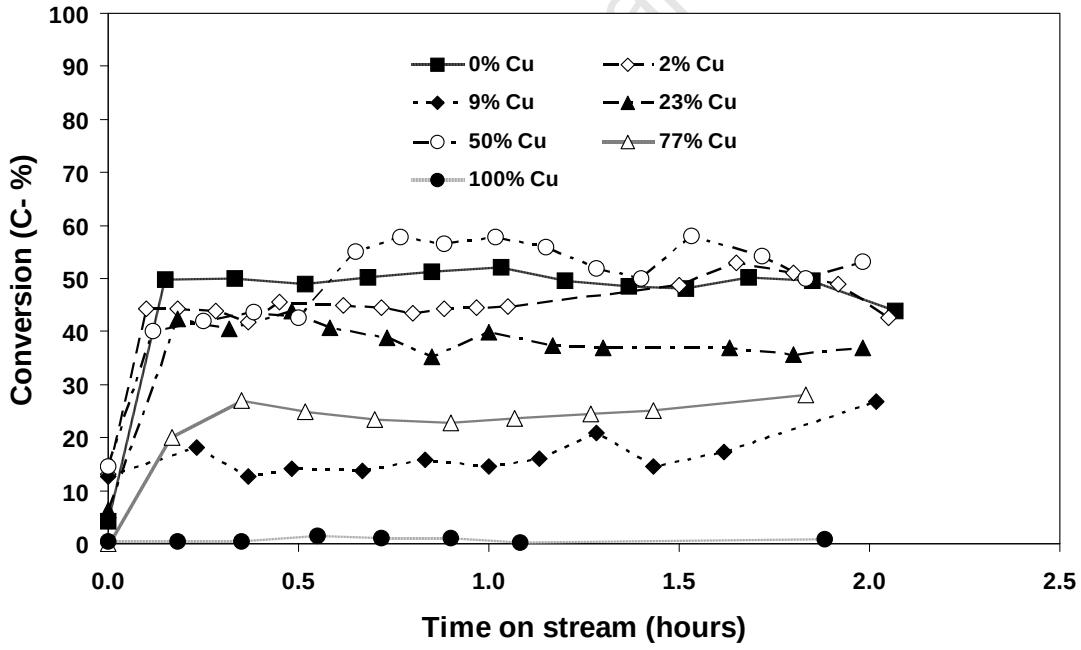

Figure 4.13 Carbon conversion as a function of time for the initial time period of 1 minute to 2 hours during Fischer-Tropsch synthesis in a fixed-bed reactor for the iron-copper catalyst series

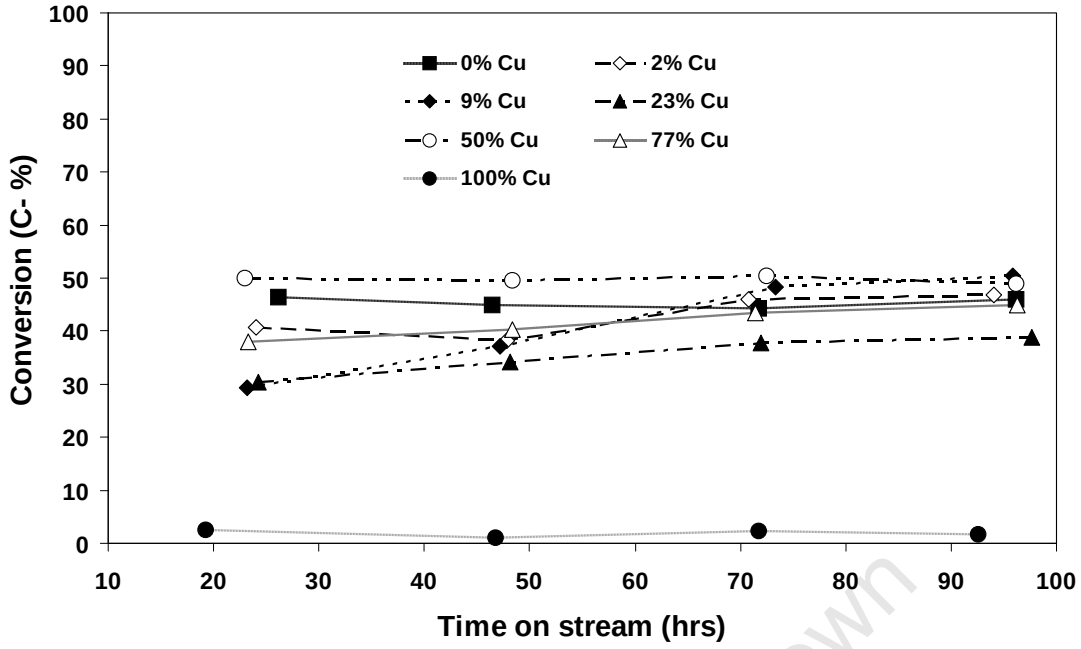

Figure 4.14 Carbon conversion as a function of time for the time period of 20 to 96 hours during Fischer-Tropsch synthesis in a fixed-bed reactor for the iron-copper catalyst series

4.4.2 Organic product formation

In the case of gas analysis for the fixed-bed reactor tests good chromatographic data could only be extracted for the carbon fraction C_1 to C_{10}. Analysis of products longer than C_{10} proved unreliable and in most cases no organic product was seen after C_{20}. Some wax formation (dark brown in colour) was observed during Fischer-Tropsch synthesis, but this does not correspond well with the chain growth probabilities shown in section 4.4.2.2, for which a higher alpha value would be expected. However, for an initial direct comparison of each catalyst, the volatile organic product is sufficient in the range that is shown.

For a more detailed examination into the product selectivity including oil and water analysis, a Berty reactor was used, as higher catalyst loadings could be achieved and more product collected; see section 4.5.

4.4.2.1 Organic products: Methane

Thermodynamically, methane is the predominant product in Fischer-Tropsch synthesis, and other products should only be produced for feeds lacking enough hydrogen for

complete conversion of carbon monoxide to methane (*Anderson*, *1984*). It is formed through the associative desorption of a methyl species with a surface hydrogen. However, the adsorbed methyl species can also act as a chain growth initiator.

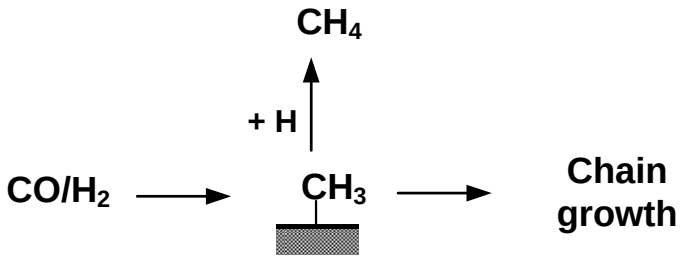

The methane selectivities for 40 and 120 minutes time on-stream, as well as 96 hours, are detailed in Table 4.14. Over the time period from 40 minutes to 96 hours the methane selectivity for all catalysts drops. This agrees well with other studies and is most likely due to the phase changes in the catalysts. Initially, the completely reduced iron is believed to have a higher "hydrogenating ability" than the subsequently formed iron carbide (*Satterfield et al.*, *1986*). Over the time periods 40 and 120 minutes all catalysts except 9 wt% Cu show comparable methane selectivity. The reason for the high methane selectivity in this catalyst could be due to its low initial activity as seen in Figure 4.13. This lower activity would coincide with a longer time needed for the catalyst to carbide in its 'transient kinetic regime', as described by Schulz *et al.* (1999 and *Claeys and Schulz*, *2004*). It appears copper has no significant effect on methane selectivity.

Table 4.14 Methane selectivities for 40 minutes, 120 minutes and 96 hours time on-stream during Fischer-Tropsch synthesis in a fixed-bed reactor for the iron-copper catalyst series

Catalyst (Cu wt%)[a]	S_{CH_4} (C- %)		
	40 min	120 min	96 hr
0	16.3	14.5	15.2
2	14.9	13.4	10.7
9	20.6	18.6	13.5
23	16.4	15.1	11.4
50	17.4	15.2	13.2
77	17.6	17.6	12.6

[a] Basis: fully reduced catalyst

4.4.2.2 Organic products: Chain growth

Fischer-Tropsch synthesis is regarded as having a stepwise mechanism sequence. This means there will either be chain growth of an adsorbed species on the catalyst surface or it will desorb from the catalyst surface as product. The probability of the species on the surface growing by one carbon number (C_{n-1} to C_n) as opposed to desorbing is described as the chain growth probability (α_{n-1}).

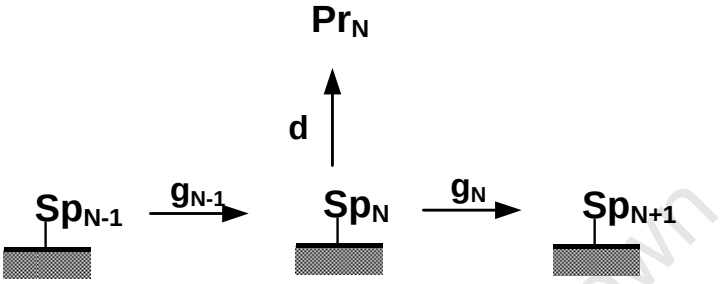

If α is independent of carbon number it can be derived from the so called Anderson-Schulz-Flory plot:

$$\frac{W_n}{n} = n \log \alpha + \text{constant} \qquad (4.1)$$

Where W_n is the mass fraction of the product species with carbon number n and α is the independent chain growth probability. Table 4.15 shows the chain growth probability for each catalyst after 40 and 120 minutes, and 96 hours, for carbon numbers between 3 and 8, as well as the chain growth probability after 96 hours for carbon numbers 3 to 10, i.e. carbon number ranges in which the actual ASF distributions showed linear behaviour. With an increase in time on-stream the alpha value increases; this result agrees well with the methane selectivity where the methane decreases with time on-stream. As the iron catalyst increases in carbide content so the average molecular weight of the product increases. Additionally, examination of the alpha value for C_{3-10} is higher than for C_{3-8} suggesting an alpha shift to the higher carbon fractions for higher carbon numbers. An increase of the chain growth probability with increasing carbon number for iron catalysts has also been reported before by (*Huff and Satterfield*, *1984* and *Claeys and Schulz*, *2004*). Copper, once again, seems to have no effect on the chain growth probability.

Table 4.15 Chain growth probabilities from VOC for 40 minutes, 120 minutes and 96 hours time on-stream during Fischer-Tropsch synthesis in a fixed-bed reactor for the iron-copper catalyst series

Catalyst (Cu wt%)[a]	Chain growth probability			
	$\alpha_{C_{3-8}}$ 40 min	$\alpha_{C_{3-8}}$ 120 min	$\alpha_{C_{3-8}}$ 96 hr	$\alpha_{C_{3-10}}$ 96 hr
0	0.50	0.62	0.66	0.69
2	0.59	0.62	0.67	0.70
9	0.51	0.61	0.65	0.68
23	0.59	0.62	0.67	0.69
50	0.59	0.62	0.65	0.67
77	0.62	0.62	0.66	0.71

[a] Basis: fully reduced catalyst

4.4.2.3 Organic products: Olefin formation

The main primary products of Fischer-Tropsch synthesis are thought to be linear hydrocarbons (paraffins and olefins) as well as linear oxygenates. The final product derived from the reactor does not always reflect the primary product, as secondary reactions can occur. The scheme below adapted from Claeys (1997) shows how alpha can re-adsorb onto the catalyst surface and undergo isomerisation to an olefin with an internal double bond, be reincorporated for further chain growth or get hydrogenated to the corresponding paraffin.

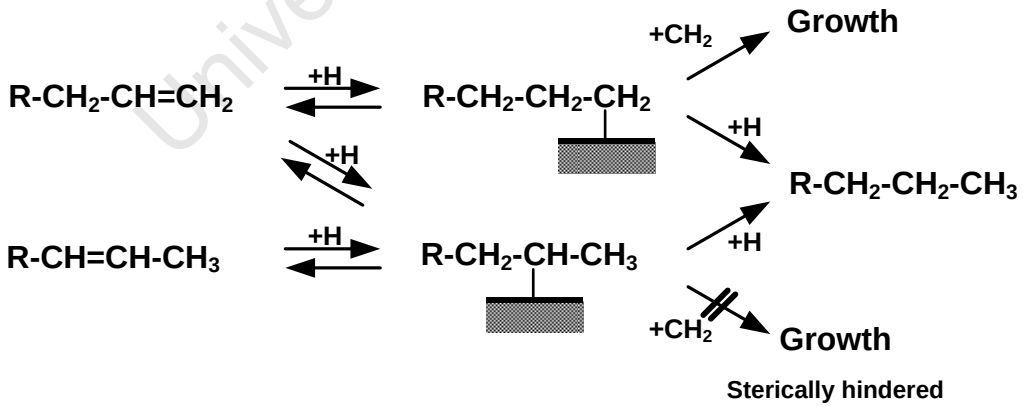

Figure 4.15 shows the molar content of olefins in the total linear hydrocarbon product as a function of carbon number after 96 hours. These molar contents for C_2 and C_3 as well as for 40 and 120 minutes are also listed in Table 4.16. Generally, carbon number independent values of this ratio indicate primary olefin selectivity, typically around 70 to 80 mol % (*Schulz and Claeys*, *1999a*). This is found in the C_3 to C_8 fraction of all

copper promoted catalysts, with a slightly lower olefin content seen with increasing copper promotion.

The relatively low olefin content in the C_2 fraction is often found in FT-products (*Schulz and Claeys*, *1999a*). It has been shown to be mainly due to the secondary hydrogenation of ethene, which is the most reactive of the olefins. Decreasing ethene contents are found at steady state with increasing copper promotion, indicating preferred secondary hydrogenation. Initially (after 40 min), the olefin content in the C_2 fraction is not affected by the copper loading and slightly higher olefin contents are obtained with all catalysts tested.

It may be speculated that copper, which facilitates hydrogen dissociation, causes increased hydrogen concentration on the iron surface, therefore leading to increased primary paraffin formation as well as an enhanced secondary hydrogenation of ethene. The latter reaction might also occur on the surface of copper itself. Temporal changes of the observed olefin contents in C_2 may also be explained by structural changes of the catalysts during their exposure to reaction conditions. This coincides with the formation of Hägg carbide crystallites, changes of crystallite sizes and the establishment of the kinetic Fischer-Tropsch regimes on the different catalysts.

It should be noted that the above effects are not caused by differences in hydrogen partial pressure as described by Dry (1981), as this did not vary in this study (see Table 4.17).

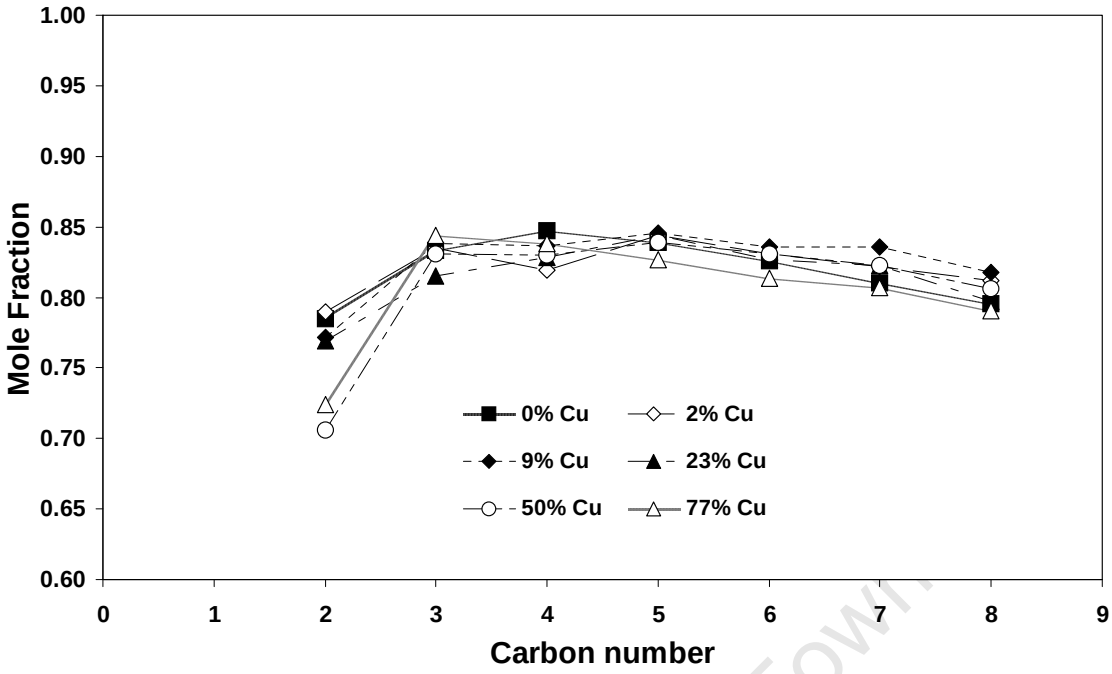

Figure 4.15 Mole fraction of olefins in linear hydrocarbon product as a function of carbon number after 96 hours during Fischer-Tropsch synthesis in a fixed-bed reactor for the iron-copper catalyst series

Table 4.16 Mole fraction of olefins in linear hydrocarbon product after 40 and 120 minutes as well as 96 hours during Fischer-Tropsch synthesis in a fixed-bed reactor for the iron-copper catalyst series

Catalyst	**Mole fraction of olefins in linear hydrocarbon product**					
(Cu wt%)[a]	C_2	C_3	C_2	C_3	C_2	C_3
	40 min		120 min		96 hr	
0	0.81	0.82	0.83	0.83	0.78	0.83
2	0.78	0.82	0.79	0.83	0.79	0.83
9	0.82	0.77	0.81	0.80	0.77	0.84
23	0.77	0.81	0.73	0.78	0.77	0.82
50	0.82	0.83	0.62	0.78	0.71	0.83
77	0.80	0.80	0.72	0.80	0.72	0.84

[a] Basis: fully reduced catalyst

Table 4.17 Average reactor hydrogen partial pressure after 40 minutes, 120 minutes and 96 hours time on-stream during Fischer-Tropsch synthesis in a fixed-bed reactor for the iron-copper catalyst series

Catalyst (Cu wt%)[a]	$p_{[H2]}$ (bar)		
	40 min	120 min	96 hr
0	12.3	11.9	9.3
2	13.1	11.5	8.7
9	12.4	12.2	8.7
23	11.9	11.8	10.0
50	13.2	12.1	8.3
77	13.0	12.9	9.9

[a] Basis: fully reduced catalyst

Figure 4.16 shows the molar content of α-olefins in the total fraction of linear olefins after 96 hours. A high fraction of α-olefins (>95%) for all carbon numbers indicates high primary product selectivity with little to no double bond shift isomerisation (*Schulz and Claeys*, *1999a*). The same ratios are shown in Table 4.18 for C_4 and C_5 including values after 40 and 120 minutes. Values for higher olefin fractions for the initial time samples cannot be reported due to no or very low selectivities to the olefins with internal double bonds. However, little to no change of the ratio over the time periods indicated shows the high primary selectivity of this product. No effect of copper can be discerned.

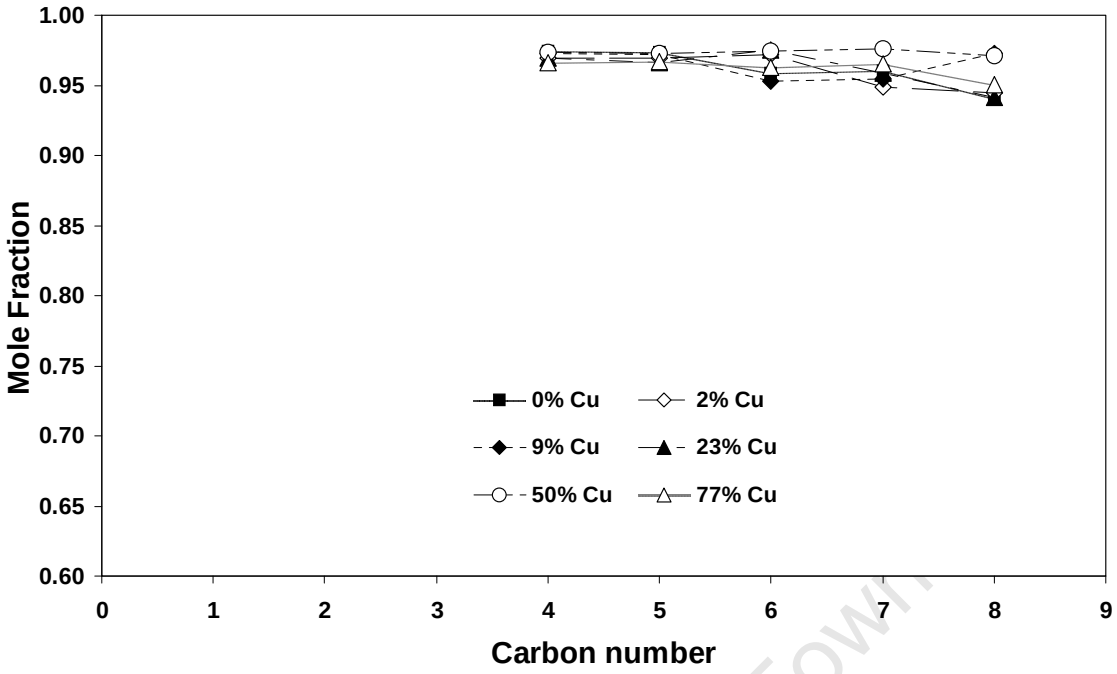

Figure 4.16 Mole fraction of α–olefins in linear olefins as function of carbon number after 96 hours time on-stream during Fischer-Tropsch synthesis in a fixed-bed reactor for the iron-copper catalyst series

Table 4.18 Mole fraction of α–olefins in linear olefins after 40 and 120 minutes as well as 96 hours during Fischer-Tropsch synthesis in a fixed-bed reactor for the iron-copper catalyst series

Catalyst	**Mole fraction of α–olefins in linear olefins**					
(Cu wt%)[a]	C_4	C_5	C_4	C_5	C_4	C_5
	40 min		120 min		96 hr	
0	0.93	0.96	0.98	0.97	0.97	0.97
2	0.98	0.98	0.97	0.98	0.97	0.97
9	1.00[b]	0.97	0.99	0.98	0.97	0.97
23	0.95	0.98	0.97	0.97	0.97	0.97
50	0.97	0.98	0.95	0.97	0.97	0.97
77	0.97	0.97	0.97	0.97	0.97	0.97

[a] Basis: fully reduced catalyst

[b] No secondary olefins identified in the chromatograph

4.4.2.4 Organic products: Branched products

Branching of the hydrocarbon product to methyl branched species can occur in one of two different pathways, as shown below. This occurs either by the secondary re-incorporation of α-olefins [1] (as shown by e.g. the co-feeding of ^{14}C labelled propene

by Schulz *et al.* (1970)) or through primary formation via the combination of an alkylidene and a methyl species [2] (*Fischer and Tropsch*, *1926* and *Craxford and Rideal*, *1939*).

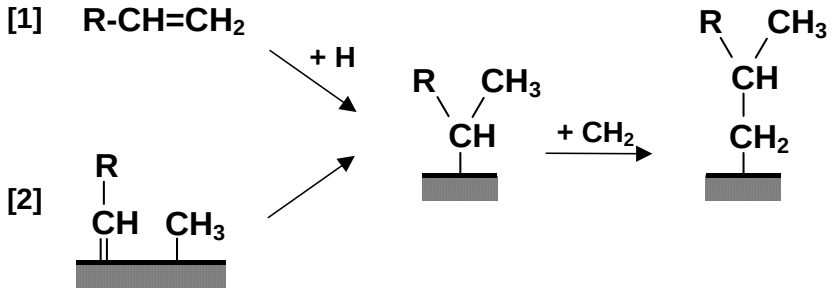

Figure 4.17 shows the molar ratio of methyl branched to linear hydrocarbons in the C_5 fraction after 40 and 120 minutes as well as 96 hours time on-stream. All catalysts that contain copper have a higher ratio for both 40 and 120 minutes time on-stream (the exception being 77 wt% Cu). It is likely that copper promotes one of the above branching mechanisms in the early life of the catalyst. The same trends were observed in other carbon number fractions, but are not shown here.

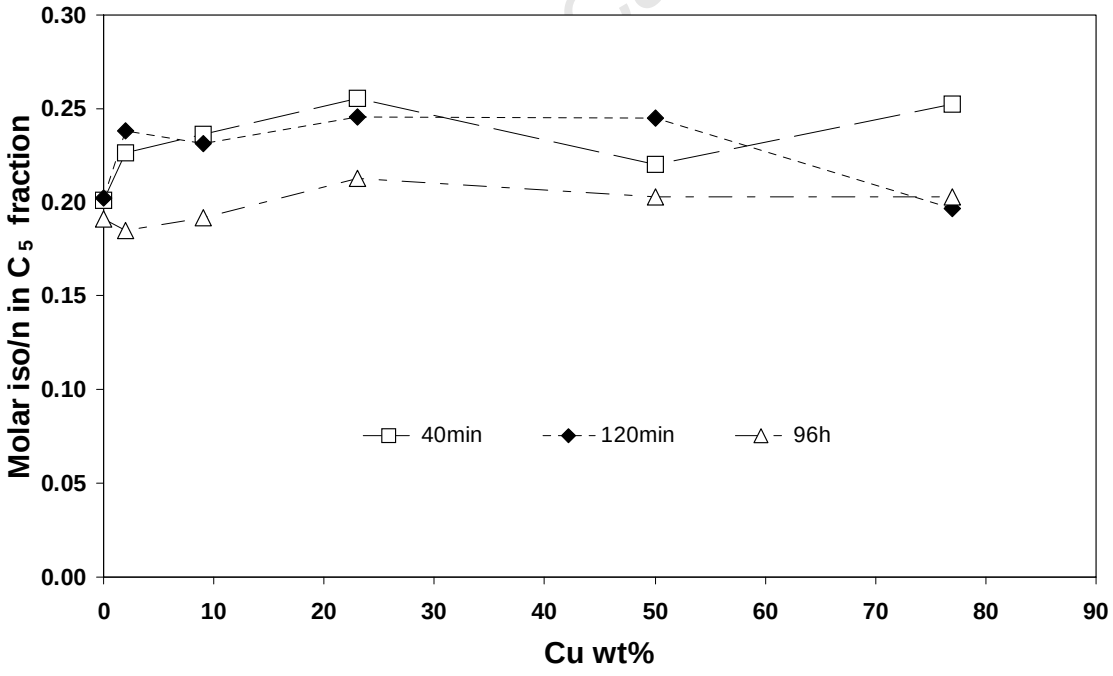

Figure 4.17 Molar ratio of methyl branched to linear hydrocarbon products in the C_5 fraction after 40 and 120 minutes as well as 96 hours during Fischer-Tropsch synthesis in a fixed-bed reactor for the iron-copper catalyst series

4.4.2.5 Organic products: Oxygenate formation

As mentioned previously oxygenates are a main product of Fischer-Tropsch synthesis. It is thought that they are formed either through the insertion of an adsorbed CO molecule into an alkyl-metal bond [1] as proposed by Pichler and Schulz (1970) or through addition of an OH group into an adsorbed ethylidyne species [2] as proposed by Johnston and Joyner (*Johnston and Joyner*, *1993*).

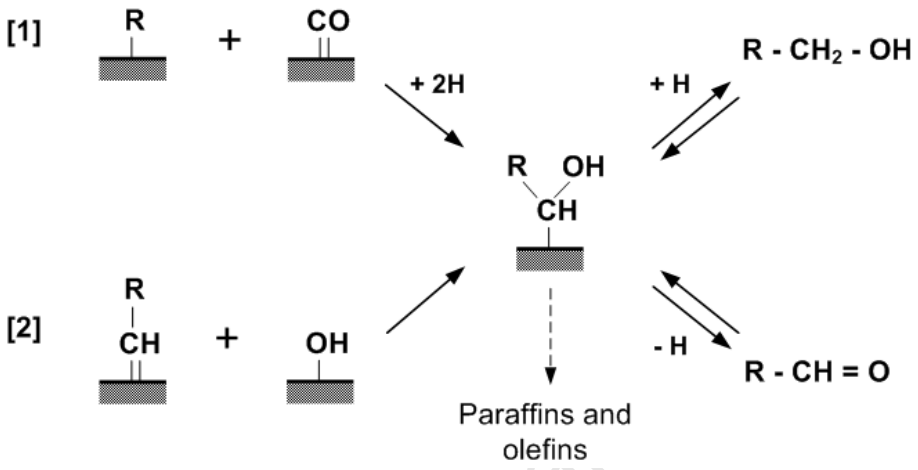

Figure 4.18 shows the fraction of primary alcohols (from C_2 to C_8 carbon number) in the total linear product (including aldehydes and ketones) as a function of carbon number after 96 hours time on-stream. Methanol is not shown, as quantitatively measuring the GC peak was not possible. An immediate trend is discernable in the C_2 fraction, where an increase in copper content increases the fraction of ethanol, with a maximum of around 45 mol% on the 50 wt% Cu catalyst (note that this corresponds to an ethanol selectivity of 4.1 % in the total organic product). Examination of the other carbon number species shows that this trend of even-more-than-doubled alcohol contents holds throughout the carbon number series.

Table 4.19 shows the same fraction only for C_2 and C_3 carbon fractions, but for 40 and 120 minutes, as well as 96 hours, time on-stream. Once again the same trend holds, except in the case of the 9 wt% Cu catalyst, where after 40 minutes it is lower than 2 and 23 but higher than 0 wt% Cu catalyst; however, after 120 minutes it seems to be comparable to the 0 wt% Cu catalyst as opposed to the 2 wt% Cu catalyst. This is probably linked to the low initial activity of the catalyst, as after 96 hours the catalyst has a higher alcohol selectivity for all carbon numbers except in the C_2 fraction where, while lower than the 2 wt% Cu copper catalyst, it is higher than the iron catalyst.

In order to confirm that this effect seen is real and not due to decreased formation rates of other hydrocarbons, the formation rates of the alcohols as a function of copper loading are listed in Table 4.20. There is a definite increase in the formation rate of alcohols up to the 50 wt% Cu catalyst, with increasing copper loading suggesting that copper enhances the formation of alcohols significantly.

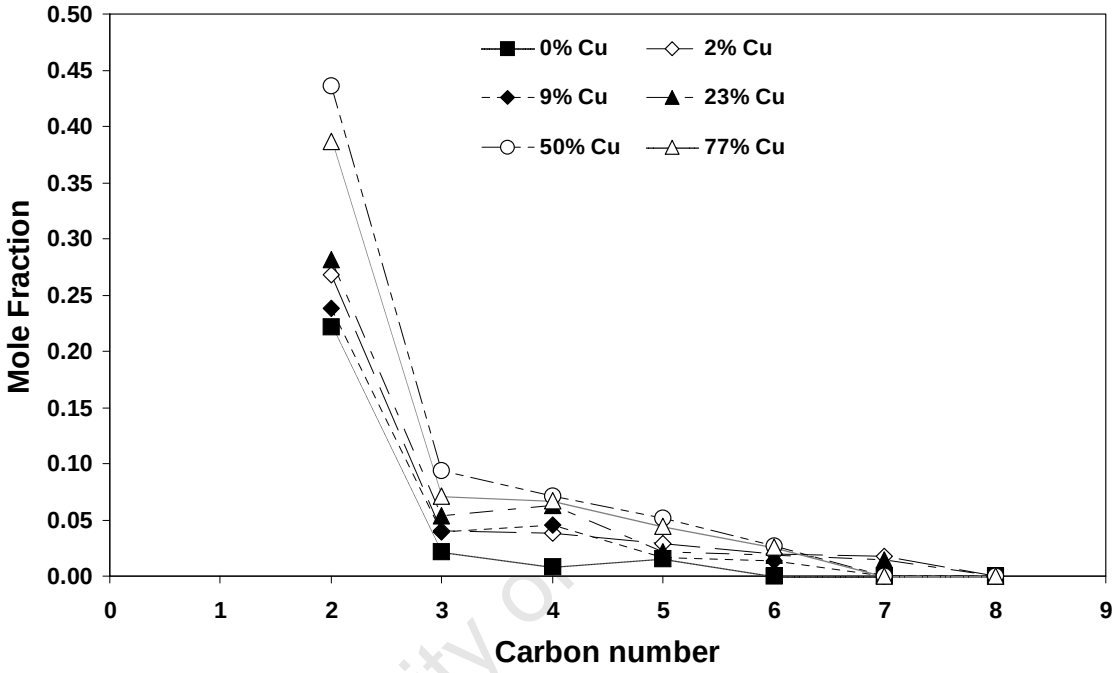

Figure 4.18 Mole fraction of primary alcohols in linear product (including aldehydes and ketones) as a function of carbon number after 96 hours during Fischer-Tropsch synthesis in a fixed-bed reactor for the iron-copper catalyst series

Table 4.19 Mole fraction of primary alcohols in linear product (including aldehydes and ketones) after 40 and 120 minutes, as well as 96 hours, during Fischer-Tropsch synthesis in a fixed-bed reactor for the iron-copper catalyst series

Catalyst (Cu wt%)[a]	Mole fraction of alcohols in linear product					
	C_2	C_3	C_2	C_3	C_2	C_3
	40 min		120 min		96 hr	
0	0.02	-[b]	0.11	0.02	0.22	0.02
2	0.27	0.07	0.24	0.03	0.27	0.04
9	0.12	0.02	0.08	0.03	0.24	0.04
23	0.32	0.04	0.30	0.05	0.28	0.05
50	0.23	0.05	0.41	0.11	0.44	0.09
77	0.19	0.03	0.23	0.04	0.39	0.07

[a] Basis: fully reduced catalyst

[b] C_3 Alcohol not discernable

Table 4.20 Rate of formation of C_2 to C_6 primary linear alcohols after 96 hours during Fischer-Tropsch synthesis in a fixed-bed reactor for the iron-copper catalyst series

Catalyst (Cu wt%)[a]	Rate of formation of alcohols $\left(\frac{\text{mole}}{\text{min} \bullet \text{g Fe}}\right)$				
	C_2	C_3	C_4	C_5	C_6
0	4.7×10^{-6}	2.8×10^{-7}	0.6×10^{-7}	6.9×10^{-8}	–[b]
2	3.7×10^{-6}	3.8×10^{-7}	2.3×10^{-7}	9.8×10^{-8}	4.0×10^{-8}
9	3.8×10^{-6}	4.4×10^{-7}	3.2×10^{-7}	6.3×10^{-8}	3.1×10^{-8}
23	5.4×10^{-6}	6.9×10^{-7}	5.2×10^{-7}	9.1×10^{-8}	4.7×10^{-8}
50	9.8×10^{-6}	12.2×10^{-7}	5.3×10^{-7}	20.0×10^{-8}	6.5×10^{-8}
77	4.1×10^{-6}	4.2×10^{-7}	2.4×10^{-7}	8.9×10^{-8}	3.1×10^{-8}

[a] Basis: fully reduced catalyst

[b] Alcohol peak not quantifiable

While no aldehyde could be identified in the FID chromatogram for the C_2 fraction, all major oxygenates (except butyric acid[10]) could be quantified from the ampoule analyses

[10] The organic acids could not be quantified from the gas analysis due to loss of the acids in the injection method (see Appendix C). This is probably due to adsorption and/or reaction of the acids in the ampoule sample introduction device.

in the C_4 fraction, viz. n-butanol-1, n-butanal and n-butanone. Their molar contents in the linear C_4 product fraction for the catalyst series are shown in Figure 4.19.

An increase in the total C_4 oxygenates is observed with increasing copper promotion; this is mainly due to a pronounced increase of the alcohol (n-butanol-1), apparently to the detriment of the aldehyde, while the ketone formation remains largely unaffected. It may be speculated that copper, on which no products are formed, aids oxygenate formation on the iron surface via spill-over of species needed to form alcohols and aldehydes. Both OH- and CO species are likely to be present on copper surfaces at reaction conditions. Similar to observations made in respect of the olefins and paraffins formed, the more hydrogen-rich product among the alcohol and the aldehyde is found with increasing copper promotion. This may again be due to increased, copper enhanced, hydrogen availability on the iron surface, leading to preferred formation of the alcohol in primary and, upon re-adsorption of the aldehyde, secondary reactions. The latter reaction might also occur on the surface of copper itself.

It may be noted though, that even at high copper promotion the partial equilibrium of aldehyde hydrogenation to alcohol is not yet reached; the closest to this ratio is the 50 wt% copper catalyst (Table 4.21). Table 4.21 also includes actual and theoretical equilibrium ratios of butan-2-one to butanol and butanal respectively. It can be seen that the actual ratios are not close to the theoretical ones, and it can be assumed that there is indeed no interaction between the ketone and the alcohol or aldehyde in the same carbon number fraction. The co-feeding work described in section 4.6 will shed some light on the possible formation routes of methyl-ketones via interaction with other oxygenates.

Secondary reactions of oxygenates can also include the less facile hydrogenation to the corresponding paraffin (*Tau et al.*, *1988*), a reaction which was more recently reported to play a minor, if any role on iron oxide and iron carbide catalysts (*Wang and Davis*, *1999*). This effect may have come into play, on copper itself, at the highest level of copper promotion, where a decrease in the molar content of all oxygenates in the C_4 fraction is observed. Again, the above effects are believed to be solely due to copper promotion, as no changes of hydrogen partial pressure, which can influence primary and secondary reactions in Fischer-Tropsch synthesis (*Dry*, *1981*), were observed.

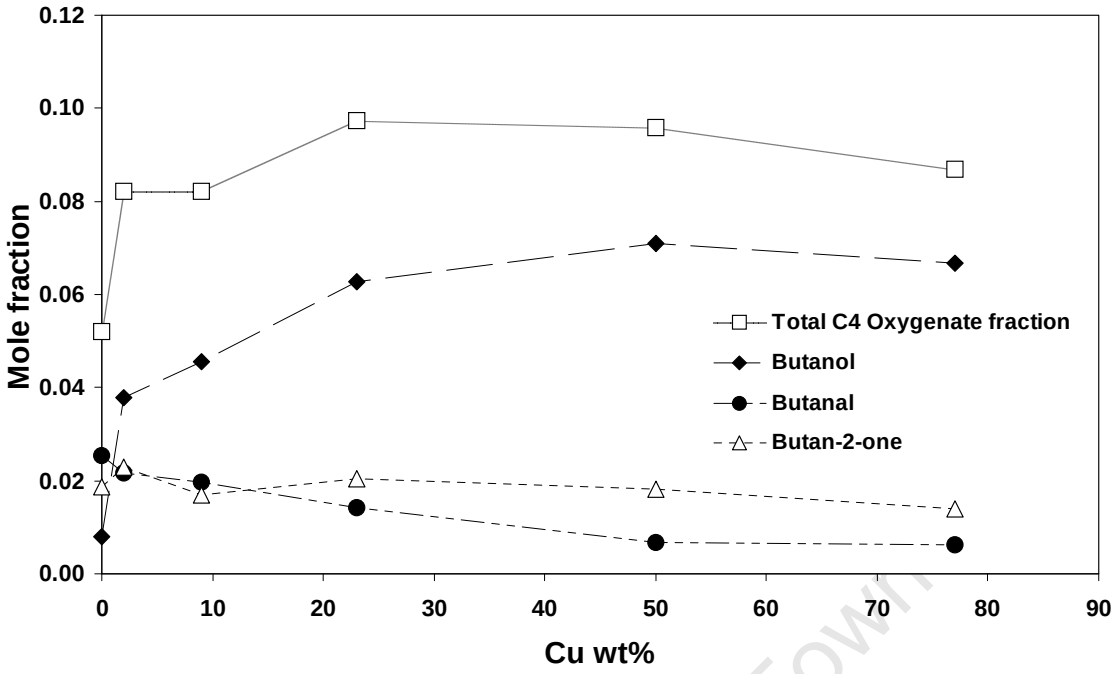

Figure 4.19 Mole fraction of oxygenates in linear C_4 products after 96 hours during Fischer-Tropsch synthesis in a fixed-bed reactor for the iron-copper catalyst series

Table 4.21 Equilibrium ratios of C_4 oxygenates (excluding butyric acid) after 96 hours during Fischer-Tropsch synthesis in a fixed-bed reactor for the iron-copper catalyst series

Reaction and ratio		**Product ratios**					
		0 wt% Cu[a]	2 wt% Cu	9 wt% Cu	23 wt% Cu	50 wt% Cu	77 wt% Cu
1-Butanol ⇔ Butan-2-one + H_2	Eq[b]	29.9	32.3	32.0	28.3	33.8	28.3
(Butan-2-one/1-Butanol)	Obs[c]	2.30	0.60	0.37	0.33	0.26	0.21
Butanal ⇔ Butan-2-one	Eq	381	381	381	381	381	381
(Butan-2-one/Butanal)	Obs	0.73	1.06	0.86	1.44	2.77	2.25
Butanal + H_2 ⇔ 1-Butanol	Eq	12.8	11.8	11.9	13.5	11.3	13.5
(1-Butanol/ Butanal)	Obs	0.32	1.75	2.32	4.44	10.7	10.7

[a] Basis: Fully reduced catalyst

[b] Eq: Expected ratio at equilibrium

[c] Obs: Observed product ratios

4.4.3 Effect of potassium

The addition of potassium to iron Fischer-Tropsch catalysts is of paramount importance; it increases the average molecular weight of the products, the olefin to paraffin ratio and the yield of C_2 and other oxygenates (*Arakawa and Bell*, *1983*). This increase of selectivity typically levels off at sufficiently high potassium loadings.

In calculating the potassium loading on the catalysts, the assumption was made that it would spread evenly over the metal surfaces of both the iron and copper (see Figure 4.20 [1]) and thus potassium loading was increased as the overall metal loading was increased. However, from the TPR data (Figure 4.3 and Figure 4.4) it was deduced that the potassium did not, in fact, spread evenly over the entire metal surface but was mainly on the iron (Figure 4.20 [2]). In order to test if the results reported above were influenced by effects of uneven potassium distribution, as opposed to a copper promotional effect, a pure iron catalyst with 10 g potassium per 100 g iron was produced (Figure 4.20 [3]) and compared with the pure iron and 50 wt% co-precipitated copper catalysts, both of which had a potassium loading of 5 g potassium per 100 g of metal. The theoretical, AAS and SEM analyses of the iron and potassium loadings of the calcined high-potassium-loaded pure iron catalyst compared to the 0 wt% Cu catalyst described earlier are shown in Table 4.22.

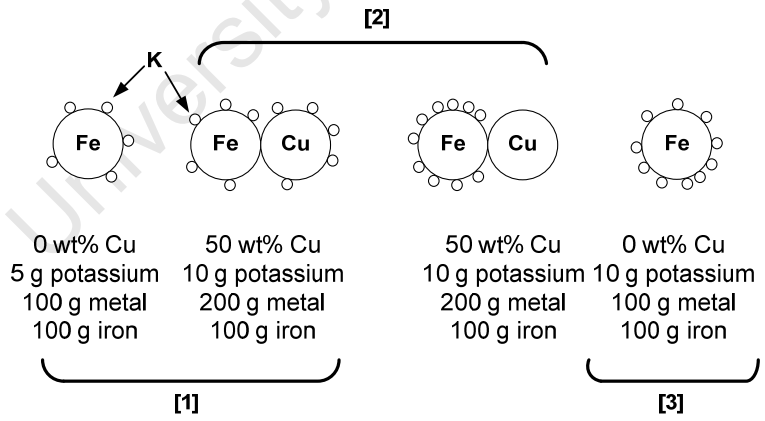

Figure 4.20 Illustration depicting the effect of potassium loadings on iron and copper-iron catalysts

Table 4.22 Theoretical and actual iron and potassium loadings and mass ratios as determined by AAS and SEM for the high potassium loaded pure iron catalyst

Catalyst	Fe : K Theory	Fe : K AAS	Fe : K SEM
Pure Fe (low potassium)	100 : 5	100 : 1.7	100 : 1.2
Pure Fe (high potassium)	100 : 10	100 : 5.1	100 : 8.3

Examination of Table 4.23 shows that all catalysts have a similar carbon conversion after 96 hours and are thus readily comparable. There also seems to be no effect on the chain growth probability, this is expected as the chain growth probability at this temperature is limited in the region of 0.7 (*Jager and Espinoza, 1995*) and will not increase with potassium loading. By comparing the C_2 olefins in hydrocarbon product for the pure iron catalysts, the effect of potassium loading can readily be seen. An increase in potassium increases the olefin yield in C_2 but not in C_3, therefore the primary selectivity seems unaffected. The same trend can be seen slightly in the alcohol fraction.

However when comparing the high-potassium-loaded catalyst to the iron-copper catalyst, the trend in the C_2 olefin content is not as expected with high-potassium loadings, suggesting copper plays a role in the secondary re-adsorption and conversion of the olefins. Once again, by comparing the iron catalysts to the copper-iron catalyst oxygenates content in the C_4 fraction, the effect can definitely not be ascribed only to a potassium effect. Clearly copper plays a role in both the formation of alcohols and increasing the oxygenate fraction in the organic product.

Table 4.23 Comparison of results for different potassium loadings on iron and copper-iron catalysts after 96 hours during Fischer-Tropsch synthesis in a fixed-bed reactor

Catalyst	Conversion (CO+CO_2) %	Chain growth probability $\alpha_{C_{3-10}}$	S_{CH_4} (C- %)	$x_i C^{=}$ [a]		$x_i C^{-OH}$ [b]		$x_i C^{-(O)}$ [c]
				C_2	C_3	C_2	C_4	C_4
0% Cu 5 g K/100 g Fe	43.7	0.69	15.2	0.78	0.83	0.22	0.008	0.052
0% Cu 10 g K/100 g Fe	41.4	0.64	11.3	0.84	0.83	0.24	0.019	0.059
50 wt% Cu 10 g K/100 g Fe	49.0	0.67	13.2	0.71	0.83	0.44	0.071	0.096

[a] Mole fraction of olefins in hydrocarbon product

[b] Mole fraction of alcohols in linear hydrocarbon product plus alcohols

[c] Mole fraction of total oxygenates in linear hydrocarbon product plus oxygenates

4.4.4 Effect of co–precipitation

To test if the copper and iron needed to be co-precipitated in order to achieve the above results, or if there was a spill-over effect from the copper to the iron a 50:50 mixture of precipitated iron and copper catalysts was prepared. Both catalysts were promoted with 5 g potassium per 100 g metal. The results of these tests are shown in Table 4.24. From the results it can be seen that the physical mixture shows an alcohol selectivity similar to, but slightly higher than that of the iron catalyst for the C_2 fraction, but is much higher (although not quite the same as the co-precipitated catalyst) for C_4. This suggests that some spill-over effect is occurring, but that to achieve the higher selectivities the copper and iron need to be closer than can be achieved by just mixing.

Table 4.24 Comparison of results for a 50 wt% copper co-precipitated copper-iron catalyst to a manual 50:50 mixture of precipitated iron and copper after 96 hours during Fischer-Tropsch synthesis in a fixed-bed reactor

Catalyst	Conversion	Chain growth probability	S_{CH_4}	x_i $C^{=}$ [a]		x_i C^{-OH} [b]		x_i $C^{-(O)}$ [c]
	$(CO+CO_2)$ %	$\alpha_{C_{3-10}}$	(C- %)	C_2	C_3	C_2	C_4	C_4
0% Cu	43.7	0.69	15.2	0.78	0.83	0.22	0.008	0.052
50 wt% Cu co-precipitated	49.0	0.67	13.2	0.71	0.83	0.44	0.071	0.096
50 wt% Cu manual mix	51.0	0.68	13.4	0.78	0.81	0.27	0.053	0.083

[a] Mole fraction of olefins in hydrocarbon product

[b] Mole fraction of alcohols in linear hydrocarbon product plus alcohols

[c] Mole fraction of total oxygenates in linear hydrocarbon product plus oxygenates

4.4.5 Summary of results using a fixed-bed reactor

While the pure copper catalyst showed no Fischer-Tropsch activity under these reaction conditions, the addition of copper to iron catalysts had no effect on the overall activity, the methane selectivity and the chain growth probability (α).

Copper was found to affect primary formation of olefins and oxygenates; it can further impact on secondary conversion of olefins and oxygenates. It has been proposed that these effects are due to higher, copper enhanced, hydrogen availability on the iron surface, leading to more hydrogen rich primary product, but also to enhancement of secondary reactions of olefins and oxygenates. These reactions might also occur on metallic copper itself. The most pronounced effect of copper is that on oxygenate selectivity, in that more than double the formation rates of alcohols are obtained on copper rich catalysts.

It may be postulated that copper, which does not promote CO bond dissociation, supplies the iron surface with molecular CO and/or OH species, which might be involved in the formation of oxygenates in the Fischer-Tropsch synthesis. To achieve this selectivity improvement the catalyst should preferably be prepared in such a way that copper is in close contact with iron, e.g. via co-precipitation.

It can further be noted that only minor changes of product selectivity were observed as a function of time on-stream. These changes were mainly increased initial methane

selectivity and lower chain growth probability (as generally observed by others (*Schulz et al.*, *1999* and *Claeys and Schulz*, *2004*)), and higher contents of methyl-branched compounds on the copper promoted catalysts. Such changes are believed to be due to structural changes of the catalysts during Fischer-Tropsch synthesis (which may have occurred rapidly at the high temperature conditions applied in this work) and the gradual establishment of the kinetic Fischer-Tropsch regime (*Schulz et al.*, *1999*), but generally these effects are not very pronounced with iron-based catalysts compared to the other Fischer-Tropsch active metals such as cobalt, nickel and ruthenium (*Schulz 2003a, 2003b* and *Claeys et al.*, *2003*).

4.5 Fischer-Tropsch synthesis - Berty reactor

A Berty reactor was used in order to produce sufficient quantities of oil and water samples for GC and GC/MS analyses of the catalyst series and for co-feeding of C_8 oxygenates on the 0 and 50 wt% Cu catalysts. The Berty reactor provides a gradientless reactor system (Appendix C), and is ideally suited for these kinetic tests as effects of varying concentration profiles of reactants and products (which can also impact on the iron catalyst phases formed) is negated. The re-testing of the catalysts at constant reactor partial pressures is discussed in this section while the co-feeding work is discussed in section 4.6.

The catalytic performance of the catalyst series was tested in the Berty reactor with a loading of 2.4 g of iron per sample. Prior to Fischer-Tropsch synthesis catalysts were activated under hydrogen, in a fluidized reactor, following the same reduction procedure mentioned previously (heating under hydrogen at a rate of 1 ºC/min to 100 ºC, holding for 1 hour, then 1 ºC/min to 400 ºC and holding for 16 hours, at ambient pressure and a space velocity of 4000 ml(NTP)/g_{Fe}/h), then transferred to the Berty reactor under argon. All tests were conducted for a minimum of 96 hours at a reaction temperature of 300 °C, a pressure of 21 bar(a) and a hydrogen to carbon monoxide to carbon dioxide ratio of 4:1:1. Steady state conversion was generally achieved after 36 to 48 hours but selectivity results have been limited to 96 hours for ease of comparison to the fixed-bed results. The carbon mass balances achieved in these experiments are around 100 +/- 8%, and run details are listed in Appendix I. It is also this series of experiments from

which the spent catalyst samples for characterisation were obtained, which are described in section 4.3.

4.5.1 Catalyst activity

Catalyst activity, expressed as carbon conversion (sum of carbon monoxide and carbon dioxide conversion) was monitored on a daily basis and is shown in Figure 4.21. As the reactor is a continuously stirred reactor and therefore has a high recycle, no differential conversions as a function of time would be meaningful; so only daily readings were taken.

After 24 hours or 1 day on-stream all the catalysts show a similar conversion of between 30 and 40%. Over the time period monitored all catalysts show comparable activity and steady state behaviour. This implies that the catalysts reach a steady state of conversion and selectivity (not shown) within 24 hours, but once again comparison of product selectivity has only been done at 96 hours on-stream.

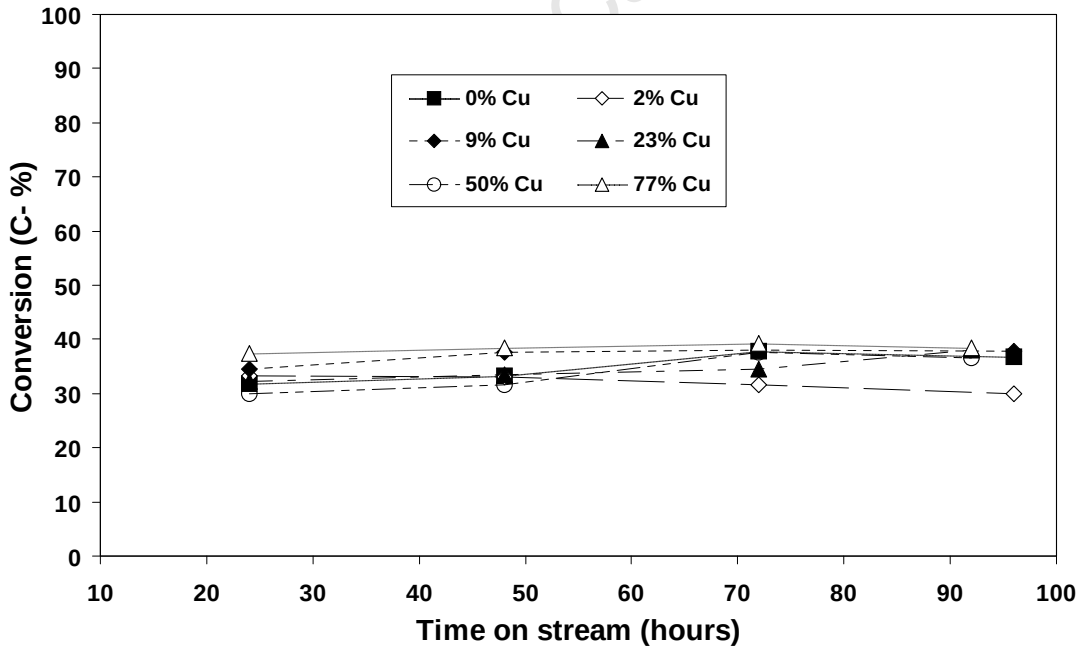

Figure 4.21 Carbon conversion as a function of time for the time period of 24 to 96 hours in a Berty reactor for the iron-copper catalyst series

The characterisation of the spent catalysts showed mainly Hägg carbide with decreasing crystallite size (50 nm to 9 nm) in catalysts with increased copper promotion (see

section 4.3). Assuming that this iron phase is the active phase for Fischer-Tropsch synthesis as reported by Anderson (1984), one would expect an increased conversion with increased copper promotion. This was however not obtained in this study. Some recent studies (*Barkhuizen et al.*, *2006*, *Bezemer et al.*, *2006, Mabaso*, *2005,* (*Mabaso et al.*, *2006* and *Welker et al.*, *2006*) indeed seem to suggest that the Fischer-Tropsch reaction is structure sensitive on the different Fischer-Tropsch-active metals, in that smaller crystallites showed lower activity than larger ones. This effect, although only reported for crystallites smaller than 10 nm, can counteract the expected higher activity of the smaller crystallites in this study.

It can be noted that conversions reported here are slightly lower than those reported in the fixed-bed tests; this is to be expected as conversions in stirred reactors are generally lower than those found in fixed-bed reactors for first order reactions (the Fischer-Tropsch reaction over iron is indeed regarded as first order with respect to hydrogen partial pressure over a wide range of conditions (*Claeys*, *1997* and *Claeys and Schulz*, *2004*)), due to the large volume difference necessary to achieve the same conversions (*Scott Fogler*, *1999*).

4.5.2 Inorganic product formation

The inorganic products of the Fischer-Tropsch synthesis are mainly water and carbon dioxide. These products, along with the feed compounds, can affect the organic product formation, and iron catalyst phase, in different ways depending on their concentration within the reactor. A study of these products is necessary in order to determine the effect of the catalyst as opposed to that of the inorganic gasses within the reactor.

4.5.2.1 Inorganic product formation: Exit partial pressures

Table 4.25 Shows the exit partial pressures (and thus the reactor partial pressures) of hydrogen, carbon monoxide, carbon dioxide and water for the catalyst series in the Berty reactor after 96 hours time on-stream. Comparison of the partial pressures shows no real variation for the catalyst series.

Table 4.25 Hydrogen, carbon monoxide, carbon dioxide and water exit partial pressure after 96 hours time on-stream during Fischer-Tropsch synthesis in a Berty reactor for the iron-copper catalyst series

Catalyst (Cu wt%)[a]	$p_{[H_2]}$ (bar)	$p_{[CO]}$ (bar)	$p_{[CO_2]}$ (bar)	$p_{[H_2O]}$ (bar)
0	12.8	0.7	4.5	2.3
2	13.0	0.9	4.4	2.0
9	11.5	0.5	4.8	3.3
23	12.5	0.8	4.3	2.5
50	12.8	0.7	4.4	2.2
77	11.8	0.6	4.9	2.6

[a] Basis: fully reduced catalyst

4.5.2.2 Inorganic product formation: Water gas shift equilibrium

As mentioned previously (2.1.1) the Fischer-Tropsch reaction can be simplified as:

$$nCO + 2nH_2 \Rightarrow -(CH_2)_n- + nH_2O \qquad (4.2)$$

where the production of water corresponds to the formation of Fischer-Tropsch product. However, on iron catalysts the water-gas shift reaction is also present and converts the produced water to CO_2. Using the exit partial pressures from Table 4.25 the equilibrium gas phase ratios for the experiments with the different catalysts can be determined (see Table 4.26) and compared to the equilibrium gas phase constant at the reaction temperature.

$$K_{p_{WGS}} = \frac{p[CO_2]\, p[H_2]}{p[CO]\, p[H_2O]} \qquad (4.3)$$

At 300 °C the equilibrium gas phase constant (K_p) of the water gas shift reaction is equal to 39.2 as calculated using Daubert *et al*. (1999).

Table 4.26 Water-gas shift chemical equilibrium ratios after 96 hours time on-stream during Fischer-Tropsch synthesis in a Berty reactor for the iron-copper catalyst series

Catalyst (Cu wt%)[a]	K_{pWGS}
0	34.5
2	32.1
9	35.5
23	26.7
50	36.6
77	38.9

[a] Basis: fully reduced catalyst

It appears that all catalysts are near to or at equilibrium for the water-gas shift reaction, as typically found at high temperature conditions (*Dry, 1981*).

4.5.3 Organic product formation: VOC

This section and its relevant sub-sections discuss the product contents as directly obtained through FID analysis from ampoule samples (except in the case of methane, where the gas was analysed through the online gas chromatograph). Section 4.5.4 discusses the composition of the collected oil and water fraction.

Again, some wax/heavy oil formation (dark brown in colour) was observed during Fischer-Tropsch synthesis, but not analysed; qualitatively the wax formation does not correspond well with the chain growth probabilities shown in section 4.5.3.2 where an alpha value well above 0.7 would be expected (*Sie et al., 1988*). However for an initial direct comparison of each catalyst the organic product is sufficient in the range that is shown.

4.5.3.1 Organic products: Methane

The methane selectivities after 96 hours time on-stream are detailed in Table 4.27. The selectivities are similar for all catalysts, but slightly lower than those obtained in the fixed-bed reactor detailed in Table 4.14. This lower methane selectivity could be related to partial pressures which are different from those found locally in the fixed-bed reactor, where relatively hydrogen-rich and CO-poor conditions exist, which promote

the formation of methane. It seems that copper causes a slight, if any, increase of methane selectivity.

Table 4.27 Methane selectivities after 96 hours time on-stream during Fischer-Tropsch synthesis in the Berty reactor for the iron-copper catalyst series

Catalyst (Cu wt%)[a]	S_{CH_4} (C- %) 96 hr
0	8.0
2	9.1
9	9.4
23	8.9
50	10.4
77	11.6

[a] Basis: fully reduced catalyst

4.5.3.2 Organic products: Chain growth

Table 4.28 shows the chain growth probability for each catalyst after 96 hours for carbon numbers between 3 and 8, as well as the chain growth probability after 96 hours for carbon numbers 8 to 14. The values for all catalysts are similar in both carbon number ranges and perhaps a slight, if any, decrease of chain growth probability can be seen. The values are also similar to those obtained in the fixed-bed reactor (detailed in Table 4.15) where no clear effect of copper was discernable.

Table 4.28 Chain growth probabilities from the VOC after 96 hours time on-stream during Fischer-Tropsch synthesis in the Berty reactor for the iron-copper catalyst series

Catalyst (Cu wt%)[a]	**Chain growth probability** $\alpha_{C_{3-8}}$ 96 hr	$\alpha_{C_{8-14}}$ 96 hr
0	0.68	0.70
2	0.65	0.66
9	0.67	0.62
23	0.66	0.68
50	0.66	0.65
77	0.65	0.63

[a] Basis: fully reduced catalyst

4.5.3.3 Organic products: Olefin formation

Figure 4.22 as well as Table 4.29 shows the molar content of linear olefins in the total linear hydrocarbon product as a function of carbon number after 96 hours. Comparison with Figure 4.15 and Table 4.16, i.e. results obtained in tests in the fixed-bed reactor, shows two major differences.

Firstly, the C_2 fraction for all catalysts has a lower overall olefin content (60 – 70%) compared to the fixed-bed reactor tests (70 – 80%) indicating more pronounced secondary ethene conversion. This difference between the two reactor systems is probably due to generally preferred secondary reactions in the back-mixed Berty reactor. At higher carbon numbers constant olefin contents in the C_3 to C_{10} fractions are found for all catalysts.

The second difference is the noteworthy drop in olefin content for the 77 wt% Cu catalyst. As this result seems to be carbon number independent, it suggests that there is a primary shift in the product selectivity to a more paraffinic product, as opposed to a secondary effect of olefin re-adsorption. The reason for these result's not being so obvious in the fixed-bed tests could possibly be the gradient concentrations of reactants and products along the fixed-bed reactor, while constant partial pressures are present in the tests using the Berty reactor.

It therefore again appears that copper impacts on both secondary and primary selectivity, via secondary hydrogenation of ethene and a primary shift to a more paraffinic product. Both effects can be explained by increased hydrogen availability promoted by copper, possibly via spill-over of hydrogen which is easily activated on copper, to the iron phases of the catalyst where the FT-reaction is taking place. In addition, secondary olefin hydrogenation is likely also to occur on the metallic copper surface.

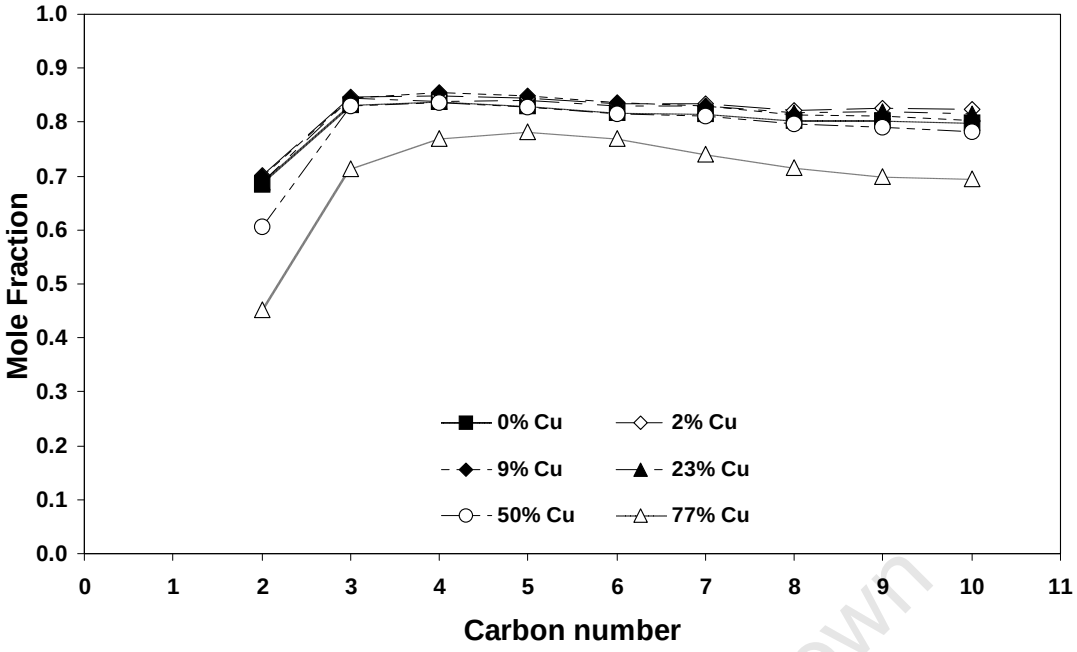

Figure 4.22 Mole fraction of linear olefins in linear hydrocarbon product as a function of carbon number after 96 hours in a Berty reactor for the iron-copper catalyst series

Table 4.29 Mole fraction of linear olefins in linear hydrocarbon product after 96 hours in a Berty reactor for the iron-copper catalyst series

Catalyst (Cu wt%)[a]	Mole fraction of olefins in linear hydrocarbon product	
	C_2	C_3
	96 hr	
0	0.68	0.83
2	0.70	0.85
9	0.70	0.84
23	0.69	0.84
50	0.61	0.83
77	0.45	0.71

[a] Basis: fully reduced catalyst

Figure 4.23 shows the molar content of α-olefins in the total olefin fraction as a function of carbon number after 96 hours. A high fraction of α-olefins (>95%) for all carbon numbers indicates high primary product selectivity with little to no olefin double bond isomerisation. Once again the 77 wt% Cu catalyst has much lower values than the rest of the catalyst series and this value decreases with an increase in carbon number.

This suggests pronounced double bond shift isomerisation could be caused by high concentrations of copper, which again can be explained by increased availability of hydrogen on the surface of the iron phases facilitated by copper. This chemisorbed hydrogen then enhances re-adsorption of olefins and their secondary reactions. In addition double bond shift isomerisation can occur on the metallic surface of copper crystallites.

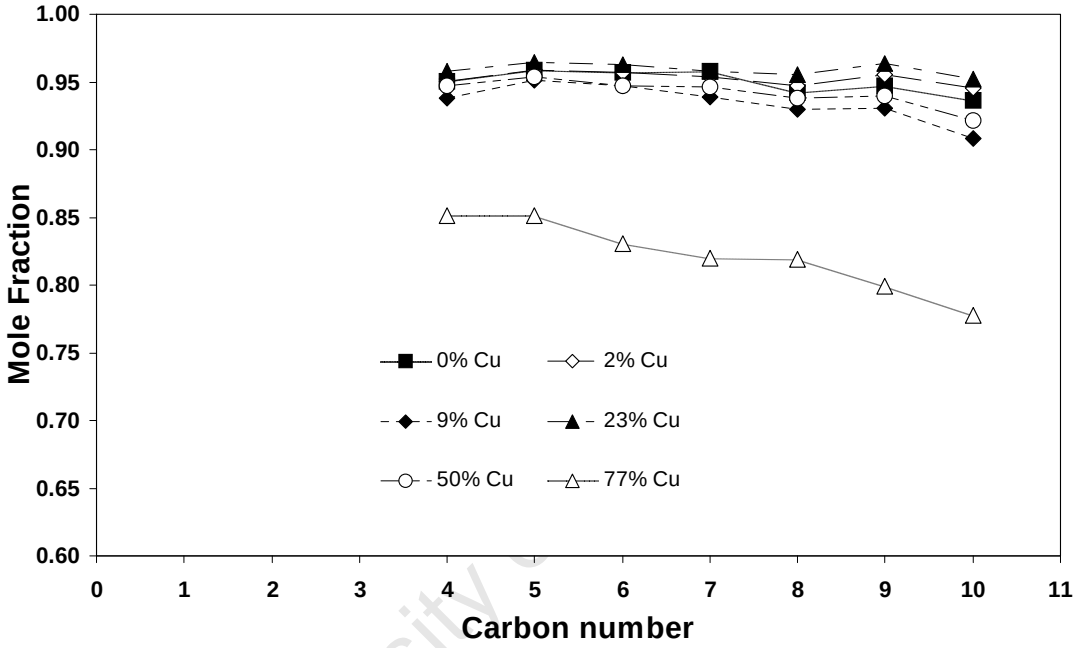

Figure 4.23 Mole fraction of α–olefins in linear olefins as a function of carbon number after 96 hours time on-stream in a Berty reactor for the iron-copper catalyst series

4.5.3.4 Organic products: Branched products

Figure 4.24 shows the molar ratio of methyl-branched to linear hydrocarbon products in the C_5 fraction. The result is similar to that of Figure 4.17 for the fixed-bed tests where a constant ratio seems to hold at around 0.2 at steady state conditions for all catalysts.

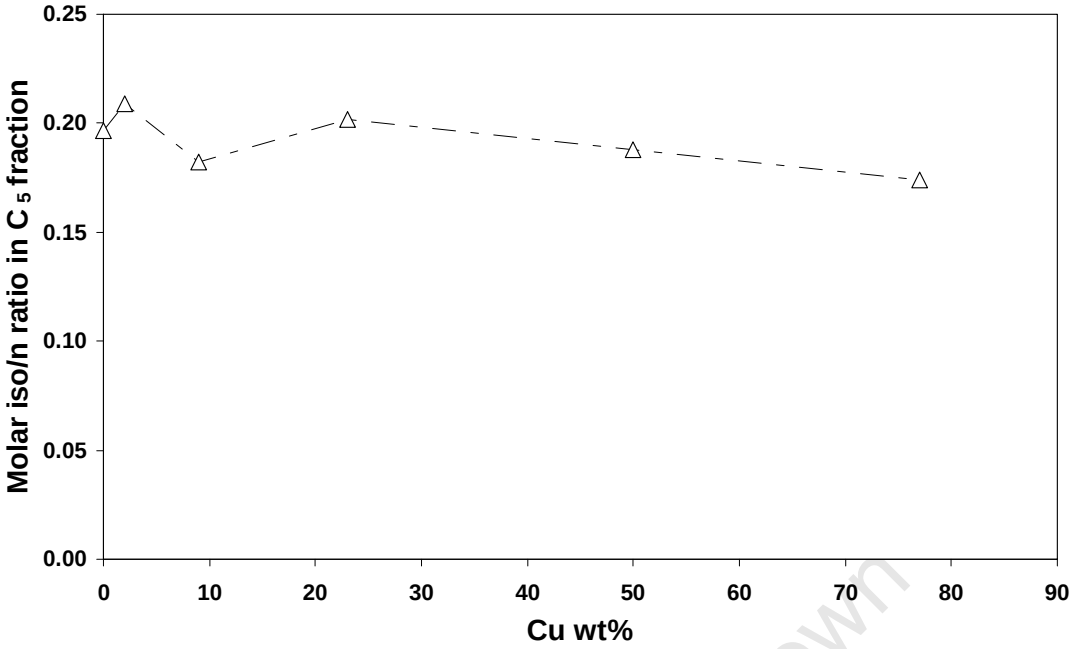

Figure 4.24 Mole ratio of methyl-branched to linear hydrocarbon products in the C_5 fraction after 96 hours in a Berty reactor for the iron-copper catalyst series

4.5.3.5 Organic products: Oxygenate formation

Figure 4.25 shows the fraction of linear alcohols (from C_2 to C_8 carbon number) in the linear product (including aldehydes and ketones) as a function of carbon number after 96 hours time on-stream. Compared to the fixed-bed results in Figure 4.18 there is really only one major difference; the 50 wt% Cu catalyst is no longer the maximum, but is now the 77 wt% Cu catalyst. Increased alcohol content can also be found in higher carbon number fractions, although this effect seems to be less pronounced in the results of the experiments conducted in the Berty reactor.

Table 4.30 shows the mole fraction of linear alcohols in the linear product for C_1 to C_3. It appears that in the C_1 fraction for all the catalysts except the 77 wt% Cu catalyst copper loading has no effect.

In this series of experiments acetaldehyde could be quantified in the C_2. It is known that this compound easily interacts with ethanol as shown below:

$$\text{Acetaldehyde} + \text{H2} \Leftrightarrow \text{Ethanol}$$

The actual ratio of ethanol to acetaldehyde is shown in Table 4.31; it can be seen that the ratio is still far away from that expected at equilibrium, although it increases with

increased copper promotion, again indicating that copper facilitates the formation of hydrogen richer products. This interaction and result is discussed in detail earlier in section 4.4.2.5.

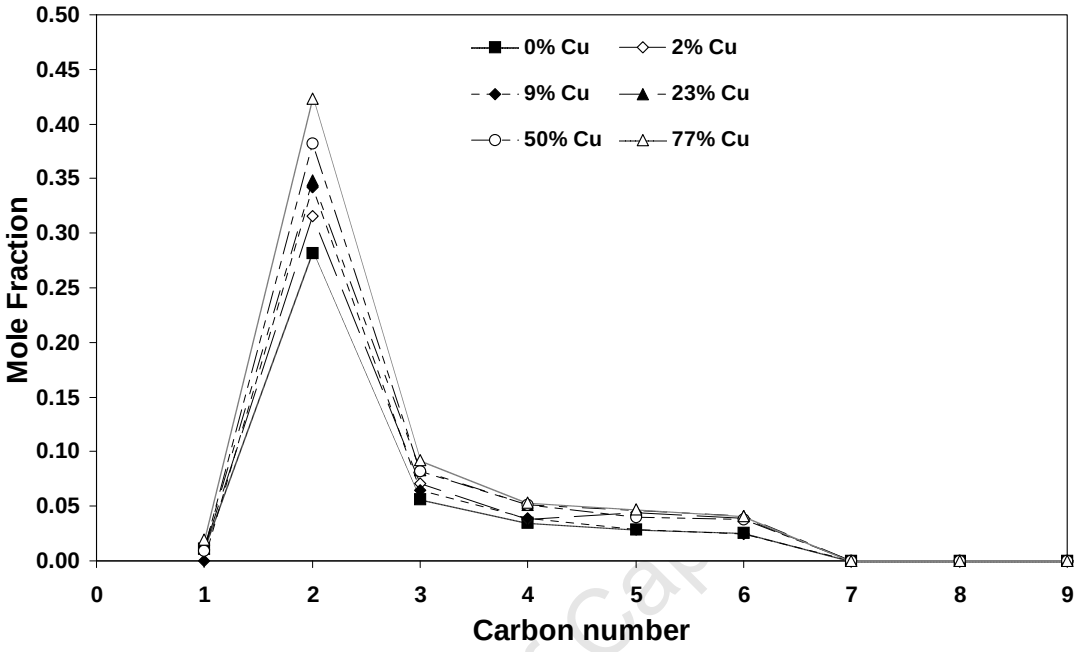

Figure 4.25 Mole fraction of alcohols in linear organic product (including aldehydes and ketones) as a function of carbon number after 96 hours during Fischer-Tropsch synthesis in a Berty reactor for the iron-copper catalyst series

Table 4.30 Mole fraction of alcohols in linear organic product (including aldehydes and ketones) after 96 hours during Fischer-Tropsch synthesis in a Berty reactor for the iron-copper catalyst series

Catalyst (Cu wt%)[a]	**Mole fraction of alcohols in linear product**		
	C_1	C_2	C_3
0	0.011	0.28	0.056
2	0.010	0.32	0.071
9	-[b]	0.34	0.065
23	0.011	0.35	0.083
50	0.010	0.38	0.082
77	0.020	0.42	0.092

[a] Basis: fully reduced catalyst

[b] Alcohol peak not discernable

Table 4.31 Equilibrium ratios of acetaldehyde and ethanol after 96 hours during Fischer-Tropsch synthesis in the Berty reactor for the iron-copper catalyst series

Reaction and ratio		Product ratios					
		0 wt% Cu[a]	2 wt% Cu	9 wt% Cu	23 wt% Cu	50 wt% Cu	77 wt% Cu
Acetaldehyde + H_2 ⇔ Ethanol	Eq[b]	138.5	140.8	125.0	135.6	138.4	128.4
Ethanol/Acetaldehyde	Obs[c]	5.3	7.7	6.3	10.5	14.7	16.2

[a] Basis: Fully reduced catalyst

[b] Eq: Expected ratio at equilibrium

[c] Obs: Observed product ratios

In the case of the organic products captured in the VOC in the Berty reactor the aldehydes and ketones could be well quantified up to their C_6 and C_7 fractions respectively. Figure 4.26 shows the fraction of aldehydes in the linear organic product. A definite trend is discernable: the aldehyde fraction can be seen to be decreasing with an increase in the copper loading of the catalysts.

Figure 4.27 shows the fraction of ketones in the linear organic product. No trend seems to be discernable with respect to copper loading.

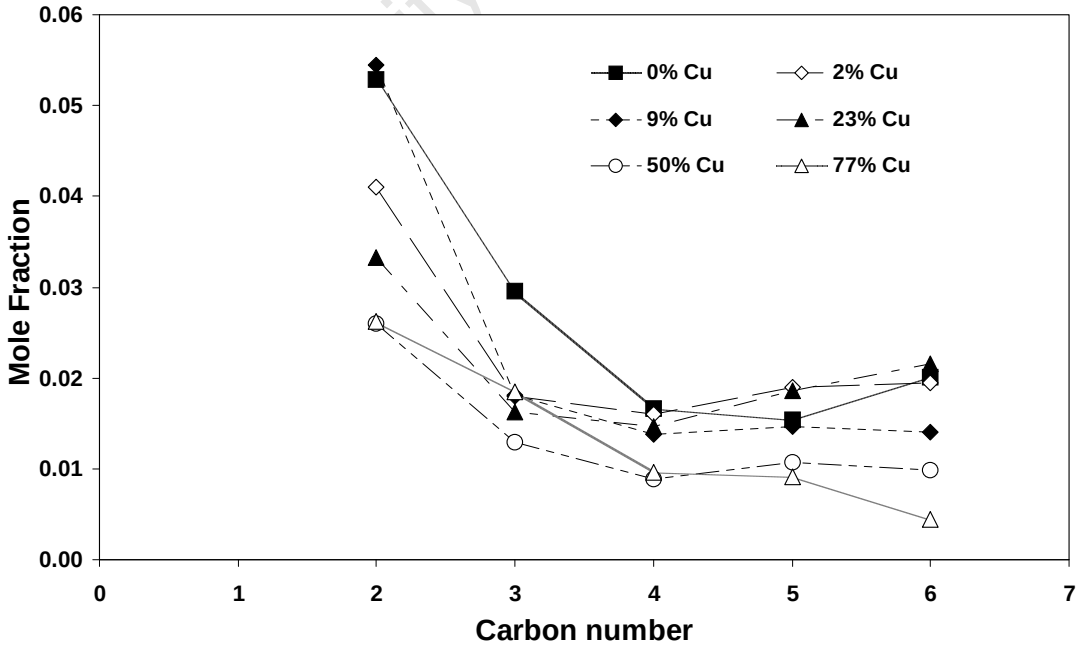

Figure 4.26 Mole fraction of aldehydes in linear organic products as function of carbon number after 96 hours during Fischer-Tropsch synthesis in a Berty reactor for the iron-copper catalyst series

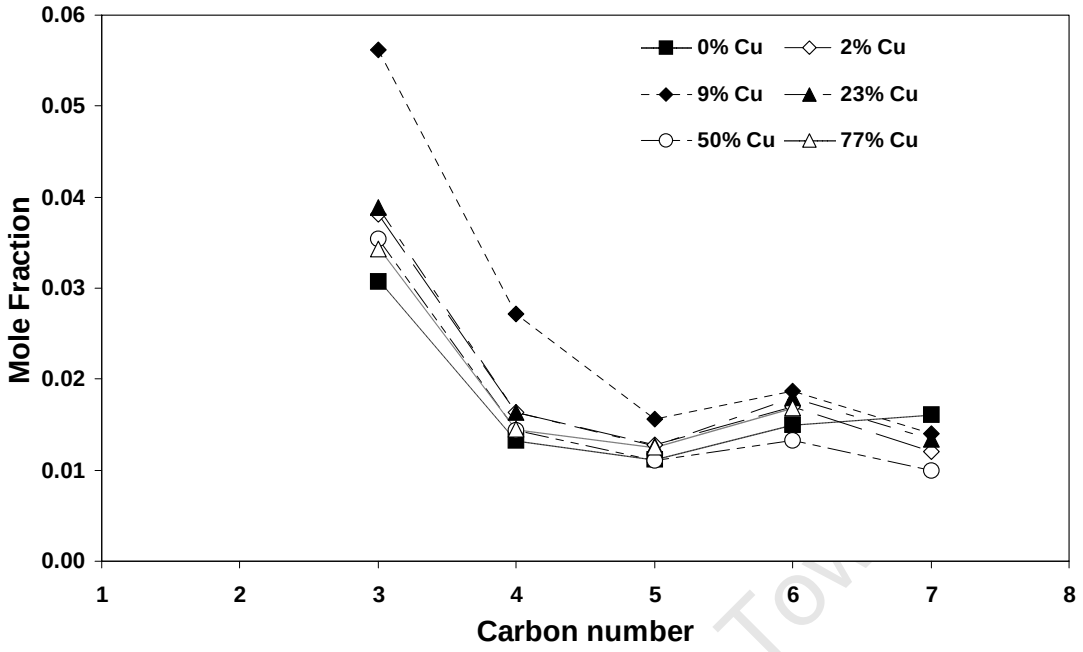

Figure 4.27 Mole fraction of ketones in linear organic products as function of carbon number after 96 hours during Fischer-Tropsch synthesis in a Berty reactor for the iron-copper catalyst series

Finally, Figure 4.28 shows the mole fraction of the linear oxygenates in the C_4 fraction (excluding butyric acid[11]) so a direct comparison with the corresponding fixed-bed data (Figure 4.19) can be made. A lower overall oxygenate fraction than found in the fixed-bed reactor is seen; this is most likely caused by the high recycle inside the Berty reactor and subsequent preferred secondary conversion in this reactor system. A comparison of product ratios with respect to partial thermodynamic equilibrium (Table 4.32) of the data obtained in the two reactor systems shows that the alcohol-aldehyde equilibrium ratios seem to have been reached on the 50 and 77 wt% Cu catalysts in the Berty reactor, suggesting fast product interaction. Once again, the more hydrogenated oxygenate product is favoured as copper promotion increases. The partial equilibria of butan-2-one with 1-butanol and butanal are also considered in Table 4.32 and it is obvious that little or no interaction between the ketone and the corresponding

[11] The organic acids could not be quantified from the gas analysis due to a loss in the acids in the injection method (see Appendix B). This is probably due to adsorption and or reaction of the acids in the ampoule sample introduction device.

oxygenates exists. A closer analysis of possible formation routes of methyl-ketones is given in section 4.6 where co-feeding of different C_8 oxygenates is discussed.

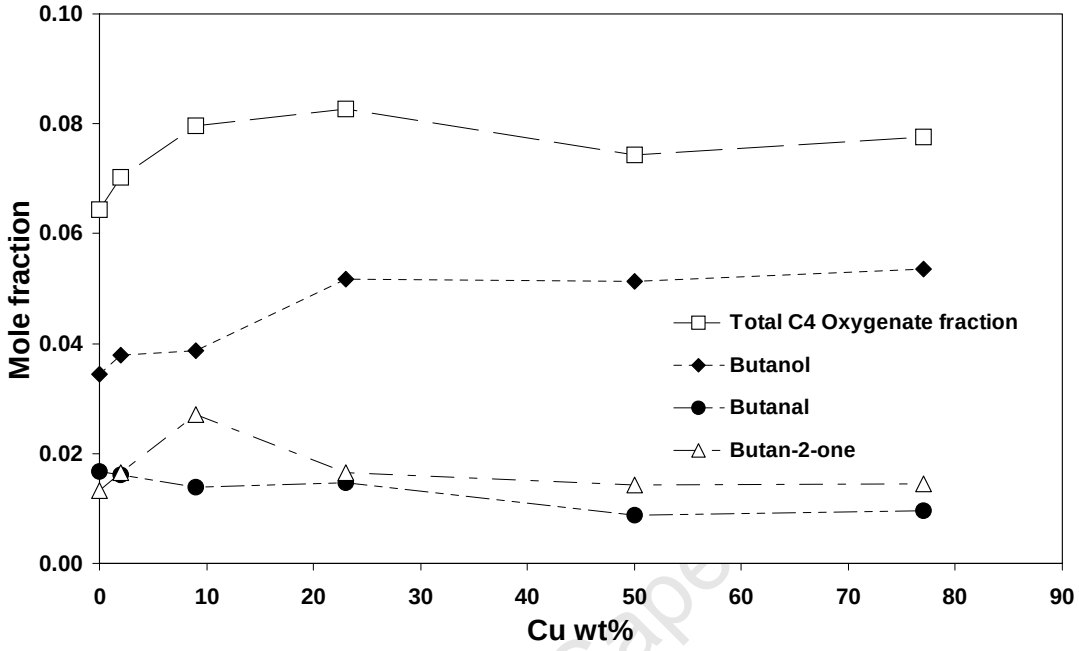

Figure 4.28 Mole fraction of oxygenates in linear C_4 products after 96 hours during Fischer-Tropsch synthesis in a Berty reactor for the iron-copper catalyst series

Table 4.32 Equilibrium ratios of C_4 oxygenates (excluding butyric acid) after 96 hours during Fischer-Tropsch synthesis in the Berty reactor for the iron-copper catalyst series

Reaction and ratio		**Product ratios**					
		0 wt% Cu[a]	2 wt% Cu	9 wt% Cu	23 wt% Cu	50 wt% Cu	77 wt% Cu
1-Butanol ⇔ Butan-2-one + H_2	Eq[b]	22.3	21.9	24.7	22.7	22.3	24.0
Butan-2-one/1-Butanol	Obs[c]	0.1	0.1	0.3	0.1	0.1	0.1
Butanal ⇔ Butan-2-one	Eq	381	381	381	381	381	381
Butan-2-one/Butanal	Obs	0.8	1.0	2.0	1.1	1.6	2.7
Butanal + H_2 ⇔ 1-Butanol	Eq	17.1	17.4	15.5	16.8	17.1	15.9
1-Butanol/ Butanal	Obs	5.9	7.8	7.6	10.0	16.6	16.0

[a] Basis: Fully reduced catalyst

[b] Eq: Expected ratio at equilibrium

[c] Obs: Observed product ratios

4.5.4 Organic product formation: Liquid product

As mentioned previously, the product from the Berty reactor included a quantifiable volume of oil and water product that could be collected from the reactor and analysed.

4.5.4.1 Liquid product – water: Soluble organic products

The short chain oxygenates are soluble in water and are found in the water fraction. However upon examination with GC-MS it was found that a fraction (in some cases quite a large fraction) of these oxygenates were also found in the oil product. This has made quantifying these oxygenates directly almost impossible. In light of this the water phase was analysed but the results were found to be extremely unreliable and are therefore not reported here. Some of the data of the water analyses are however used in the evaluation of results discussed in section 4.6.

4.5.4.2 Liquid product – oil

As the analysis of the water fraction was not possible, and extremely variable, due to a mixture of light oxygenates in both the water and oil phases, as well as possible loss of the more volatile components, another method for identification of the oxygenate product was sought. The oil fraction captured proved to contain a high percentage of long chain products and so this phase was examined as a possible method of isolating the different oxygenate components, including acids (which due to adsorption phenomena could not be analysed using the ampoule technique), and identifying their interaction.

4.5.4.3 Liquid product – oil: Carbon fraction captured – FID

Due to the complexity of the GC trace only the alpha olefins, n-paraffins and 1-alcohols were identified and quantified. Figure 4.29 shows a typical logarithmic plot of the corrected area of total organic products (alpha olefins, n-paraffins and 1-alcohols) divided by carbon number, versus carbon number (ASF plot) as obtained from FID analysis of the oil phase collected during an experiment in the Berty reactor. A straight line with negative slope is the expected result for a product having an Anderson Schulz-

Flory distribution. It can be seen that for carbon numbers 5, 6 and 7 the whole liquid hydrocarbon fraction has not been captured as there is a positive slope for these products. The plot shows that the full product fractions have been successfully captured from C_8.

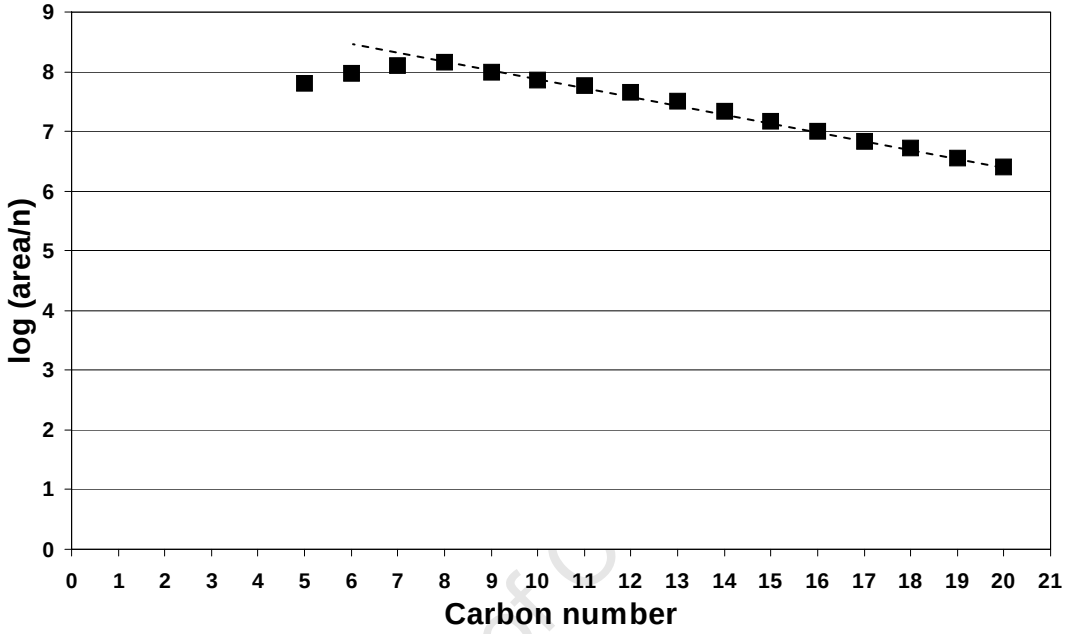

Figure 4.29 A typical log of the carbon specific area of organic products divided by carbon number from the FID analysis after 96 hours during Fischer-Tropsch synthesis from a Berty reactor for one of the catalysts in the iron-copper series

4.5.4.4 Liquid product – oil: Olefin formation

As only the alpha olefins, n-paraffins and 1-alcohols were identified and quantified within the oil FID chromatogram, it makes direct comparison with the previous VOC samples discussed above impossible. However comparison of the fraction of α-olefins in α-olefins plus linear paraffin product can be done on the VOC sample and the oil sample. The combined result is shown in Figure 4.30 where the VOC is shown from C_2 to C_7 and oil fraction from C_8 to C_{20}.

For the VOC product spectrum the results are very similar to the results obtained from olefins in linear hydrocarbon product. This is due to the small amount of internal olefins formed under these conditions, which were included in the previous graph

(Figure 4.22). Comparison of the VOC results and the ratio obtained from the oil product shows that initially (C_8 to C_{10}) the trend is similar for the gas product (not shown in this plot). However, at higher carbon numbers there is a sharp decline in the ratio and it seems that there are less α-olefins in the product. This carbon number dependent loss of olefins has been shown to be due to secondary olefin hydrogenation and or incorporation, caused by increased retention times of these long chain products in the reactor and/or the pores of the catalyst particles, as a consequence of increasing solubility and diffusivity (*Schulz and Claeys*, *1999a* and *Iglesia et al.*, *1993*). The decline of the α-olefins, and thus these secondary effects, seems to be more pronounced on the highly copper promoted catalysts.

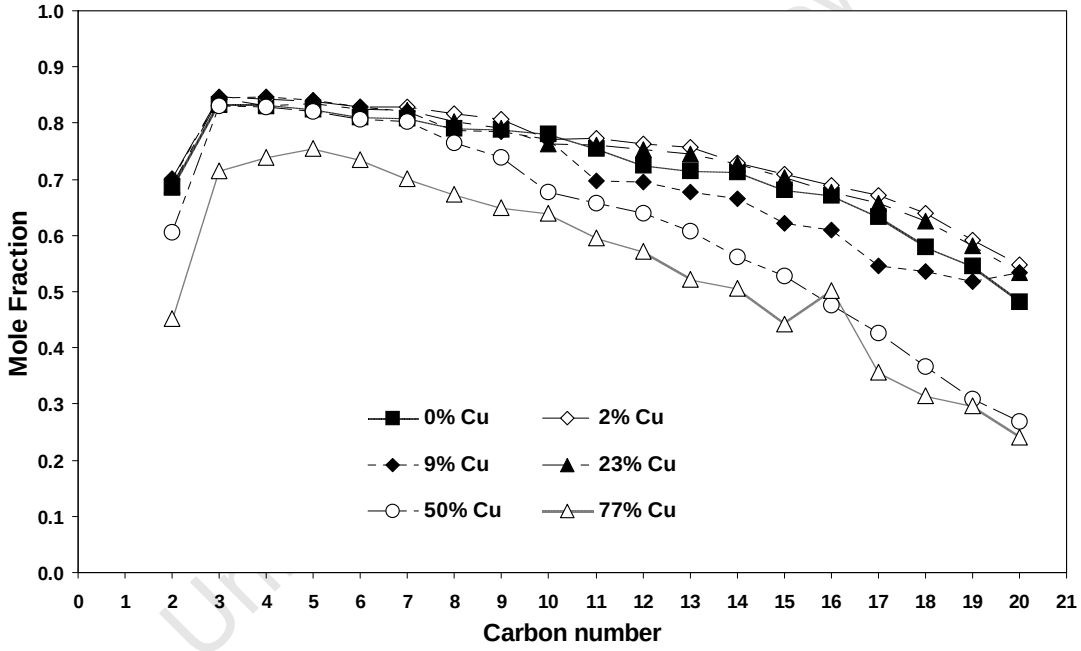

Figure 4.30 Mole fraction of linear α-olefins in α-olefins plus linear paraffins in the VOC (C_2 to C_7) and oil product (C_8 to C_{20}) as a function of carbon number after 96 hours in a Berty reactor for the iron-copper catalyst series

4.5.4.5 Liquid product – oil: Oxygenate formation – FID

Examination of the quantified 1-alcohol fraction in the identified linear product fraction obtained through FID analysis once again resulted in extremely messy results. Additionally, the aldehydes, ketones and acids could not be extracted at all. This suggests that the peak separation and quantification could not be done successfully for

these product classes in the oil samples. So another method of examination of the oxygenate spectrum was sought.

4.5.4.6 Liquid product – oil: Oxygenate formation – MS

Due to the high concentration of hydrocarbons in the oil chromatogram from the FID and the poor separation of the products of interest, another method was sought to quantify the product spectrum. Recent advances in mass spectrometry have made the attachment of mass spectrometers to gas chromatograph columns a much cheaper option than in the past. Mass spectrometers add the ability to selectively extract ions from a chromatograph, thereby adding an ability to extract compound-specific products out of an extremely complex chromatogram.

For the most part each particular product family has a specific or unique m/z ion that can be extracted from a TIC chromatogram. The following ions can be extracted to identify the oxygenate product classes of interest: m/z=31 for 1-alcohols, m/z=44 for aldehydes, m/z=58 for methyl-ketones and m/z=60 for carboxylic acids; they were extracted from total ion chromatograms. Figure's 3.7, 3.8, 3.9, 3.10, 3.11 and 3.12 in the previous section show the extracted ion chromatograms together with the corresponding FID chromatogram. The different product classes are now clearly visible, including the acids.

The actual oxygenate products in the C_8 fraction were confirmed by means of analysis of the oil, which was spiked with the component of interest. As responses on the MS detector (both TIC and extracted ions), unlike FID responses, are often non-linear, careful (and usually compound-specific) calibration is required. The C_8 oxygenates were chosen for identification and calibrated against n-decene. The non-linear molar response factors (quadratic function) for 1-octanol, octanal, octan-2-one and octanoic acid, as calibrated using n-decene as the tie component are shown in Table 3.11 (calibration curves and histograms are shown in Appendix E).

The mole fractions of the C_8 oxygenates in the oil sample using the extracted ion specific areas for the period 72 to 96 hours are shown in Figure 4.31 for the catalyst series. The results obtained show (the previously seen) high oxygenate selectivity for the higher-copper containing catalysts (the results for the 2 wt% Cu catalysts – shown in grey – appear to be out of line for unknown reasons). A similar trend to that seen in the

C_4 product (Figure 4.19) is seen, where the alcohol content increases to the detriment of the aldehyde with increased copper loading.

The fraction of octanoic acid can be quantified in the oil sample and the effect of copper on the acid selectivity can be examined. Here, while the fraction of acid is relatively low on the pure iron catalyst, there seems to be a decrease in the acid fraction with copper loading. Additionally, the acid seems to behave similarly to the ketone for all samples. The trend of the alcohols and aldehydes on the high loaded copper catalysts seems to still be in agreement with that seen in the lower carbon numbers in the gas phase product. An increase in copper leads to a decrease in the aldehyde fraction, and an increase in the alcohol and overall oxygenate fractions.

Thermodynamically (Table 4.33) the ratio of aldehydes to alcohols is very near (or even at) equilibrium for the 50 and 77 Cu wt% catalysts, a result in agreement with that seen on the C_4 VOC product fraction (Table 4.21 and Table 4.32). The other two reactions of interest thermodynamically are the formation of octanoic acid via octanal or 1-octanol. Both these reactions are at (or close to) thermodynamic equilibrium for the whole catalyst series, suggesting an extremely fast interaction between these compounds, while (as perhaps to be expected) no such interaction seems to exist between octan-2-one and 1-octanol or octanal respectively.

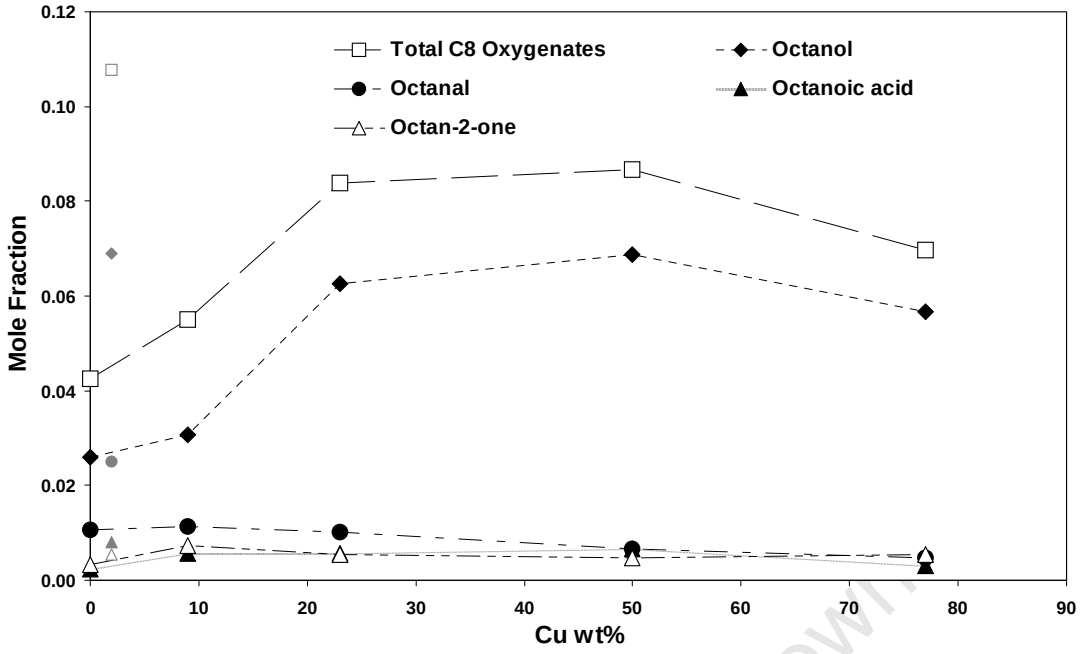

Figure 4.31 Mole fraction of C_8 oxygenates in linear hydrocarbon and oxygenate products in product oil after 96 hours during Fischer-Tropsch synthesis in a Berty reactor for the iron-copper catalyst series using the TIC m/z ion specific areas

Table 4.33 Equilibrium ratios of C_8 oxygenates in product oil after 96 hours during Fischer-Tropsch synthesis in a Berty reactor for the iron-copper catalyst series using the TIC m/z ion specific areas

Reaction and ratio		Product ratios					
		0 wt% Cu[a]	2 wt% Cu	9 wt% Cu	23 wt% Cu	50 wt% Cu	77 wt% Cu
Octanoic acid + H_2 ⇔ Octan-2-one + H_2O	Eq[b]	1170	1342	741	1024	1226	944
Octan-2-one/ Octanoic acid	Obs[c]	1.54	0.73	1.16	0.82	0.90	1.38
1-Octanol ⇔ Octan-2-one + H_2	Eq	38.3	37.7	42.5	39.1	38.3	41.3
Octan-2-one/1-Octanol	Obs	0.13	0.08	0.24	0.09	0.08	0.09
Octanal ⇔ Octan-2-one	Eq	415	415	415	415	415	415
Octan-2-one/ Octanal	Obs	0.36	0.23	0.64	0.59	0.77	1.01
1-Octanol + H_2O ⇔ Octanoic acid +2H_2	Eq	0.03	0.03	0.06	0.04	0.03	0.04
Octanoic acid/1-Octanol	Obs	0.09	0.10	0.20	0.11	0.09	0.07
Octanal + H_2O ⇔ Octanoic acid + H_2	Eq	0.35	0.31	0.56	0.41	0.34	0.44
Octanoic acid/ Octanal	Obs	0.24	0.32	0.55	0.72	0.85	0.73
Octanal + H_2 ⇔ 1-Octanol	Eq	10.8	11.0	9.8	10.6	10.8	10.0
1-Octanol /Octanal	Obs	2.7	3.1	2.7	6.4	9.8	11.2

[a] Basis: Fully reduced catalyst

[b] Eq: Expected ratio at equilibrium

[c] Obs: Observed product ratios

4.5.4.7 Summary of results using a Berty reactor

Results of the runs conducted in the Berty reactor agreed well with those seen previously in a fixed-bed reactor for the catalyst series. The addition of copper to iron catalysts had no effect on overall activity and exit/reactor partial pressures. A slight increase of methane selectivity with a corresponding decrease of the chain growth probability with increasing copper content might be discernable. This is in contrast to the results obtained in the fixed-bed reactors where no clear trend was observed.

Once again copper was found to affect the olefin content in the hydrocarbon product, where an increase in copper loading led to the more hydrogenated product in the C_2 fraction and in very high carbon number fractions (>C_8). In addition, a shift of primary selectivity towards a more paraffinic product could be identified from the comparatively

low carbon number independent olefin content in the C_3 to C_8 fraction of the product from the highly copper promoted catalyst.

It is therefore proposed that copper impacts on both primary hydrocarbon product formation (alpha-olefin versus paraffin), and secondary olefin consumption (hydrogenation and double bond shift isomerisation). This is most likely via facile hydrogen activation and subsequent hydrogen surface enrichment of the active iron phases. In addition, secondary olefin reactions may take place on the surface of copper.

As in the experiments in the fixed-bed reactor, the most significant effect of copper promotion is a pronounced increase in the amount of oxygenates, in particular alcohols. It could again be shown that there appears to be a rapid interaction between 1-alcohols and the corresponding aldehydes, in particular in copper promoted catalysts where the corresponding partial equilibria were obtained in different carbon number fractions.

A method for the quantification of long chain oxygenates using GC/MS techniques was developed, which also enabled the identification and quantification of the carboxylic acids. Thermodynamic analysis of partial equilibria indicates that an interaction between acids, and alcohols or aldehydes, takes place as previously proposed by Dry (1981).

A detailed analysis of possible interactions of oxygenates and the role of copper on these reactions is discussed in the next section on the basis of co-feeding experiments of C_8 oxygenates on two different catalysts.

4.6 C_8 Oxygenate co-feeding – Berty

The results in the previous section led to questions being asked around the oxygenate interaction on the catalyst, and how copper affects this interaction. As it was shown earlier that the acids could not be captured quantitatively in the gas samples and that the shorter chain oxygenates were not captured solely in one phase (mixture in water and oil), it was decided that the oxygenates in the oil fraction (as identified by GC-MS) should be quantified and examined. The C_8 oxygenates were chosen as they were easy to quantify and they were entirely captured in the oil fraction.

1-Octanol, octanal, octan-2-one and octanoic acid were co-fed with the feed gas (H_2, CO and CO_2) through the use of a saturator for a 48 hour period between 48 and 96 hours time online on the 0 and 50 wt% Cu catalysts. The feeding rates of the oxygenate compounds were determined by the temperature of the saturator. Rates approximately 10-100 times that of the normal formation rate of the compound were sought. The feeding rate was chosen large enough to see clear effects on the oxygenate reactions, but low enough so that their presence should not impact on the overall synthesis gas conversion.

As the Fischer-Tropsch hydrocarbon products cannot be reliably determined in the VOC gas phase after carbon number 12, the oxygenates after carbon number 7, and acids not at all. The captured oil product was used to determine the formation rates. In order to do this a 'tie' component was required to work back the formation rates to the gas phase FID and the internal standard of neo-hexane.

To determine the best 'tie' component the elution times of the desired products as well as other hydrocarbon products was examined. The C_8-oxygenates elute at different times in the chromatogram, the ketone and aldehyde exit just before n-decene while 1-octanol exits between the C_{10} and C_{11} hydrocarbons, octanoic acid exits the GC-MS between the C_{11} and C_{12} hydrocarbons. Also the full hydrocarbon spectrum can only be captured in the oil phase after C_7 (Figure 4.29). For these reasons n-decene was decided upon as the 'tie' component.

4.6.1 Confirmation of baseline and steady state

Before co-feeding could be done, confirmation that the product selectivities were at a steady state after 48 hours was needed. The previous section already demonstrated that steady state activity was reached after 24 hours. Additional analysis of the VOC and oil product confirmed that product selectivity did not change after 48 hours for both catalysts. These results can be seen in Appendix J. This confirmed that steady state was reached within 48 hours, and the resulting changes in the product selectivities would be caused by the interaction of the co-fed components, and would not be due to the transient conditions during the experiments.

4.6.2 Product analysis

Due to the high concentration of hydrocarbons overlapping with the peaks of oxygenates in the oil chromatogram from the FID analysis, extracted ion chromatograms were used for quantification of the C_8 oxygenates (as described previously) through the use of the calibration functions, and the vapour pressures of the oxygenates as determined by Daubert *et al*. (1999).

Other components that were monitored, in addition to the four co-fed components were 2-octanol, octylacetate[12], nonan-2-one, and ethyl caprylate[13]. However, only nonan-2-one was calibrated against n-decene (Table 4.34), while the formation of the other components was followed qualitatively, i.e. via the relative changes of peak areas in the corresponding extracted ion chromatogram relative to 1-decene. The compounds, their specific elution time in the oil TIC chromatogram, and their compound specific ion are detailed in Table 4.35.

Figure 4.32 shows the extracted ion chromatograms for ions m/z=31 (alcohols), m/z=44 (aldehydes), m/z=58 (ketones) and m/z=60 (acids) for a baseline condition at 96 hours using the copper promoted catalyst. Comparison of these chromatograms to those during co-feeding are a simple way of identifying obvious changes in the product spectrum upon co-feeding of the different components. Information on the co-feeding experiments in addition to the results reported below can be found in Appendices K to N.

Table 4.34 Calibrated molar response factors for nonan-2-one (m/z = 58) using n-decene (m/z = 55) as a tie component.

Compound	m/z	Tie ratio	x^2	x	c	R^2
Nonan-2-one	58	58/55	0.104	0.097	-0.0004	0.98

Table 4.35 Details of other components that were monitored during the co-feeding of C_8 oxygenates.

Monitored component	Elution time (min)	Monitored m/z ion
2-Octanol	± 13.4	45

[12] Acetic acid octyl ester

[13] Octanoic acid ethyl ester

Nonan-2-one	± 16.2	58
Ethyl caprylate	± 19.6	88
Octylacetate	± 20.0	70

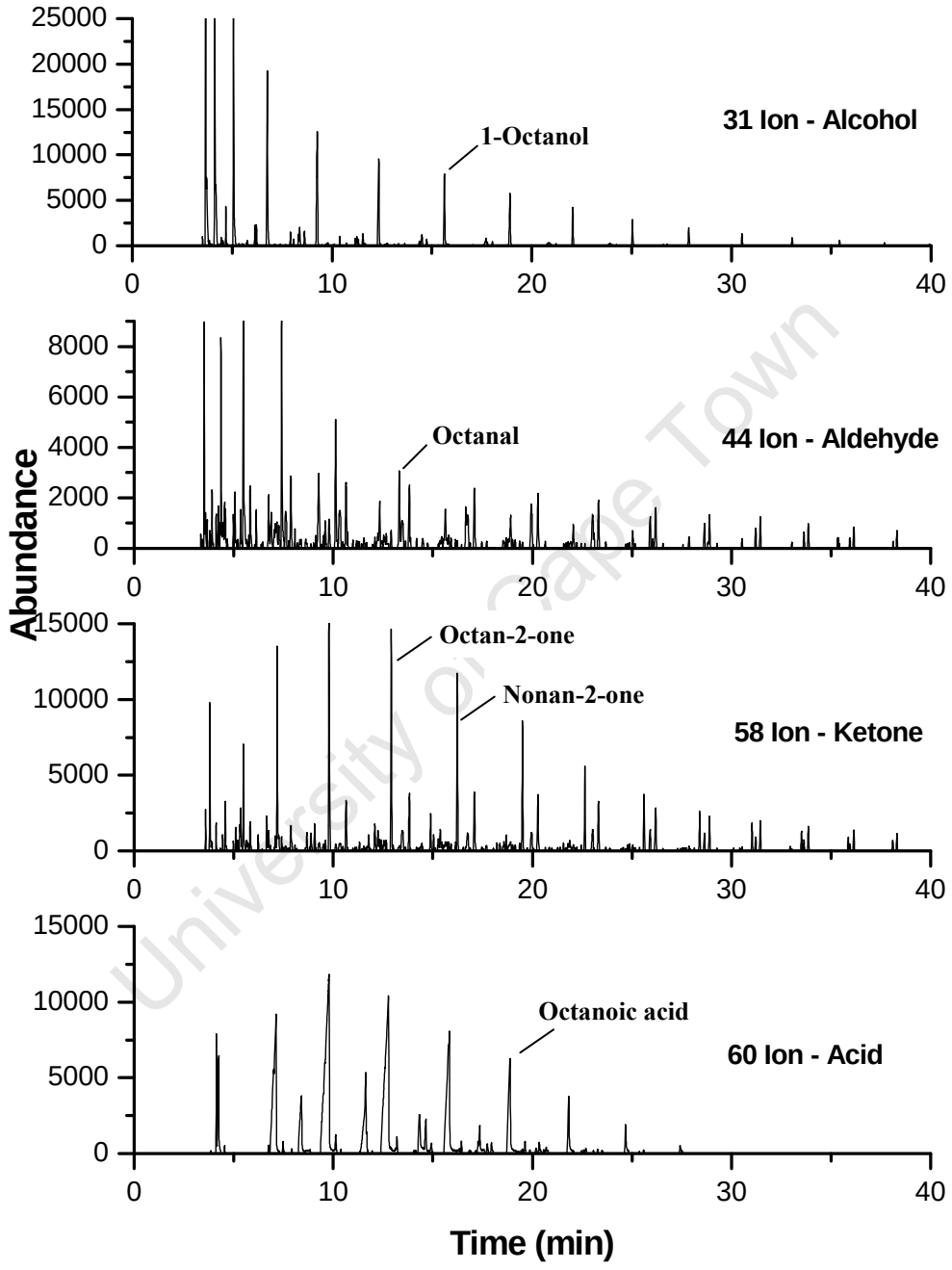

Figure 4.32 Extracted ion chromatograms of 50 wt% Cu catalyst baseline (with no feeding) after 96 hours TOL during Fischer-Tropsch synthesis in a Berty reactor for ions m/z=31 (alcohols), m/z=44 (aldehydes), m/z=58 (ketones) and m/z=60 (acids)

4.6.3 Co-feeding of 1-octanol

1-Octanol was co-fed with syn-gas using a saturator attached to the feed line of the Berty reactor. Successful co-feeding of 1-octanol during the periods 48 to 96 hours was confirmed via analysis of the feed gas; it was also seen that 1-octanol was not converted completely in these experiments as large quantities of 1-octanol was present in the product oil.

Figure 4.33 and Figure 4.34 show the extracted ion chromatograms of the main oxygenates of interest after 96 hours runtime, i.e. after 48 hours of co-feeding, for the two catalysts tested. The major reactions which 1-octanol undergoes can immediately be seen. These include formation of octanal, but also the additional formation of octanoic acid and nonan-2-one (and subsequently a very small increase of 2-nonanol, see section 4.6.5). The formation of nonan-2-one during this co-feeding may help identify formation routes of methyl-ketones, a reaction which, like the formation of carboxylic acids, is typically not considered in reports dealing with the formation of oxygenates during Fischer-Tropsch synthesis. A detailed discussion of these findings can be found at the end of this chapter after the sections dealing with the co-feeding of the other oxygenates.

In addition to the flow rates of the C_8 oxygenates and nonan-2-one, the formation rates of major C_7, C_8 and C_9 hydrocarbons (n-paraffins and α-olefins) were monitored closely before and during co-feeding (results are listed in Appendix K). A significant increase in the formation of these hydrocarbon fractions during co-feeding would point towards hydrogenation (increase of C_8), or incorporation (increase of C_9) of the co-fed component, in this case 1-octanol. Figure 4.35 depicts the molar formation rates of hydrocarbons during co-feeding in comparison to those obtained at baseline conditions for the experiment with the non-copper promoted iron catalyst. It can clearly be seen that the hydrocarbon formation rates in these two carbon numbers remain largely unaffected during 1-octanol addition, indicating that 1-octanol hydrogenation or incorporation do not play a role in this experiment, or cannot be identified by the applied method, due to the relatively small amount of oxygenate added compared to the amount of hydrocarbons formed. ^{14}C labelled ethanol (a more sensitive method), showed incorporation into growing chains and has previously been reported to occur over iron catalysts (*Tau et al.*, *1987*).

It may further be noted that the small amounts of 1-octanol added did not affect the syn-gas conversion, as unchanged conversion levels were found throughout all co-feeding experiments (supporting data are listed in Appendix K). Additionally, product selectivity, such as molar olefin contents and molar α-olefin content remained completely unaffected by the co-feeding.

An attempt was made to conduct mass balances on the fed 1-octanol, and exiting molar flow rates of the main C_8 oxygenates and nonan-2-one, taking base case formation of all compounds into account (Appendix K). The formation of octan-2-one was not considered in these mass balances as it seems kinetically unlikely that this component can form from terminal oxygen groups; this is also supported by the unchanged formation rates of octan-2-one during co-feeding. In these mass balances, closure values of larger than 100% were found (150-500%), indicating that (apparently) more products were formed from 1-octanol than 1-octanol was fed. This is likely to be due to problems of the feed analysis, and therefore an alternative mass balance was conducted where it was assumed that the co-fed oxygenate, in this case 1-octanol, only reacted to form octanal, octanoic acid and nonan-2-one. After subtracting the formation rates before co-feeding, the conversion of 1-octanol and the selectivity to octanal, octanoic acid and nonan-2-one can be established.

Table 4.36 shows these results, which allow a direct comparison of the oxygenate reactions (extent and selectivity) on the two different catalysts.

Although the conversion of 1-octanol over the copper promoted catalyst was more than twice that of the conversion over the 0 wt% Cu catalyst, very similar product selectivities were obtained, and almost exclusively octanal was formed (selectivity > 97%), indicating a preferred dehydrogenation of 1-octanol. Earlier it was shown that the alcohol content of the catalyst increased with copper loading to the detriment of the aldehyde. In light of the co-feeding results it suggests that the interaction between the two oxygenates is rapid and is readily promoted by copper. Among the other two products, nonan-2-one was the preferred one with almost 2% selectivity, and almost 1% octanoic acid was formed from the converted 1-octanol.

In addition to these major reactions a number of possible minor reactions were followed by monitoring extracted ion chromatograms, corresponding to 2-octanol, octylacetate and ethyl caprylate relative to n-decene during 1-octanol co-feeding. Table 4.37 shows peak area ratios of these ions relative to that of 1-decene for both catalysts. An example

of extracted ion chromatograms obtained during co-feeding of 1-octanol with the copper promoted iron catalyst is shown in Figure 4.36 and Appendix K.

As mentioned previously the m/z 45 ion of 2-octanol has been hard to isolate during the baseline experiments. Once again, for the 1-octanol co-feeding it was not readily visible as a product using the 0 wt% Cu catalyst. This is probably due to its low selectivity for the iron catalyst. For the 50 wt% Cu catalyst however, a marked increase in the selectivity compared to the 0 wt% Cu suggests that the iso-alcohol selectivity is higher over the 50 wt% Cu catalyst. This is probably due to hydrogenation of the corresponding methyl-ketone, in this case octan-2-one (see also section 4.6.5). A temporal change of the peak area ratio was not obtained on either catalyst during co-feeding of 1-octanol, indicating no interaction between the two alcohols (1-octanol and 2-octanol). This is to be expected, as it would include a shift of the OH group.

The formation of octylacetate seems to increase sharply once 1-octanol is introduced into the reactor. The formation of octylacetate is most likely through the esterification of 1-octanol and acetic acid. However, this result cannot be verified due to the problems in analysing the acid in either the gas or water phase, as discussed previously.

Ethyl caprylate seems to increase slightly with 1-octanol addition. The route of formation of ethyl caprylate from octanol would most likely be through the esterification reaction of octanoic acid (formed from the co-fed 1-octanol) with ethanol. The formation of ethanol from FID analysis does not seem to change over this time period. The formation rate of ethanol is, however, orders of magnitude larger than that of the components investigated here, so that only a relatively small amount of the ethanol would be converted, possibly too small to be detected.

Both ethyl caprylate and octylacetate are likely to be formed via esterification reactions as discussed above. These reactions are typically acid catalysed and not metal catalysed and it is not clear if such acidic centres are present on the catalysts used. It may be speculated that these esters can be formed in non-catalysed, homogeneous reactions. Alternatively, if these species were formed on metallic or carbide surfaces of the iron catalysts used via interaction of suitable surface species, one might also expect the formation of esters containing C_1 groups, which are the dominant surface species on a working Fischer-Tropsch catalyst. The identification of such esters in the product spectra was, however, not successful.

Additional product work-up identified two small peaks between the linear hydrocarbon peaks in carbon numbers 17 and 18 on both the FID and TIC chromatograms. Identification of these peaks proved to be problematic, but it is thought that one of the peaks relates to the C_{16} ester (octanoic acid octylester as identified using GC-MS techniques), while the second peak could not be identified.

Table 4.36 1-Octanol conversion and product selectivity for both 0 and 50 wt% Cu catalyst assuming octanal, octanoic acid and nonan-2-one are the only products formed.

0 wt% Cu catalyst 1-Octanol co-feeding		
Time on-stream of analysis (hrs)	74	96
1-Octanol conversion (%)	4.6	4.1
Octanal selectivity (%)	92.4	94.9
Octanoic acid selectivity (%)	4.7	2.8
Nonan-2-one selectivity (%)	2.9	2.3
50 wt% Cu catalyst 1-Octanol co-feeding		
Time on-stream of analysis (hrs)	72	80
1-Octanol conversion (%)	12.0	11.5
Octanal selectivity (%)	97.9	97.8
Octanoic acid selectivity (%)	1.2	1.5
Nonan-2-one selectivity (%)	0.8	0.7

Table 4.37 Ratio of extracted ion (m/z) areas of 2-octanol (m/z=45), octylacetate (m/z=70) and ethyl caprylate (m/z=88) over decene (m/z=55) during 1-octanol co-feeding

			0 wt% Cu catalyst 1-Octanol co-feeding			
TOL	48	54	74	96	104	120
Feeding	no		1-Octanol		no	no
$\frac{\text{Area 2-Octanol}}{\text{Area Decene}}$	-	-	-	0.015	-	0.018
$\frac{\text{Area Octylacetate}}{\text{Area Decene}}$	0.031	0.027	0.124	0.212	0.203	0.205
$\frac{\text{Area Ethyl capralate}}{\text{Area Decene}}$	0.023	0.024	0.033	0.038	0.037	0.039
			50 wt% Cu catalyst 1-Octanol co-feeding			
TOL	48	72	80	96	121	
Feeding	no		1-Octanol		no	
$\frac{\text{Area 2-Octanol}}{\text{Area Decene}}$	0.047	0.027	0.027	0.027	0.028	
$\frac{\text{Area Octylacetate}}{\text{Area Decene}}$	0.020	0.121	0.217	0.265	0.193	
$\frac{\text{Area Ethyl capralate}}{\text{Area Decene}}$	0.016	0.029	0.038	0.046	0.038	

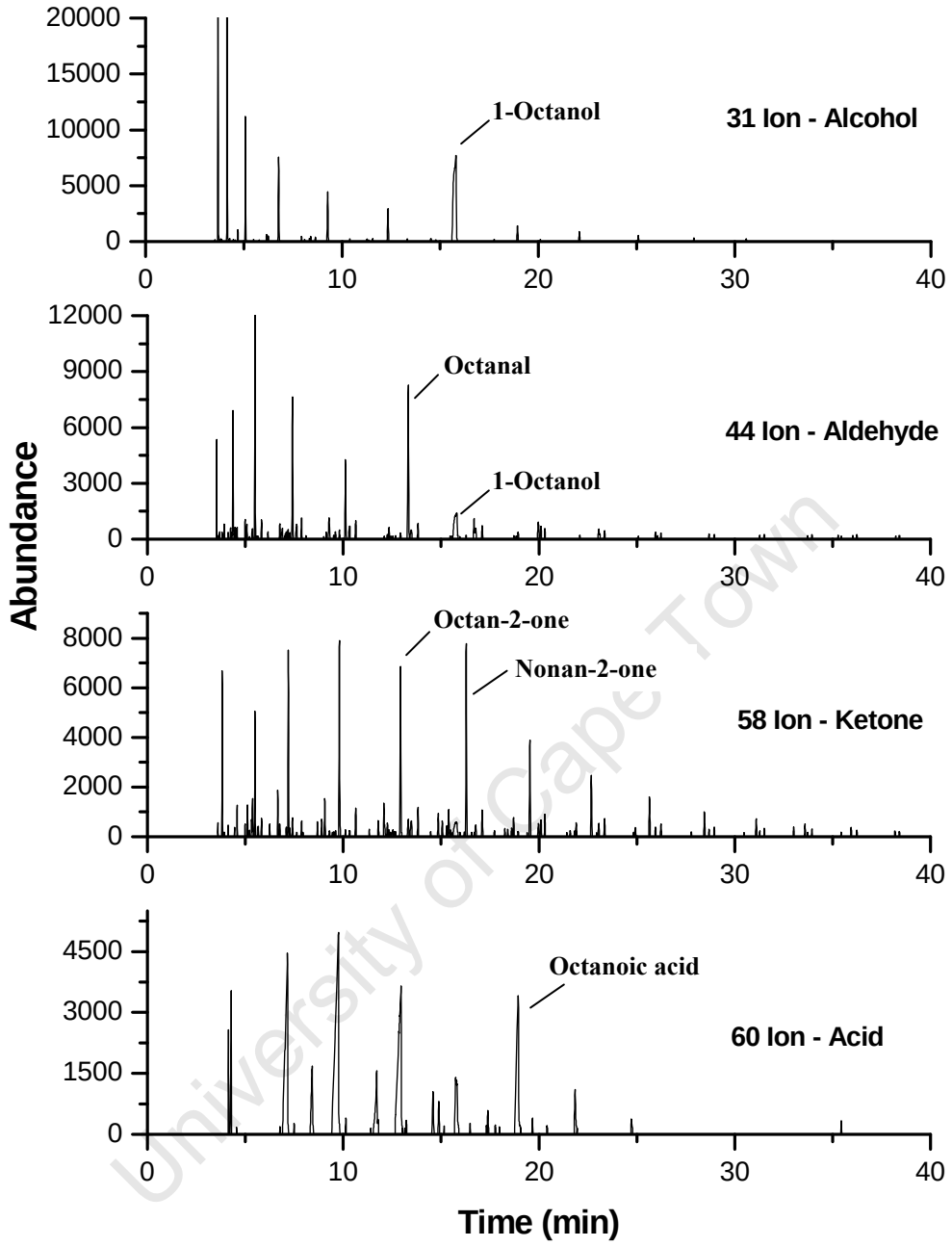

Figure 4.33 Extracted ion chromatograms of 0 wt% Cu catalyst with 1-octanol co-feeding after 96 hours TOL during Fischer-Tropsch synthesis in a Berty reactor for ions m/z=31 (alcohols), m/z=44 (aldehydes), m/z=58 (ketones) and m/z=60 (acids)

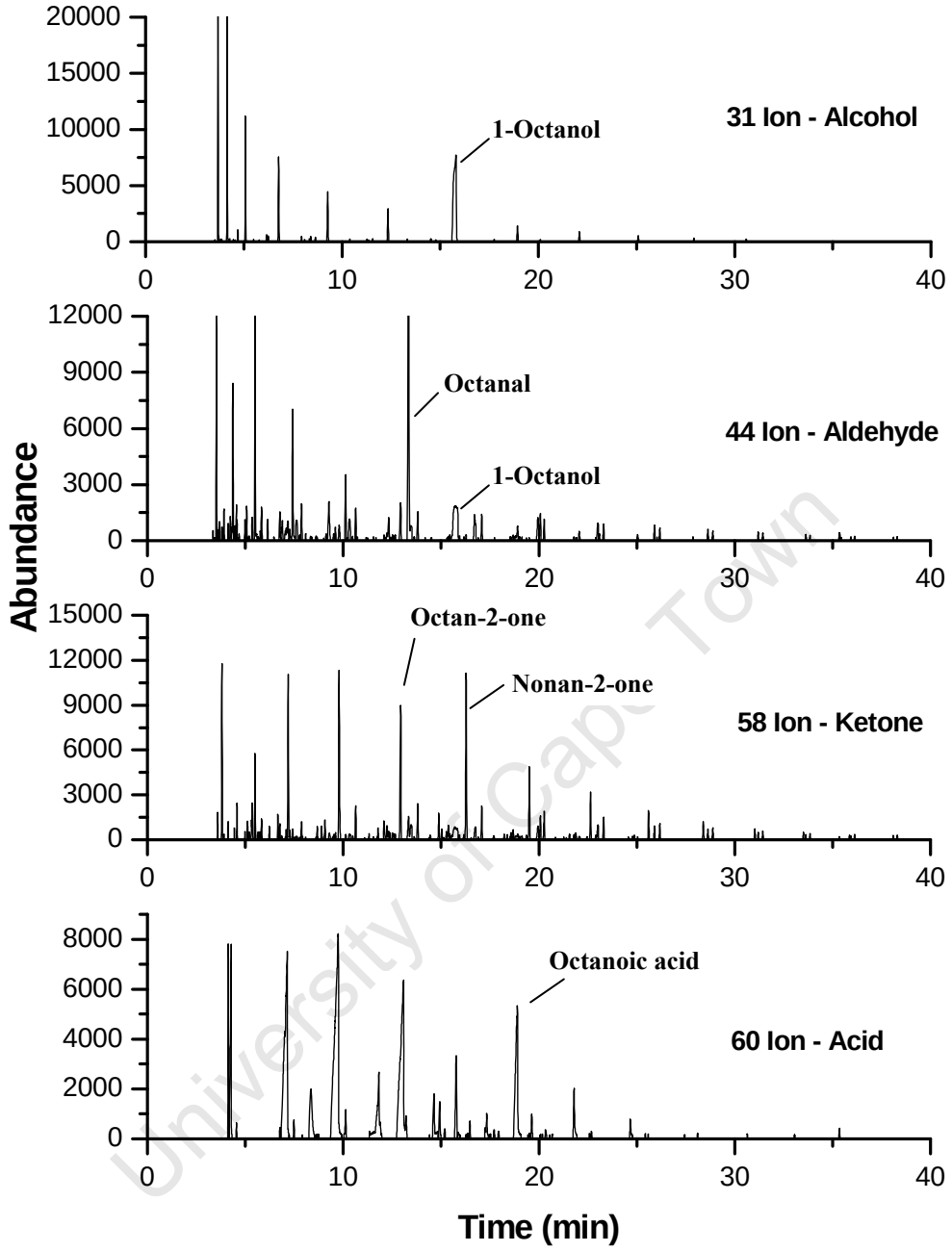

Figure 4.34 Extracted ion chromatograms of 50 wt% Cu catalyst with 1-octanol co-feeding after 96 hours TOL during Fischer-Tropsch synthesis in a Berty reactor for ions m/z=31 (alcohols), m/z=44 (aldehydes), m/z=58 (ketones) and m/z=60 (acids)

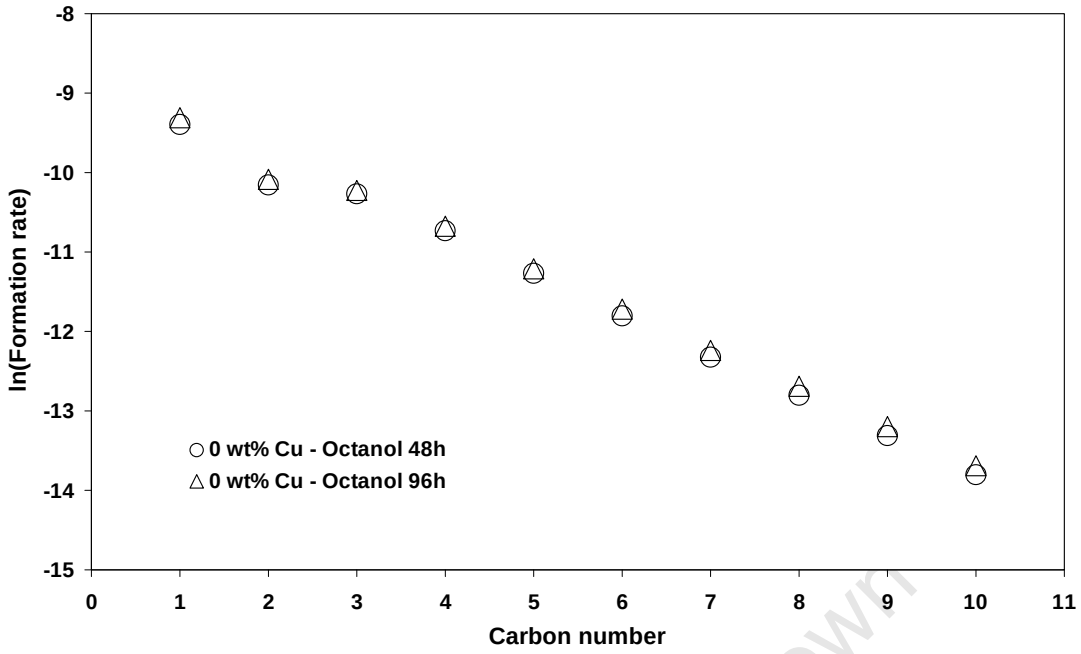

Figure 4.35 ASF plot of natural log of formation rates of linear hydrocarbons versus carbon number for 48 and 96 hours with the 0 wt% Cu catalyst during 1-octanol co-feeding

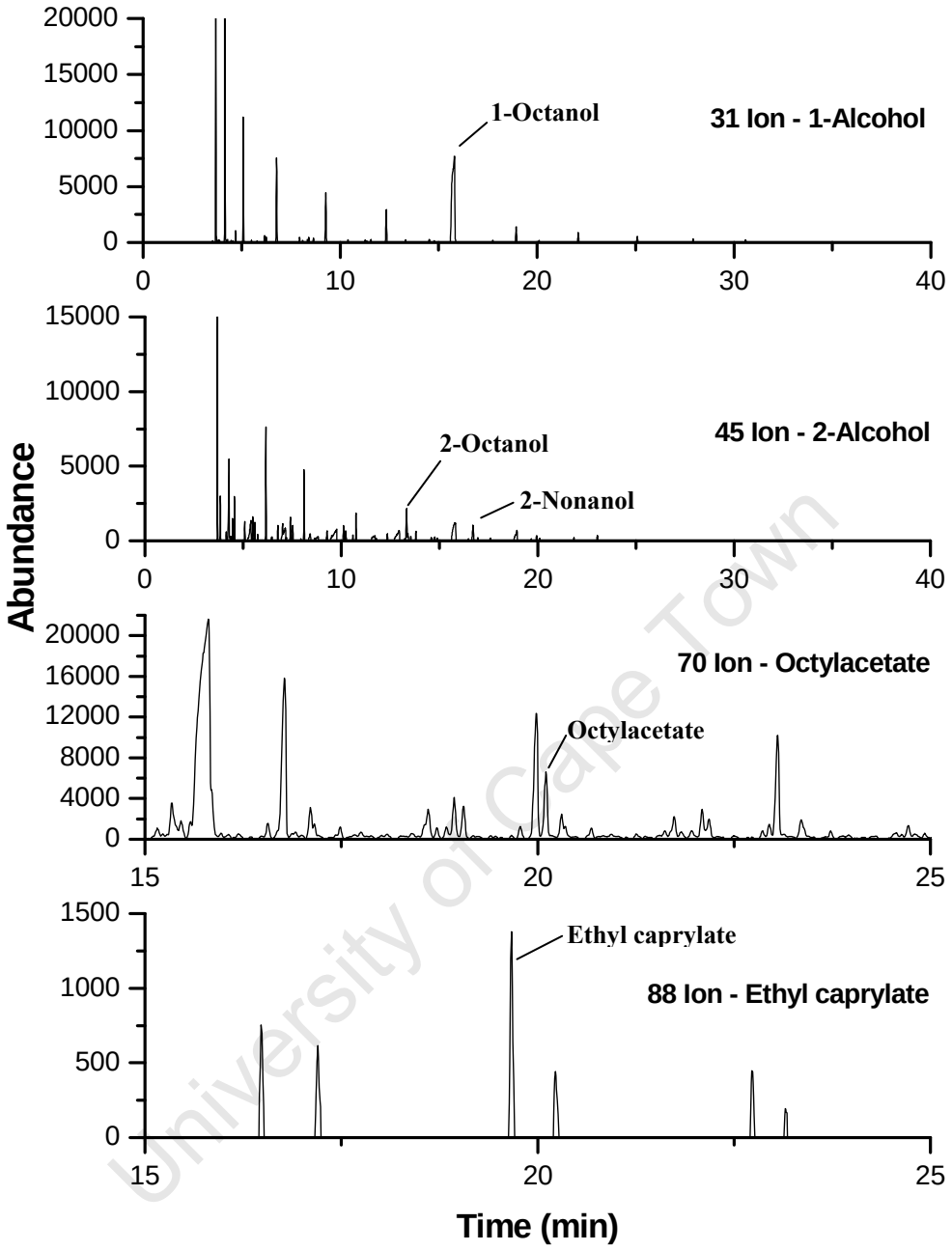

Figure 4.36 The corresponding extracted ion chromatograms including that of the primary alcohols of 0 wt% Cu catalyst with 1-octanol co-feeding after 96 hours TOL during Fischer-Tropsch synthesis in a Berty reactor for ions m/z=31 (1-alcohols), m/z=45 (2-alcohols), m/z=70 (octylacetate) and m/z=60 (ethyl caprylate)

4.6.4 Co-feeding of octanal

Octanal was co-fed with syn-gas using a saturator attached to the feed line of the Berty reactor. Again no effects on the synthesis gas conversion and no shifts in the overall hydrocarbon product formation and selectivity were seen during octanal co-feeding (for data see Appendix L). There were certain selectivity shifts within the C_8 and C_9 oxygenate fraction as evidenced in the extracted ion chromatograms obtained during co-feeding (Figure 4.37 and Figure 4.38). Again it is evident that an inter-conversion of the oxygenates is taking place and 1-octanol, octanoic acid and nonan-2-one (and subsequently a very small amount of 2-nonanol, see section 4.6.5) are formed upon addition of octanal during Fischer-Tropsch synthesis using the two different iron catalysts. Octan-2-one formation was again not affected.

Again, a direct mass balance was problematic, and a modified mass balance around the co-fed octanal was conducted assuming the formation of the three above listed oxygenates only (Table 4.38).

The conversion levels are generally much higher than those obtained with 1-octanol, indicating that octanal is the much more reactive component of the two. As with the result seen with 1-octanol, the copper-iron catalyst increases the conversion of the fed oxygenate (90% compared to around 70%). The major product, in particular with the copper promoted iron catalyst, is 1-octanol (>90%), which, in conjunction with the results described on 1-octanol co-feeding in the previous section, clearly indicates a very rapid interaction/inter-conversion of these two oxygenates. Almost 10% of the co-fed octanal was converted to octanoic acid on the copper free iron catalyst while only around 3% octanoic acid selectivity was obtained on the copper-iron catalyst. Only a relatively small amount of the converted octanal, i.e. less than 2%, yielded nonan-2-one.

Table 4.39 shows the area ratios of extracted ion chromatograms corresponding to 2-octanol, octylacetate and ethyl caprylate relative to decene during octanal co-feeding. Additional chromatograms are supplied in Appendix L.

Again the m/z 45 ion of 2-octanol has been hard to isolate for the 0 wt% Cu catalyst, while the concentration of secondary alcohols seems to be higher on the copper promoted iron catalyst. As expected the co-feeding of octanal does not impact on the 2-octanol concentration, while some increase in the formation of the two monitored esters

seems to occur. Additionally, the two peaks described in section 4.6.3 above were again seen between the C_{17} and C_{18} linear hydrocarbon peaks.

Table 4.38 Octanal conversion and product selectivity for both 0 and 50 wt% Cu catalyst assuming 1-octanol, octanoic acid and nonan-2-one are the only products formed.

0 wt% Cu catalyst Octanal co-feeding			
Time on-stream of analysis (hrs)	73	88	96
Octanal conversion (%)	58.8	63.7	68.5
1-Octanol selectivity (%)	88.4	91.5	87.9
Octanoic acid selectivity (%)	10.4	7.1	10.2
Nonan-2-one[a] selectivity (%)	1.2	1.4	1.9
50 wt% Cu catalyst Octanal co-feeding			
Time on-stream of analysis (hrs)	73	88	96
Octanal conversion (%)	86.2	89.5	90.5
1-Octanol selectivity (%)	96.3	97.1	96.9
Octanoic acid selectivity (%)	3.5	2.8	2.9
Nonan-2-one[a] selectivity (%)	0.24	0.07	0.17

[a] Formation rate assumed using response factor of octan-2-one

Table 4.39 Ratio of extracted ion (m/z) areas of 2-octanol (m/z=45), nonan-2-one (m/z=58), octylacetate (m/z=70) and ethyl caprylate (m/z=88) over decene (m/z=55) during octanal co-feeding

				0 wt% Cu catalyst Octanal co-feeding			
TOL	48	68	73	88	96	113	120
Feeding	no	Octanal				no	no
Area 2-Octanol / Area Decene	n/a [a]	n/a [a]	n/a [a]	n/a [a]	n/a [a]	n/a [a]	0.019
Area Octylacetate / Area Decene	0.022	0.067	0.084	0.089	0.086	0.087	0.075
Area Ethyl capralate / Area Decene	0.033	0.043	0.054	0.053	0.055	0.064	0.069
				50 wt% Cu catalyst Octanal co-feeding			
TOL	48	65	73	88	96	113	120
Feeding	no	Octanal				no	no
Area 2-Octanol / Area Decene	0.049	0.031	0.035	n/a [a]	0.038	0.042	0.046
Area Octylacetate / Area Decene	0.190	0.092	0.167	0.168	0.200	0.180	0.175
Area Ethyl capralate / Area Decene	n/a [a]	0.051	0.083	0.088	0.115	0.127	0.132

[a] Peak too small to be identified

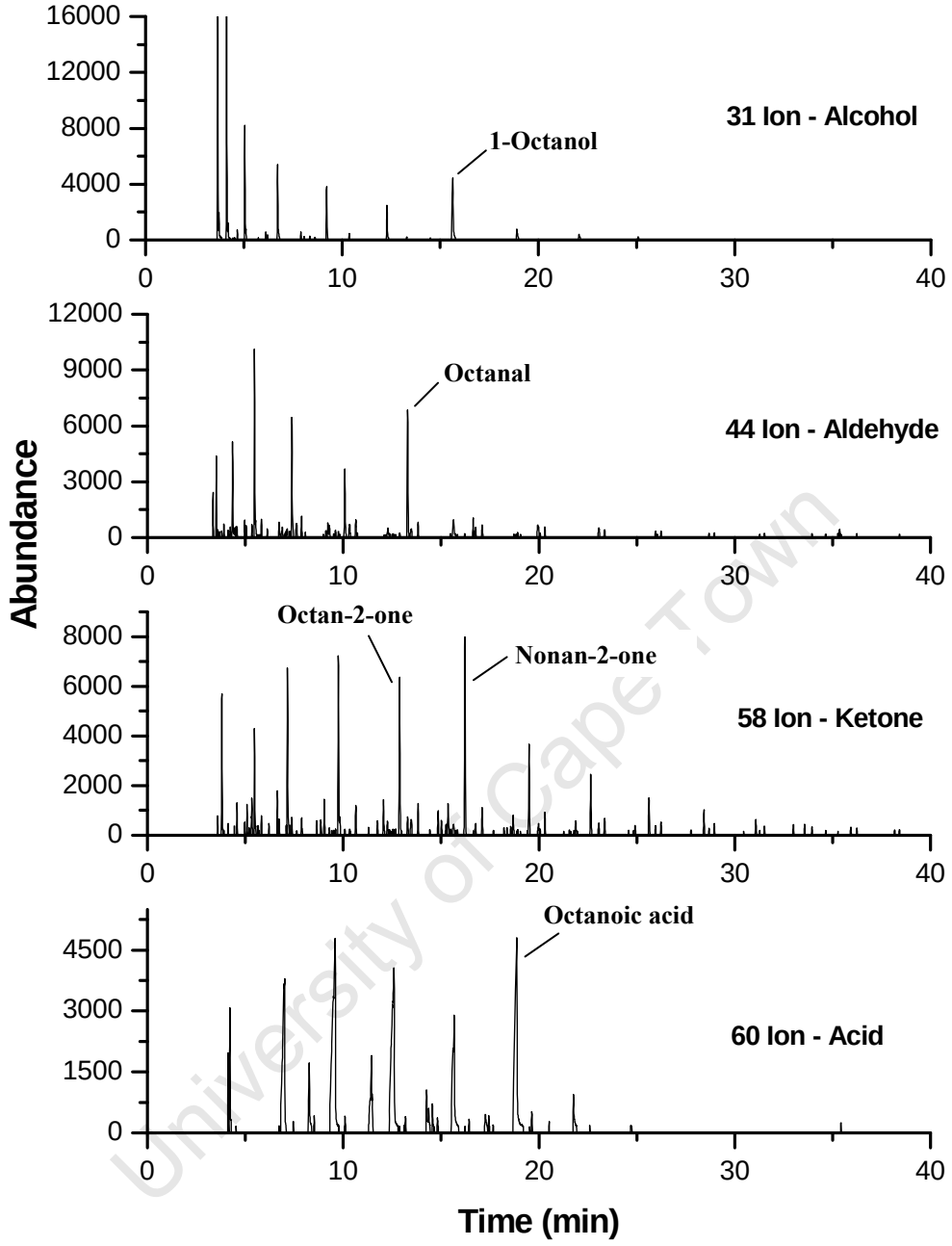

Figure 4.37 Extracted ion chromatograms of 0 wt% Cu catalyst with octanal co-feeding after 96 hours TOL during Fischer-Tropsch synthesis in a Berty reactor for ions m/z=31 (alcohols), m/z=44 (aldehydes), m/z=58 (ketones) and m/z=60 (acids)

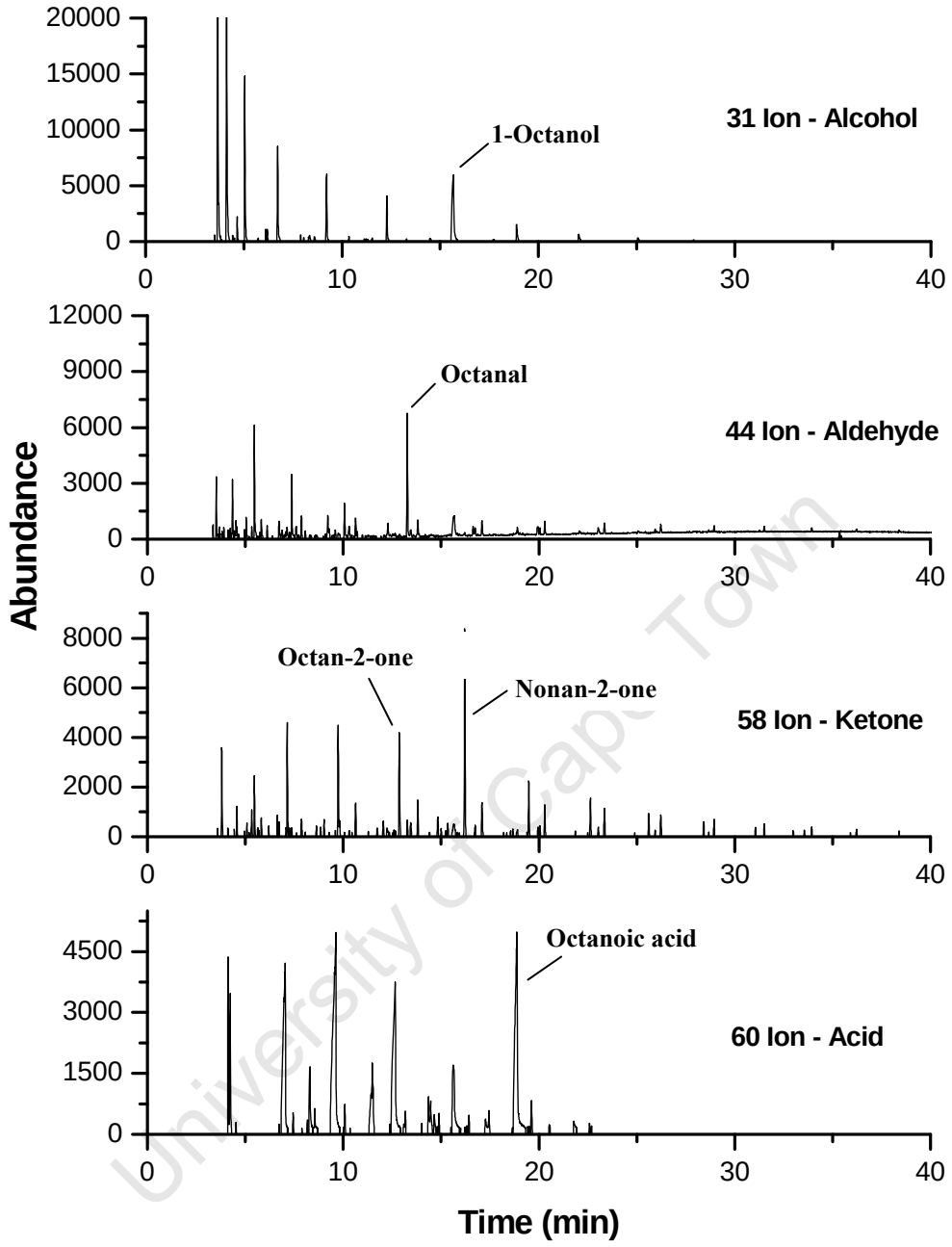

Figure 4.38 Extracted ion chromatograms of 50 wt% Cu catalyst with octanal co-feeding after 96 hours TOL during Fischer-Tropsch synthesis in a Berty reactor for ions m/z=31 (alcohols), m/z=44 (aldehydes), m/z=58 (ketones) and m/z=60 (acids)

4.6.5 Co-feeding of octan-2-one

The co-feeding of octan-2-one did not affect the synthesis gas conversion, or the hydrocarbon formation rates and selectivities (for data see Appendix M). It can therefore be concluded that, as with the other co-fed components, octan-2-one was not hydrogenated to the corresponding paraffin or incorporated into growing chains. In addition, no change in the iso-to-n paraffin ratio was observed in the C_9 fraction, indicating that no branched compounds were formed originating from the incorporation of this ketone; this reaction had previously been reported upon co-feeding of 2-propanol, which readily interconverts with acetone (*Kummer et al.*, *1951 and 1953* and *Tau et al.*, *1988*).

From the extracted ion chromatograms that were obtained during co-feeding of octan-2-one with the two different catalysts (Figure 4.39 and Figure 4.40) the reactions of the co-fed octan-2-one can possibly be identified. The results described in the two previous sections showed an increased formation of nonan-2-one upon co-feeding of 1-octanol and octanal. A reverse reaction of the methyl-ketone should therefore result in increased formation of oxygenates with a chain length of n-1, i.e. the C_7 oxygenates in this case. However, an inspection of the extracted ion chromatograms does not suggest an increased formation of 1-heptanol, heptanal or heptanoic acid (which can be included in this consideration since the interconversion of oxygenates was identified in the previous sections). A close inspection of formation rates of the C_7 and C_8 oxygenates shows that while the formation rates of C_8 oxygenates (1-alcohol, aldehyde and acid) remain unchanged during co-feeding, those of the C_7 oxygenates are not affected, or even seem to decrease slightly in comparison to the base case condition (48 hours time on-stream) without co-feeding (see Figure 1.39 and Figure 1.40 and Table M.3 in Appendix M).

Note: the increase of the “octanal” peak in the extracted ion chromatogram m/z=44 in the experiment with the copper promoted iron catalyst is due to increased formation of 2-octanol (see below) which also has an m/z 44 fragment in its histogram. The two products elute extremely close to each other from the GC-MS and so it is hard to separate them using this ion. So while it is unclear why the formation of some C_7 oxygenates decreased slightly, it is important to note that the reverse reaction of the methyl-ketone to the oxygenates of the next lower carbon number does not occur. As

no significant formation of these oxygenates was observed, no (modified) mass balance around these compounds was conducted for the octan-2-one co-feeding experiments.

Table 4.40 shows the area ratios of the extracted ion corresponding to 2-octanol, octylacetate and ethyl caprylate relative to decene during octan-2-one co-feeding. Additional chromatograms are supplied in Appendix M.

It can clearly be seen that large amounts of 2-octanol are formed during the co-feeding. This is further highlighted by extracted ion chromatograms m/z=45 for co-feeding product of the experiments with the two catalysts, shown in Figure 4.41. The formation of the secondary alcohol from the co-fed octan-2-one was in fact so pronounced that it could be followed in the FID spectra, and the conversion to this product could be calculated as being: 4.9 % for the iron catalyst and 17.9 % for the copper promoted iron catalyst, which again indicates that a much higher conversion was obtained in the hydrogenation reaction over the copper promoted catalyst.

As expected, no effect on the formation of octylacetate or methyl caprylate can be seen through the feeding of octan-2-one.

Table 4.40 Ratio of extracted ion (m/z) areas of 2-octanol (m/z=45), octylacetate (m/z=70) and ethyl caprylate (m/z=88) over decene (m/z=55) during octan-2-one co-feeding

			0 wt% Cu catalyst				
			Octan-2-one co-feeding				
TOL	48	53	72	77	93	117	126
Feeding	no	Octan-2-one				no	no
Area 2-Octanol / Area Decene	n/a [a]	0.021	1.084	1.023	0.757	0.387	0.239
Area Octylacetate / Area Decene	n/a [a]	n/a [a]	n/a [a]	0.016	n/a [a]	n/a [a]	0.022
Area Ethyl capralate / Area Decene	n/a [a]	n/a [a]	n/a [a]	0.013	n/a [a]	0.018	0.020
			50 wt% Cu catalyst				
			Octan-2-one co-feeding				
TOL	48	56	72	92	96		
Feeding	no	Octan-2-one					
Area 2-Octanol / Area Decene	0.008	0.014	1.821	1.548	1.335		
Area Octylacetate / Area Decene	n/a [a]	n/a [a]	n/a [a]	n/a [a]	n/a [a]		
Area Ethyl capralate / Area Decene	n/a [a]	n/a [a]	n/a [a]	n/a [a]	n/a [a]		

[a] Peak too small to be quantified

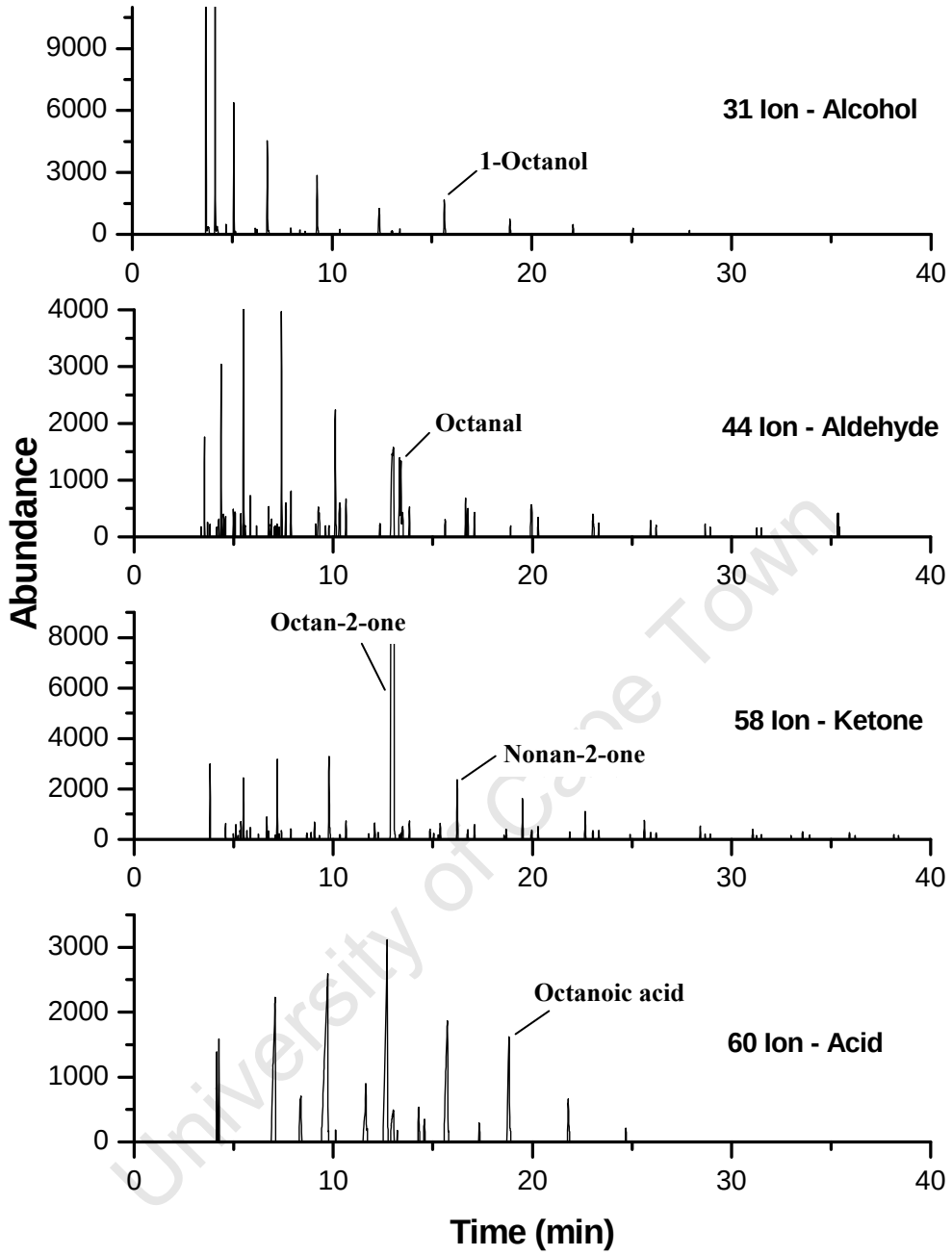

Figure 4.39 Extracted ion chromatograms of 0 wt% Cu catalyst with octan-2-one co-feeding after 96 hours TOL during Fischer-Tropsch synthesis in a Berty reactor for ions m/z=31 (alcohols), m/z=44 (aldehydes), m/z=58 (ketones) and m/z=60 (acids)

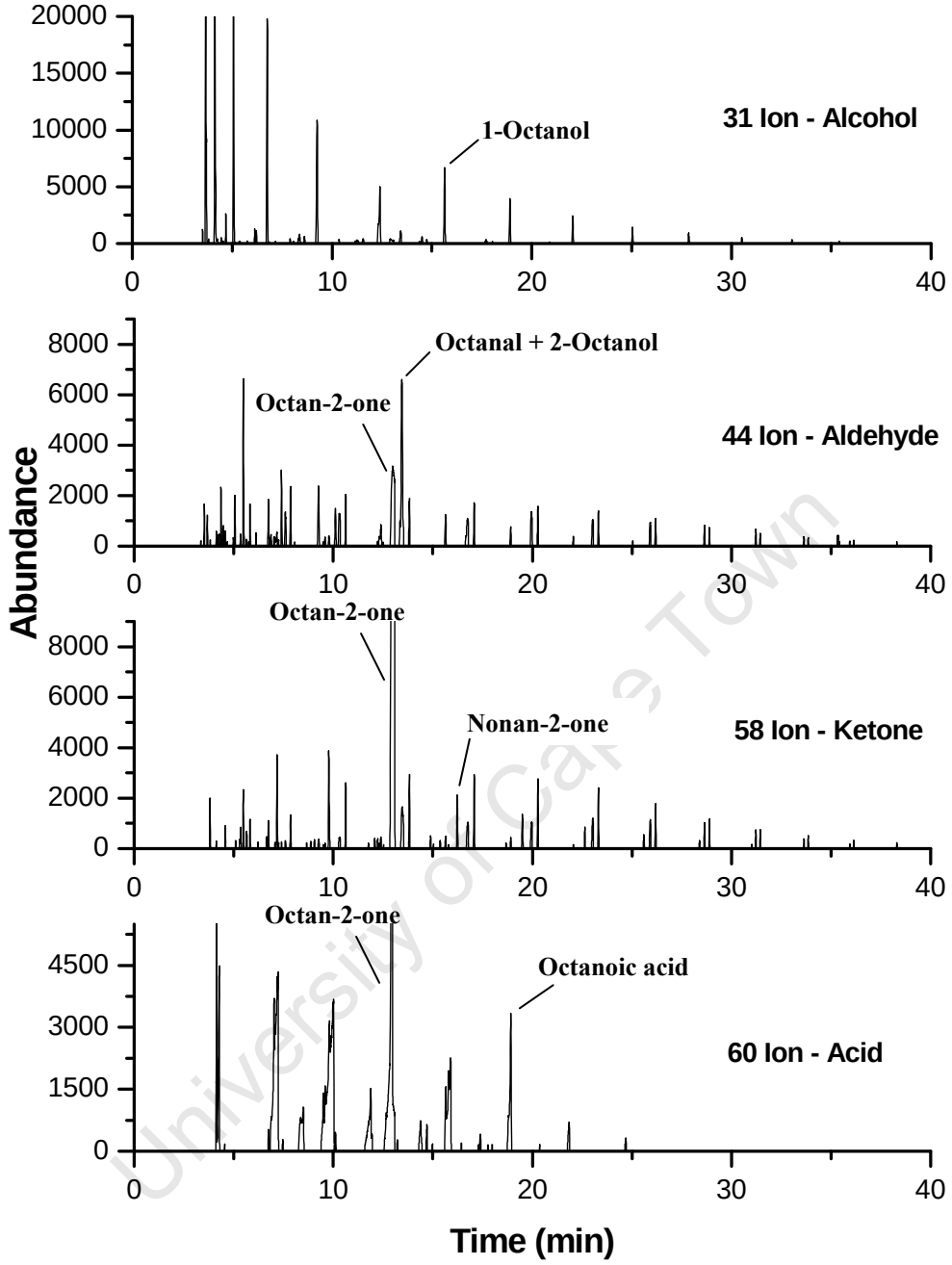

Figure 4.40 Extracted ion chromatograms of 50 wt% Cu catalyst with octan-2-one co-feeding after 96 hours TOL during Fischer-Tropsch synthesis in a Berty reactor for ions m/z=31 (alcohols), m/z=44 (aldehydes), m/z=58 (ketones) and m/z=60 (acids)

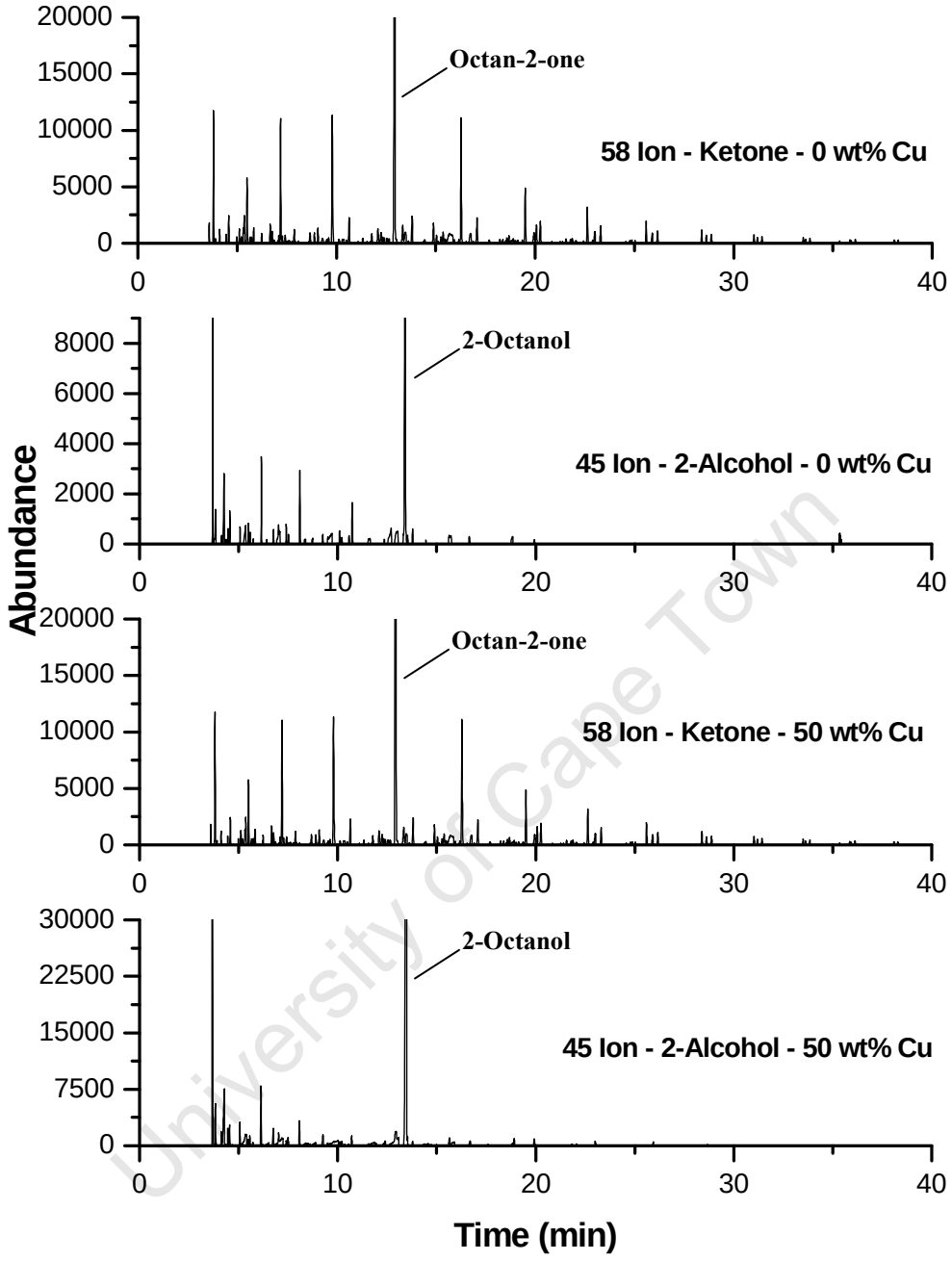

Figure 4.41 Extracted ion chromatograms of 0 and 50 wt% Cu catalyst with octan-2-one co-feeding after 96 hours TOL during Fischer-Tropsch synthesis in a Berty reactor for ions m/z=58 (ketones) and m/z=45 (2-alcohols)

4.6.6 Co-feeding of octanoic acid

As in the co-feeding of all previously discussed oxygenates the addition of octanoic acid during Fischer-Tropsch synthesis using the two different catalysts did not affect synthesis gas conversion. Also, hydrocarbon product selectivity and formation rates of C_8 and C_9 hydrocarbons were not affected by the small amounts of octanoic acid which were co-fed indicating that no, or no significant, hydrogenation to the corresponding paraffin (in this case, octane) or incorporation into growing chains occurred (for data see Appendix N).

An examination of the extracted ion chromatograms of the oxygenates of interest again reveals that octanoic acid also interacts with the other oxygenates, as clearly the formation of additional 1-octanol, octanal and nonan-2-one can be seen (Figure 4.42 and Figure 4.43). As expected, additional octan-2-one formation was not detectable upon octanoic acid co-feeding.

A direct mass balance from ingoing and outgoing flow in this experiment in particular was difficult, as a feed analysis using the offline ampoule sampling technique was not possible due to loss of this component upon sample introduction on the offline GC (Appendix N). Therefore, again, a modified mass balance has been conducted assuming the formation of the above listed products only (Table 4.41).

The same octanoic acid conversion of about 70% was obtained on both catalysts, and about 98% of the converted acid yielded 1-octanol plus octanal on both catalysts, but at different ratios, namely, around 3:1 with the iron catalyst compared to 10:1 with the copper promoted catalyst. This again indicated that a more “hydrogenated” product is achieved on the copper promoted catalyst. Less than 2% of the converted octanoic acid was converted to nonan-2-one on both catalysts.

Table 4.42 shows the area ratios of extracted ion chromatograms corresponding to 2-octanol, octylacetate and ethyl caprylate relative to decene during octanoic acid co-feeding. Additional chromatograms are supplied in Appendix N.

As expected the addition of octanoic acid did not impact on the formation of the secondary alcohol, 2-octanol, while increased formation rates of the two monitored esters octylacetate and ethyl caprylate can be seen on both catalysts in apparently equal quantities. It may again be speculated that the formation of ethyl caprylate is a direct result of an esterification of octanoic acid and ethanol, while octylacetate may have

formed via esterification of acetic acid and additional 1-octanol which originated from the co-fed octanoic acid. Again, no direct evidence for these esterification reactions could be found in the formation rates of the corresponding C_2 oxygenates analysed from the water phase. As in the case of 1-octanol (section 4.6.3) and octanal (4.6.4) co-feeding an additional peak was seen between the C_{17} and C_{18} linear hydrocarbon peaks. Unlike the previous cases however only one peak was seen (and identified as octanoic acidoctyl ester using GC-MS techniques). It is thought that the formation of octanoic acid octyl ester is via the esterification of the co-fed C_8 acid.

Table 4.41 Octanoic acid conversion and product selectivity for both 0 and 50 wt% Cu catalyst assuming 1-octanol, octanal, and nonan-2-one are the only products formed.

0 wt% Cu catalyst Octanoic acid co-feeding			
Time on-stream of analysis (hrs)	72	80	96
Octanoic acid conversion (%)	75.5	72.0	68.6
1-octanol selectivity (%)	65.0	65.6	67.3
Octanal selectivity (%)	32.9	32.6	30.7
Nonan-2-one selectivity (%)	2.1	1.8	2.0
50 wt% Cu catalyst Octanoic acid co-feeding			
Time on-stream of analysis (hrs)	72	89	96
Octanoic acid conversion (%)	61.4	70.5	68.5
1-octanol selectivity (%)	88.9	88.6	89.8
Octanal selectivity (%)	10.2	10.26	9.0
Nonan-2-one selectivity (%)	1.0	1.1	1.2

Table 4.42 Ratio of extracted ion (m/z) areas of 2-octanol (m/z=45), nonan-2-one (m/z=58), octylacetate (m/z=70) and ethyl caprylate (m/z=88) over decene (m/z=55) during octanoic acid co-feeding

			0 wt% Cu catalyst				
			Octanoic acid co-feeding				
TOL	48	56	72	80	96	103	120
Feeding	no		Octanoic acid			no	no
Area 2-Octanol / Area Decene	n/a [a]	0.010	0.020	0.011	0.015	0.017	0.019
Area Octylacetate / Area Decene	0.018	0.021	0.052	0.073	0.092	0.108	0.107
Area Ethyl capralate / Area Decene	0.009	0.024	0.355	0.401	0.403	0.420	0.341
			50 wt% Cu catalyst				
			Octanoic acid co-feeding				
TOL	48	65	72	89	96	113	123
Feeding	no		Octanoic acid			no	no
Area 2-Octanol / Area Decene	0.023	0.033	0.042	0.036	0.036	0.030	0.040
Area Octylacetate / Area Decene	0.026	0.041	0.071	0.080	0.090	0.085	0.104
Area Ethyl capralate / Area Decene	0.027	0.128	0.273	0.288	0.306	0.276	0.316

[a] Peak too small to be quantified

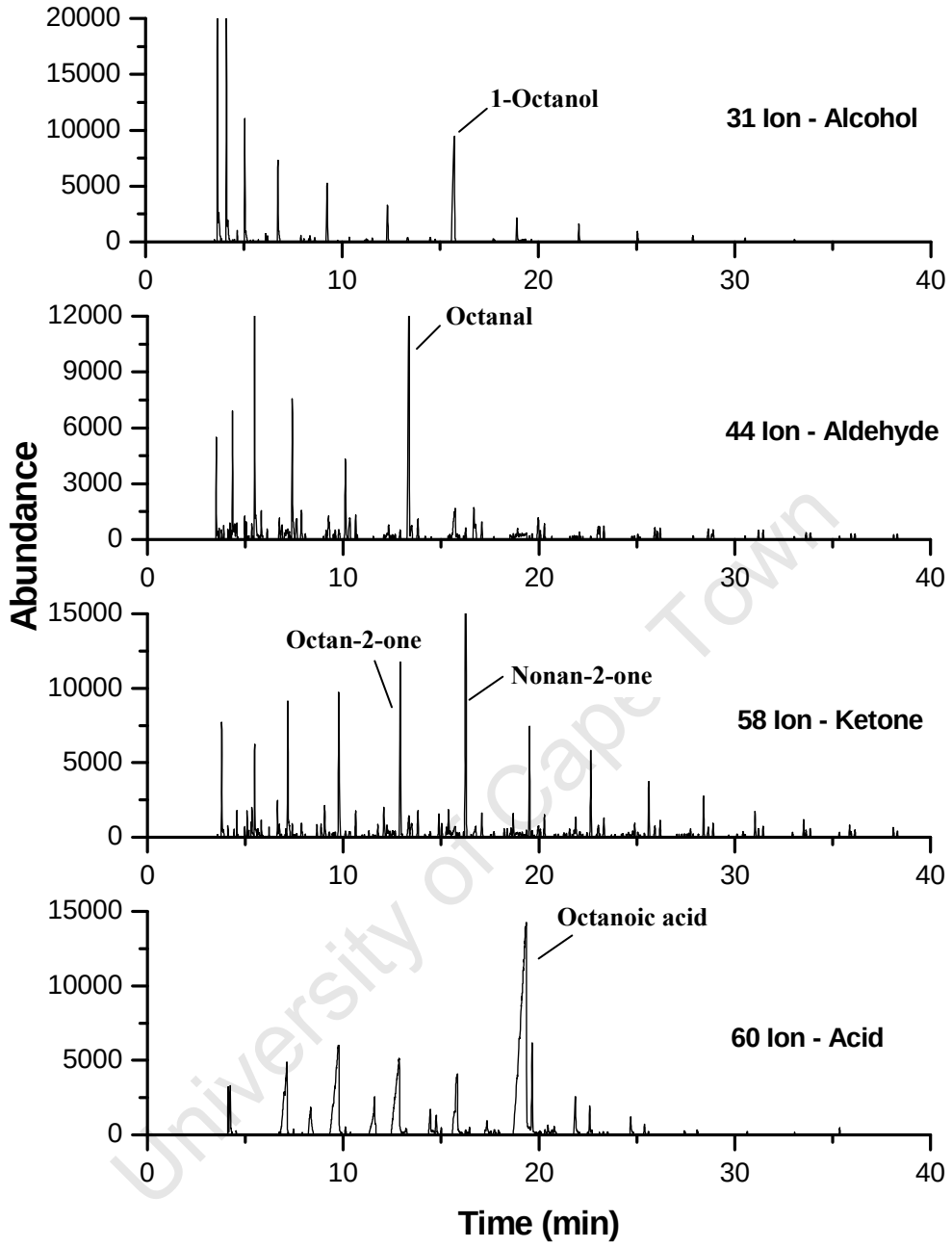

Figure 4.42 Extracted ion chromatograms of 0 wt% Cu catalyst with octanoic acid co-feeding after 96 hours TOL during Fischer-Tropsch synthesis in a Berty reactor for ions m/z=31 (alcohols), m/z=44 (aldehydes), m/z=58 (ketones) and m/z=60 (acids)

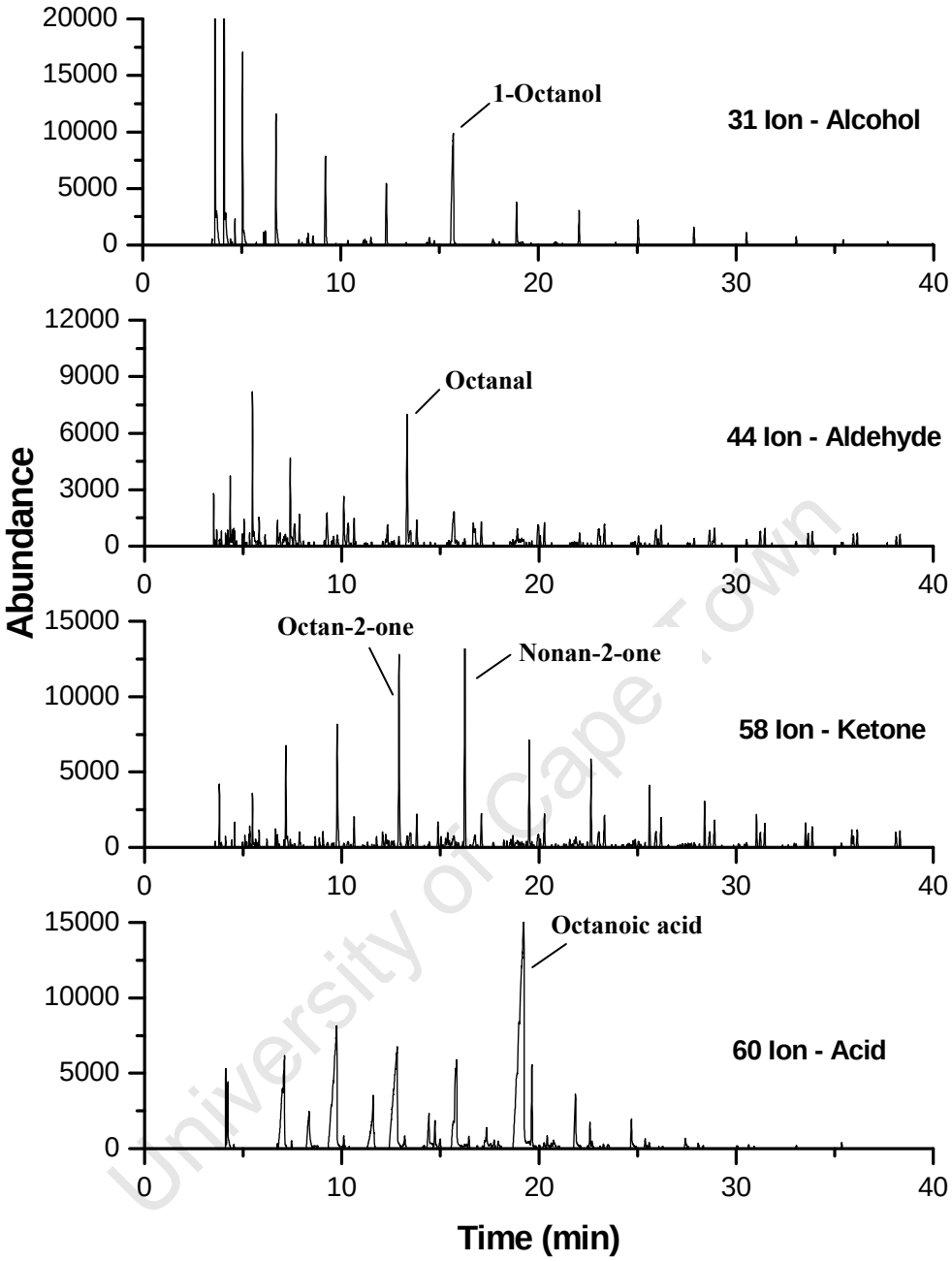

Figure 4.43 Extracted ion chromatograms of 50 wt% Cu catalyst with octanoic acid co-feeding after 96 hours TOL during Fischer-Tropsch synthesis in a Berty reactor for ions m/z=31 (alcohols), m/z=44 (aldehydes), m/z=58 (ketones) and m/z=60 (acids)

4.6.7 Discussion and summary of co-feeding results

The results on the co-feeding of the different oxygenates indicate close interaction of these components, and they provide important insight on mechanistic steps of the formation of oxygenates in the Fischer-Tropsch regime and the role of copper on these reactions. In the following discussion the thermodynamic feasibility of some reactions of relevance is reviewed and, taking the results from the co-feeding experiments into account, a reaction scheme for the formation and inter-conversion of oxygenates is proposed. In these considerations, hydrogenation of oxygenates to the corresponding hydrocarbon and incorporation into growing chains was not included, as no direct evidence for these reactions could be found in the co-feeding experiments described above.

Table 4.43 lists a number of reactions that might occur between the oxygenates, together with theoretic thermodynamic ratios to be expected at the actual reaction conditions (taking partial pressures of syn-gas, CO_2 and water into account) and the actual ratios of the corresponding oxygenates. This consideration indicates the thermodynamic feasibility of a reaction and how close an actual reaction is to its equilibrium. The data shown are for 96 hours time online and are shown as a function of the copper loading in the catalyst. Some of these reactions were discussed in section 4.5, but as additional reactions are now taken into account, the findings of the co-feeding work are used to substantiate or discard some of the listed reactions.

Table 4.43 Equilibrium ratios of C_8 oxygenates and nonan-2-one in product oil after 96 hours during Fischer-Tropsch synthesis in a Berty reactor for the iron-copper catalyst series using the TIC m/z ion specific areas

Reaction and ratio		Product ratios					
		0 wt% Cu[a]	2 wt% Cu	9 wt% Cu	23 wt% Cu	50 wt% Cu	77 wt% Cu
[A] Octanal + H_2 ⇔ 1-Octanol	Eq[b]	10.8	11.0	9.8	10.6	10.8	10.0
1-Octanol /Octanal	Obs[c]	2.7	3.1	2.7	6.4	9.8	11.2
[B] 1-Octanol + H_2O ⇔ Octanoic acid +2H_2	Eq	0.03	0.03	0.06	0.04	0.03	0.04
Octanoic acid/1-Octanol	Obs	0.09	0.10	0.20	0.11	0.09	0.07
[C] Octanal + H_2O ⇔ Octanoic acid + H_2	Eq	0.35	0.31	0.56	0.41	0.34	0.44
Octanoic acid/ Octanal	Obs	0.24	0.32	0.55	0.72	0.85	0.73
[D] Octanal + CO + 2H_2 ⇔ Nonan-2-one + H_2O	Eq	612092	861500	230235	573580	631899	358485
Nonan-2-one / Octanal	Obs	1.13	0.58	0.96	0.63	0.71	1.12
[E] 1-Octanol + CO + H_2 ⇔ Nonan-2-one + H_2O	Eq	56539	78268	23564	54087	58380	35700
Nonan-2-one /1-Octanol	Obs	0.27	0.19	0.53	0.46	0.60	0.82
[F] Octanoic acid + CO + 2H_2 ⇔ Nonan-2-one + 2H_2O	Eq	247116	392427	65293	206999	267570	125910
Nonan-2-one / Octanoic acid	Obs	0.10	0.06	0.20	0.07	0.06	0.07
[G] Octanal ⇔ Octan-2-one	Eq	415	415	415	415	415	415
Octan-2-one/ Octanal	Obs	0.36	0.23	0.64	0.59	0.77	1.01
[H] 1-Octanol ⇔ Octan-2-one + H_2	Eq	38.3	37.7	42.5	39.1	38.3	41.3
Octan-2-one/1-Octanol	Obs	0.13	0.08	0.24	0.09	0.08	0.09
[I] Octanoic acid + H_2 ⇔ Octan-2-one + H_2O	Eq	1170	1342	741	1024	1226	944
Octan-2-one/ Octanoic acid	Obs	1.54	0.73	1.16	0.82	0.90	1.38
[J] Octanoic acid + Acetic acid ⇔ Nonan-2one + CO_2 + H_2	Eq	1996	1097	1546	1817	1318	1996
Nonan-2-one / Octanoic acid	Obs	0.10	0.06	0.20	0.07	0.06	0.07

[a] Basis: Fully reduced catalyst

[b] Eq: Expected ratio at equilibrium

[c] Obs: Observed product ratios

Reaction [A] considers the conversion of octanal to 1-octanol. The co-feeding experiments have shown that this is a relatively facile and reversible reaction, which is enhanced by the presence of copper in the catalyst. At high copper loadings even thermodynamic equilibrium is reached. It is likely that copper promotion increases

hydrogen availability on the iron phases of the catalyst, therefore enhancing hydrogenation/dehydrogenation reactions. It is also likely that these reactions, similar to the hydrogenation of olefins (see section 4.4.2.3 and 4.5.3.3), occur on the metallic surface of copper itself. This reaction has been described before to occur during FT-synthesis (*Dry*, *1981*, *Schulz et al.*, *1970* and *Tau et al.*, *1987*) and it was reported that it reaches thermodynamic equilibrium in the C_2 fraction only at High Temperature Fischer-Tropsch conditions (600 K), but not at lower temperatures (510 K) (*Dry*, *2004*).

A significant finding of the co-feeding experiments is the observation of octanoic acid formation upon the addition of octanal and 1-octanol. Indeed, reactions [B] and [C] in Table 4.43 are at thermodynamic equilibrium, suggesting interaction between the acid and 1-octanol and octanal (which themselves are interacting strongly). Thermodynamic equilibrium of ethanol and acetic acid was earlier reported to occur at high temperatures by Dry (2004), but no direct evidence for this reaction was shown. Furthermore, the co-feeding of octanoic acid showed that the reverse reaction to the primary alcohol and the aldehyde does take place. For these reactions no clear effect of copper can be seen from the co-feeding work. It can thus be assumed that these reactions occur, unaided by copper, on the surface of the working iron catalyst only. But it is likely that the inter-conversion of these products and also their primary formation proceeds via a common intermediate.

Another significant finding of the co-feeding studies of this work includes the formation of nonan-2-one upon co-feeding of 1-octanol, octanal and octanoic acid, all of which interact with each other. Table 4.43 lists three reactions [D], [E] and [F] which take the conversion of these compounds to nonan-2-one into account, and it can be seen that the formation of nonan-2-one is thermodynamically highly favourable. The actual observed ratios of the corresponding compounds relative to nonan-2-one, however, indicate that equilibrium is not reached. It was further noted that methyl-ketones are not formed from oxygenates of the same carbon number, as evidenced in the co-feeding experiments where no additional formation of octan-2-one was detected during co-feeding of C_8 oxygenates. These reactions, although thermodynamically feasible (see reactions [G], [H] and [I]), would be hard to explain kinetically, as they would include a shift of the functional group from the terminal to internal carbon atoms. The formation of nonan-2-one from the three oxygenates, which seems unaffected by the presence of copper, suggests that the formation of methyl-ketones is also linked with the inter-

conversion of these oxygenates, and it is likely that it takes place via the same intermediate. It was noted, however, that the reverse reaction of a methyl-ketone to form the corresponding oxygenates of the next lower carbon number did not occur as was shown in the octan-2-one co-feeding experiments. The step of methyl-ketone formation should therefore be considered irreversible.

The only reaction that was observed during the co-feeding of octan-2-one was the formation of 2-octanol. This hydrogenation is similar to that of octanal to yield 1-octanol and it is believed to be rapid and enhanced by the presence of copper, possibly also occurring on the copper surface. This reversible hydrogenation reaction was earlier also reported to occur during the Fischer-Tropsch synthesis by Kummer *et al.*, (1951 and 1953), Dry (1981 and 2004) and Tau *et al.*, (1988). Dry reports that in the C_3 fraction, again only at high temperatures, thermodynamic equilibrium between acetone and 2-propanol is reached.

From the above observations a kinetic scheme was developed (Figure 4.44) which assumes a common precursor for the formation and inter-conversion of the oxygenates of interest. The studies do not allow for this conclusion if certain oxygenates are formed via secondary pathways only. Similar to the formation and reactions of hydrocarbons (olefins and paraffins) it is assumed that all oxygenates can form as primary products and be inter-converted into other products via secondary reactions. The primary and secondary pathways are likely to occur through the same intermediate(s), in this case an oxygen-containing species, namely an acyl group [1] which can be hydrogenated to species [2] in a reversible reaction (Figure 4.44). The formation of these intermediates can be explained via the CO insertion mechanism (*Pichler and Schulz*, *1970*) or, alternatively, an OH addition to an alkylidene species as proposed by Johnston and Joyner (*Johnston and Joyner*, *1993*) (see also sections 1.2.1 and 1.4.2.5). Species [1] and species [2] are assumed to interconvert rapidly.

From species [1], upon hydrogen addition, primary alcohols can form, while hydrogen addition to species [2] leads to the formation of the corresponding aldehyde. Both products can easily re-adsorb and be inter-converted. These hydrogenation/dehydrogenation reactions are generally very facile on metallic surfaces, and copper is likely to promote them via enhancing hydrogen availability. An addition of an OH surface species to species [2] would explain the formation of acids, again in a reversible reaction, while the addition of a CH_3 group could explain the formation of

methyl-ketones from the same precursor. The latter reaction appears to be irreversible, and methyl-ketones can only react further to form secondary alcohols in a reversible reaction, as also indicated in (Figure 4.44). In further side reactions esters can be formed from primary alcohols and acids, but it is not clear if these reaction proceed on metallic catalyst surfaces.

It should be noted that the proposed type of reaction for the formation of the methyl-ketone, which includes the addition of a methyl species, should, in principle, also account for formation of ethyl-, propyl- etc. ketones via the addition of the corresponding alkyl species. The latter products are typically not reported as products of Fischer-Tropsch synthesis, and it is likely that they are only present in low quantities. C_1 surface species are however regarded as by far the most abundant on a working Fischer-Tropsch catalyst, and consequently mainly methyl-ketones should be formed via the proposed reaction (these products could not however, be found successfully using the methods available). It should be noted that an alternative reaction pathway for the secondary formation of methyl-ketones has been proposed by Dry (2004), who considered a ketonisation reaction which includes the conversion of acids.

$$2\text{acetic acid} \Leftrightarrow \text{acetone} + CO_2 + H_2O \qquad (4.4)$$

where $\Delta G^R_{300\,°C} = -65.2$ kJ/mol

This reaction has been found to approach thermodynamic equilibrium at High Temperature Fischer-Tropsch conditions. The corresponding ketonisation type reaction for octanoic acid plus acetic acid [J] is included in Table 4.43 for the experiments of this thesis, and the equilibrium composition is not obtained. The equilibrium ratio is, however, closer than the direct reaction route from octanoic acid. Similar to the discussion above, a combination of acids of longer chain lengths would also yield ketones other than methyl-ketones. Indeed, some evidence for the occurrence of a ketonisation type reaction was reported by Wang and Davis (1999), who reacted 1-octanol over Fe_2O_3 and iron carbide and found a symmetrical C_{15} ketone, believed to be formed via the ketonisation of octanal which formed from 1-octanol dehydrogenation. Their model studies were however conducted in the absence of synthesis gas, and a CH_3 addition as proposed in Figure 4.44 could therefore not take place.

The studies of this work also showed the appearance of an unidentified peak at high carbon numbers, but not during octanoic acid co-feeding (the common peak is thought

to be octanoic acid octyl ester). Furthermore it can be noted that during the co-feeding of octan-2-one no increase of heptanoic acid was observed, which one would expect from the reverse reaction of the ketonisation of heptanoic acid and acetic acid:

$$\text{heptanoic acid} + \text{acetic acid} = \text{octan-2-one} + CO_2 + H_2O \qquad (4.5)$$

Where $\Delta G^{R}_{300°C}$ = -69.1 kJ/mol.

The proposed reaction mechanism in Figure 4.44 is therefore considered the more likely one. It must be added that aspects of this mechanism were, in principle, originally proposed by Schulz (1977b), but the results of this work provide experimental evidence for it.

Figure 4.45 attempts to indicate which reactions are affected by copper as a promoter in the Fischer-Tropsch catalyst. As highlighted in Sections 4.4 and 4.5, enhanced overall selectivity of oxygenates was achieved with copper promotion. According to the kinetic scheme it is therefore likely that copper helps to promote the primary formation of the oxygenate precursor species [1] and [2], which readily interact. Copper can therefore either be assumed to promote the CO insertion step or the addition of OH groups. It was noted that virtually no syn-gas conversion was achieved during the experiments with the pure copper catalyst using the synthesis gas ($4H_2$:$1CO$:$1CO_2$), not even activity of the reverse water gas shift reaction. It can therefore be assumed that no OH species (which may then have spilt over to the iron phases) were formed on the copper surface. Also, the addition of copper did not clearly impact on the formation of acids, which according to the mechanism proposed also includes the addition of OH species. It is therefore perhaps more likely, although still speculative, that copper activates CO groups which it then provides to the iron phases where increased amounts of surface species [1] and [2] are produced, and from there the corresponding oxygenates are formed.

Copper clearly enhanced the hydrogenation/dehydrogenation activity of the catalyst likely to occur via hydrogen spillover to the iron surfaces, although these reactions probably also occur on the copper surface itself. This impacts on the interaction between the aldehyde and 1-alcohol, and the methyl-ketone and 2-alcohol, and generally leads to the more thermodynamically favourable products, which at these conditions are the hydrogen richer products, i.e. the alcohols.

In summary, the co-feeding experiments show strong interaction of the major oxygenates formed during Fischer-Tropsch synthesis. It could be shown that acids can be formed in reversible reactions from 1-alcohols and aldehydes. In addition, methyl-ketones can be formed from these three oxygenates in an irreversible reaction. It was proposed that all products are formed in primary and secondary reactions and that a common intermediate exists in these reactions. Copper helps to promote the primary formation of this intermediate but also promotes secondary partial hydrogenation reactions, leading to primary and secondary alcohols.

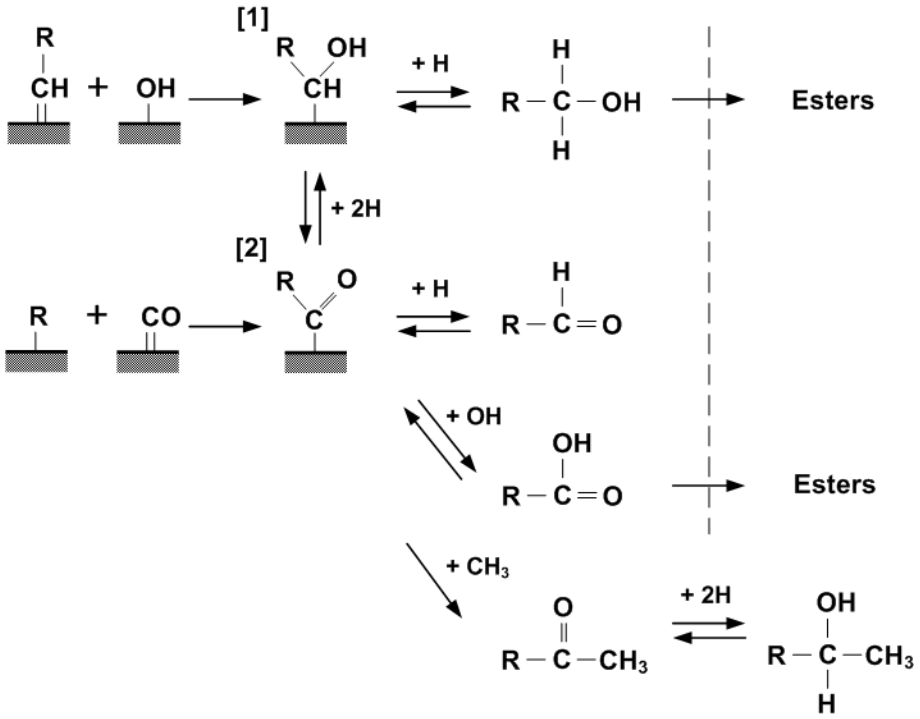

Figure 4.44 Kinetic scheme of oxygenate formation and interaction as seen from co-feeding tests

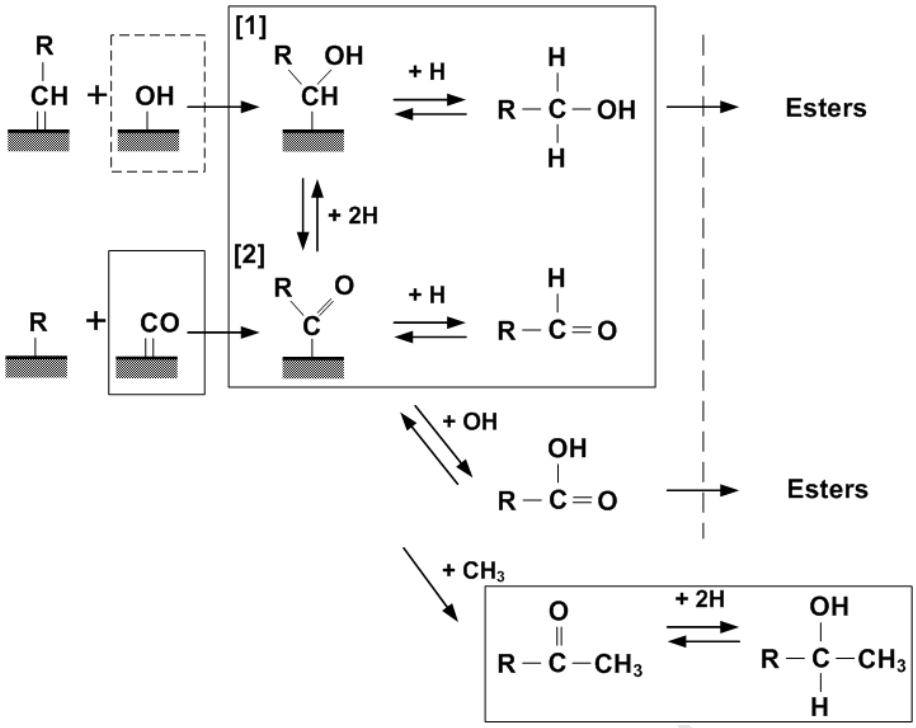

Figure 4.45 Kinetic scheme of oxygenate formation and interaction as seen from co-feeding tests with copper promoted routes highlighted

Chapter 5

Conclusions and recommendations

Full summaries are supplied after every section in the preceding chapter. However, the major observations and conclusions will be discussed here again.

Preparation and characterisation of calcined, reduced and spent co-precipitated iron-copper catalysts

Iron catalysts with varying copper loadings were successfully prepared via the co-precipitation of their nitrates. After calcination in air at 400 °C characterisation of these catalysts showed that an increase in the addition of copper in the co-precipitation process formed small (x-ray amorphous) iron crystallites whose phase could not be successfully determined using the techniques employed.

Upon reduction under hydrogen the copper oxides and iron phases were successfully reduced to their pure metal states and the promotional effect of copper on the rate of reduction was clearly seen (lowering the initial reduction temperature of the iron by 100 °C). The iron crystallites formed crystals of the same size (approx. 30-35 nm) for all the catalysts, while the copper crystallites increased in size with copper loading. Additionally, the assumption that the loaded potassium spreads evenly across both metal surfaces was not confirmed, as evidenced in the TPR of the pure copper sample. It was shown that the potassium had a higher affinity for the iron than the copper.

During synthesis the metallic iron changed to a combination of mainly Hägg carbide and some magnetite, as expected during normal Fischer-Tropsch synthesis (the ratio of these two phases seems constant, and was not affected by the catalyst copper loading). The copper phase was seen to be the same as that after reduction (i.e. pure metallic phase).

As with the calcined catalysts the crystallite sizes of the iron phases seem to decrease with copper loading while the copper crystallite sizes increase.

Fischer-Tropsch synthesis – effect of copper on product selectivity

The pure copper catalyst showed no Fischer-Tropsch activity under these reaction conditions, and the addition of copper to iron catalysts had no effect on the overall activity of the catalysts. While the fixed-bed results showed that copper did not affect the methane selectivity and the chain growth probability (α), a slight increase in methane selectivity with a corresponding decrease of the chain growth probability with increasing copper content might be discernable in the Berty reactor results.

Copper was found to affect the olefin contents in the hydrocarbon product, where an increase in copper loading led to the more hydrogenated product in the C_2 fraction (seen in both reactors) and in very high carbon number fractions ($>C_8$ – only seen in the Berty reactor). In addition, a shift of primary selectivity towards a more paraffinic product could be identified in the Berty reactor – from the comparatively low carbon number independent olefin contents in the C_3 to C_8 fraction of the product from the highly copper promoted catalyst.

It is therefore proposed that copper impacts on both primary hydrocarbon product formation (alpha-olefin versus paraffin), and secondary olefin consumption (hydrogenation and double bond shift isomerisation). This is most likely via facile hydrogen activation and subsequent hydrogen surface enrichment of the active iron phases. In addition, secondary olefin reactions may take place on the surface of copper.

The most significant effect of copper promotion, however, is the pronounced increase in the amount of oxygenates, in particular alcohols. It could be shown that there appears to be a rapid interaction between 1-alcohols and the corresponding aldehydes, in particular on copper promoted catalysts, where the corresponding partial equilibria were

obtained in different carbon number fractions with the Berty reactor. It was also shown that this result is not due to potassium but a true copper effect.

It was postulated that copper, which does not promote CO bond dissociation, supplies the iron surface with molecular CO species, which might be involved in the formation of oxygenates in the Fischer-Tropsch synthesis. To achieve this selectivity improvement the catalyst should preferably be prepared in such a way that copper is in close contact with iron, e.g. via co-precipitation, as was shown with catalyst mixtures on the fixed-bed tests.

A method for the quantification of long chain oxygenates using GC/MS techniques was developed, which also enabled the identification and quantification of the carboxylic acids from liquid product samples. Thermodynamic analysis of partial equilibria indicates that an interaction between acids, and alcohols or aldehydes takes place.

Co-feeding of C_8 oxygenates – mechanistic conclusions

The results on the co-feeding of the different oxygenates indicate close interaction of these components; they provide important insight on mechanistic steps of the formation of oxygenates in the Fischer-Tropsch regime and the role of copper on these reactions. Figure 5.1 shows the reaction scheme devised from the feeding experiments. It was shown that 1-octanol, octanal and octanoic acid all readily interact, possibly through an acyl intermediate, and that these reactions are reversible. Additionally, nonan-2-one was found to be a product of all three oxygenates when fed over both catalysts, suggesting that the n+1 methyl-ketone is formed through the addition of a CH_3 group to the acyl intermediate. This reaction, however, is not reversible, as shown by the octan-2-one feeding tests. The methyl-ketone is readily hydrogenated to the methyl-alcohol (in this case 2-octanol with octan-2-one feeding). It is thought that this reaction (as with 1-octanol and octanal) is reversible, but this has not been shown. The oxygenates were not seen to be hydrogenated to hydrocarbons nor incorporated for chain growth in any of the feeding tests.

The addition of copper to the iron catalyst and its effects on the product selectivities during co-feeding, showed that in all cases the more hydrogenated product (in this case the alcohol) was preferred. The conversions of octanol, octanal and octan-2-one were also enhanced by copper.

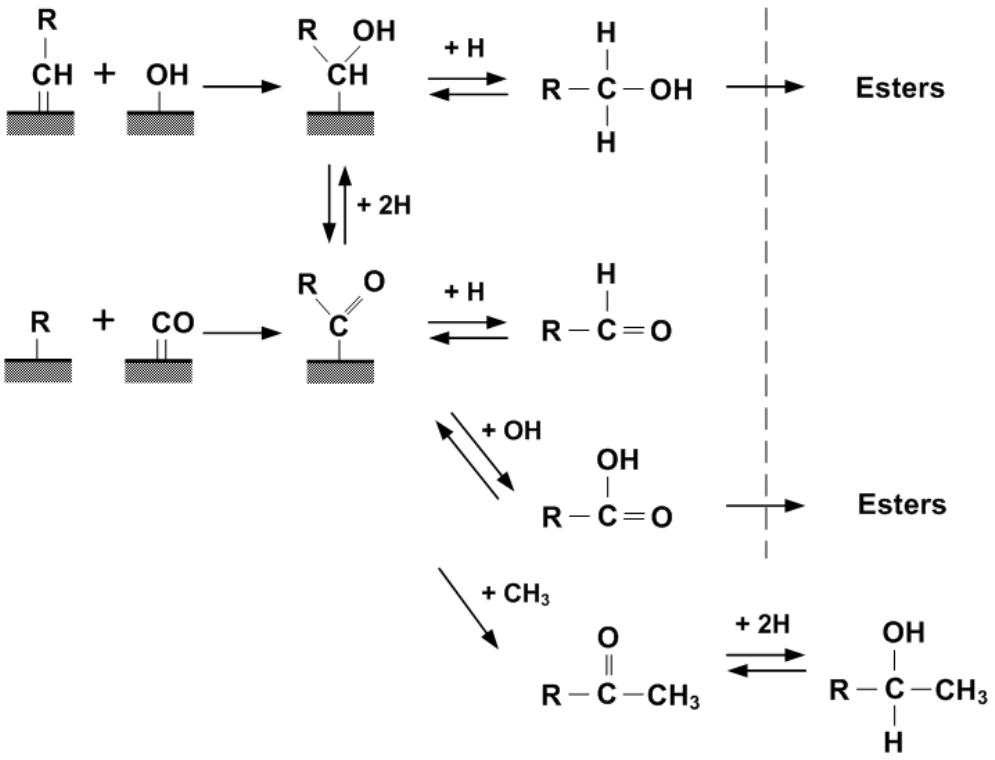

Figure 5.1 Kinetic scheme of oxygenate formation and interaction

Copper and iron Fischer-Tropsch

Enhanced overall selectivity of oxygenates was achieved with copper promotion. It is therefore likely that copper helps to promote the primary formation of the oxygenate precursor species which readily interact to form oxygenate products. As no water gas shift activity was seen on the copper, it is proposed that no OH species (which may then have spilt over to the iron phases) were formed on the copper surface. Also, the addition of copper did not clearly impact on the formation of acids, which, according to the mechanism proposed, also includes the addition of OH species. It is therefore more likely, although still speculative, that copper activates CO groups which it then provides to the iron phases, where increased amounts of the surface acyl species, and from there the corresponding oxygenates are formed.

Copper clearly enhanced the hydrogenation/dehydrogenation activity of the catalyst; this is likely to occur via hydrogen spillover to the iron surfaces, although these reactions probably also occur on the copper surface itself. This impacts on the interaction between the aldehyde and 1-alcohol, and the methyl-ketone and 2-alcohol,

and generally leads to the more thermodynamically favourable products, which at these conditions are the hydrogen richer products, i.e. the alcohols.

Suggested further work

While this report has attempted to be as thorough as possible, certain areas have been identified that would create a better understanding of the results seen and perhaps a more rounded explanation.

Of immediate interest is the copper-iron interaction and how close the copper needs to be to the iron for the enhanced selectivities to take effect. The first point of further examination should be the reduction aspect of the catalysts. It is thought that the catalysts used in these experiments could have been reduced completely at lower temperatures so as to reduce effects of copper sintering and associated loss of copper surface area for copper-iron interaction. Subsequent to this, the testing of mixtures of copper and iron as well as the addition and removal of copper to iron during reduction could also be examined.

Additionally, the use of the 'reverse micelle', or microemulsion technique, to create small crystallites of supported copper and iron, or small crystallites of the one and normal sized crystallites of the other, could enhance the understanding of the surface interactions. Further examination could also be done on other supported catalysts and this would be especially helpful in the 100 wt% Cu catalyst as further work with it was discarded after no activity was seen.

For the catalyst characterisation, most of the methods used were bulk techniques that examined the bulk phase and interaction of the catalysts. It is plausible that there is some surface interaction of both the metals (copper and iron) as well as interesting effects of adsorbed syngas that could be seen through the use of surface characterisation methods.

In the case of the co-feeding tests, the feeding of an iso-alcohol such as 2-octanol would complete the understanding of the surface interactions of the oxygenates. In the case of the octan-2-one feeding experiments, where it seemed a decrease in the C_7 oxygenates was seen, further work would need to be done in to establish the nature of this seemingly strange interaction. Also, as no hydrogenation or incorporation of any of the

co-fed components to hydrocarbons was seen, these tests could possibly be repeated using ^{13}C or ^{14}C tagged compounds, to verify this finding.

BIBLIOGRAPHY

Anderson, K.G. & Ekerdt, J.G. (1985), 'Study of Fischer-Tropsch synthesis over $FeSiO_2$: Effect of diethylamine on hydrocarbon and alcohol production', *Journal of Catalysis*, no. 95, pp. 602.

Anderson, R.B. (1984), *The Fischer-Tropsch Synthesis*, Academic press, inc., Orlando.

Arakawa, H. & Bell, A.T. (1983), 'Effects of potassium promotion on the activity and selectivity of iron Fischer-Tropsch catalysts', *Ind. Eng. Chem. Process Des. Dev.*, vol. 22, no. 1, pp. 97-103.

Arakawa, H., Takeuchi, K., Matsuzaki T., & Sugi, Y. (1984), 'Effect of Metal Dispersion on the Activity and Selectivity of Rh/Sio2 Catalyst for High Pressure Co Hydrogenation', *Chemistry Letters*, vol. 13, no. 9, pp.1607-1610.

Baker, R. & Rodriguez, N. (1994), 'A Review of the Use of In Situ Electron Microscopy Techniques for the Study of Iron-Based Catalysts for Coal Conversion Processes', *Energy & Fuels*, vol. 8, no. 2, pp. 330.

Barkhuizen, D., Mabaso, I., Viljoen, E., Welker, C., Claeys, M., van Steen, E. & Fletcher, J. (2006), 'Experimental approaches to the preparation of supported metal nanoparticles', *Pure Applied Chemistry*, vol. 78, no. 9, pp. 1759-1769.

Bhasin, M.M., Bartley, W.J., Ellgen, P.C. & Wilson, T.P. (1978), 'Synthesis gas conversion over supported rhodium and rhodium-iron catalysts', Journal of Catalysis, vol. 54, no. 2, pp 120-128.

Bezemer, G., Bitter, J., Kuipers, H., Oosterbeek, H., Holewijn, J., Xu, X., Kapteijn, F., van Dillen, A., de Jong, K. &, (2006), 'Cobalt particle size effects in the Fischer-Tropsch reaction studied with carbon nanofiber supported catalysts', *Journal of American Chemical Society*, vol. 128, pp. 3956.

Bukur, D., Okabe, K., Rosynek, P., Li, C., Wang, D., Rao, K. & Huffman, G. (1995), 'Activation studies with a precipitated iron catalyst for Fischer-Tropsch synthesis', *Journal of Catalysis*, vol. 155, pp. 353-365.

Campos-Martín, J.M., Fierro, J.L.G., Guerrero-Ruiz, A., Herman, R.G. & Klier, K. (1996), 'Promoter Effect of Cesium on C–C Bond Formation during Alcohol Synthesis from CO/H_2over Cu/ZnO/Cr_2O_3Catalysts', Journal of Catalysis, vol. 163, no. 2, pp 418-428.

Chen, W.M., Ding, Y.J., Jiang, D.H., Wang, T., & Luo, H.Y. (2006), 'A selective synthesis of acetic acid from syngas over a novel Rh nanoparticles/nanosized SiO2 catalysts', *Catalysis Communications*, vol. 7, no. 8, pp. 559-562.

Chichen, G.C., Spencer, M.S., Waugh, K.C. & Whan, D.A. (1986), *Faraday Symp. Chem. Soc.*, 21, paper 18.

Chichen, G.C., Waugh, K.C. & Whan, D.A. (1986), 'The activity and state of the copper surface in methanol synthesis catalysts', *Applied Catalysis*, vol. 25, pp 101-107.

Chichen, G.C., Spencer, M.S., Waugh, K.C. & Whan, D.A. (1987), 'Promotion of methanol synthesis and the water-gas shift reactions by adsorbed oxygen on supported copper catalysts', *J. Chem. Soc., Faraday Trans*. 1, 83, pp 2193-2212.

Claeys, M. & Schulz, H. (2004), 'Effects of internal mass transfer on activity and selectivity in iron based Fischer-Tropsch synthesis', *Prepr. Pap.-Am. Chem. Soc., Div. Pet. Chem.*, vol. 49, no. 2, pp. 195.

Claeys, M. & van Steen, E. (2004), Basic studies. In A. Steynberg & M. Dry (Ed.), *Fischer-Tropsch Technology, vol 152 of Studies in surface science and catalysis*, (Chapter 8) Amsterdam:Elsiveir.

Claeys, M. (1997), *Selectivität, Elementarschritte und kinetische Modellierung bei der Fischer-Tropsch-Synthese*. Universität Fridericiana Karlsruhe.

Claeys, M., Cowan, R. & Schulz, H. (2003), 'Temporal changes of Fischer-Tropsch activity and selectivity using ruthenium: Fischer-Tropsch catalysis-science and practice', *Topics in catalysis*, vol. 26, no. 1-4, pp. 139-143(4).

Craxford, S. & Rideal, E. (1939), 'Die Fischer-Tropsch synthese von kohlonwasserstoffen und einige verwandte reaktionen', *Brennstoff Chemie*, no. 20, pp. 263.

Daubert, T. (1999), *Physical and thermodynamic properties of pure chemicals: evaluated process design data*, Taylor and Francis, Philadelphia, Pensilvania, USA.

Davis, B. (2001), 'Fischer-Tropsch synthesis: current mechanism and futuristic needs', *Fuel processing technology*, vol. 71, no. 71, pp. 157-166.

Davis, B.H. (1993), *^{14}C tracer studies of the Fischer-Tropsch Synthesis*, International Conference on Catalysis and Catalytic Processing, 24-27 October 1993 Cape Town, South Africa.

Dry, M. (1981), Catalysis - Science and Technology. In John R. Anderson and Michel Boudart (Ed.), *Volume 1*, (pp. 159-255). Berlin Heidelburg:Springer-Verlag.

Dry, M. (1982), 'Catalytic aspects of industrial Fischer-Tropsch synthesis', *Journal of Molecular Catalysis*, no. 17, pp. 133-144.

Dry, M. (1996), 'Practical and theoretical aspects of the catalytic Fischer-Tropsch process', *Applied Catalysis A: General*, no. 138, pp. 319-344.

Dry, M. (2002), 'The Fischer-Tropsch process: 1950 - 2000', *Catalysis Today*, no. 71, pp. 227-241.

Dry, M. (2004), Chemical concepts used for engineering purposes. In A. Steynberg & M. Dry (Ed.), *Fischer-Tropsch Technology, vol 152 of Studies in surface science and catalysis*, (Chapter 3) Amserdam:Elsevier.

Dry, M.E. & Oosthuien, G.J. (1968), 'The correlation between catalyst surface basicity and hydrocarbon selectivity in te Fischer-Tropsch synthesis', *Journal of Catalysis*, no. 11, pp. 18-24.

Dry, M.E. (1990), 'The Fischer-Tropsch process - commercial aspects', *Catalysis Today*, no. 6, pp. 183.

Dry, M.E. (2003), Chapter 3. *Encyclopaedia of Catalysis*, New York, U.S.A. John Wiley and Sons.

Dry, M.E., Shingles, T. & van H. Botha, C.S. (1970), 'Factors influencing the formation of carbon on iron Fischer-Tropsch catalysts', *Journal of Catalysis*, no. 17, pp. 341-346.

Eidus, Y. T., (1967) 'The mechanism of the Fischer-Tropsch reaction and he initiated Hydropolymerisation of alkenes, from radiochemical kinetic data.' *Russian Chemical Reviews,* Vol. 36, no. 5, pp. 338.

Emmett et al as referenced in Anderson, R.A. (1984), *The Fischer-Tropsch synthesis*, Academic press, inc., Orlando.

Erley, W., McBreen, P. & Ibach, H. (1983), 'Evidence for CH_x surface species after the hydrogenation of CO over an Fe(110) single crystal surface', *Journal of Catalysis*, no. 84, pp. 229.

Ertl, G., Knözinger, H. & Weitkamp, J. (1997), *Handbook of heterogeneous catalysis*, VCH, Weinheim, Federal Republic of Germany.

Fischer, F. & Tropsch, H. (1926), 'The synthesis of petroleum at atmospheric pressures from gasification products from coal', *Brennstoff Chemie*, no. 7, pp. 97-104.

Forzatti, P., Tronconi, E. & Pasquon, I. (1991), 'Higher Alcohol Synthesis', Catalysis Reviews, vol. 33, no. 1 & 2 pp 109–168.

Hanaoka, T., Arakawa, H., Matsuzaki, T., Sugi, Y., Kanno K., & Abe, Y. (2000) 'Ethylene hydroformylation and carbon monoxide hydrogenation over modified and unmodified silica supported rhodium catalysts', *Catalysis Today*, vol. 58, no. 4, pp. 271-280

Herman, R.G. (2000), 'Advances in catalytic synthesis and utilization of higher alcohols', Catalysis today, vol. 55, no. 3, pp 233-245.

Hindermann, J.P., Hutchings, G.J. & Kiennemann, A. (1993), 'Mechanistic aspects of the formation of hydrocarbons and alcohols from CO hydrogenation', *catal. rev. -sci. eng.*, vol. 35, no. 1, pp. 1-127.

Huff, G. & Satterfield, C. (1984), 'Evidence for two chain growth probabilities on iron catalysts in the Fischer-Tropsch synthesis', *Journal of Catalysis*, no. 85, pp. 370-379.

Iglesia, E., Reyes, S.C., Madon, R.J. & Soled, S.L. (1993), 'Selectivity Control and Catalyst Design in the Fischer-Tropsch Synthesis: Sites, Pellets, and Reactors', *Advances in catalysis*, no. 39, pp. 221-302.

Jager, B. & Espinoza, R. (1995), 'Advances in low temperature Fischer-Tropsch synthesis', *Catalysis Today*, vol 23, no. 1, pp. 17-28.

Jager, B. (1997), 'Developments in Fischer-Tropsch Technology', *Natural Gas Conversion IV, Studies in Surface Science and Catalysis*, vol. 107, pp. 219-224.

Jin, Y. & Datye, A. (2000), 'Phase transformations in iron Fischer-Tropsch catalysts during temperature-programmed reduction', *Journal of Catalysis*, vol. 196, pp. 8-17.

Johnston, P. & Joyner, R. (1993), *Structure-function relationships in heterogeneous catalysis: The embedded surface molecule approach and its applications*, Elsevier, Budapest, Hungary.

Kaiser, R. (1969), *Chromatographie in der Gasphase*, Bibliographisches Institut, Mannheim.

Kaminsky, M., Winograd, N., Geoffroy, G. & Vannice, M.A. (1986), 'Direct SIMS observation of methylidyne, methylene and methyl intermediates on a Ni(III) methanation catalyst', *Journal of American Chemical Society*, no. 108, pp. 1315.

Kieffer, R., Kiennemann, A., Rodriguez, M., Bernal, S., & Rodriguez-Izquierdo, J.M. (1988) 'Promoting effect of lanthana in the hydrogenation of carbon monoxide over supported rhodium catalysts', *Applied Catalysis*, vol. 42, no. 1, pp. 77-89

Kummer, J.T., Podgurski, H., Spencer, W., Emmet, P.H. (1951), 'Mechanistic studies of the Fischer-Tropsch synthesis: addition of radioactive alcohols', *Journal of the American Chemical Society*, vol. 73, pp. 564.

Kummer, J.T. & Emmet, P.H. (1953), 'Fischer-Tropsch synthesis mechanism studies: the addition of radioactive alcohols to the synthesis gas', *Journal of the American Chemical Society*, vol. 75, pp. 5177.

Li, S., Krishnamoorthy, S., Li, A., Meitzner, G.D. & Iglesia, E. (2002), 'Promoted iron-based catalysts for the Fischer-Tropsch synthesis: design, synthesis, site densities and catalytic properties', *Journal of Catalysis*, no. 206, pp. 202-217.

Li, S., Li, A., Krishnamoorthy, S. & Iglesia, E. (2001), 'Effects of Zn, Cu, and K promoters on the structure and on the reduction, carburization, and catalytic behaviour of iron-based Fisher-Tropsch synthesis catalysts', *catalysis letters*, vol. 77, no. 4, pp. 197-205.

Luo, H.Y., Zhang, W., Zhou, H.W., Huang, S.Y., Lin, P.Z., Ding, Y.J., Lin, L.W. (2001) 'A study of Rh-Sm-V/SiO_2 catalysts for the preparation of C_2-oxygenates from syngas', *Applied catalysis A:General*, vol. 214, pp. 161-166

Luo, M., O'Brien, R.J., Bao, S. & Davis, B.H. (2003), 'Fischer-Tropsch synthesis: induction and steady-state activity of high-alpha potassium promoted iron catalysts', *Applied Catalysis A: General*, no. 239, pp. 111-120.

Mabaso, I., van Steen, E. & Claeys, M. (2006), *Fischer-Tropsch synthesis on supported iron crystallites of different size*, DGMK-Tagungsbericht 2006 4-6 October; Dresden, Germany.

Mabaso, I.E. (2005), *Nanosized iron crystallites for Fischer-Tropsch synthesis*. University of Cape Town.

Maitlis, P.M., Quyoum, R., Long, H.C. & Turner, M.L. (1999), 'Towards a chemical understanding of the Fischer-Tropsch reaction: alkene formation', *Applied Catalysis A: General* , no. 186, pp. 363-374.

Mansker, L.D., Jin, Y., Bukur, D.B. & Datye, A.K. (1999), 'Characterization of slurry phase iron catalysts for Fischer-Tropsch synthesis', *Applied Catalysis A: General* , no. 186, pp. 277-296.

McMurry, J. (1996), *Organic chemistry / John McMurry*, Brooks/Cole publishing company.

Nowicki, L. (2005), 'Kinetics of CO hydrogenation on modified Cu/ZnO catalyst in a slurry reactor', *Chemical Engineering and Processing*, vol. 44, no. 3, pp 383-391.

Nunan, J.G., Bogdan, C.E., Klier, K., Smith, K.J., Young, Chyi-Woei, Herman, R.G. (1989), 'Higher alcohol and oxygenate synthesis over cesium-doped Cu/ZnO catalysts', *Journal of Catalysis*, vol. 116, no.1, pp 195-221.

O'Brien, R.J., Xu, L., Spicer, R.L., Bao, S., Milburn, D. & Davis, B.H. (1997), 'Activity and selectivity of precipitated iron Fischer-Tropsch catalysts', *Catalysis Today*, no. 36, pp. 325-334.

Patzlaff, J., Liu, Y., Graffmann, C. & Gaube, J. (1999), 'Studies on product distributions of iron and cobalt catalyzed Fischer-Tropsch synthesis', *Applied Catalysis A: General* , no. 86, pp. 109-119.

Pichler, H. & Roelen, O. (1957) 'Mitteldrucksynthese' in *Ullmanns Encyklopadie der technischen Chemie*. Urban & Schwarzenberg, München-Berlin.

Pichler, H. & Schulz, H. (1970), 'Neuere erkenntnisse auf dem gebiet der synthese von kohlenwasserstoffen aus CO und H_2', *Chemie-Ing.-Techn.*, vol. 42, no. 18, pp. 1162-1174.

Pijolat, M. & Perrichon, V. (1985), 'Synthesis of Alcohols from CO and H_2 on a Fe/Al_2O_3 catalyst at 8-30 bars pressure', *Applied Catalysis* , no. 3, pp. 321-333.

Razzaghi, A., Hindermann, J.P. & Kiennemann, A. (1984), *Applied Catalysis*, vol. 13, no. 1, pp. 193-210.

Roelen, O. (1938), 849,548, DRP.

Rottig, W. (1955a), 911,848, Ruhrchemie.

Rottig, W. (1955b), 923,127, Ruhrchemie.

Rottig, W. (1956), 937,706, Ruhrchemie.

Satterfield, C.N., Hanlon, R.T., Tung, S.E., Zou, Z. & Papaefthymiou, G.C. (1986), 'Initil behaviour of a reduced fused-magnetite catalyst in the Fischer-Tropsch synthesis', *Ind. Eng. Chem. Prod. Res. Dev.*, vol. 25, no. 3, pp. 401-407.

Schulz, H. & Claeys, M. (1999a), 'Reactions of a-olefins of different chain length added during Fischer-Tropsch synthesis on a cobalt catalyst in a slurry reactor', *Applied Catalysis A: General*, vol. 186, pp. 71-90.

Schulz, H. & Claeys, M. (1999b), 'Kinetic modelling of Fischer-Tropsch product distributions', *Applied Catalysis A: General* , no. 186, pp. 91-107.

Schulz, H. & Nehren, S. (1986), 'Die Herstellung van Gas/Dampf - Eichgemischem für die Gaschromatographie', *Erdöl und Kohle - Petrochemie*, vol. 39, pp. 93.

Schulz, H., Rao, B.R. & Elstner, M. (1970), '^{14}C-Studien zum Reaktionmechanismus der Fischer-Tropsch-Synthese', *Erdöl und Kohle*, vol. 22, pp. 651.

Schulz, H., Schaub, G., Claeys, M. & Riedel, T. (1999), 'Transient initial kinetic regimes of Fischer-Tropsch synthesis', *Applied Catalysis A: General*, vol. 186, pp. 215-227.

Schulz, H. & Zein el Deen, A. (1977a), 'New concepts and results concerning the mechanism of carbon monoxide hydrogenation. I. Organic oxygen compounds produced during medium pressure synthesis with Iron catalysts', *Fuel Proc. Techn.*, vol. 1, pp. 247.

Schulz, H. (1977b) 'Molekülaufbau bei der Fischer-Tropsch Synthese. Reaktionsschritte des Molekülaufbaus durch katalytische Umsetzung von Kohlenmonoxid und Wasserstoff', *Erdöl und Kohle*, vol. 22, pp. 651.

Schulz, H., (2003a), 'Major and minor reactions in Fischer–Tropsch synthesis on cobalt catalysts', *Topics in Catalysis*, vol. 26, pp. 73-85.

Schulz, H., (2003b), 'Spatial constraints and frustrated reactions in Fischer-Tropsch synthesis', *Catalysis Today*, vol. 84, pp. 67-70.

Scott-Fogler, H. (1999), *Elements of chemical reaction engineering*, Prentice-Hall International, Inc., Upper Saddle River, New Jersey.

Sie, S., Eilers, J. & Minderhout, J. (1988), 'Consequences of Fischer-Tropsch chain growth kinetics for process mode selection and product selectivity.' In M. T. M.J. Phillips (Ed.), (pp. 743-750). Proc. 9th Int. Catalysis Congress, The Chem. Institute of Canada, Ottawa, Canada.

Smith, K.J., Anderson, R.B. (1983), 'The higher alcohol synthesis over promoted Cu/ZnO catalysts', *The Canadian Journal of Chemical Engineering*, vol. 61, no. 1, pp 40-45.

Snel, R. & Espinoza, R.L. (1989), 'Fischer-Tropsch synthesis on iron -based catalysts: the effect of co-feeding small oxygenates', *Journal of Molecular Catalysis*, no. 54, pp. 213-223.

Spencer, M.S. (1999), 'The role of surface oxygen on copper metal in catalysts for the synthesis of methanol', *Catalysis Letters*, vol. 60, no. 1-2, pp 45-49.

Steynberg, A.P. (2004), Introduction to Fischer-Tropsch technology - Chapter 1. In A. Steynberg & M. Dry (Ed.), *Fischer-Tropsch Technology*, (pp. 1). Amsterdam:Elsevier.

Storch, H.H., Golumbic, N. & Anderson, R.B. (1951), *The Fischer-Tropsch and Related Syntheses*, John Wiley & Sons, New York U.S.A.

Subramanyam, K. & Rao, M.R.A.. (1970b), 'Adsorption of hydrogen and carbon monoxide and their mixtures on iron Fischer-Tropsch catalysts. Part II Adsorption of hydrogen and carbon monoxide and their mixtures on iron Fischer-Tropsch catalysts. Part I', *J. Res. Inst. Catalysis, Hokkaido Univ.*, vol. 18, no. 3, pp. 115-123.

Subramanyam, K. & Rao, M.R.A. (1970a), 'Adsorption of hydrogen and carbon monoxide and their mixtures on iron Fischer-Tropsch catalysts. Part II', *J. Res. Inst. Catalysis, Hokkaido Univ.*, vol. 18, no. 3, pp. 124-141.

Sugier, A. & Freund, E. (1978), US 4,122,110, IFP.

Sugier, A. & Freund, E. (1981), US 4,291,126, IFP.

Tago, T., Hanaoka, T., Dhupatemiya, P., Hayashi, H., Kishida, M. & Wakabayashi, K. (2000), 'Effects of Rh content on catalytic behavior in CO hydrogenation with Rh–silica catalysts prepared using microemulsion', *Catalysis Letters*, vol. 64, no. 1, pp. 27-31.

Tau, L., Dabbagh, H., Bao, S. & Davis, B.H. (1990), 'Fischer-Tropsch synthesis. Evidence for two chain growth mechanisms', *Catalysis Letters*, no. 7, pp. 127-140.

Tau, L., Dabbagh, H., Bao, S., Chawla, B. & Davis, B. (1988), 'Incorporation of carbon-14 labelled compounds during Fischer-Tropsch synthesis'. *Proceedings of the 9th international conference on catalysis, Calgary*, 1988, Vol. 2, The Chemical Institute of Canada, Ottowa.

Tau, L., Robinson, R., Ross, R.D. & Davis, B.H. (1987), 'Oxygenates formed from ethanol during Fischer-Tropsch synthesis', *Journal of Catalysis*, no. 105, pp. 335-341.

Teng, B., Zhang, C., Yang, J., Cao, D., Chang, J., Xiang, H. & L, Y. (2005), 'Oxygenate kinetics in Fischer-Tropsch synthesis over an industrial Fe-Mn catalyst', *Fuel* , vol. 84, pp. 791-800.

Underwood, R.P. & Bell, A.T. (1987), 'Influence of particle size on carbon monoxide hydrogenation over silica- and lanthana-supported rhodium', *Applied Catalysis*, vol. 34, pp. 289-310.

Underwood, R.P. & Bell, A.T. (1988), 'Lanthana-promoted Rh/SiO2: I. Studies of CO and H2 adsorption and desorption', *Journal of Catalysis*, vol. 109, no. 1, pp. 61-75.

Vedage, G.A., Himelfarb, P.B., Simmons, G.W., Klier, K. (1985), 'Alkali-promoted copper-zinc oxide catalysts for low alcohol synthesis', *A.C.S. symposium series*, no. 279, pp 295-312.

Visagie, J.L., van Zyl, A.J., Gonvender, N. & Dlamini, H.T. (2001), WO 2003/043734 A1, Sasol technology (proprietary) limited.

Wang, C.J. & Ekerdt, J.G. (1984), 'Evidence for alkyl intermediates during Fischer-Tropsch synthesis and their relation to hydrocarbon products', *Journal of Catalysis*, no. 86, pp. 239.

Wang, Y. & Davis, B.H. (1999), 'Fischer-Tropsch synthesis. Conversion of alcohols over iron oxide and iron carbide catalysts', *Applied Catalysis A: General*, no. 180, pp. 277-285.

Welker, C., Moss, J., van Steen, E. & Claeys, M. (2006), *Closing the gap between homogeneous and heterogeneous ruthenium-based Fischer-Tropsch synthesis*, DGMK-Tagungsbericht 2006 4-6 October; Dresden, Germany.

van Steen, E. & Claeys, M. (2008), 'Fischer-Tropsch catalysts for the biomass-to-liquid (BTL)-process', *Chemical Engineering Technology*, vol. 31, no. 5, pp. 655-666.

van Zyl, A.J., Visagie, J.L., Govender, N.S. & de Villiers, D. (2004a), WO 2004/047986 A1, Sasol technology (proprietary) limited.

van Zyl, A.J., Visagie, J.L., Preston, H., Mdleleni M. M., Dlamini, H.T. & Motjope, T.R. (2004b), US 2004/152791 A1, Sasol technology (proprietary) limited.

Wilson, T.P., Kasai, P.H. & Ellgen, P.C. (1981), 'The state of manganese promoter in rhodium-silica gel catalysts', *Journal of Catalysis*, vol. 69, no. 1, pp 193-201.

Xiaoding, X., Doesburg, E.B.M., & Scholten, J.J.F. (1987), 'Synthesis of higher alcohols from syngas – recently patented catalysts and tentative ideas on the mechanism', *Catalysis Today*, vol. 2, pp. 125-170.

Appendices

Appendix A

Nitrate and ammonia volumes used in catalyst co-precipitation

Table A.1 Calibration and volumes of cold solutions needed for catalyst precipitation

Catalyst (Cu wt%)[a]	**Volume 1 molar iron nitrate solution** (ml)	**Volume 1 molar copper nitrate solution** (ml)	**Volume 25 wt% ammonia solution** (ml)
0	500	0	525
2	484	16	525
9	428	72	500
23	333	167	468
50	187	313	410
77	76	424	369
100	0	500	300

[a] Basis: Fully reduced catalyst

Appendix B

Ampoule breaker

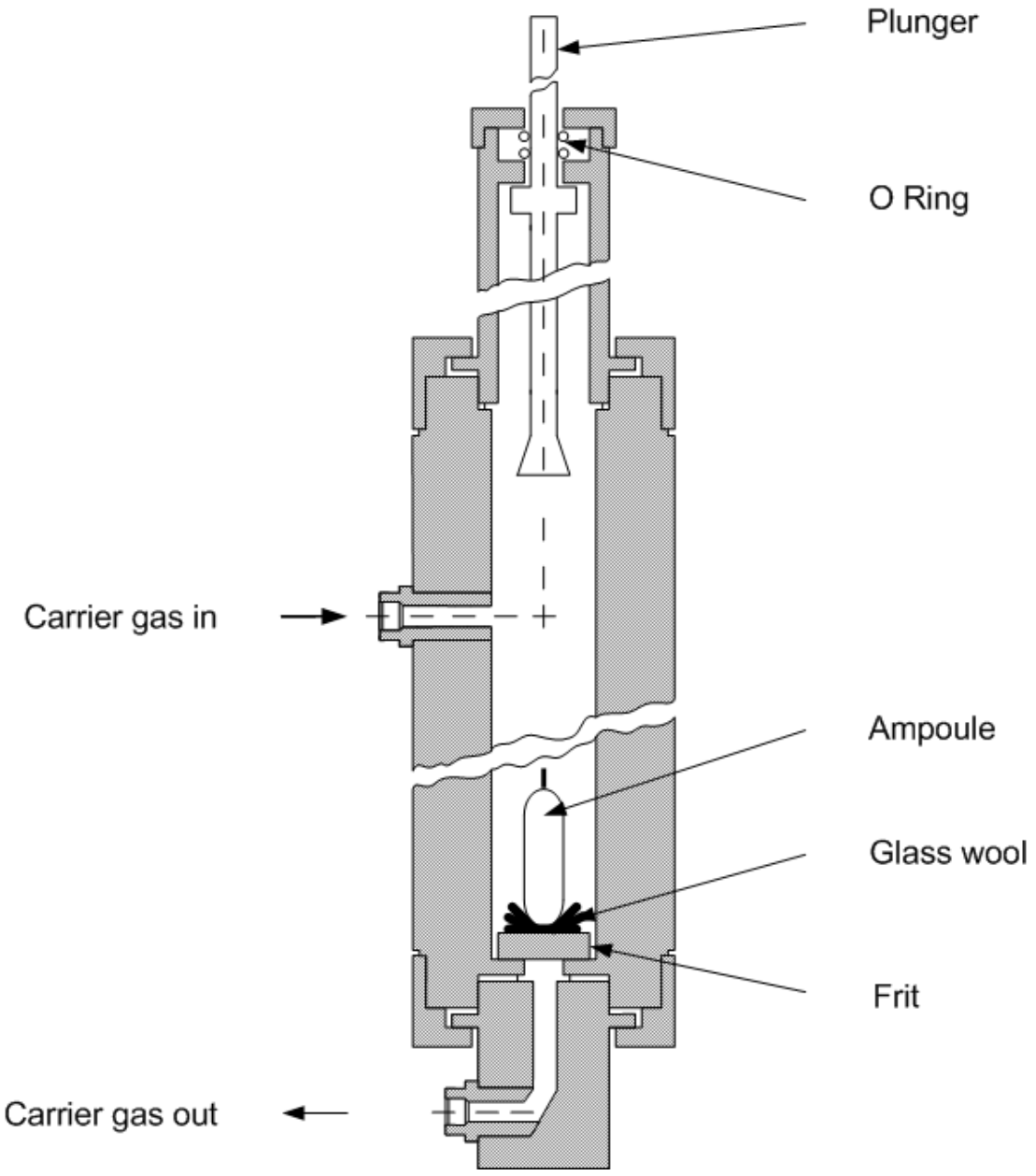

Figure B.1 Ampoule breaker system of GC FID and GC-MS analysis

Appendix C

Characterisation of the Berty reactor

The flow profile in the Berty reactor was characterised by a residence time study under reaction conditions. The study was performed utilising a slightly different feed to allow for continuous monitoring of the CO_2-concentration using an on-line IR-detector. At initial conditions the feed stream contained 0% CO_2. This was adjusted as a step change from 0 to 5% while keeping the feed velocity constant by lowering the CO feed percentage by 5%. The reactor was loaded with SiC to mimic realistic operating conditions with the presence of a solid.

Prior to the residence time study, the volume of the reactor and the internals were estimated. The rest volume in the reactor with all internals in place was estimated by measuring pressure increase upon a constant flow rate into the reactor of 0.1190±0.0035 litre (STP)/min. The reactor volume was then estimated by:

$$V = \frac{v \cdot p}{d\Delta p / dt} = \frac{0.119 \cdot \frac{litre}{\min} \cdot 103 \cdot kPa}{0.3515 \cdot \frac{kPa}{s} \cdot 60 \cdot \frac{s}{\min}} = 0.581 \pm 0.034 litres$$

Three different set-ups were employed, viz. the Berty reactor with just the outer shell in, the Berty reactor with the outer shell, the big and the medium rings in, and the Berty reactor with all internals in. The residence time distribution studies were performed at two different flow rates of the gas (1.01 and 2.02 litre (STP)/min).

Figure C.1 shows a typical response to the step change:

$$F(t) = 1 - \frac{C_{CO_2,t=t}}{C_{CO_2,t=\infty}}$$

From the response in the step change the experimentally determined residence time is determined:

$$\tau_{exp} = \int_{t=0}^{t=\infty} t \cdot E(t) \cdot dt \qquad \text{with} \qquad E(t) = \frac{dF(t)}{dt}$$

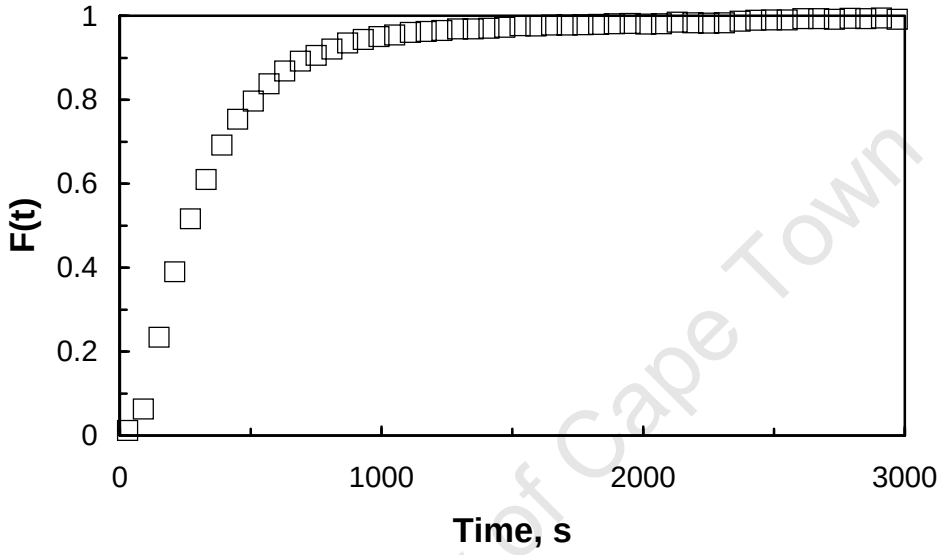

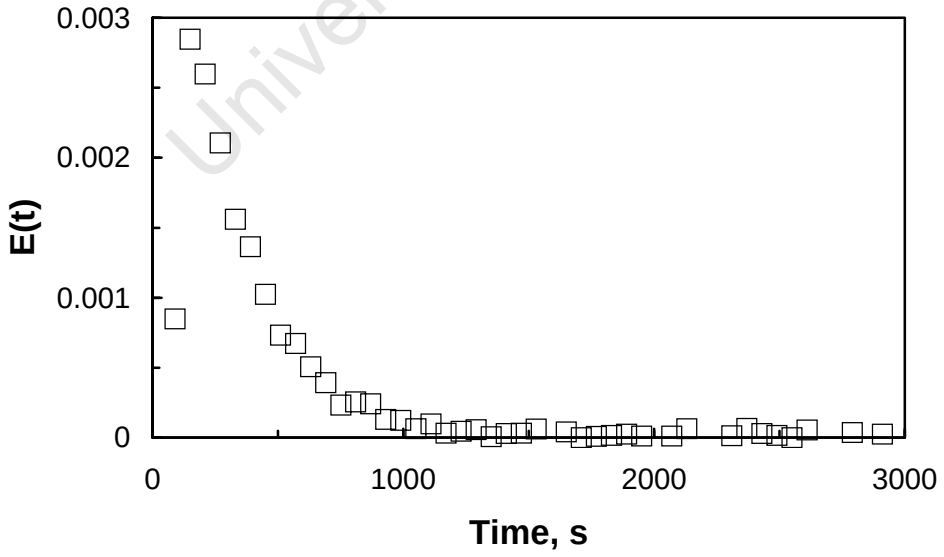

Figure 5.2 Residence time distribution (F(t) and E(t)) for the Berty reactor characterisation tests

The behaviour of the reactor system is obtained by plotting 1-F(t) on a semi-logarithmic plot versus time (Figure C.2). The response of an ideal CSTR on a step input in a semi-logarithmic plot of 1-F(t) versus time should give a straight line. It can be clearly recognised despite the scatter in the data that the Berty reactor does not operate as a single CSTR. The two different slopes in the plot indicates that the reactor is operating as two CSTRs (the initial change in the slope close to time equals zero can be attributed to the volume of the measuring cell, which also acts as a mini-CSTR).

Principally two models can be considered to evaluate the residence time distribution of the Berty reactor, viz. CSTRs operating in series, parallel operating CSTRs and two CSTRs with interchange (Figure C.3). The resulting mathematical models for both situations are rather similar, although their physical interpretation differs significantly.

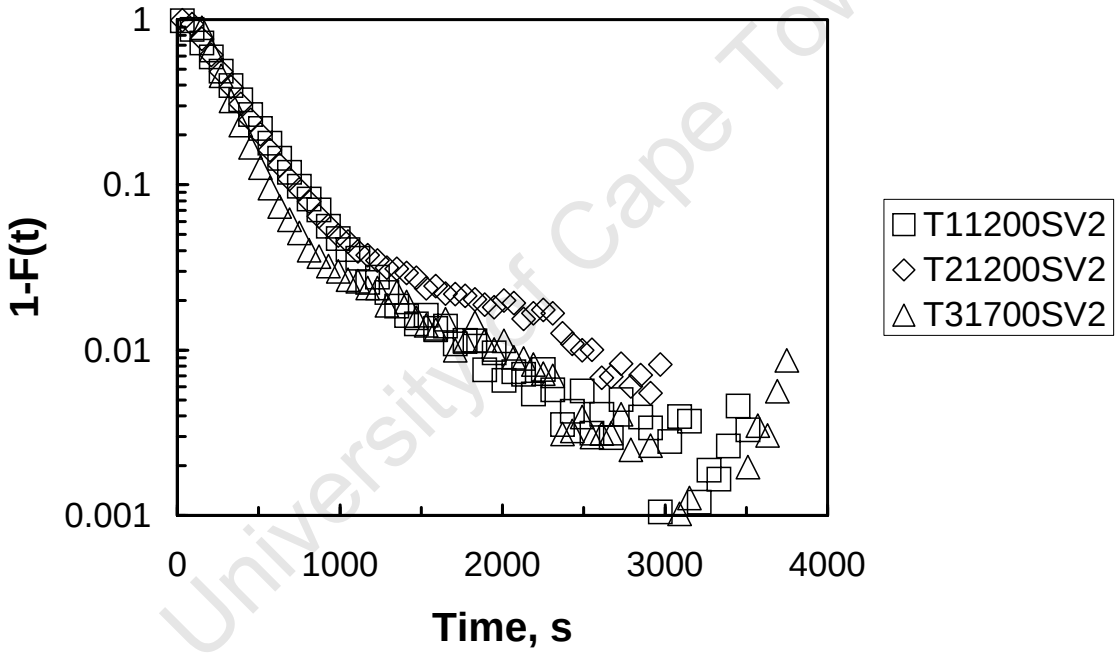

Figure C.1 Semi-logarithmic residence time distribution plots as a function of time for 3 different test conditions, i.e. T11200SV2: $\tau_{theoretical}$ = 4.92 min; T211200SV2: $\tau_{theoretical}$ = 3.92 min; T31700SV2: $\tau_{theoretical}$ = 2.69 min)

The response of each of the systems (CSTRs in series, CSTRs in parallel, and two CSTRs with interchange of mass all can be described by following generalised expression:

$$1-F(t)=f\cdot e^{-\frac{t+c}{\tau_1}}+(1-f)\cdot e^{-\frac{t+c}{\tau_2}}$$

This four-parameter model was used to model the experimentally observed residence time distribution (the term c is included here to account for the flow through the piping and the detector). This means automatically that any distinction between the models is not possible and physical inspection must be used to distinguish between the various, possible flow models. The only relevant information that can be obtained is on the deviation of the reactor from an ideal CSTR.

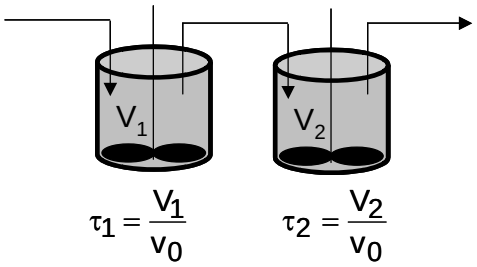

$$\tau_1 = \frac{V_1}{v_0} \qquad \tau_2 = \frac{V_2}{v_0}$$

$$F(t) = 1 - \frac{\tau_1}{\tau_1 - \tau_2} \cdot e^{-\frac{t}{\tau_1}} + \frac{\tau_2}{\tau_1 - \tau_2} \cdot e^{-\frac{t}{\tau_2}}$$

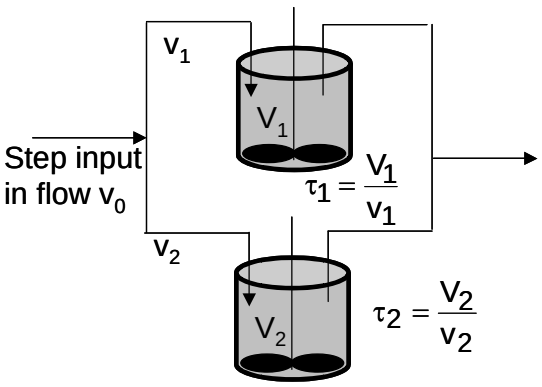

$$F(t) = 1 - \frac{v_1}{v_0} \cdot e^{-\frac{t}{\tau_1}} - \frac{v_2}{v_0} \cdot e^{-\frac{t}{\tau_2}}$$

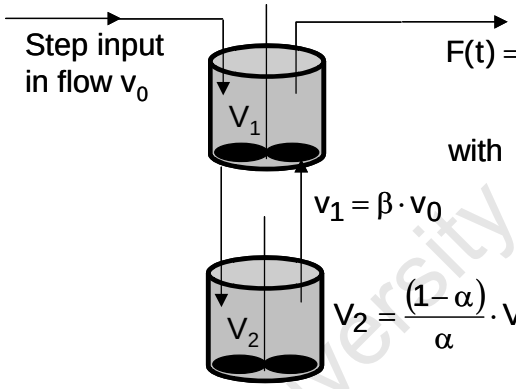

$$F(t) = 1 - \frac{(\alpha \cdot m_1 + \beta + 1) \cdot e^{\frac{m_2 \cdot t}{\tau}} - (\alpha \cdot m_2 + \beta + 1) \cdot e^{\frac{m_1 \cdot t}{\tau}}}{\alpha \cdot (m_1 - m_2)}$$

$$\text{with } m_{1,2} = \left(\frac{1 - \alpha + \beta}{2 \cdot \alpha \cdot (1 - \alpha)} \right) \cdot \left(-1 \pm \sqrt{1 - \frac{4 \cdot \alpha \cdot \beta \cdot (1 - \alpha)}{(1 - \alpha + \beta)^2}} \right)$$

Figure C.2 Different models for describing the response to a step input function in a system involving two CSTRs

Table C.1 Fit of experimentally determined residence distribution function to

$$1-F(t) = f \cdot e^{-\frac{t+c}{\tau_1}} + (1-f) \cdot e^{-\frac{t+c}{\tau_2}}$$

Test	$\tau_{theoretical}$ min	Stirrer speed rpm	c min	f	τ_1 min	τ_2 min
A SV1	9.81	1700	-1.81	0.47	7.05	12.65
B SV1	9.77	1200	-1.72	0.91	9.10	36.11
C SV1	9.76	700	-3.14	1.00	7.63	-
A SV2	4.92	1700	-2.43	1.00	3.91	
B SV2	4.92	1200	-1.25	0.97	4.52	22.23
C SV1	7.82	1700	-1.47	0.91	7.53	135.6
D SV1	7.78	1200	-1.71	0.92	7.25	20.71
E SV1	7.78	700	-2.20	0.85	6.95	16.56
D SV2	3.92	1700	-0.48	0.98	4.10	25.11
E SV2	3.92	1200	-1.84	0.91	3.48	18.53
F SV1	5.37	1700	-2.09	0.97	4.42	639.7
G SV1	5.34	1200	-2.27	0.92	4.84	58.10
H SV1	5.33	700	-1.98	0.95	4.65	85.67
F SV2	2.69	1700	-1.02	0.97	2.51	54.73
G SV2	2.69	1200	-1.60	1.00	1.64	-

In general, the Berty reactor system can be described as a single CSTR (for more than 90%), with a small volume, which may act as a second CSTR. At lower gas velocities the reactor seems to tend to behave more like two CSTRs.

Appendix D

Loss of acids in ampoule method

Table D.1 FID areas on oxygenate liquid injection – standard solution

	Injection 1	**Injection 2**	**Injection 3**
Octan-2-one Area	815872157	673597128	663704979
Octanal Area	589741120	482856822	478063916
Octanol Area	806522145	666838478	657428720
Octanoic acid Area	824598449	694104292	671130315
1-Decene	827063977	683245292	673648630

Table D.2 Ratio of oxygenates to decene on liquid injection

	Injection 1	**Injection 2**	**Injection 3**
Octan-2-one/1-Decene	0.99	0.99	0.99
Octanal/1-Decene	0.71	0.71	0.71
Octanol/1-Decene	0.98	0.98	0.98
Octanoic acid/1-Decene	1.00	1.02	1.00

Table D.3 FID areas on oxygenate ampoule injection – standard solution

	Ampoule 1	**Ampoule 2**	**Ampoule 3**
Octan-2-one Area	1516824408	913278471	404606513
Octanal Area	1044260182	568230795	284710348
Octanol Area	1502149345	875144825	384081567
Octanoic acid Area	664977573	390473364	112480959
1-Decene	1600032598	969188614	415241840

Table D.4 Ratio of oxygenates to decene on ampoule injection

	Ampoule 1	Ampoule 2	Ampoule 3
Octan-2-one/1-Decene	0.95	0.94	0.97
Octanal/1-Decene	0.65	0.59	0.69
Octanol/1-Decene	0.94	0.90	0.92
Octanoic acid/1-Decene	0.42	0.40	0.27

The loss of the acid in the ampoule breaking method can clearly be seen in the comparison of the acid to decene ratio in Table D.2 and Table D.4.

Appendix E

Calibration curves and histograms

E.1 Calibration curves

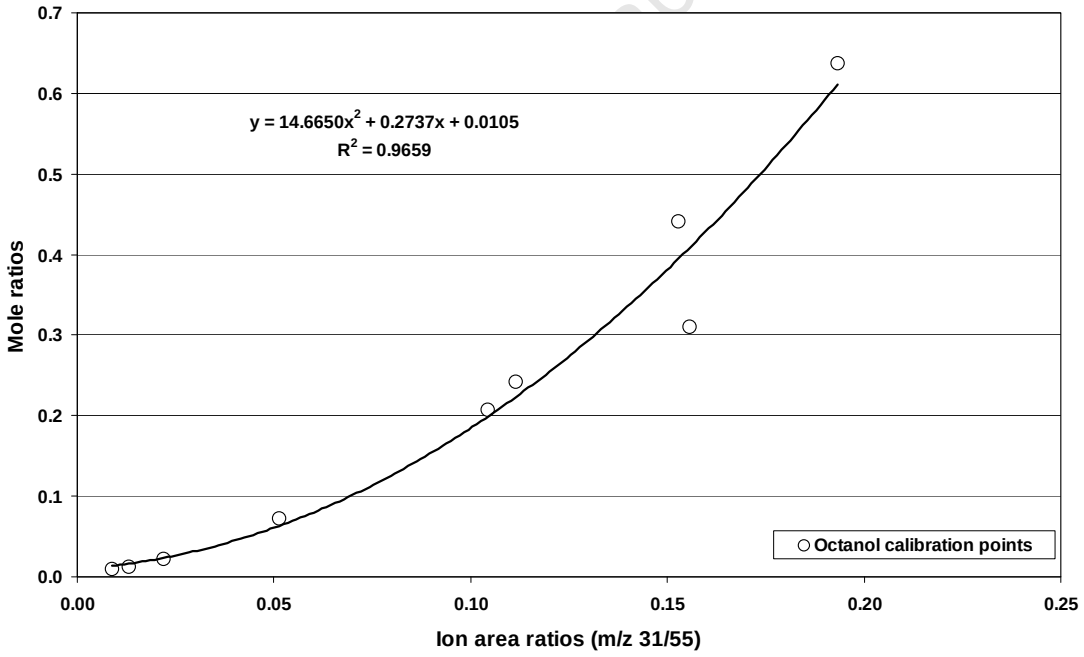

Figure E.1 Calibration curve for the m/z = 31 ion of 1-octanol and the m/z = 55 ion of decene

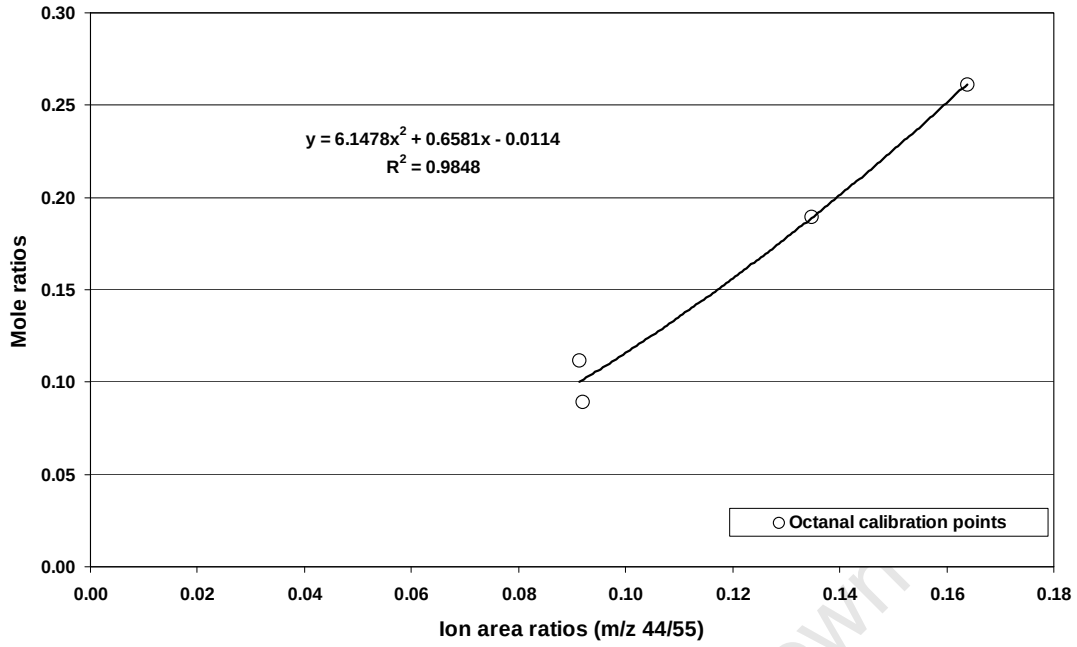

Figure E.2 Calibration curve for the m/z = 44 ion of octanal and the m/z = 55 ion of decene

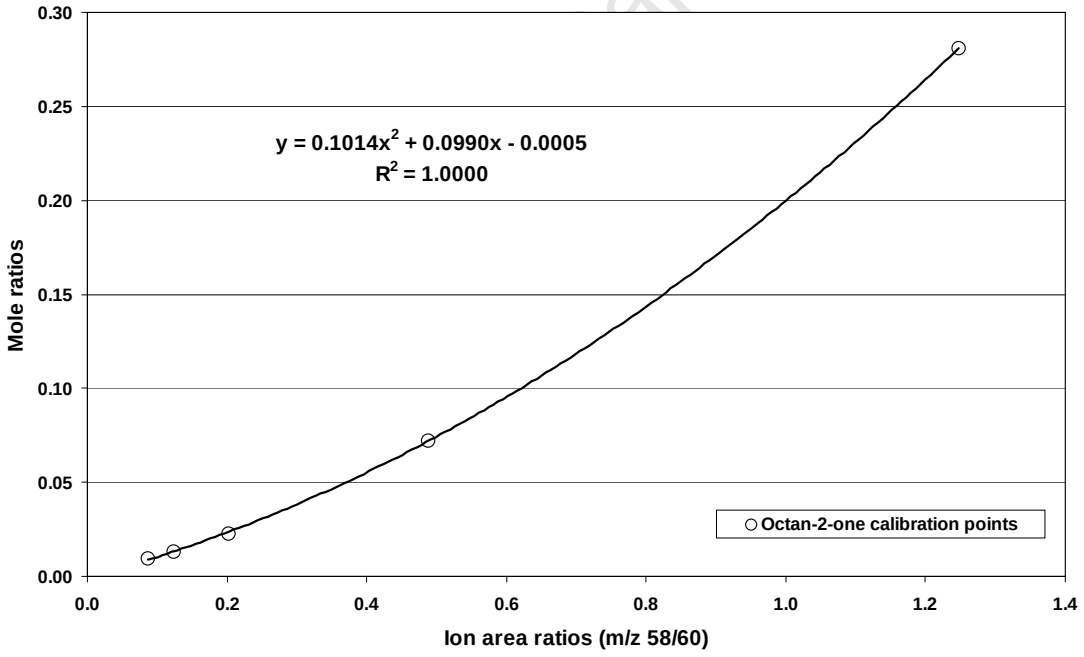

Figure E.3 Calibration curve for the m/z = 58 ion of octan-2-one and the m/z = 55 ion of decene

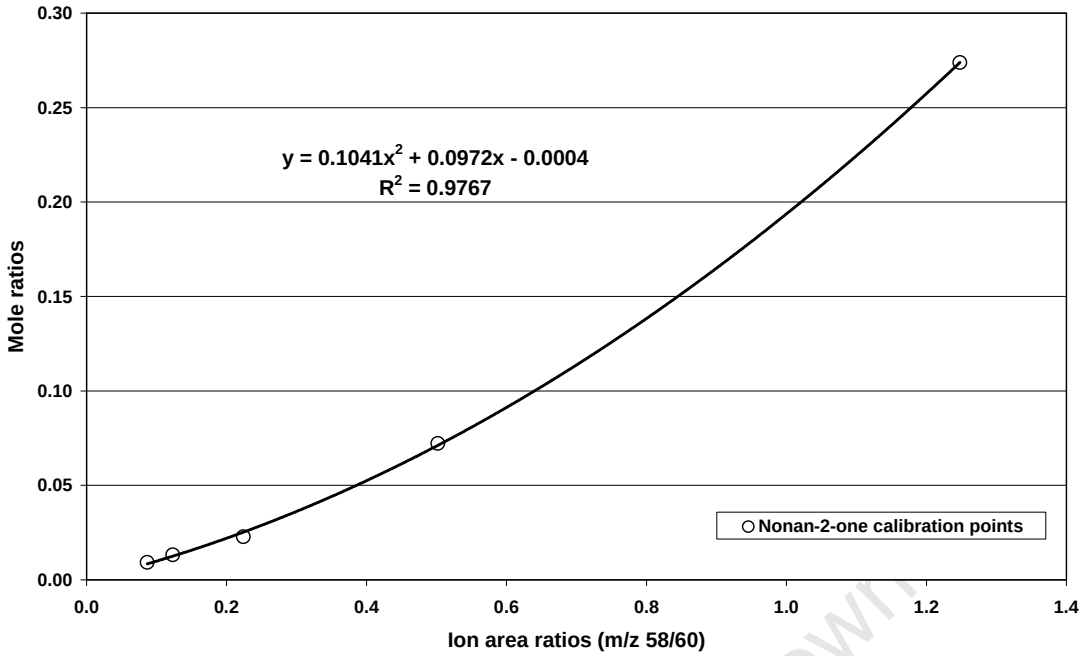

Figure E.4 Calibration curve for the m/z = 58 ion of nonan-2-one and the m/z = 55 ion of decene

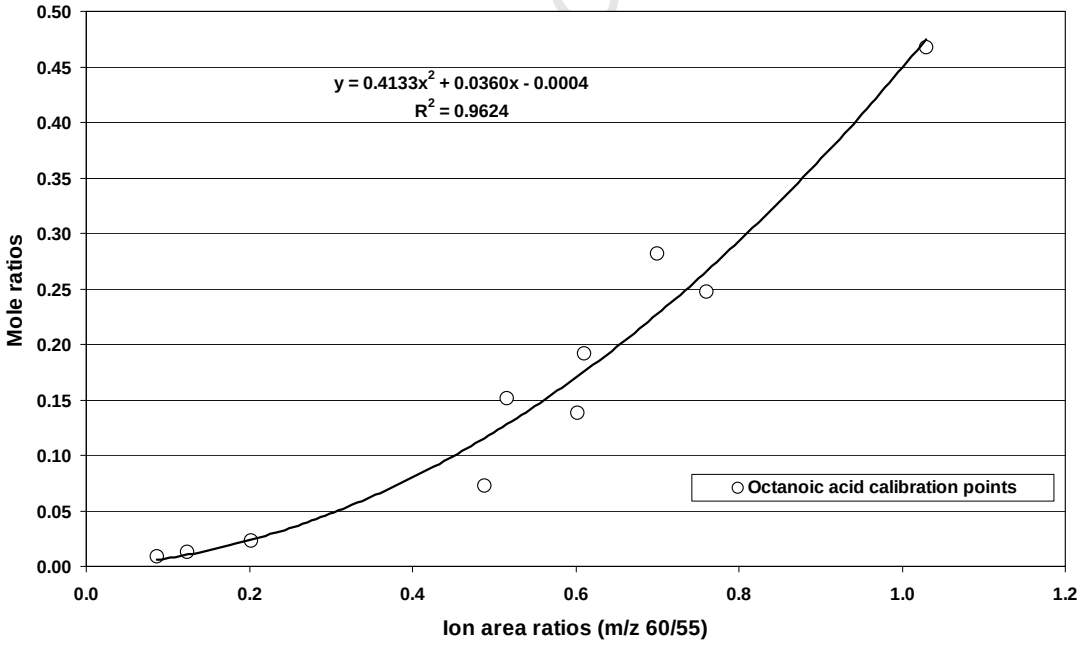

Figure E.5 Calibration curve for the m/z = 60 ion of octanoic acid and the m/z = 55 ion of decene

E.2 Histograms

Name: 1-Octanol

Formula: $C_8H_{18}O$

MW: 130 CAS#: 111-87-5 NIST#: 228852 ID#: 18348

Contributor: Japan AIST/NIMC Database- Spectrum MS-NW- 942

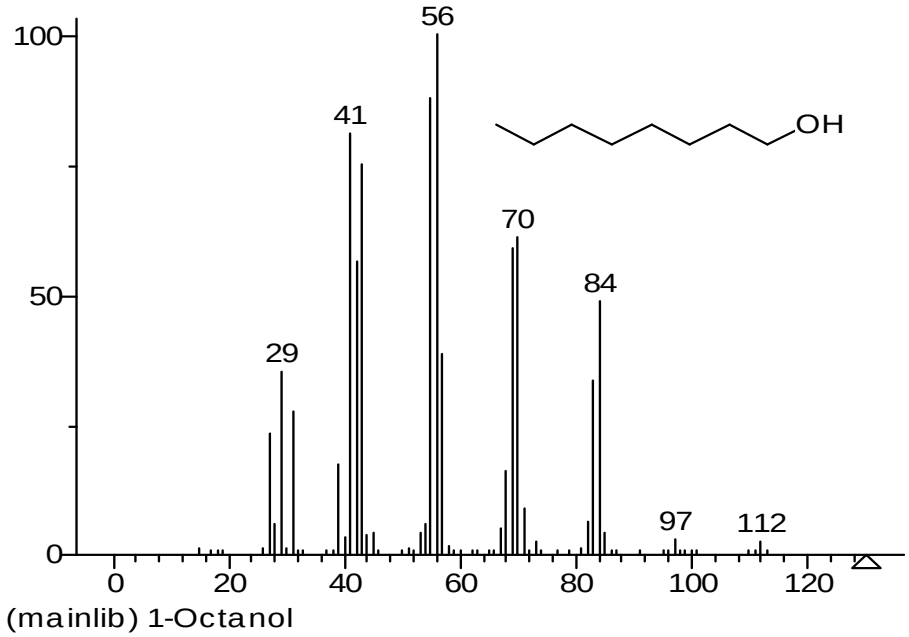

Name: Octanal

Formula: $C_8H_{16}O$

MW: 128 CAS#: 124-13-0 NIST#: 114738 ID#:

Contributor: NIST Mass Spectrometry Data Center, 1990.

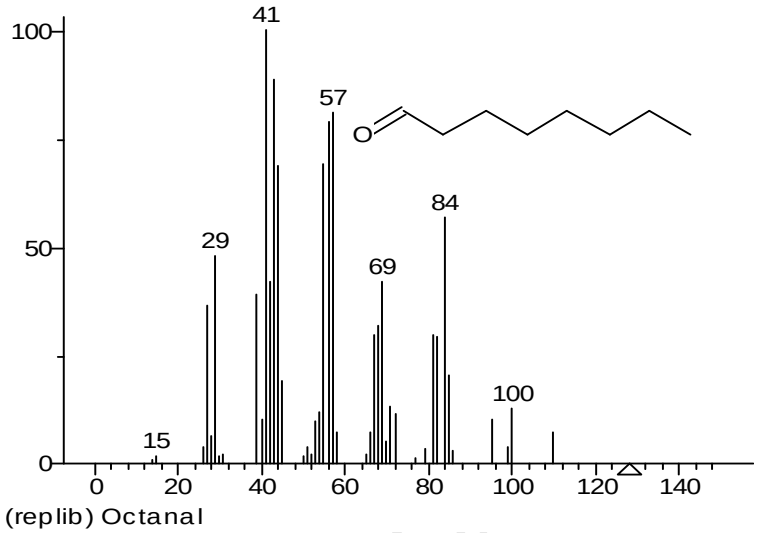

Name: 2-Octanone

Formula: $C_8H_{16}O$

MW: 128 CAS#: 111-13-7 NIST#: 61746 ID#: 2222

Contributor: D.HENNEBERG, MAX-PLANCK INSTITUTE, MULHEIM, WEST GERMANY

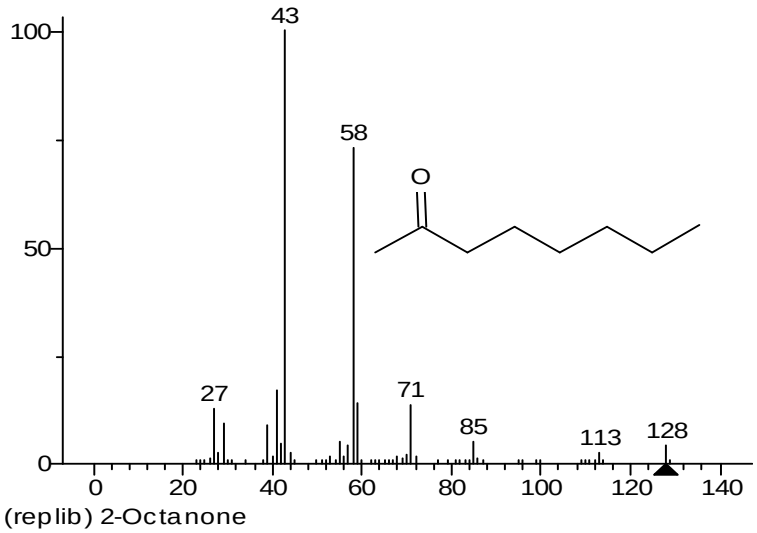

Name: 2-Nonanone

Formula: $C_9H_{18}O$

MW: 142 CAS#: 821-55-6 NIST#: 288967 ID#: 2223

Contributor: James Little,Eastman Chem.Co.,Kingsport,TN

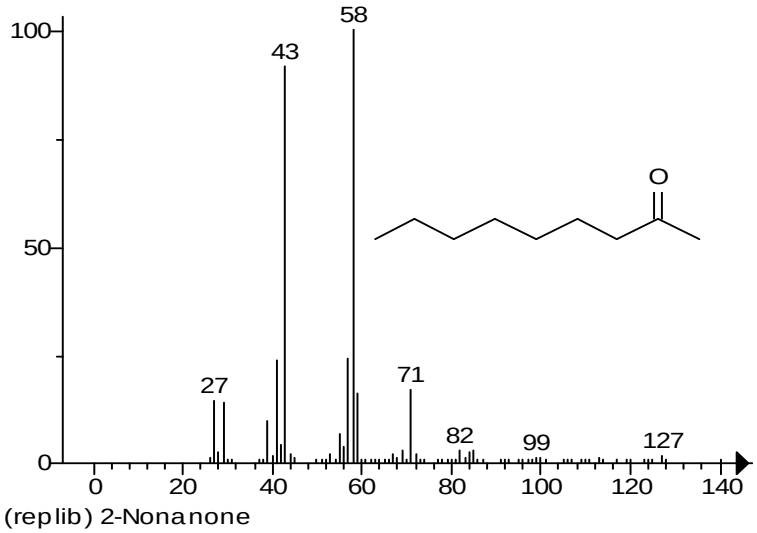

Name: Octanoic Acid

Formula: $C_8H_{16}O_2$

MW: 144 CAS#: 124-07-2 NIST#: 291498 ID#: 6793

Contributor: NIST Mass Spectrometry Data Center, 1998.

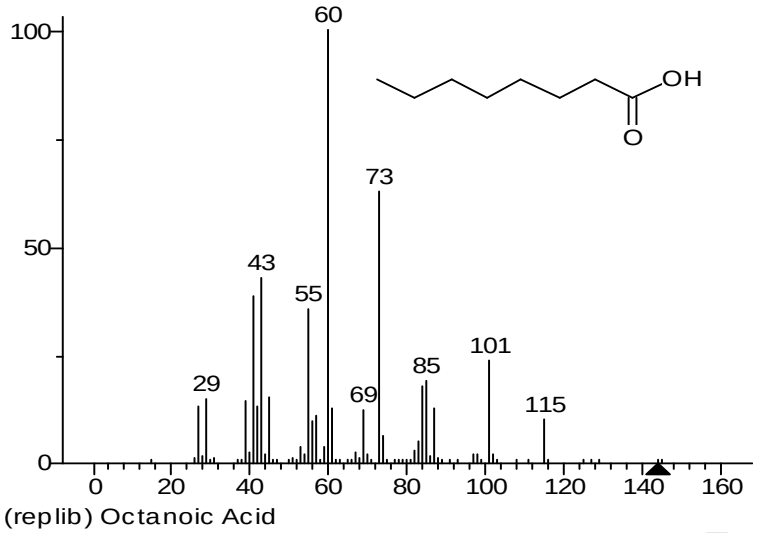

Appendix F

Thermodynamic calculations

Table F.1 Thermodynamic equilibrium co-efficients and Gibbs free energies of reaction for reactions of oxygenates to hydrocarbons in the Fischer-Tropsch sysnthesis

Reaction	K_a	ΔG^R (573 K) kJ/mol (Daubert *et al.*)
Ethanol ⇔ Ethene + H_2O	252	-26.35
Acetaldehyde + H_2 ⇔ Ethene + H_2O	2735	-37.71
Acetic acid + 2 H_2 ⇔ Ethene + 2 H_2O	322	-27.51
Ethanol + H_2 ⇔ Ethane + H_2O	253687401	-92.21
Acetaldehyde + 2 H_2 ⇔ Ethane + H_2O	2750212348	-103.57
Acetic acid + 3 H_2 ⇔ Ethane + 2 H_2O	323587018	-93.37
Butanoic acid +2 H_2 ⇔ Butene + 2 H_2O	6637	-41.94
1-Butanol ⇔ Butene + H_2O	14863	-45.78
Butanal + H_2 ⇔ Butene + H_2O	19928	-47.17
Butan-2-one + H_2 ⇔ Butene + H_2O	52	-18.85
2-Butanol ⇔ Butene + H_2O	198	-25.20
Butanoic acid +3 H_2 ⇔ Butane + 2 H_2O	254279324	-92.22
1-Butanol + H_2 ⇔ Butane + H_2O	569442895	-96.07
Butanal + 2 H_2 ⇔ Butane + H_2O	763503868	-97.46
Butan-2-one + 2 H_2 ⇔ Butane + H_2O	2002610	-69.14
2-Butanol + H_2 ⇔ Butane + H_2O	7585969	-75.49
C8-Acid +2 H_2 ⇔ Octene + 2 H_2O	22319	331.54
C8-1-Alcohol ⇔ Octene + H_2O	18916	-47.71

C8-Aldehyde + H_2 ⇔ Octene + H_2O	45.6	-46.93
C8-Ketone + H_2 ⇔ Octene + H_2O	432	-18.20
C8-2-Alcohol ⇔ Octene + H_2O	364666243	-28.91
C8-Acid +3 H_2 ⇔ Octane + 2 H_2O	859479604	-93.94
C8-1-Alcohol + H_2 ⇔ Octane + H_2O	728461644	-98.03
C8-Aldehyde + 2 H_2 ⇔ Octane + H_2O	1756263	-97.24
C8-Ketone + 2 H_2 ⇔ Octane + H_2O	16627431	-68.52
C8-2-Alcohol + H_2 ⇔ Octane + H_2O	22319	-79.23

Table F.2 Thermodynamic equilibrium co-efficients and Gibbs free energies of reaction for reactions of oxygenates in the Fischer-Tropsch sysnthesis

Reaction	K_a	ΔG^R (573 K) kJ/mol (Daubert *et al.*)
Acetic acid + 2 H_2 ⇔ Ethanol + H_2O	1.28	-1.16
Acetaldehyde + H_2 ⇔ Ethanol	10.84	-11.36
Acetaldehyde + H_2O ⇔ Acetic acid + H_2	8.50	-10.20
Ethanol ⇔ Ethene + H_2O	252	-26.35
Acetaldehyde + H_2 ⇔ Ethene + H_2O	2735	-37.71
Acetic acid + 2 H_2 ⇔ Ethene + 2 H_2O	322	-27.51
Ethanol + H_2 ⇔ Ethane + H_2O	253687401	-92.21
Acetaldehyde + 2 H_2 ⇔ Ethane + H_2O	2750212348	-103.57
Acetic acid + 3 H_2 ⇔ Ethane + 2 H_2O	323587018	-93.37
Butanoic acid + H_2 ⇔ Butan-2-one + H_2O	127	-23.08
1-Butanol ⇔ Butan-2-one + H_2	284	-26.92
Butanal ⇔ Butan-2-one	381	-28.32
2-Butanol ⇔ Butan-2-one + H_2	3.79	-6.35
1-Butanol + H_2O ⇔ Butanoic acid +2 H_2	2.24	-3.84
Butanal + H_2O ⇔ Butanoic acid + H_2	3.00	-5.24
2-Butanol + H_2O ⇔ Butanoic acid +2 H_2	0.03	16.74
Butanal + H_2 ⇔ 1-Butanol	1.34	-1.40
1-Butanol ⇔ 2-Butanol	33.5	-20.58
Butanal + H_2 ⇔ 2-Butanol	1.34	-1.40
Butanoic acid +2 H_2 ⇔ Butene + 2 H_2O	6637	-41.94
1-Butanol ⇔ Butene + H_2O	14863	-45.78
Butanal + H_2 ⇔ Butene + H_2O	19928	-47.17
Butan-2-one + H_2 ⇔ Butene + H_2O	52	-18.85
2-Butanol ⇔ Butene + H_2O	198	-25.20
Butanoic acid +3 H_2 ⇔ Butane + 2 H_2O	254279324	-92.22
1-Butanol + H_2 ⇔ Butane + H_2O	569442895	-96.07
Butanal + 2 H_2 ⇔ Butane + H_2O	763503868	-97.46
Butan-2-one + 2 H_2 ⇔ Butane + H_2O	2002610	-69.14
2-Butanol + H_2 ⇔ Butane + H_2O	7585969	-75.49
Octanoic acid + H_2 ⇔ Octan-2-one + H_2O	207.64	-25.43
1-Octanol ⇔ Octan-2-one + H_2	489.38	-29.51
Octanal ⇔ Octan-2-one	414.78	-28.72

1-Octanol + H_2O ⇔ Octanoic acid +2 H_2	2.36	-4.09
Octanal + H_2O ⇔ Octanoic acid + H_2	2.00	-3.30
1-Octanol ⇔ Octanal + H_2	1.18	-0.79
Octanoic acid + CO + 2 H_2 ⇔ C9-Ketone + 2 H_2O	10775	-44.24
1-Octanol + CO + H_2 ⇔ C9-Ketone + H_2O	13886	-45.45
Octanal + CO + 2 H_2 ⇔ C9-Ketone + H_2O	11769	-44.67

Appendix G

XRD – calcined catalyst

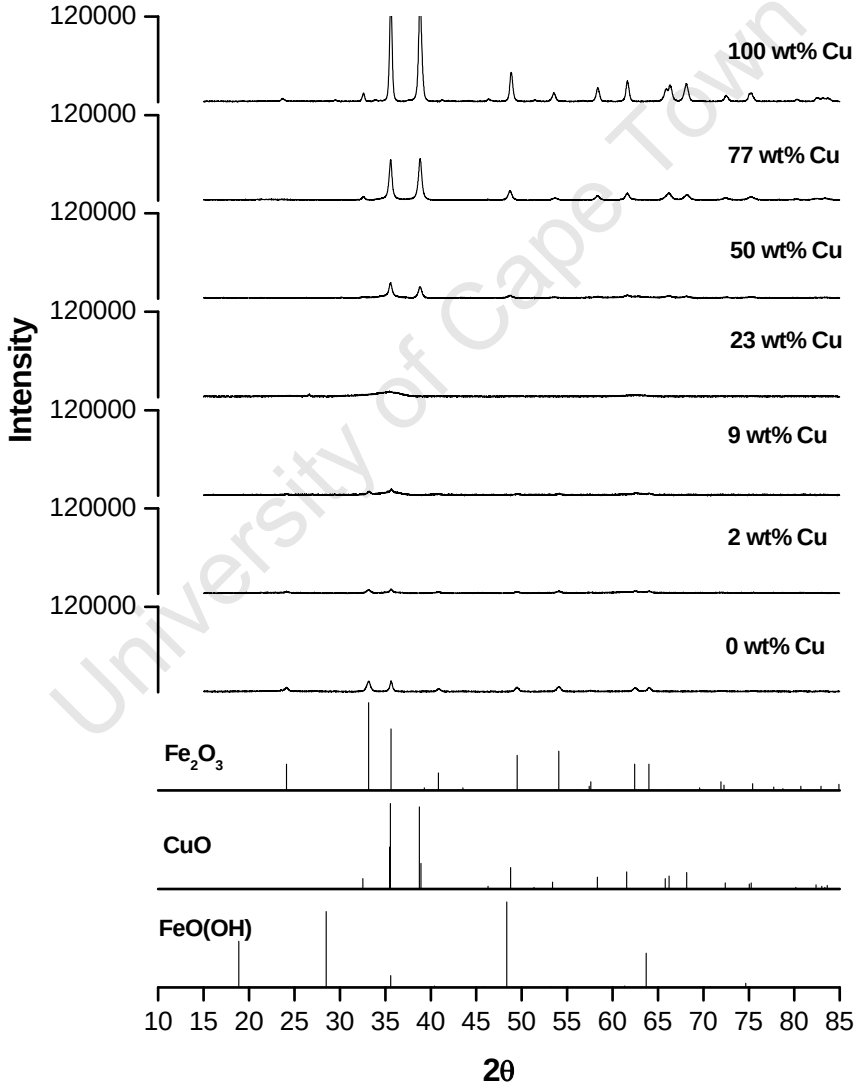

Figure G.1 XRD diffractograms of calcined catalyst series with same scale on the y-axis

Appendix H

Details, selected flows and results for the Fixed-bed tests

H.1 Catalyst loading and conversions

Table H.1 Catalyst loadings and time on-stream conversions for the Fixed-bed reactor

	0% Cu	2% Cu	9% Cu	23% Cu	50% Cu	77% Cu
Mass catalyst loaded (g)	0.6903	0.7039	0.7495	0.9019	1.3793	1.4950[a]
Mass SiC loaded (g)	0.5001	0.5006	0.5009	0.5013	0.5006	0.4998
24 hours (time)	26.2	24.0	23.2	24.3	23.0	23.2
CO conversion (TCD)	94.7	84.2	65.0	84.4	94.1	92.0
Carbon conversion (TCD)	46.4	40.8	29.3	30.4	50.0	38.0
48 hours (time)	46.4	47.9	47.2	48.1	48.4	48.4
CO conversion (TCD)	94.4	86.8	75.3	87.2	92.2	94.7
Carbon conversion (TCD)	45.0	38.2	37.1	34.1	49.7	40.4
72 hours (time)	71.7	70.8	73.4	72.0	72.4	71.4
CO conversion (TCD)	92.7	90.3	85.5	90.4	92.5	96.1
Carbon conversion (TCD)	44.2	46.1	48.2	38.0	50.4	43.5

96 hours (time)	96.2	94.1	95.9	97.7	96.2	96.3
CO conversion (TCD)	93.0	86.8	89.1	93.3	93.5	97.3
Carbon conversion (TCD)	45.9	46.9	50.5	38.8	49.0	45.0

[a] Half catalyst loaded – flow rates also halved

H.2 Mass balance after 96 hours time on-stream

Table H.2 Flows in and out and the carbon balance after 96 hours time on-stream for the Fixed-bed reactor

	0% Cu	2% Cu	9% Cu	23% Cu	50% Cu	77% Cu[a]
	mol/min	mol/min	mol/min	mol/min	mol/min	mol/min
H_2 in	1.34E-03	1.35E-03	1.36E-03	1.38E-03	1.32E-03	7.23E-04
CO in	3.54E-04	3.14E-04	3.23E-04	3.57E-04	3.25E-04	1.52E-04
CO_2 in	3.54E-04	3.41E-04	3.41E-04	3.26E-04	3.27E-04	1.71E-04
H_2 out	8.36E-04	7.09E-04	7.50E-04	8.73E-04	6.45E-04	4.55E-04
CO out	4.22E-05	4.16E-05	3.65E-05	2.38E-05	2.05E-05	9.14E-06
CO_2 out	3.57E-04	3.06E-04	2.85E-04	3.94E-04	3.01E-04	1.67E-04
CH_4 out TCD	1.82E-05	1.94E-05	1.79E-05	2.83E-05	2.43E-05	1.22E-05
CH_4 out FID	3.20E-05	2.34E-05	2.90E-05	3.23E-05	3.18E-05	1.57E-05
Approx of HC's out[b]	9.59E-05	7.01E-05	8.69E-05	9.68E-05	9.54E-05	4.72E-05
EtOH out	7.50E-06	6.92E-06	7.08E-06	9.07E-06	1.34E-05	5.65E-06
H_2O out TCD	6.71E+00	7.49E+00	8.80E+00	4.20E+00	7.66E+00	3.26E+00
H_2O out O balance	3.00E-04	3.34E-04	3.93E-04	1.88E-04	3.42E-04	1.46E-04
Carbon in permanent gasses	7.09E-04	6.55E-04	6.65E-04	6.83E-04	6.52E-04	3.24E-04
Carbon out permanent gasses	3.99E-04	3.48E-04	3.21E-04	4.18E-04	3.22E-04	1.76E-04
Carbon out product[c]	2.10E-04	2.18E-04	2.15E-04	2.83E-04	2.41E-04	1.24E-04
Carbon balance closure	**85.9 %**	**86.5 %**	**80.6 %**	**102.6 %[d]**	**86.3 %**	**92.9 %**

[a] Half catalyst loaded – flow rates also halved

[b] Used FID exit methane times 3

[c] Used total area of FID relative to internal standard

[d] Could be high due to high exiting CO_2

H.3 Rates of formation after 96 hours time on-stream

Table H.3 Rate of formation of selected hydrocarbons and alcohols after 96 hours time on-stream for the catalyst series in a Fixed-bed reactor

Carbon number	**0% Cu** $\left(\frac{\text{mole}}{\text{min} \bullet \text{g Fe}}\right)$	**2% Cu** $\left(\frac{\text{mole}}{\text{min} \bullet \text{g Fe}}\right)$	**9% Cu** $\left(\frac{\text{mole}}{\text{min} \bullet \text{g Fe}}\right)$	**23% Cu** $\left(\frac{\text{mole}}{\text{min} \bullet \text{g Fe}}\right)$	**50% Cu** $\left(\frac{\text{mole}}{\text{min} \bullet \text{g Fe}}\right)$	**77% Cu** $\left(\frac{\text{mole}}{\text{min} \bullet \text{g Fe}}\right)$
			α-olefins			
2	1.23E-05	7.04E-06	8.51E-06	9.75E-06	8.41E-06	4.43E-06
3	9.69E-06	7.04E-06	8.40E-06	9.23E-06	8.75E-06	4.46E-06
4	6.02E-06	4.47E-06	5.28E-06	5.94E-06	5.44E-06	2.69E-06
5	3.47E-06	2.60E-06	2.98E-06	3.31E-06	3.02E-06	1.53E-06
6	2.14E-06	1.58E-06	1.79E-06	1.93E-06	1.81E-06	9.18E-07
7	1.30E-06	1.01E-06	1.12E-06	1.18E-06	1.14E-06	5.71E-07
8	8.54E-07	6.42E-07	6.85E-07	7.10E-07	7.32E-07	3.63E-07
9	6.19E-07	4.26E-07	4.21E-07	4.16E-07	4.90E-07	2.61E-07
10	3.89E-07	2.66E-07	2.30E-07	2.11E-07	2.85E-07	1.67E-07
			Linear olefins			
2	1.23E-05	7.04E-06	8.51E-06	9.75E-06	8.41E-06	4.43E-06
3	9.69E-06	7.04E-06	8.40E-06	9.23E-06	8.75E-06	4.46E-06
4	6.17E-06	4.61E-06	5.42E-06	6.13E-06	5.59E-06	2.78E-06
5	3.57E-06	2.69E-06	3.06E-06	3.42E-06	3.11E-06	1.58E-06
6	2.23E-06	1.63E-06	1.88E-06	1.98E-06	1.92E-06	9.54E-07
7	1.36E-06	1.06E-06	1.17E-06	1.23E-06	1.17E-06	5.91E-07
8	9.09E-07	6.79E-07	7.04E-07	7.54E-07	7.54E-07	3.82E-07
9	6.72E-07	4.60E-07	4.44E-07	4.65E-07	5.08E-07	2.79E-07
10	4.38E-07	2.66E-07	2.30E-07	2.32E-07	2.85E-07	1.67E-07
			Linear parafins			
1	3.20E-05	2.34E-05	2.90E-05	3.23E-05	3.18E-05	1.57E-05

2	3.38E-06	1.87E-06	2.51E-06	2.93E-06	3.51E-06	1.69E-06
3	1.94E-06	1.39E-06	1.62E-06	2.09E-06	1.79E-06	8.22E-07
4	1.11E-06	1.02E-06	1.06E-06	1.27E-06	1.15E-06	5.38E-07
5	6.86E-07	4.96E-07	5.60E-07	6.31E-07	5.96E-07	3.31E-07
6	4.69E-07	3.31E-07	3.68E-07	4.14E-07	3.93E-07	2.18E-07
7	3.17E-07	2.30E-07	2.31E-07	2.65E-07	2.53E-07	1.42E-07
8	2.33E-07	1.58E-07	1.57E-07	1.92E-07	1.81E-07	1.01E-07
9	1.98E-07	1.27E-07	1.25E-07	1.32E-07	1.48E-07	1.77E-07
10	1.55E-07	8.01E-08	8.79E-08	8.34E-08	1.06E-07	1.81E-07

Appendix I

Details, selected flows and results for the Berty tests

I.1 Catalyst loading and conversions

Table I.1 Catalyst loadings and time on-stream conversions for the Berty reactor

	0% Cu	2% Cu	9% Cu	23% Cu	50% Cu	77% Cu
Mass catalyst loaded (g)	2.4002	2.4480	2.6405	3.1200	4.8002	10.4099
			24 hours			
CO conversion (TCD)	75.9	77.8	82.5	75.4	76.0	87.9
Carbon conversion (TCD)	31.8	33.3	34.6	32.1	30.0	37.4
			48 hours			
CO conversion (TCD)	81.4	77.6	85.0	78.1	76.9	88.4
Carbon conversion (TCD)	33.3	33.0	37.5	33.4	31.7	38.4
			72 hours			
CO conversion (TCD)	83.4	77.8	86.7	80.7	84.3	89.6
Carbon conversion (TCD)	37.8	31.7	38.0	34.5	37.6	39.2
			96 hours			
CO conversion (TCD)	83.5	77.7	86.1	82.0	83.6	87.7

Carbon conversion (TCD)	36.7	30.0	37.8	38.0	36.5	38.5

I.2 Mass balance after 96 hours time on-stream

Table I.2 Flows in and out and the carbon balance after 96 hours time on-stream for the Berty reactor

	0% Cu	**2% Cu**	**9% Cu**	**23% Cu**	**50% Cu**	**77% Cu**
	mol/min	mol/min	mol/min	mol/min	mol/min	mol/min
H_2 in	4.91E-03	4.65E-03	4.41E-03	4.90E-03	4.94E-03	4.58E-03
CO in	1.14E-03	1.10E-03	8.70E-04	1.15E-03	1.11E-03	1.11E-03
CO_2 in	9.93E-04	9.73E-04	1.26E-03	1.01E-03	9.53E-04	1.02E-03
H_2 out	3.31E-03	3.37E-03	2.89E-03	3.28E-03	3.24E-03	2.87E-03
CO out	1.88E-04	2.27E-04	1.20E-04	2.08E-04	1.81E-04	1.36E-04
CO_2 out	1.16E-03	1.14E-03	1.21E-03	1.13E-03	1.13E-03	1.17E-03
CH_4 out TCD	6.28E-05	6.49E-05	7.58E-05	7.32E-05	7.78E-05	9.45E-05
CH_4 out FID	7.42E-05	6.99E-05	9.67E-05	8.11E-05	7.89E-05	8.04E-05
Approx of HC's out[a]	2.23E-04	2.10E-04	2.90E-04	2.43E-04	2.37E-04	2.41E-04
EtOH out	2.33E-05	2.53E-05	4.18E-05	2.80E-05	2.84E-05	3.79E-05
H_2O out TCD	1.32E+01	1.17E+01	1.83E+01	1.50E+01	1.23E+01	1.40E+01
H_2O out O balance	5.91E-04	5.24E-04	8.18E-04	6.69E-04	5.50E-04	6.25E-04
Carbon in permanent gasses	2.14E-03	2.08E-03	2.13E-03	2.16E-03	2.06E-03	2.12E-03
Carbon out permanent gasses	1.35E-03	1.36E-03	1.33E-03	1.34E-03	1.31E-03	1.30E-03
Carbon out product[b]	5.96E-04	5.51E-04	9.25E-04	5.70E-04	5.68E-04	6.96E-04
Carbon balance closure	**91.2 %**	**92.2 %**	**105.6 %**[c]	**88.4 %**	**91.1 %**	**94.3 %**

[a] Used FID exit methane times 3

[b] Used total area of FID relative to internal standard

[c] Could be high due to low incoming CO

I.3 Rates of formation after 96 hours time on-stream

Table I.3 Rate of formation of selected hydrocarbons after 96 hours time on-stream for the catalyst series in a Berty reactor

Carbon number	0% Cu $\left(\frac{\text{mole}}{\text{min} \bullet \text{g Fe}}\right)$	2% Cu $\left(\frac{\text{mole}}{\text{min} \bullet \text{g Fe}}\right)$	9% Cu $\left(\frac{\text{mole}}{\text{min} \bullet \text{g Fe}}\right)$	23% Cu $\left(\frac{\text{mole}}{\text{min} \bullet \text{g Fe}}\right)$	50% Cu $\left(\frac{\text{mole}}{\text{min} \bullet \text{g Fe}}\right)$	77% Cu $\left(\frac{\text{mole}}{\text{min} \bullet \text{g Fe}}\right)$
			α-olefins			
2	2.31E-05	2.30E-05	3.19E-05	2.27E-05	1.88E-05	1.55E-05
3	2.10E-05	2.21E-05	3.61E-05	2.08E-05	2.14E-05	2.26E-05
4	1.22E-05	1.28E-05	2.28E-05	1.20E-05	1.22E-05	1.35E-05
5	7.23E-06	7.25E-06	1.38E-05	7.00E-06	7.14E-06	8.02E-06
6	4.49E-06	4.26E-06	8.24E-06	4.23E-06	4.27E-06	5.00E-06
7	2.91E-06	2.57E-06	4.99E-06	2.64E-06	2.65E-06	2.78E-06
8	1.97E-06	1.60E-06	3.05E-06	1.74E-06	1.70E-06	1.66E-06
9	1.38E-06	1.01E-06	1.87E-06	1.15E-06	1.12E-06	9.97E-07
10	9.89E-07	6.45E-07	1.12E-06	7.82E-07	7.51E-07	6.21E-07
			Linear olefins			
2	2.31E-05	2.30E-05	3.19E-05	2.27E-05	1.88E-05	1.55E-05
3	2.10E-05	2.21E-05	3.61E-05	2.08E-05	2.14E-05	2.26E-05
4	1.28E-05	1.34E-05	2.43E-05	1.25E-05	1.29E-05	1.58E-05
5	7.54E-06	7.57E-06	1.45E-05	7.26E-06	7.48E-06	9.42E-06
6	4.69E-06	4.45E-06	8.70E-06	4.39E-06	4.50E-06	6.02E-06
7	3.04E-06	2.69E-06	5.31E-06	2.76E-06	2.80E-06	3.39E-06
8	2.09E-06	1.69E-06	3.28E-06	1.82E-06	1.82E-06	2.03E-06
9	1.46E-06	1.05E-06	2.01E-06	1.19E-06	1.19E-06	1.25E-06
10	1.06E-06	6.82E-07	1.24E-06	8.22E-07	8.14E-07	7.98E-07
			Linear parafins			
1	7.42E-05	6.99E-05	9.67E-05	8.11E-05	7.89E-05	8.04E-05
2	1.06E-05	9.81E-06	1.37E-05	1.02E-05	1.23E-05	1.87E-05

3	4.23E-06	4.00E-06	6.70E-06	3.85E-06	4.38E-06	9.03E-06
4	2.46E-06	2.40E-06	4.16E-06	2.44E-06	2.54E-06	4.76E-06
5	1.55E-06	1.39E-06	2.59E-06	1.39E-06	1.56E-06	2.61E-06
6	1.04E-06	8.81E-07	1.70E-06	8.97E-07	1.02E-06	1.80E-06
7	6.88E-07	5.34E-07	1.09E-06	5.69E-07	6.49E-07	1.19E-06
8	5.13E-07	3.66E-07	7.49E-07	4.07E-07	4.61E-07	8.06E-07
9	3.59E-07	2.23E-07	4.67E-07	2.62E-07	3.16E-07	5.38E-07
10	2.66E-07	1.46E-07	3.04E-07	1.85E-07	2.26E-07	3.49E-07

Table I.4 Rate of formation of selected oxygenates after 96 hours time on-stream for the catalyst series in a Berty reactor

Carbon number	**0% Cu** $\left(\frac{\text{mole}}{\text{min} \bullet \text{g Fe}}\right)$	**2% Cu** $\left(\frac{\text{mole}}{\text{min} \bullet \text{g Fe}}\right)$	**9% Cu** $\left(\frac{\text{mole}}{\text{min} \bullet \text{g Fe}}\right)$	**23% Cu** $\left(\frac{\text{mole}}{\text{min} \bullet \text{g Fe}}\right)$	**50% Cu** $\left(\frac{\text{mole}}{\text{min} \bullet \text{g Fe}}\right)$	**77% Cu** $\left(\frac{\text{mole}}{\text{min} \bullet \text{g Fe}}\right)$
			Linear alcohols			
1	8.31E-07	7.21E-07	0.00E+00	9.13E-07	7.71E-07	1.63E-06
2	1.43E-05	1.61E-05	2.58E-05	1.86E-05	2.00E-05	2.63E-05
3	1.61E-06	2.11E-06	3.23E-06	2.38E-06	2.44E-06	3.43E-06
4	5.62E-07	6.46E-07	1.19E-06	8.45E-07	8.55E-07	1.20E-06
5	2.77E-07	4.31E-07	5.13E-07	4.32E-07	3.87E-07	6.02E-07
6	1.57E-07	2.27E-07	2.72E-07	2.34E-07	2.20E-07	3.43E-07
			Linear aldeydes			
2	2.68E-06	2.09E-06	4.12E-06	1.77E-06	1.36E-06	1.63E-06
3	8.44E-07	5.38E-07	9.01E-07	4.65E-07	3.84E-07	6.84E-07
4	2.73E-07	2.72E-07	4.26E-07	2.39E-07	1.47E-07	1.20E-07
5	1.48E-07	1.84E-07	2.64E-07	1.74E-07	1.04E-07	1.17E-07
6	1.23E-07	1.12E-07	1.55E-07	1.24E-07	5.83E-08	3.67E-08
7	1.53E-07	1.56E-07	1.89E-07	1.64E-07	1.01E-07	0.00E+00
			Linear ketones			
3	8.76E-07	1.14E-06	2.79E-06	1.11E-06	1.05E-06	1.27E-06

4	2.17E-07	2.79E-07	8.40E-07	2.68E-07	2.39E-07	3.23E-07
5	1.08E-07	1.24E-07	2.83E-07	1.19E-07	1.06E-07	1.61E-07
6	9.20E-08	9.79E-08	2.06E-07	1.04E-07	7.78E-08	1.41E-07
7	6.35E-08	4.12E-08	9.55E-08	4.76E-08	3.59E-08	0.00E+00

Appendix J

Co-feeding: Baseline tests

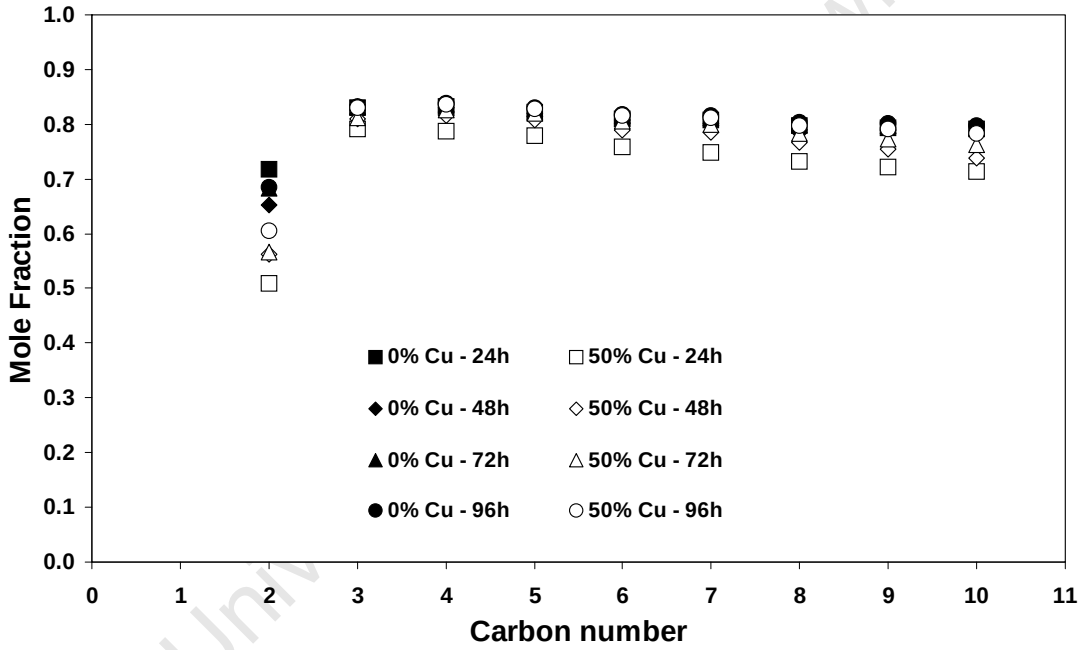

Figure J.1 Olefins in linear hydrocarbons as a function of carbon number for the 0 and 50 wt% Cu catalysts from 24 to 96 hrs time on-stream in a Berty reactor

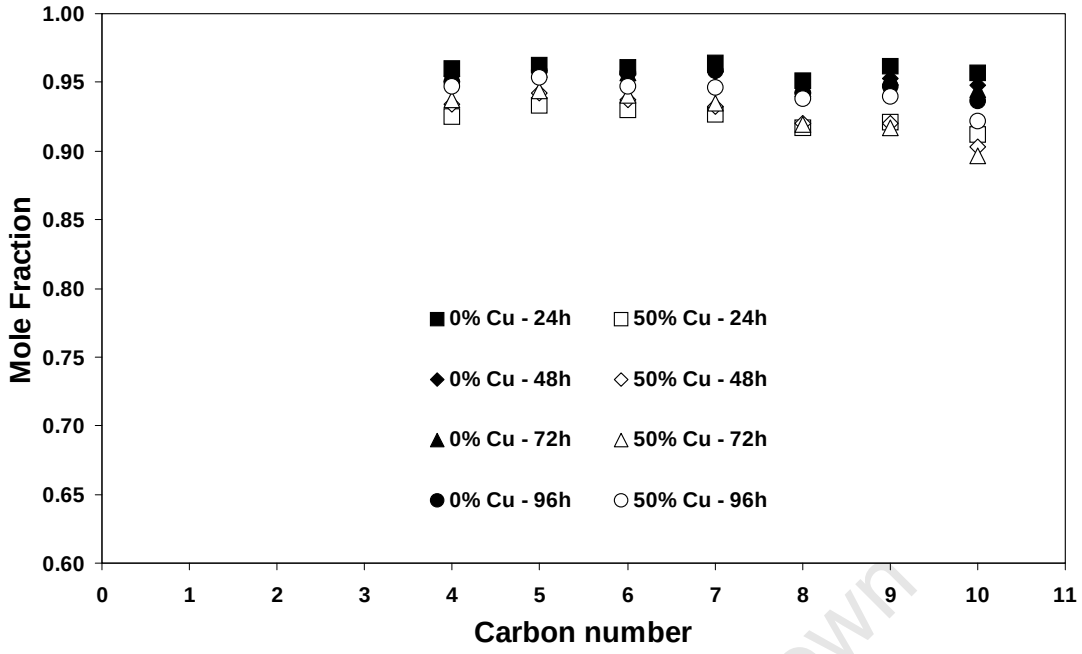

Figure J.2 α-Olefins in linear olefins as a function of carbon number for the 0 and 50 wt% Cu catalysts from 24 to 96 hrs time on-stream in a Berty reactor

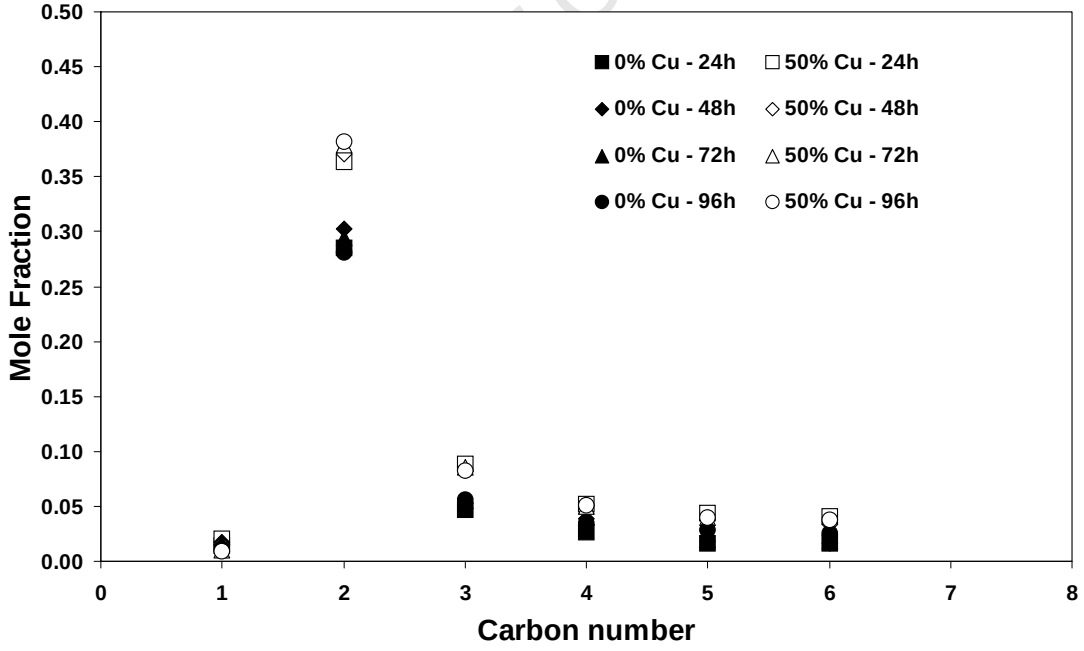

Figure J.3 Alcohols in linear hydrocarbons as a function of carbon number for the 0 and 50 wt% Cu catalysts from 24 to 96 hrs time on-stream in a Berty reactor

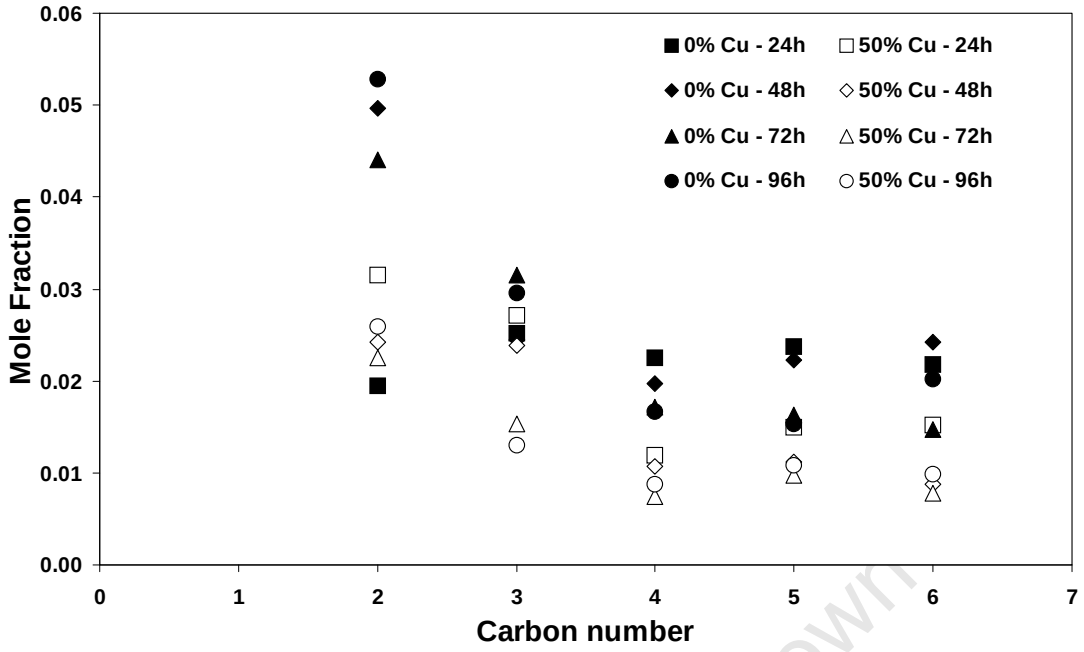

Figure J.4 Aldehydes in linear hydrocarbons as a function of carbon number for the 0 and 50 wt% Cu catalysts from 24 to 96 hrs time on-stream in a Berty reactor

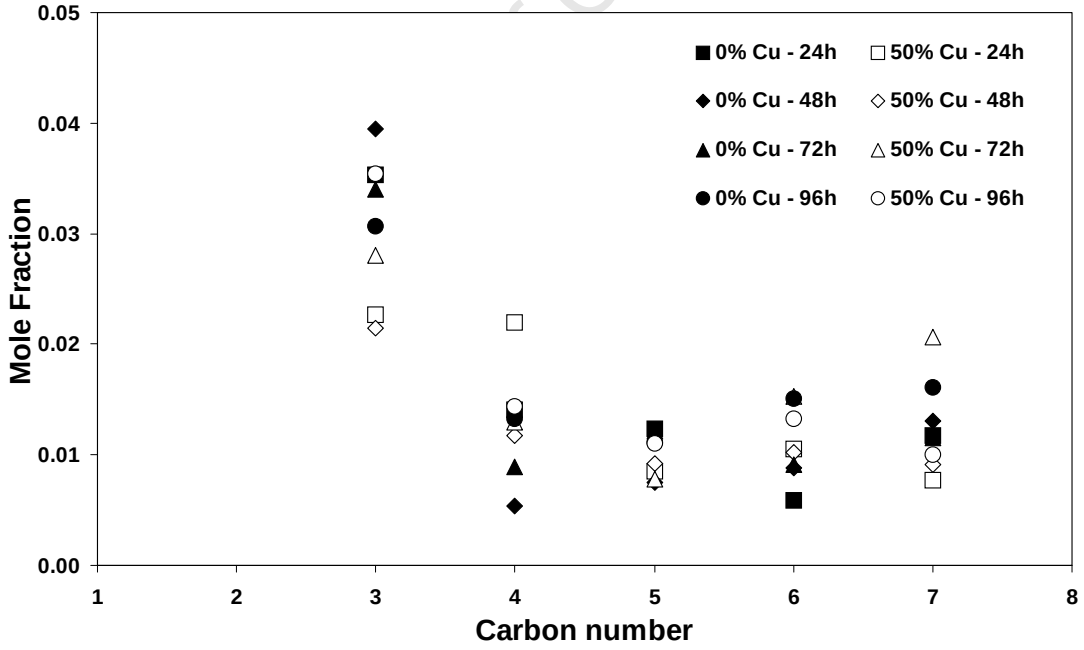

Figure J.5 Ketones in linear hydrocarbons as a function of carbon number for the 0 and 50 wt% Cu catalysts from 24 to 96 hrs time on-stream in a Berty reactor

Table J.1 Mole fraction of the C_8 oxygenates in linear C_8 hydrocarbons for the baseline runs

0 wt% Cu Baseline				
TOL	24	48	72	96
Feeding	no	no	no	no
$\frac{\text{Octanol}}{(\text{Octane} + \text{Octene})}$	0.037	0.032	0.027	0.023
$\frac{\text{Octanal}}{(\text{Octane} + \text{Octene})}$	0.016	0.016	0.011	0.008
$\frac{\text{Octan-2-one}}{(\text{Octane} + \text{Octene})}$	0.004	0.004	0.003	0.003
$\frac{\text{Octanoic acid}}{(\text{Octane} + \text{Octene})}$	0.007	0.004	0.003	0.002
50 wt% Cu Baseline				
TOL	24	48	72	96
Feeding	no	no	no	no
$\frac{\text{Octanol}}{(\text{Octane} + \text{Octene})}$	0.102	0.091	0.075	0.063
$\frac{\text{Octanal}}{(\text{Octane} + \text{Octene})}$	0.010	0.009	0.007	0.006
$\frac{\text{Octan-2-one}}{(\text{Octane} + \text{Octene})}$	0.006	0.006	0.005	0.005
$\frac{\text{Octanoic acid}}{(\text{Octane} + \text{Octene})}$	0.020	0.011	0.007	0.005

Table J.2 Equilibrium ratios of C_8 oxygenates in product oil for the baseline runs during Fischer-Tropsch synthesis in a Berty reactor using the TIC m/z ion specific areas

0 wt% Cu Baseline					
Reaction and ratio		**Product ratios**			
		24h	48h	72h	96h
Octanoic acid + H_2 ⇔ Octan-2-one + H_2O	Eq[a]	1577	1554	1071	1170
Octan-2-one/ Octanoic acid	Obs[b]	0.51	0.96	1.32	1.54
1-Octanol ⇔ Octan-2-one + H_2	Eq	36.4	37.1	38.6	38.3
Octan-2-one/1-Octanol	Obs	0.10	0.12	0.13	0.13
Octanal ⇔ Octan-2-one	Eq	415	415	415	415
Octan-2-one/ Octanal	Obs	0.23	0.25	0.30	0.36
1-Octanol + H_2O ⇔ Octanoic acid +2H_2	Eq	0.02	0.02	0.04	0.03
Octanoic acid/1-Octanol	Obs	0.20	0.12	0.09	0.09
Octanal + H_2O ⇔ Octanoic acid + H_2	Eq	0.26	0.27	0.39	0.36
Octanoic acid/ Octanal	Obs	0.46	0.26	0.23	0.24
Octanal + H_2 ⇔ 1-Octanol	Eq	11.4	11.2	10.8	10.8
1-Octanol /Octanal	Obs	2.3	2.1	2.4	2.7
50 wt% Cu catalyst					
Reaction and ratio		**Product ratios**			
		24h	48h	72h	96h
Octanoic acid + H2 ⇔ Octan-2-one + H2O	Eq	2038	1673	1093	1226
Octan-2-one/ Octanoic acid	Obs	0.29	0.49	0.74	0.90
1-Octanol ⇔ Octan-2-one + H2	Eq	36.0	36.7	39.0	38.3
Octan-2-one/1-Octanol	Obs	0.06	0.06	0.07	0.08
Octanal ⇔ Octan-2-one	Eq	415	415	415	415
Octan-2-one/ Octanal	Obs	0.57	0.64	0.73	0.77
1-Octanol + H2O ⇔ Octanoic acid +2H2	Eq	0.02	0.02	0.04	0.03
Octanoic acid/1-Octanol	Obs	0.20	0.13	0.09	0.09

Octanal + H2O ⇔ Octanoic acid + H2	Eq	0.20	0.25	0.38	0.34
Octanoic acid/ Octanal	Obs	1.93	1.32	0.99	0.85
Octanal + H2 ⇔ 1-Octanol	Eq	11.5	11.3	10.6	10.8
1-Octanol /Octanal	Obs	9.8	10.5	10.4	9.8

[a] Eq: Expected ratio at equilibrium

[b] Obs: Observed product ratios

Appendix K

Co-feeding: 1-Octanol

K.1 Run details

Table K.1 Catalyst loadings and time on-stream conversions for 1-octanol co-feeding

	0% Cu	50% Cu
Mass catalyst loaded (g)	2.4001	4.8017
Time on line (hours)	24	24
CO conversion (TCD)	86.8	84.2
Carbon conversion (TCD)	38.0	37.8
Time on line (hours)	48	48
CO conversion (TCD)	86.7	86.5
Carbon conversion (TCD)	40.3	39.7
Time on line (hours)	74	72
CO conversion (TCD)	89.7	86.6
Carbon conversion (TCD)	41.5	36.8
Time on line (hours)	96	80
CO conversion (TCD)	89.0	86.3
Carbon conversion (TCD)	40.5	33.6
Time on line (hours)	120	96
CO conversion (TCD)	89.6	87.2
Carbon conversion (TCD)	40.7	38.9
Time on line (hours)		121
CO conversion (TCD)		87.7
Carbon conversion (TCD)		41.6

K.2 GC-FID results

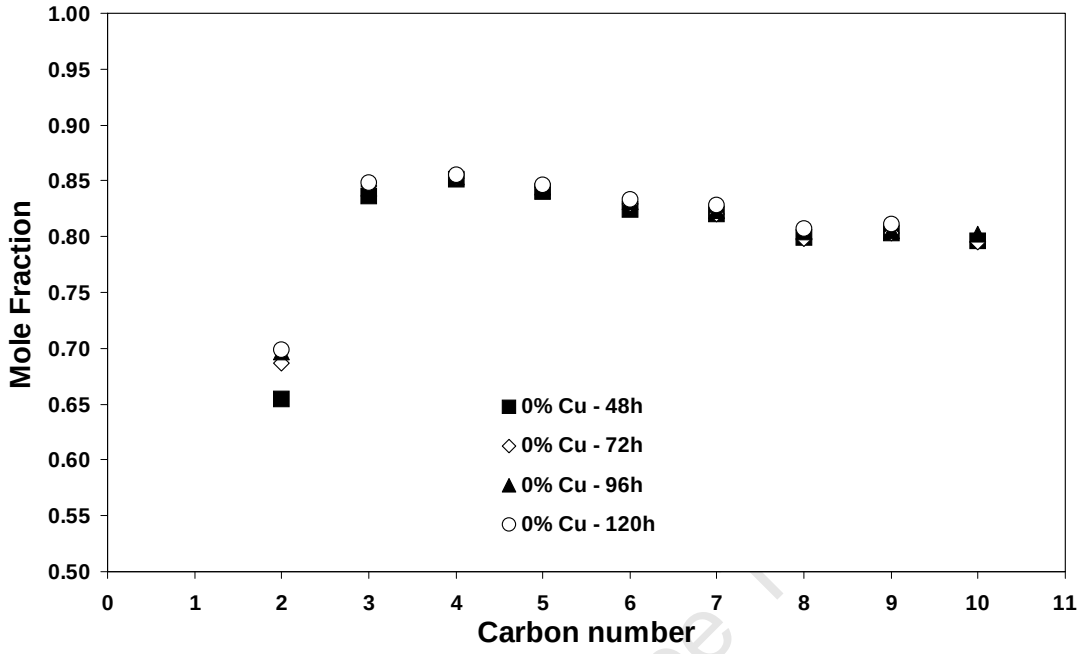

Figure K.1 Mole fraction of linear olefins in linear hydrocarbon product on the 0 wt% Cu catalyst for 1-octanol co-feeding

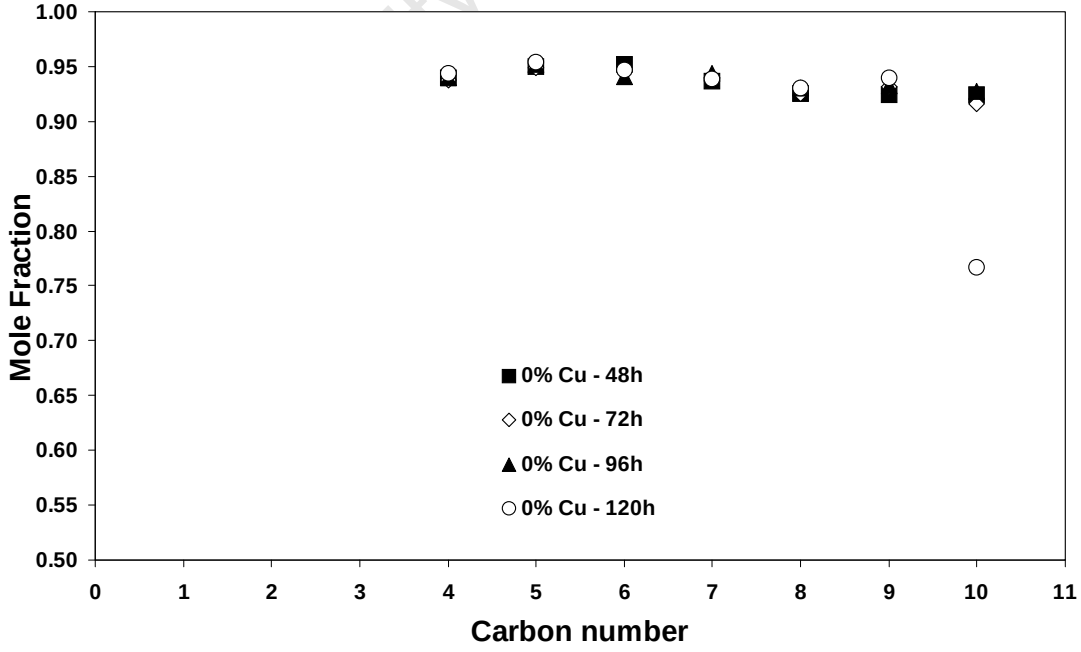

Figure K.2 Mole fraction of α–olefins in linear olefins on the 0 wt% Cu catalyst for 1-octanol co-feeding

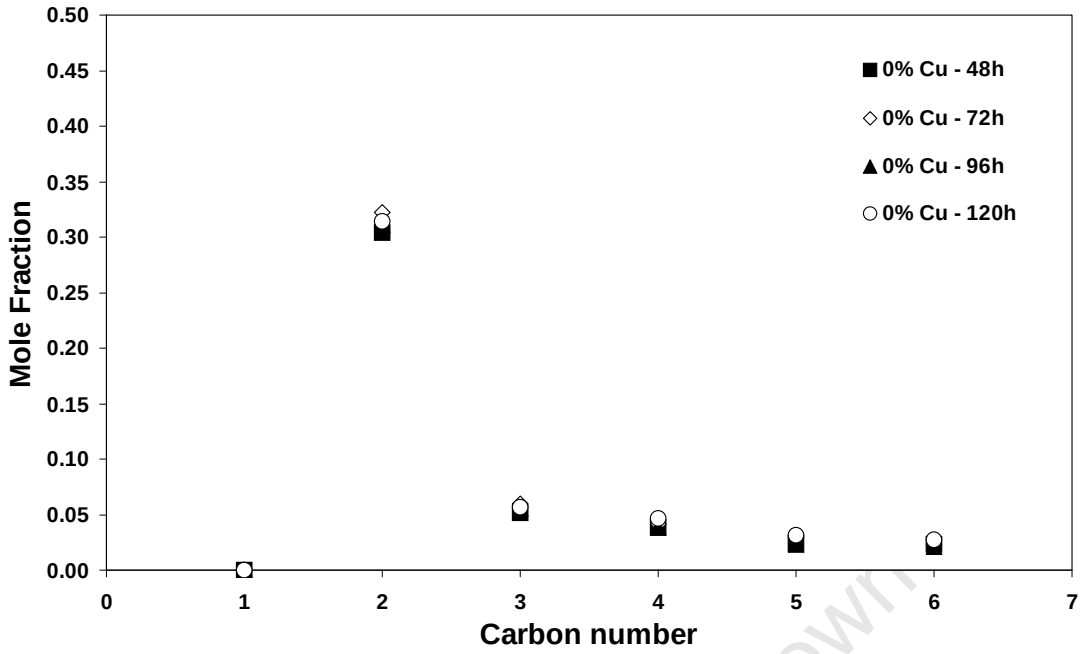

Figure K.3 Mole fraction of alcohols in linear product (excluding aldehydes and ketones) on the 0 wt% Cu catalyst for 1-octanol co-feeding

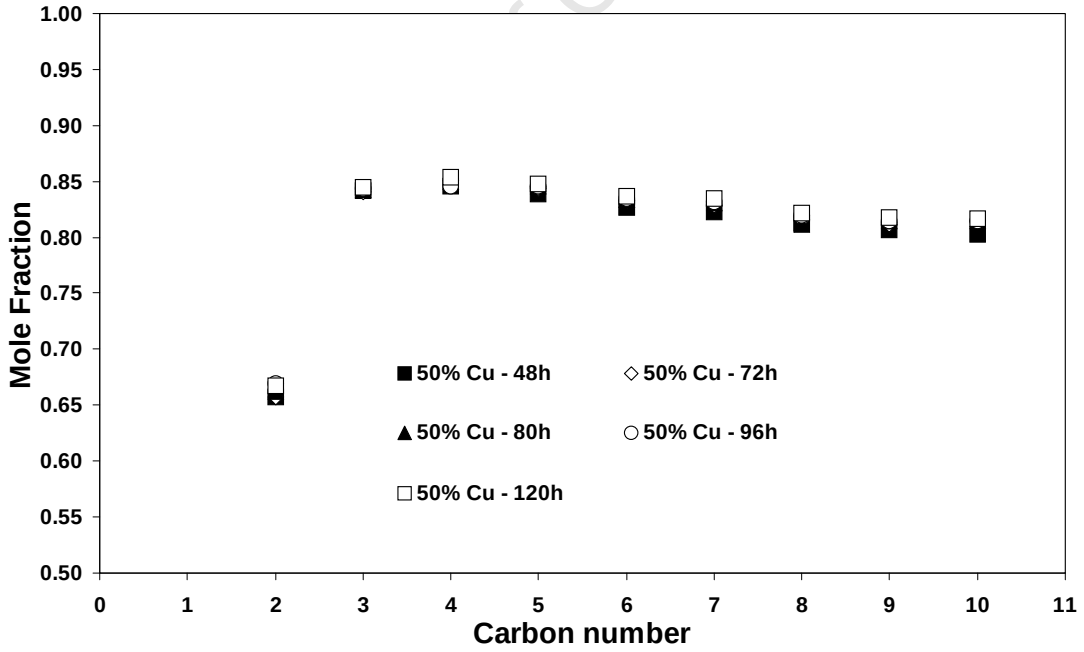

Figure K.4 Mole fraction of linear olefins in linear hydrocarbon product on the 50 wt% Cu catalyst for 1-octanol co-feeding

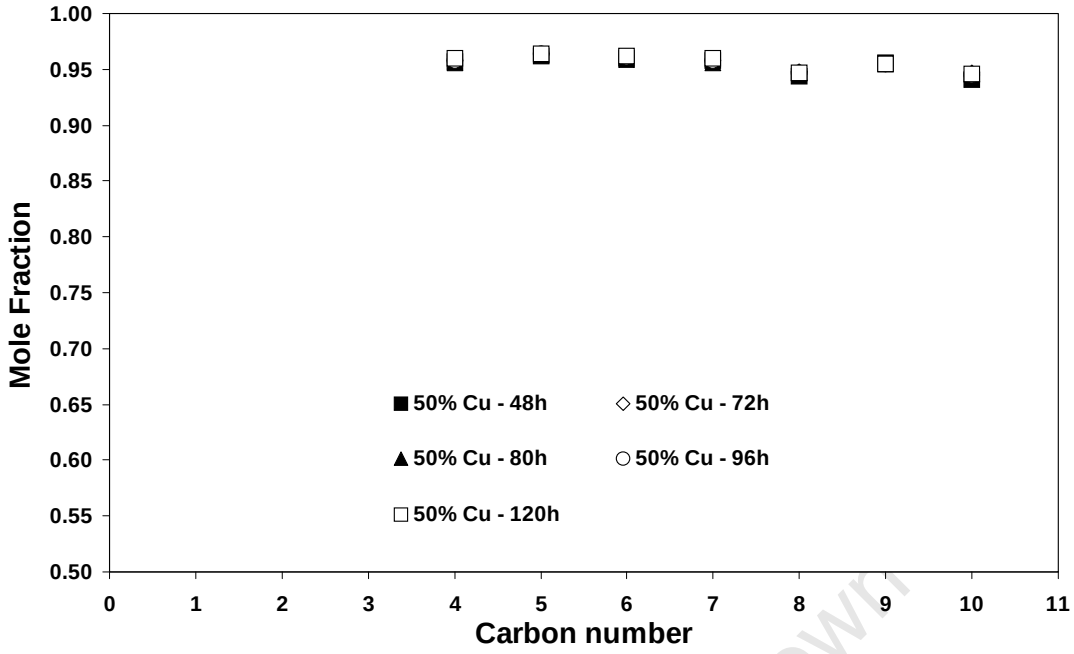

Figure K.5 Mole fraction of α–olefins in linear olefins on the 50 wt% Cu catalyst for 1-octanol co-feeding

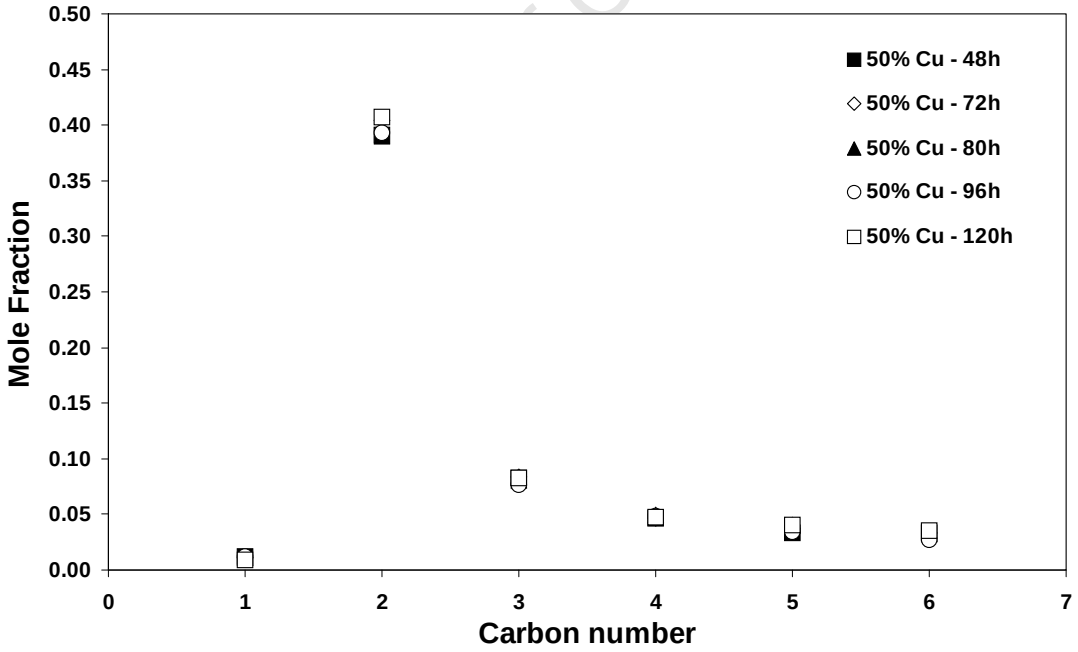

Figure K.6 Mole fraction of alcohols in linear product (excluding aldehydes and ketones) on the 50 wt% Cu catalyst for 1-octanol co-feeding

K.3 GC-MS results

Table K.2 Molar balance of 1-octanol fed to C_8 oxygenate products for both 0 and 50 wt% Cu catalysts.

0 wt% Cu catalyst			
1-Octanol co-feeding			
Time on-stream of analysis (hrs)	74	96	
Feed rate (μmoles/min)	5.309	0.632	
Average feed rate (μmoles/min)		2.971	
Exit 1-Octanol (μmoles/min)		9.559	
Exit Octanal (μmoles/min)		0.434	
Exit Nonan-2-one (μmoles/min)		0.021	
Exit Octanoic acid (μmoles/min)		0.041	
C_8 Balance closure (less baseline flows)		186.0 %	
50 wt% Cu catalyst			
1-Octanol co-feeding			
Time on-stream of analysis (hrs)	72	80	96
Feed rate (μmoles/min)	0.445	1.160	1.256
Average feed rate (μmoles/min)		0.803	1.208
Exit 1-Octanol (μmoles/min)		0.786	0.770
Exit Octanal (μmoles/min)		5.289	6.109
Exit Nonan-2-one (μmoles/min)		0.671	0.662
Exit Octanoic acid (μmoles/min)		0.012	0.013
C_8 Balance closure (less baseline flows)		505.3%	531.3%

Table K.3 Molar flow rates (in μmol/min) of 1-octanol, octanal, octan-2-one, octanoic acid, nonan-2-one, heptane + heptane, octane + octene, and nonane + nonene for 1-octanol co-feeding

			0 wt% Cu 1-Octanol feeding			
TOL	48	54	74	96	104	120
Feeding	no		Octanol		no	no
1-Octanol	0.090	0.089	4.408	9.559	5.071	1.009
Octanal	0.048	0.042	0.239	0.434	0.171	0.037
Octan-2-one	0.014	0.013	0.016	0.017	0.013	0.004
Octanoic acid	0.030	0.027	0.040	0.041	0.024	0.006
Nonan-2-one	0.011	0.011	0.017	0.021	0.014	0.004
Heptane + Heptene	4.46	-	4.76	4.84	-	4.81
Octane + Octene	2.77	-	3.07	3.06	-	2.97
Nonane + Nonene	1.66	-	1.84	1.85	-	1.70
			50 wt% Cu 1-Octanol feeding			
TOL	48	72	80	96	121	
Feeding	no		1-Octanol		no	
1-Octanol	0.105	3.058	5.289	6.109	2.749	
Octanal	0.010	0.404	0.671	0.662	0.152	
Octan-2-one	0.014	0.014	0.016	0.015	0.008	
Octanoic acid	0.012	0.017	0.023	0.022	0.013	
Nonan-2-one	0.007	0.010	0.018	0.020	0.011	
Heptane + Heptene	3.55	3.87	3.89	3.92	4.02	
Octane + Octene	2.30	2.52	2.52	2.50	2.61	
Nonane + Nonene	1.48	1.62	1.57	1.54	1.64	

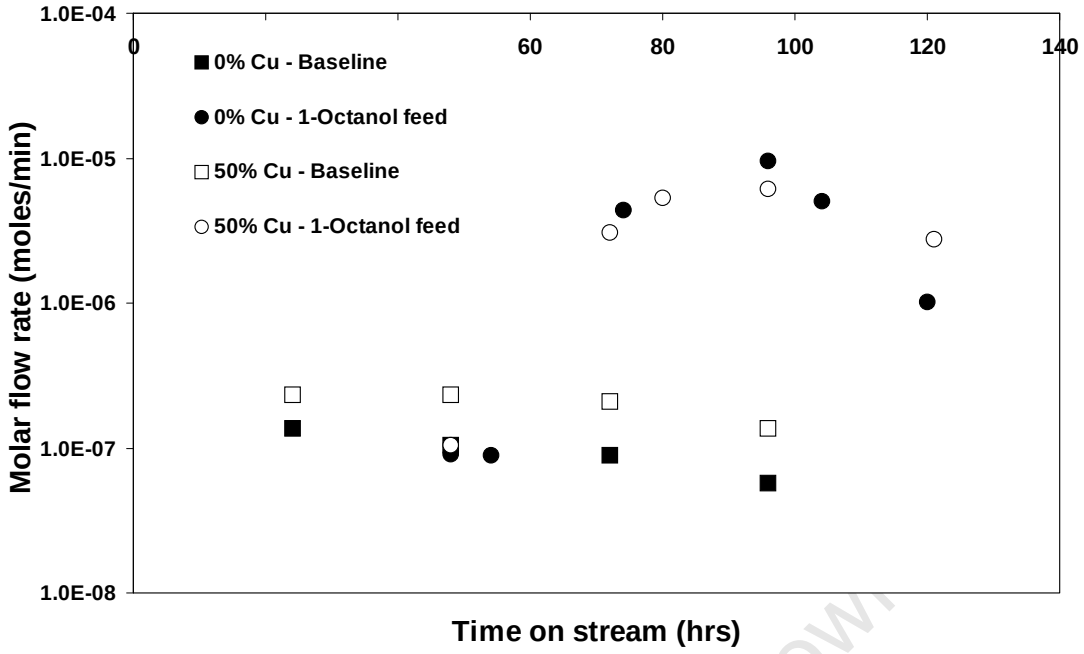

Figure K.7 1-Octanol flow rate as calculated in product oil for 0 and 50 wt% Cu catalysts for both baseline and 1-octanol co-feeding experiments

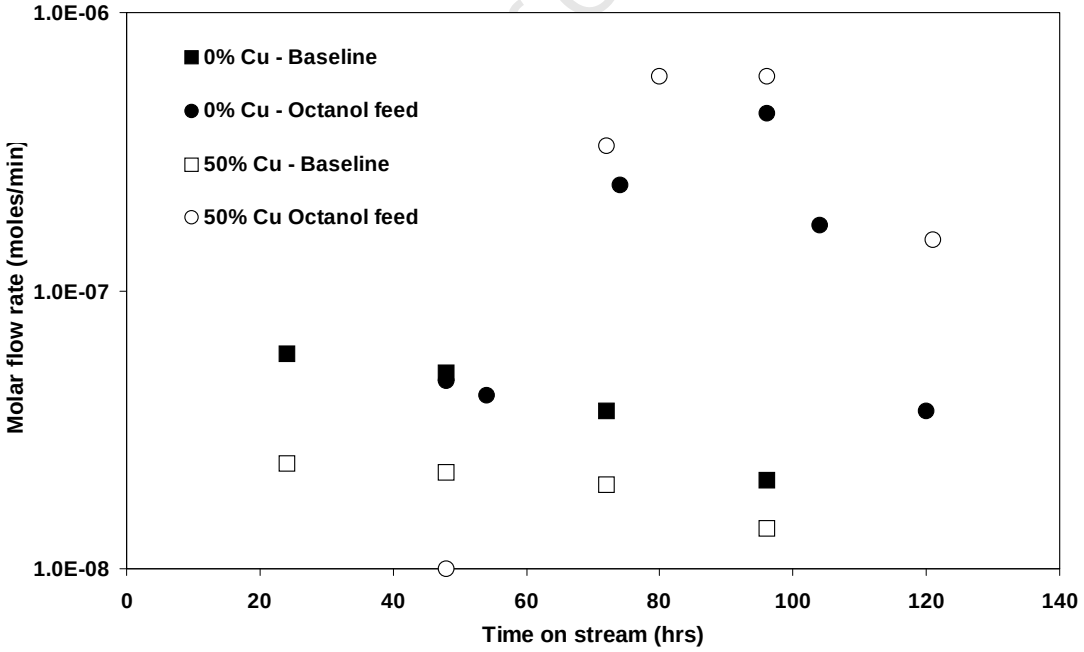

Figure K.8 Octanal flow rate in product oil for 0 and 50 wt% Cu catalysts for both baseline and 1-octanol co-feeding experiments

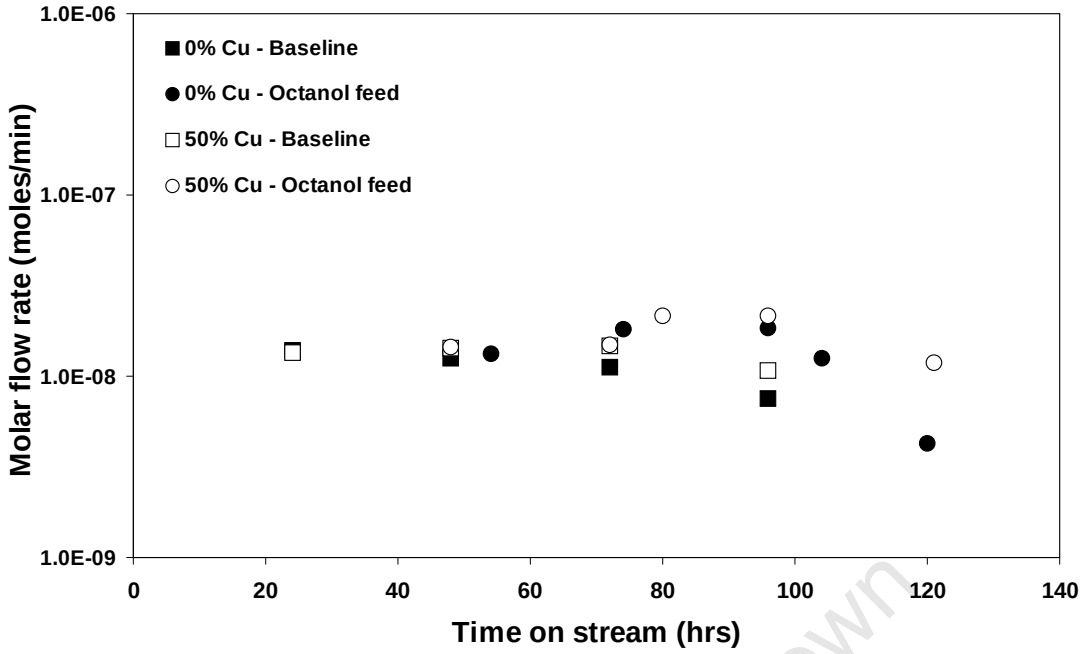

Figure K.9 Octan-2-one flow rate in product oil for 0 and 50 wt% Cu catalysts for both baseline and 1-octanol co-feeding experiments

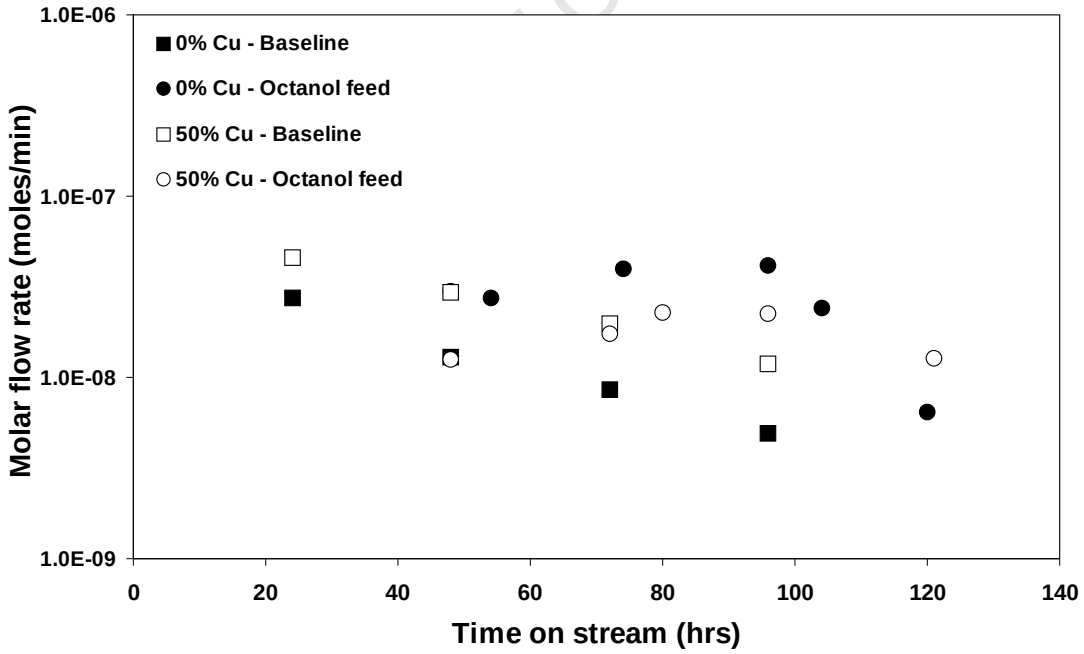

Figure K.10 Octanoic acid flow rate in product oil for 0 and 50 wt% Cu catalysts for both baseline and 1-octanol co-feeding experiments

The ASF plot of natural log of formation rates of linear hydrocarbons verse carbon number for 48 and 96 hours with the 0 wt% Cu catalyst during 1-octanol co-feeding is shown in the main text.

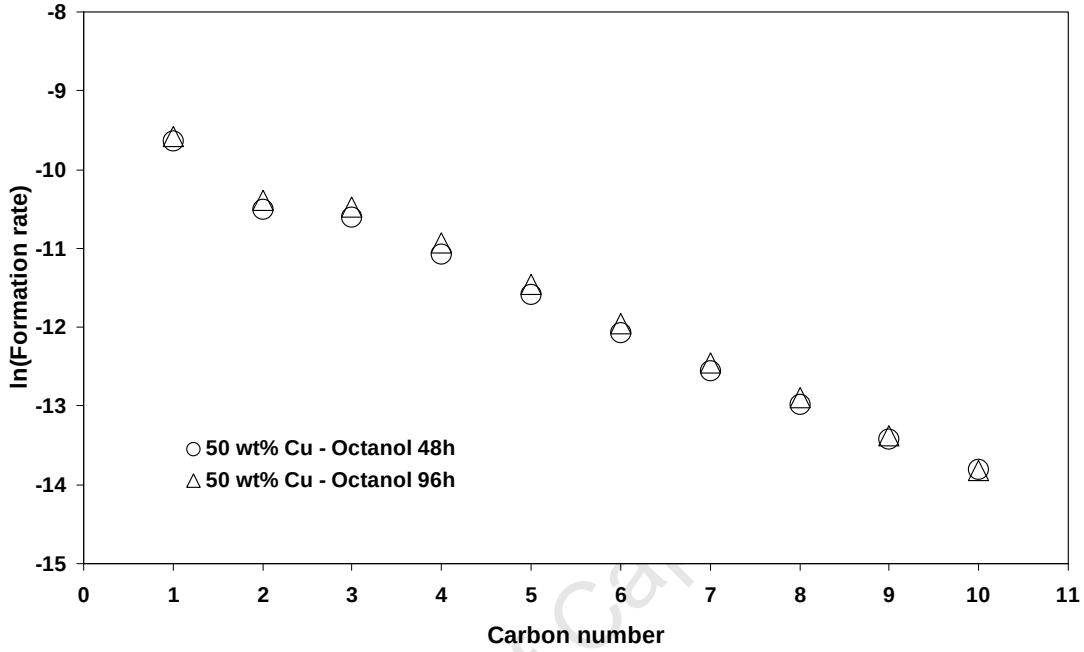

Figure K 11 ASF plot of natural log of formation rates of linear hydrocarbons verse carbon number for 48 and 96 hours with the 50 wt% Cu catalyst during 1-octanol co-feeding

The corresponding extracted ion chromatograms including that of the primary alcohols of 0 wt% Cu catalyst with 1-octanol co-feeding after 96 hours TOL during Fischer-Tropsch synthesis in a Berty reactor for ions m/z=31 (1-alcohols), m/z=45 (2-alcohols), m/z=70 (octylacetate) and m/z=88 (ethyl caprylate) is shown it the main text.

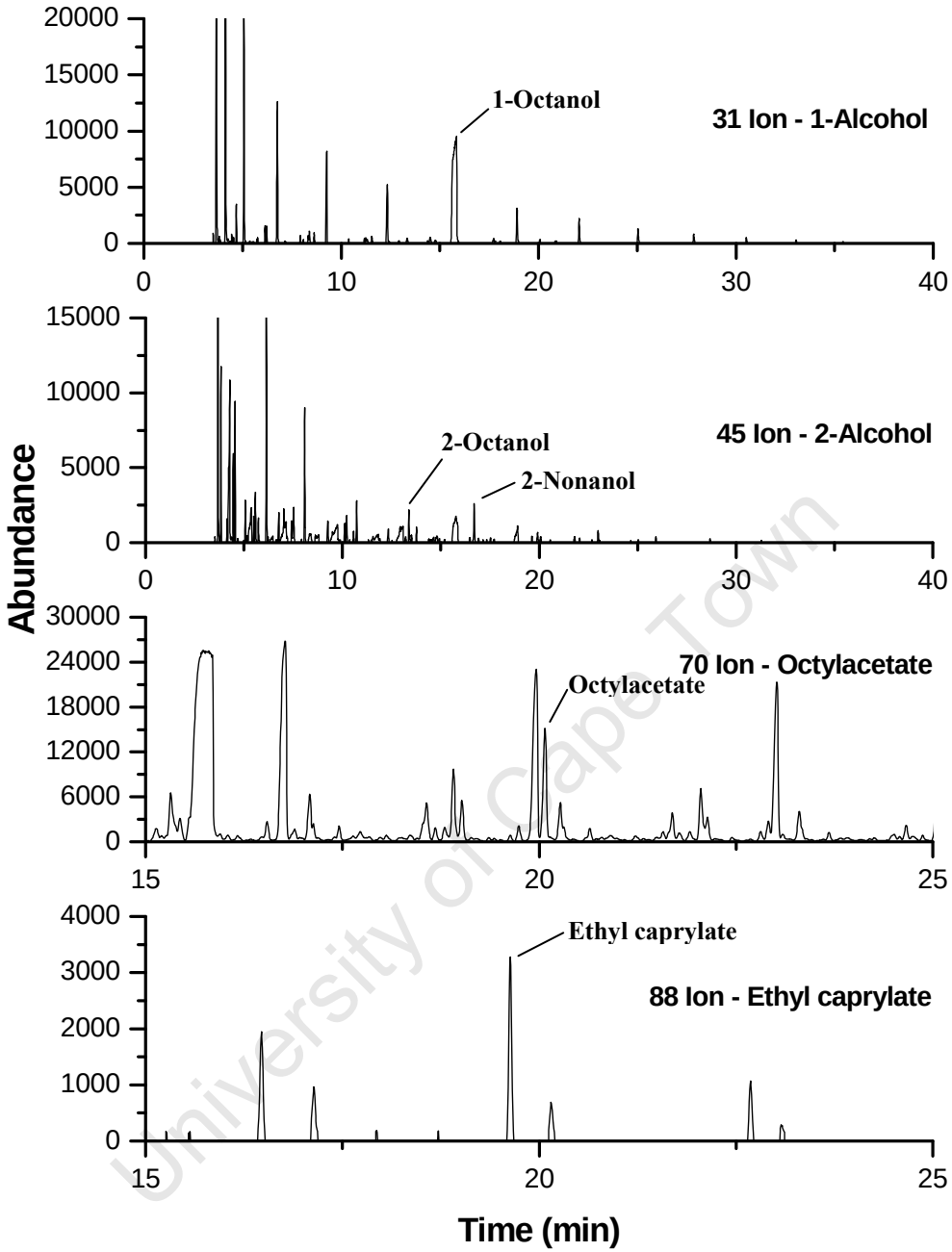

Figure K.12 The corresponding extracted ion chromatograms including that of the primary alcohols of 50 wt% Cu catalyst with 1-octanol co-feeding after 96 hours TOL during Fischer-Tropsch synthesis in a Berty reactor for ions m/z=31 (1-alcohols), m/z=45 (2-alcohols), m/z=70 (octylacetate) and m/z=88 (ethyl caprylate)

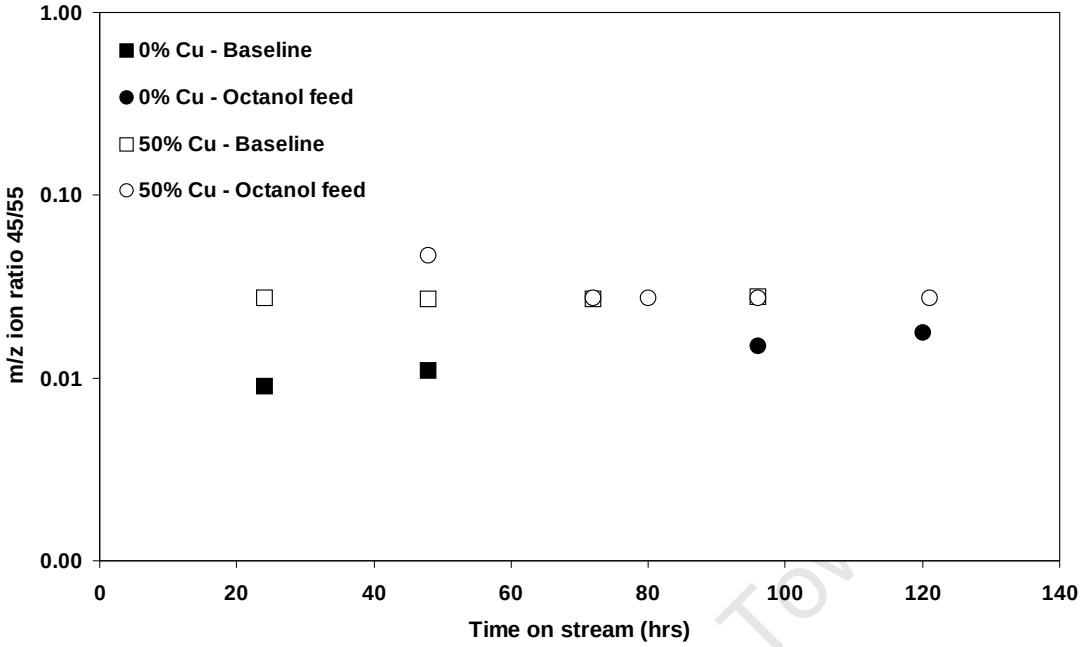

Figure K.13 Ion m/z for 2-octanol (45/55) in product oil for 0 and 50 wt% Cu catalysts for both baseline and 1-octanol co-feeding experiments

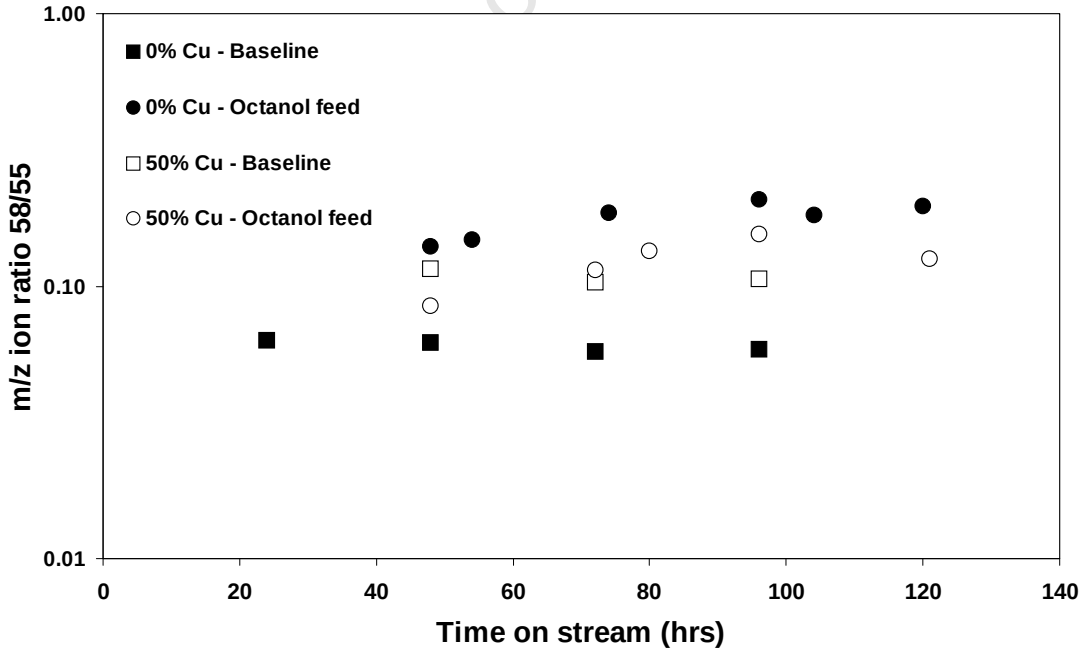

Figure K.14 Ion m/z for nonan-2-one (58/55) in product oil for 0 and 50 wt% Cu catalysts for both baseline and 1-octanol co-feeding experiments

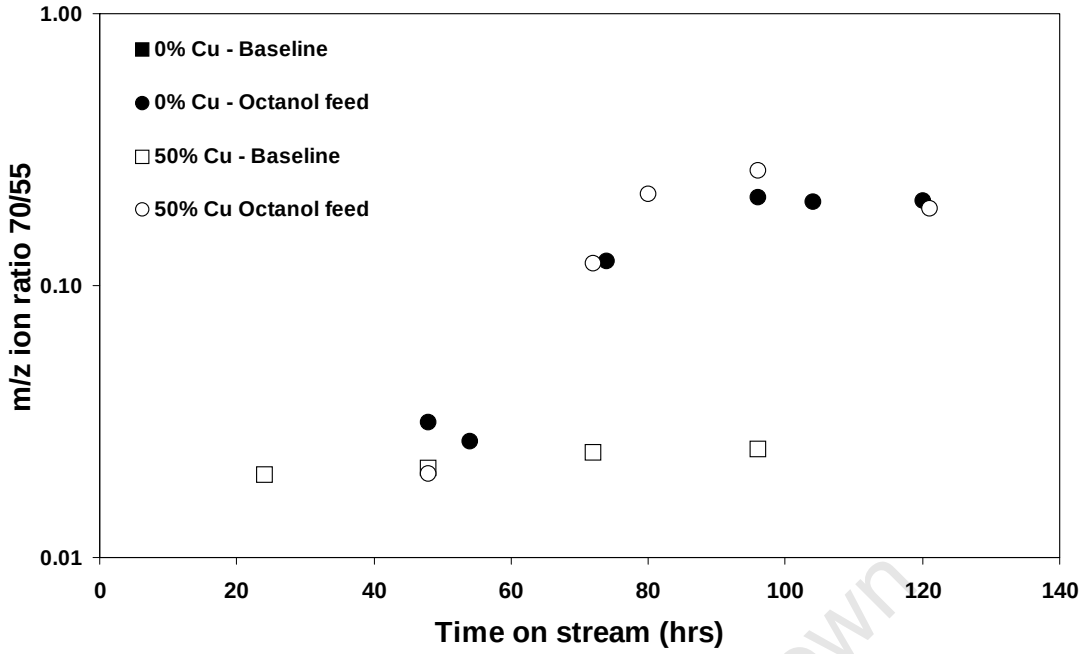

Figure K.15 Ion m/z for octylacetate (70/55) in product oil for 0 and 50 wt% Cu catalysts for both baseline and 1-octanol co-feeding experiments

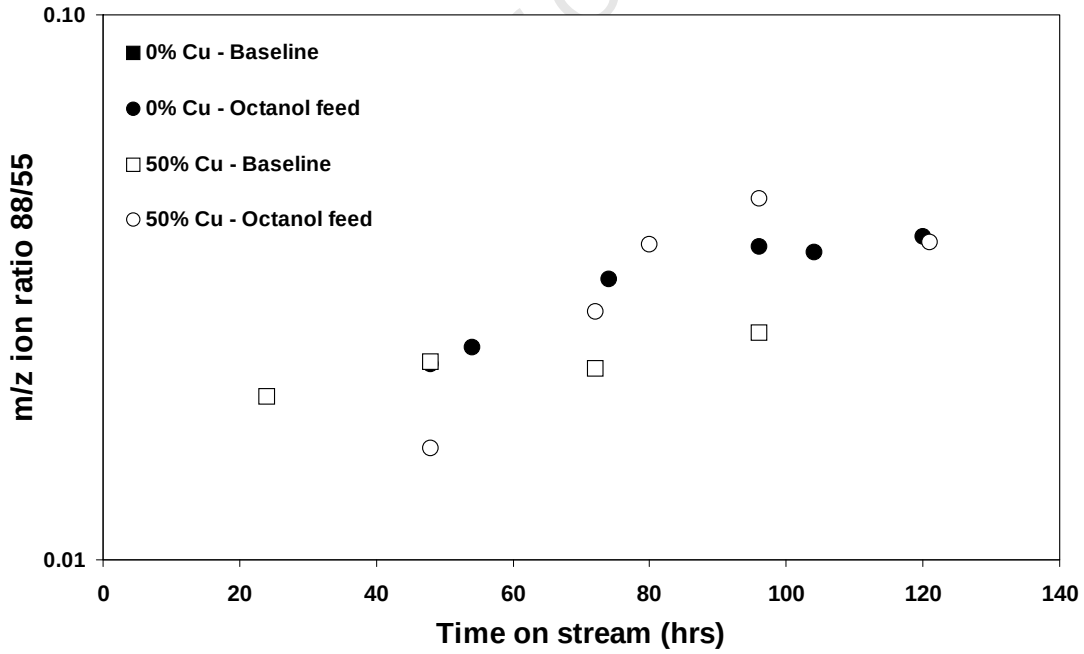

Figure K.16 Ion m/z for ethyl caprylate (88/55) in product oil for 0 and 50 wt% Cu catalysts for both baseline and 1-octanol co-feeding experiments

K.4 Thermodynamics

Table K.4 Equilibrium ratios of C_8 oxygenates in product oil with 1-octanol co-feeding during Fischer-Tropsch synthesis in a Berty reactor for the 0 wt% Cu catalyst using the TIC m/z ion specific areas

Reaction and ratio		**Product ratios**			
		48h	72h	96h	120h
Octanoic acid + H_2 ⇔ Octan-2-one + H_2O	Eq[a]	762	786	836	792
Octan-2-one/ Octanoic acid	Obs[b]	0.46	0.46	0.45	0.66
1-Octanol ⇔ Octan-2-one + H_2	Eq	42.4	41.7	41.3	42.1
Octan-2-one/1-Octanol	Obs	0.152	0.004	0.002	0.004
Octanal ⇔ Octan-2-one	Eq	415	415	415	415
Octan-2-one/ Octanal	Obs	0.29	0.08	0.04	0.12
1-Octanol + H_2O ⇔ Octanoic acid +2H_2	Eq	0.056	0.053	0.049	0.053
Octanoic acid/1-Octanol	Obs	0.33	0.01	0.00	0.01
Octanal + H_2O ⇔ Octanoic acid + H_2	Eq	0.54	0.53	0.50	0.52
Octanoic acid/ Octanal	Obs	0.63	0.17	0.09	0.17
Octanal + H_2 ⇔ 1-Octanol	Eq	9.8	10.0	10.0	9.9
1-Octanol /Octanal	Obs	1.89	18.45	22.02	27.28
Octanoic acid + CO + 2H_2 ⇔ Nonan-2-one + 2H_2O	Eq	88217	70852	85591	75349
Nonan-2-one / Octanoic acid	Obs	0.38	0.44	0.50	0.68
1-Octanol + CO + H_2 ⇔ Nonan-2-one + H_2O	Eq	30959	24114	27387	25442
Nonan-2-one /1-Octanol	Obs	0.13	0.004	0.002	0.004
Octanal + CO + 2H_2 ⇔ Nonan-2-one + H_2O	Eq	302587	240110	275219	250770
Nonan-2-one / Octanal	Obs	0.24	0.07	0.05	0.12

[a] Eq: Expected ratio at equilibrium

[b] Obs: Observed product ratios

Table K.5 Equilibrium ratios of C_8 oxygenates in product oil with 1-octanol co-feeding during Fischer-Tropsch synthesis in a Berty reactor for the 50 wt% Cu catalyst using the TIC m/z ion specific areas

Reaction and ratio		**Product ratios**				
		48h	72h	80h	96h	120h
Octanoic acid + H_2 ⇔ Octan-2-one + H_2O	Eq[a]	968	1313	1823	1077	866
Octan-2-one/ Octanoic acid	Obs[b]	1.15	27.20	15.47	8.49	4.71
1-Octanol ⇔ Octan-2-one + H_2	Eq	39.4	37.8	37.0	38.8	39.9
Octan-2-one/1-Octanol	Obs	0.14	0.16	0.07	0.03	0.02
Octanal ⇔ Octan-2-one	Eq	415	415	415	415	415
Octan-2-one/ Octanal	Obs	1.43	1.17	0.53	0.29	0.39
1-Octanol + H_2O ⇔ Octanoic acid +2H_2	Eq	0.041	0.029	0.020	0.036	0.046
Octanoic acid/1-Octanol	Obs	0.119	0.006	0.004	0.004	0.005
Octanal + H_2O ⇔ Octanoic acid + H_2	Eq	0.43	0.32	0.23	0.39	0.48
Octanoic acid/ Octanal	Obs	1.24	0.04	0.03	0.03	0.08
Octanal + H_2 ⇔ 1-Octanol	Eq	10.5	11.0	11.2	10.7	10.40
1-Octanol /Octanal	Obs	10.44	7.56	7.88	9.23	18.07
Octanoic acid + CO + 2H_2 ⇔ Nonan-2-one + 2H_2O	Eq	143630	255904	500367	166631	105168
Nonan-2-one / Octanoic acid	Obs	0.55	0.58	0.50	0.59	0.86
1-Octanol + CO + H_2 ⇔ Nonan-2-one + H_2O	Eq	39723	52136	73459	41413	32501
Nonan-2-one /1-Octanol	Obs	0.07	0.003	0.002	0.002	0.004
Octanal + CO + 2H_2 ⇔ Nonan-2-one + H_2O	Eq	418661	571541	822631	442654	337870
Nonan-2-one / Octanal	Obs	0.68	0.03	0.02	0.02	0.07

[a] Eq: Expected ratio at equilibrium

[b] Obs: Observed product ratios

Appendix L

Co-feeding: Octanal

L.1 Run details

Table L.1 Catalyst loadings and time on-stream conversions for octanal co-feeding

	0% Cu	50% Cu
Mass catalyst loaded (g)	2.4002	4.7998
Time on line (hours)	26.5	24
CO conversion (TCD)	86.4	79.2
Carbon conversion (TCD)	36.6	31.9
Time on line (hours)	48	48
CO conversion (TCD)	87.2	83.0
Carbon conversion (TCD)	38.0	36.0
Time on line (hours)	68	65
CO conversion (TCD)	88.3	80.8
Carbon conversion (TCD)	39.5	29.2
Time on line (hours)	73	73
CO conversion (TCD)	88.6	83.6
Carbon conversion (TCD)	40.7	32.5
Time on line (hours)	88	88
CO conversion (TCD)	88.5	91.1
Carbon conversion (TCD)	39.0	44.0
Time on line (hours)	96	96
CO conversion (TCD)	88.1	88.0
Carbon conversion (TCD)	36.1	40.3
Time on line (hours)	120	120
CO conversion (TCD)	88.3	85.8
Carbon conversion (TCD)	34.8	37.1

L.2 GC-FID results

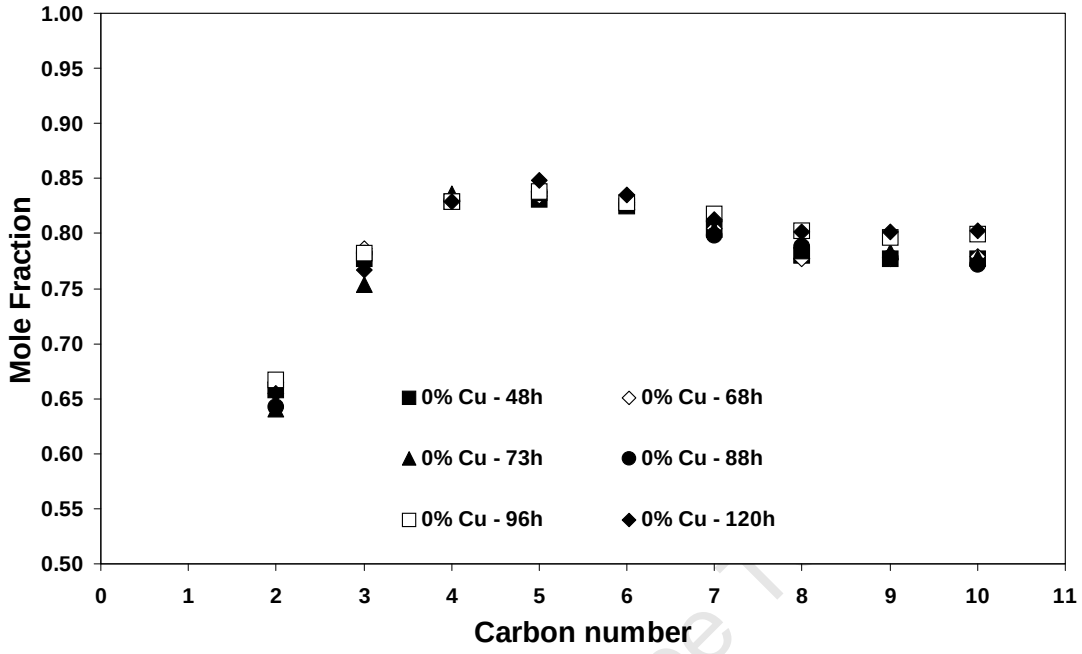

Figure L.1 Mole fraction of linear olefins in linear hydrocarbon product on the 0 wt% Cu catalyst for octanal co-feeding

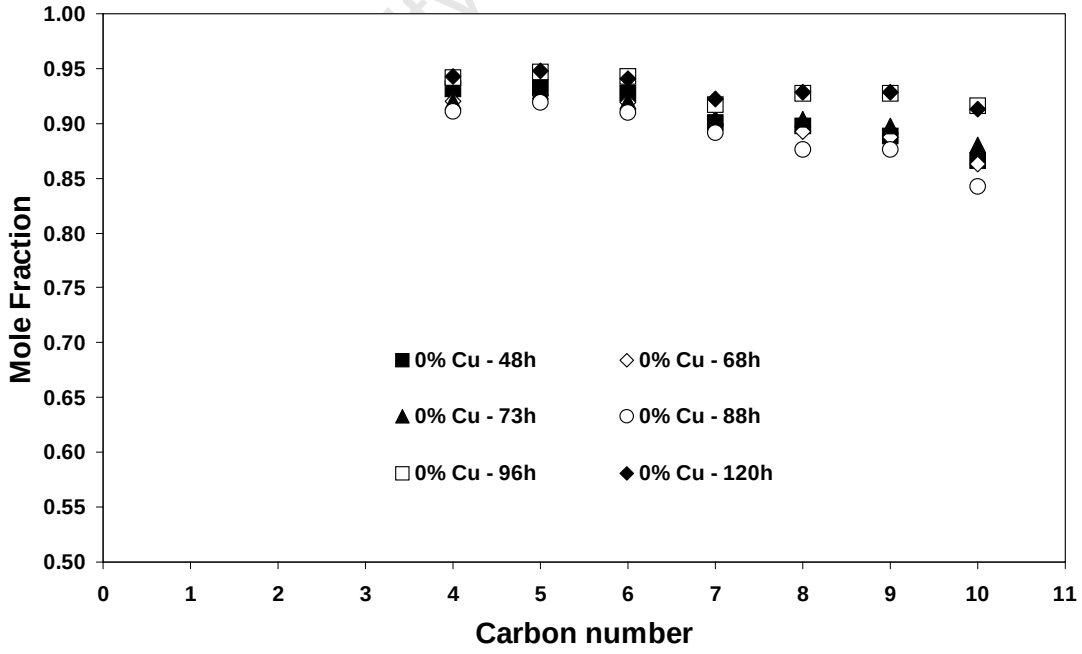

Figure L.2 Mole fraction of α−olefins in linear olefins on the 0 wt% Cu catalyst for octanal co-feeding

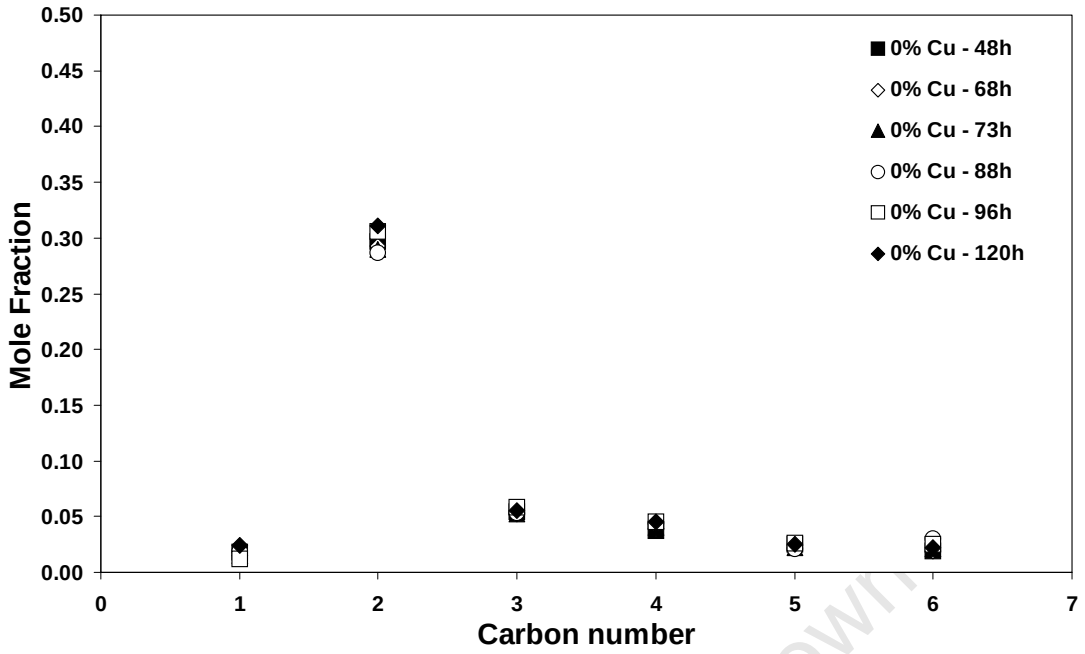

Figure L.3 Mole fraction of alcohols in linear product (excluding aldehydes and ketones) on the 0 wt% Cu catalyst for octanal co-feeding

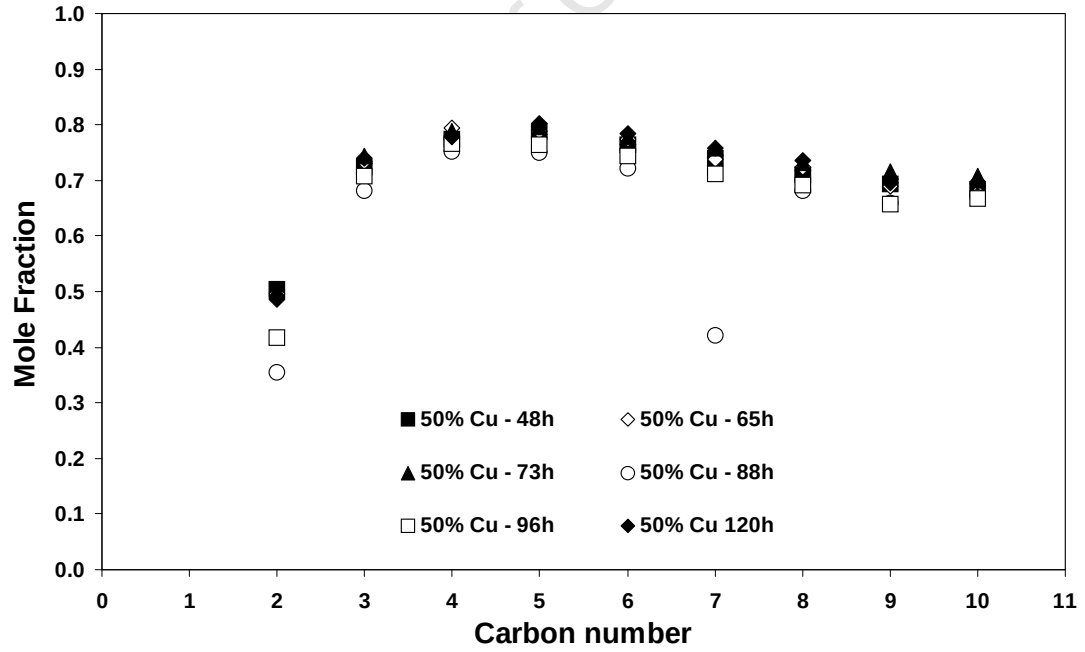

Figure L.4 Mole fraction of linear olefins in linear hydrocarbon product on the 50 wt% Cu catalyst for octanal co-feeding

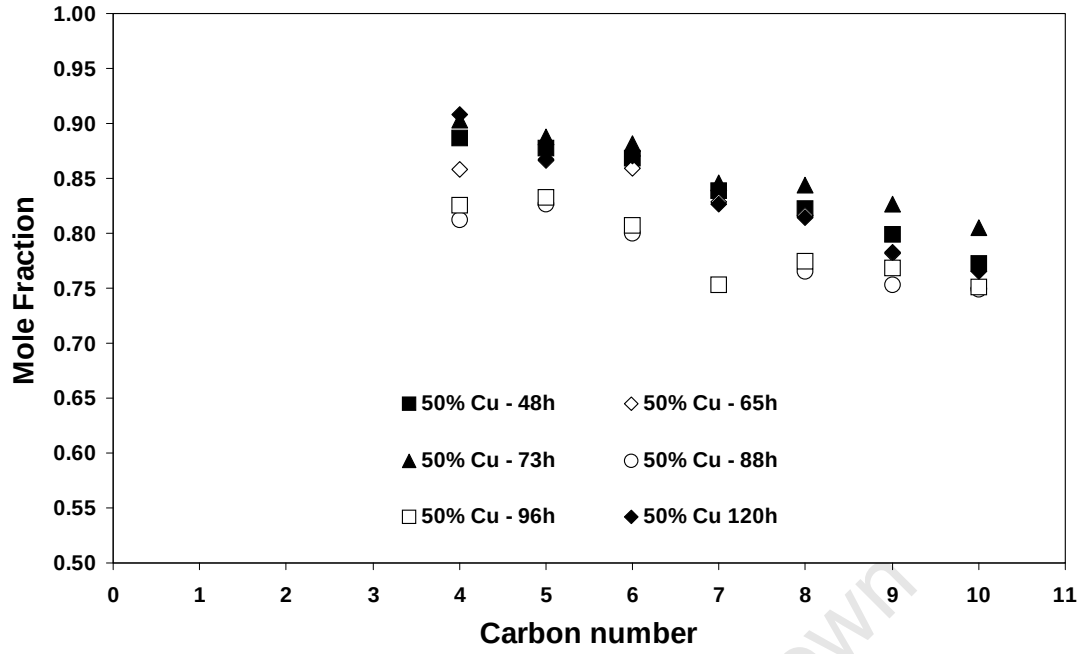

Figure L.5 Mole fraction of α–olefins in linear olefins on the 50 wt% Cu catalyst for octanal co-feeding

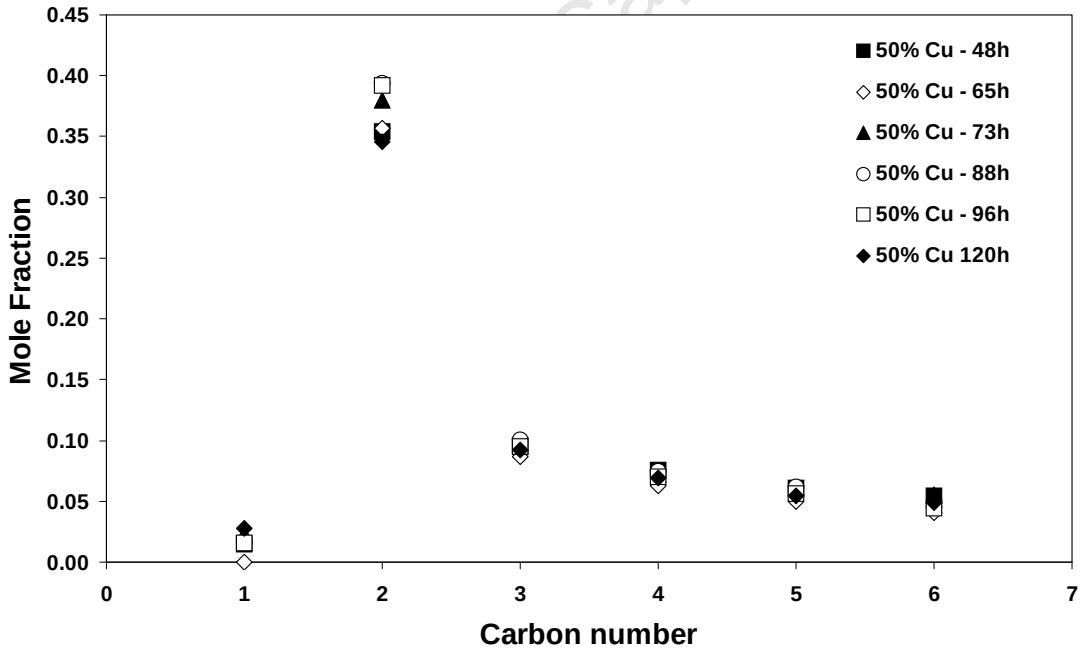

Figure L.6 Mole fraction of alcohols in linear product (excluding aldehydes and ketones) on the 50 wt% Cu catalyst for octanal co-feeding

L.3 GC-MS results

Table L.2 Molar balance of octanal fed to C_8 oxygenate products for both 0 and 50 wt% Cu catalysts.

0 wt% Cu catalyst				
Octanal co-feeding				
Time on-stream of analysis (hrs)	68	73	88	96
Feed rate (µmoles/min)	0.577	0.228	0.142	0.078
Average feed rate (µmoles/min)		0.402	0.185	0.110
Exit 1-Octanol (µmoles/min)		1.338	0.944	0.781
Exit Octanal (µmoles/min)		1.031	0.575	0.407
Exit Nonan-2-one (µmoles/min)		0.031	0.027	0.029
Exit Octanoic acid (µmoles/min)		0.173	0.092	0.106
C_8 Balance closure (less baseline flows)		411.4%	631.0%	788.8%
50 wt% Cu catalyst				
Octanal co-feeding				
Time on-stream of analysis (hrs)	65	73	88	96
Feed rate (µmoles/min)	0.105	0.344	0.317	0.339
Average feed rate (µmoles/min)		1.524	0.330	0.328
Exit 1-Octanol (µmoles/min)		3.697	2.420	2.772
Exit Octanal (µmoles/min)		0.572	0.280	0.298
Exit Nonan-2-one (µmoles/min)		0.021	0.014	0.017
Exit Octanoic acid (µmoles/min)		0.126	0.066	0.078
C8 Balance closure (less baseline flows)		135.7%	592.0%	713.6%

Table L.3 Molar flow rates (in µmol/min) of octanol, octanal, octan-2-one, octanoic acid, nonan-2-one, heptane + heptane, octane + octene, and nonane + nonene for octanal co-feeding

				0 wt% Cu Octanal feeding			
TOL	48	68	73	88	96	113	120
Feeding	no		Octanal			no	no
1-Octanol	0.105	1.124	1.338	0.944	0.781	0.448	0.383
Octanal	0.053	0.940	1.031	0.575	0.407	0.185	0.129
Octan-2-one	0.014	0.015	0.017	0.015	0.019	0.020	0.024
Octanoic acid	0.027	0.034	0.173	0.092	0.106	0.077	0.082
Nonan-2-one	0.014	0.024	0.031	0.027	0.029	0.025	0.027
Heptane + Heptene	4.60	4.72	4.71	4.70	4.95	-	4.82
Octane + Octene	2.91	3.04	2.98	3.01	2.99	-	2.93
Nonane + Nonene	1.71	1.78	1.79	1.76	1.83	-	1.78
				50 wt% Cu Octanal feeding			
TOL	48	65	73	88	96	113	120
Feeding	no		Octanal			no	no
1-Octanol	0.651	1.427	3.697	2.420	2.772	1.844	1.408
Octanal	0.067	0.187	0.572	0.280	0.298	0.160	0.104
Octan-2-one	0.005	0.007	0.010	0.006	0.007	0.009	0.009
Octanoic acid	0.015	0.069	0.126	0.066	0.078	0.059	0.066
Nonan-2-one	0.013	0.009	0.021	0.014	0.017	0.016	0.015
Heptane + Heptene	3.93	3.98	4.05	2.12	4.08	-	3.98
Octane + Octene	2.51	2.57	2.51	2.33	2.39	-	2.45
Nonane + Nonene	1.57	1.56	1.55	1.36	1.39	-	1.46

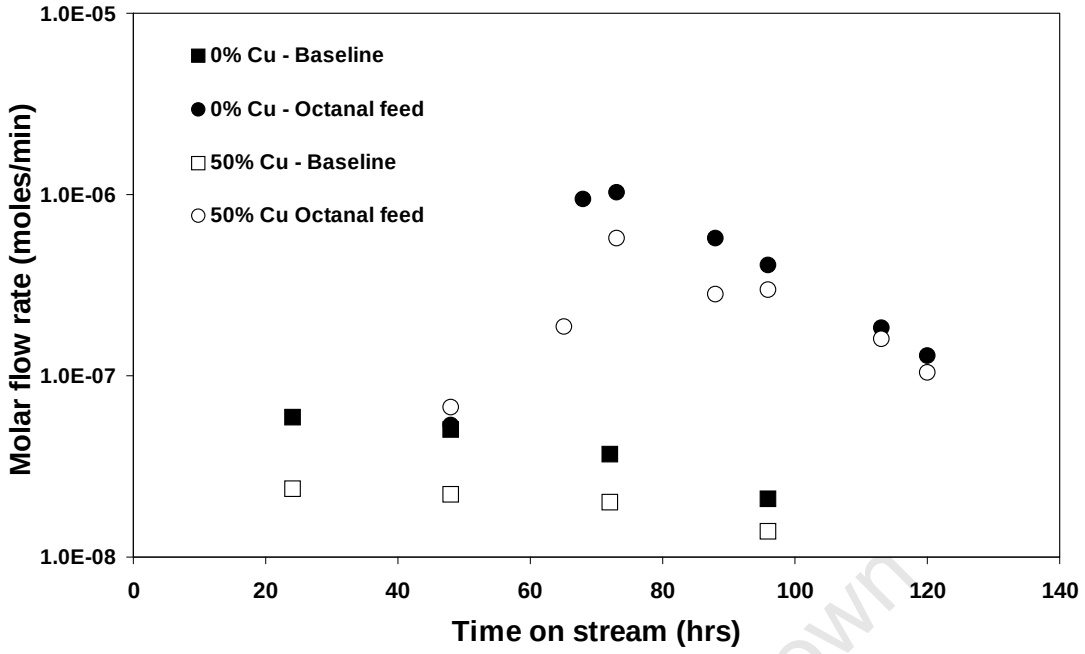

Figure L.7 Octanal flow rate in product oil for 0 and 50 wt% Cu catalysts for both no feeding and octanal co-feeding experiments

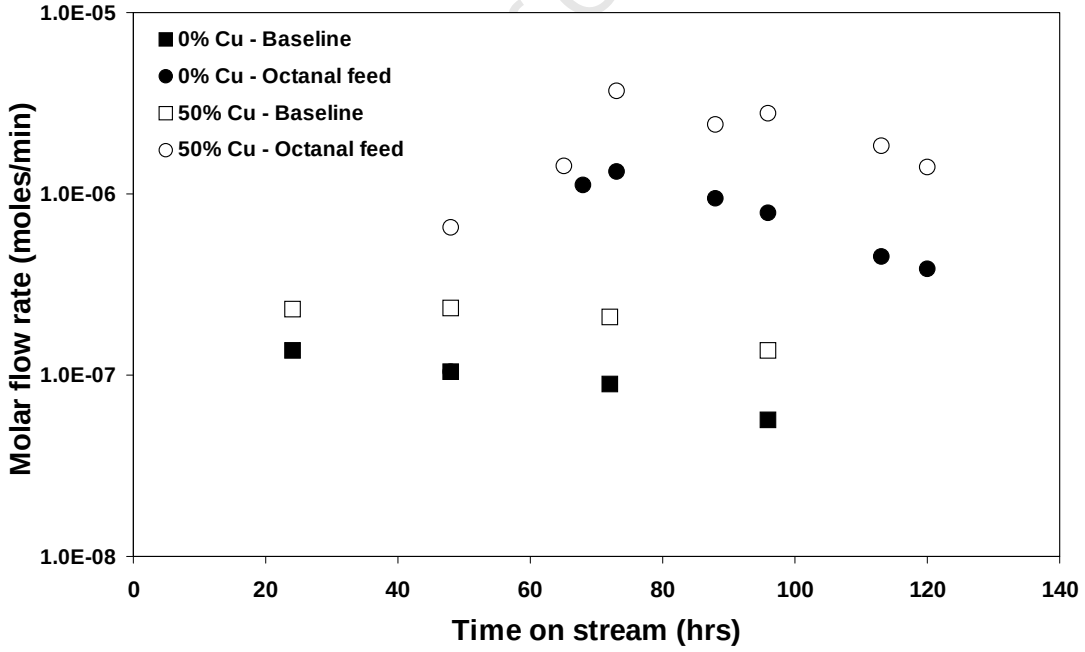

Figure L.8 1-Octanol flow rate in product oil for 0 and 50 wt% Cu catalysts for both baseline and octanal co-feeding experiments

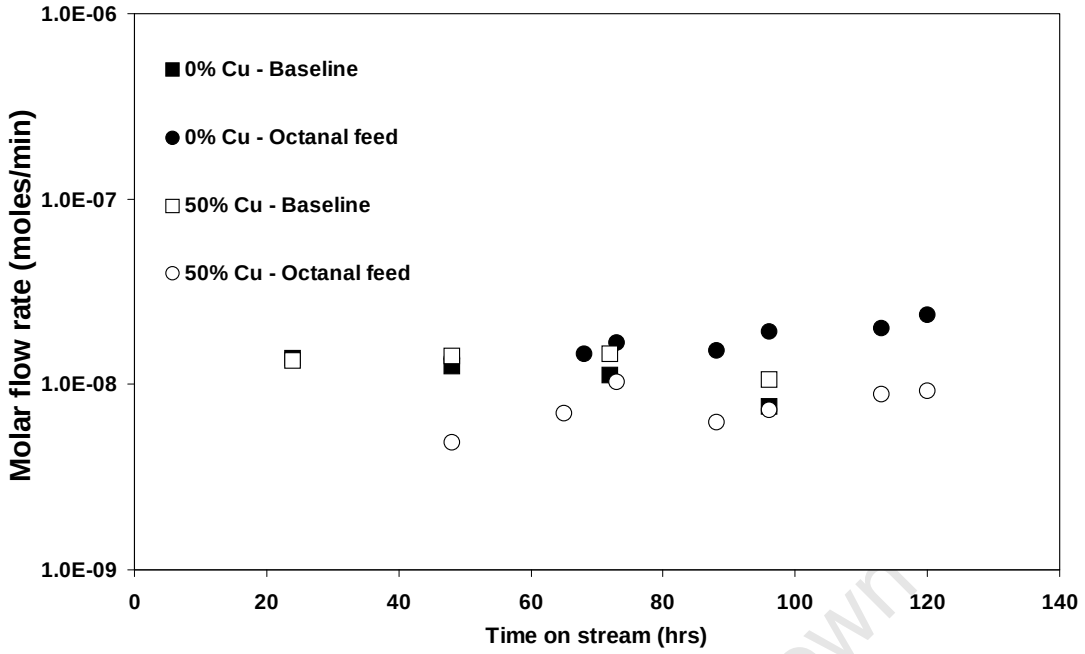

Figure L.9 Octan-2-one flow rate in product oil for 0 and 50 wt% Cu catalysts for both baseline and octanal co-feeding experiments

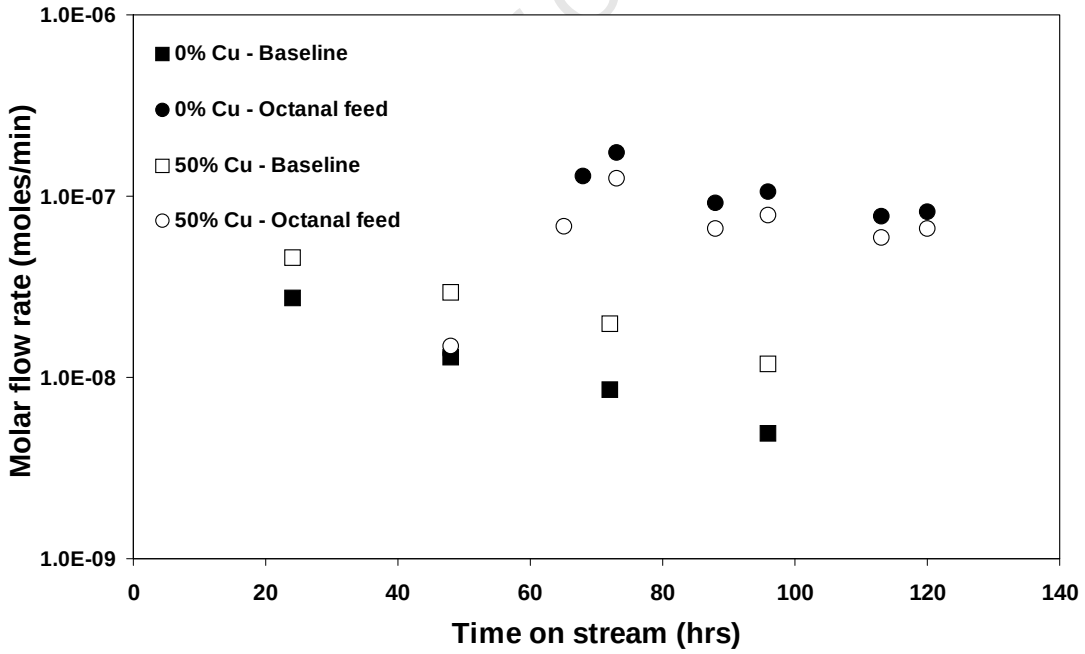

Figure L.10 Octanoic acid flow rate in product oil for 0 and 50 wt% Cu catalysts for both baseline and octanal co-feeding experiments

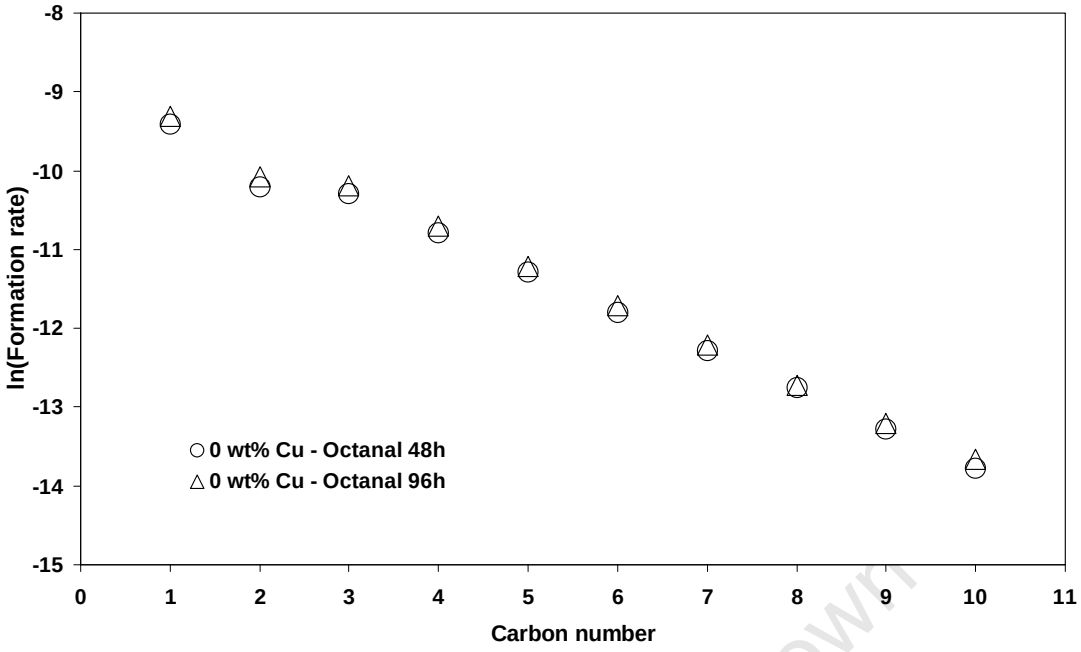

Figure L.11 ASF plot of natural log of formation rates of linear hydrocarbons verse carbon number for 48 and 96 hours with the 0 wt% Cu catalyst during 1-octanal co-feeding

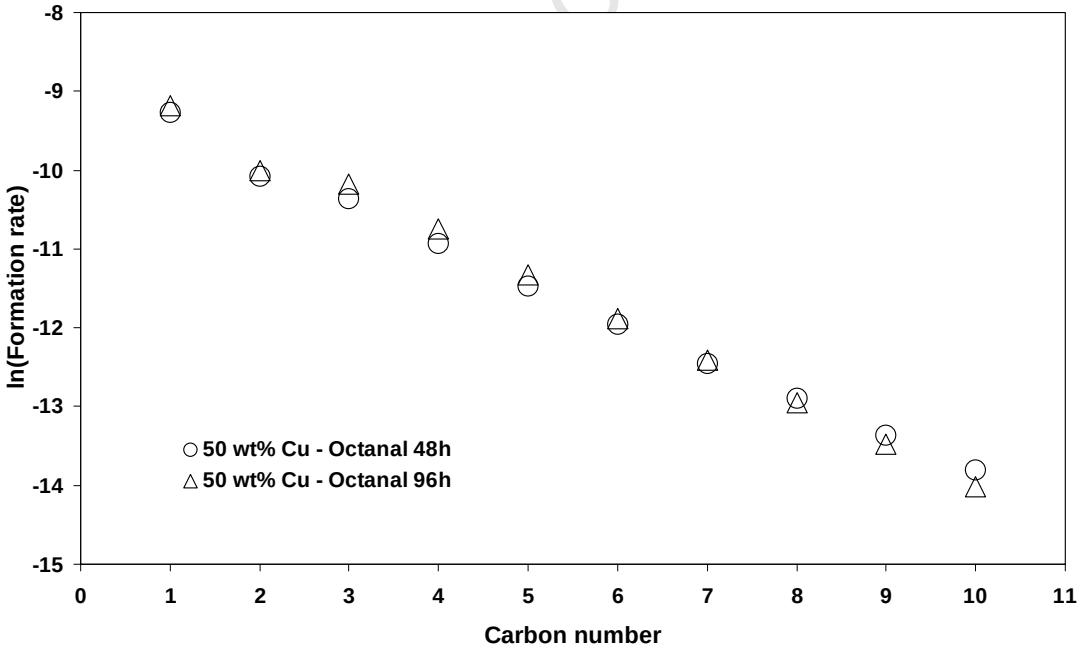

Figure L.12 ASF plot of natural log of formation rates of linear hydrocarbons verse carbon number for 48 and 96 hours with the 50 wt% Cu catalyst during 1-octanal co-feeding

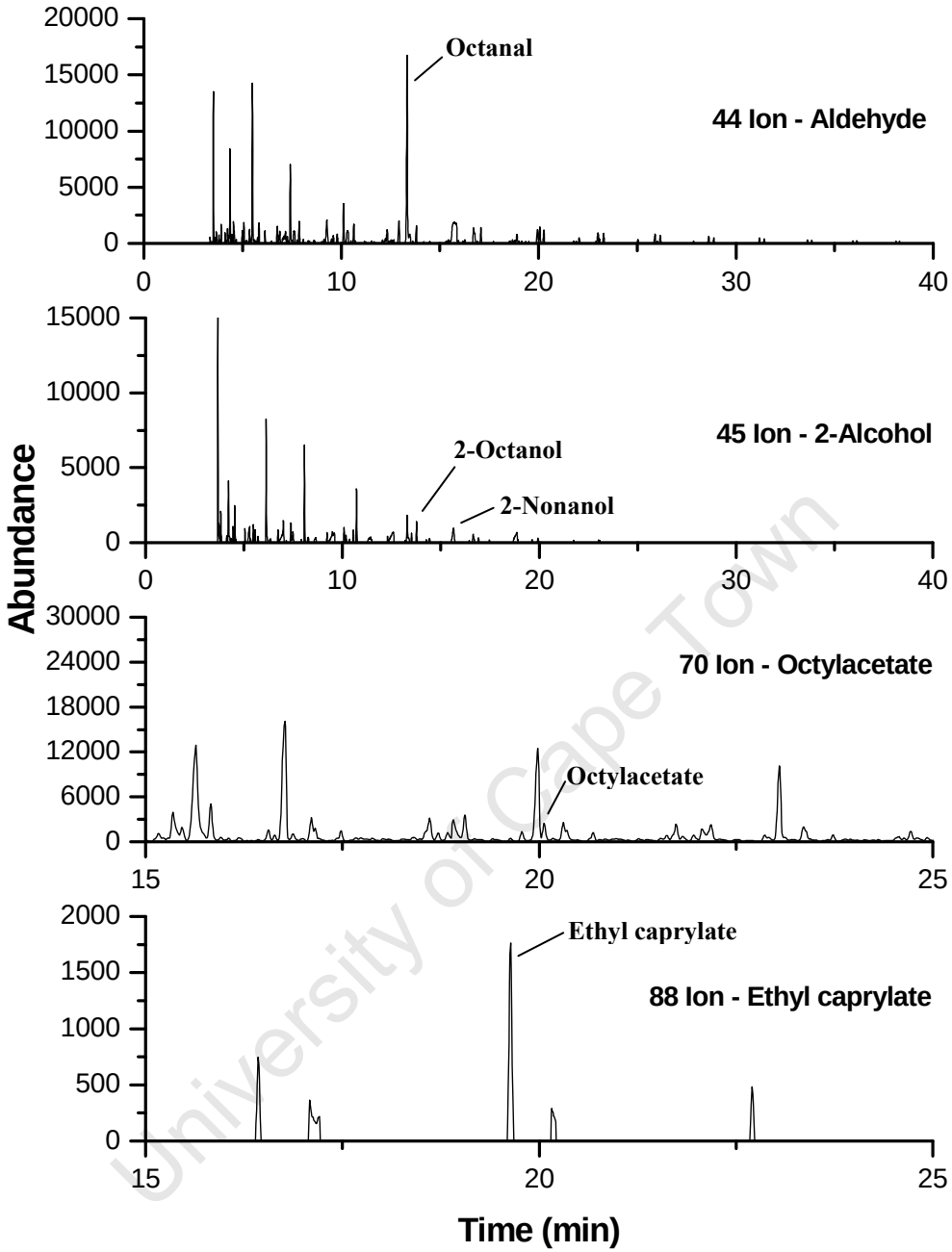

Figure L.13 The corresponding extracted ion chromatograms including that of the aldehydes of 0 wt% Cu catalyst with octanal co-feeding after 96 hours TOL during Fischer-Tropsch synthesis in a Berty reactor for ions m/z=31 (1-alcohols), m/z=45 (2-alcohols), m/z=70 (octylacetate) and m/z=88 (ethyl caprylate)

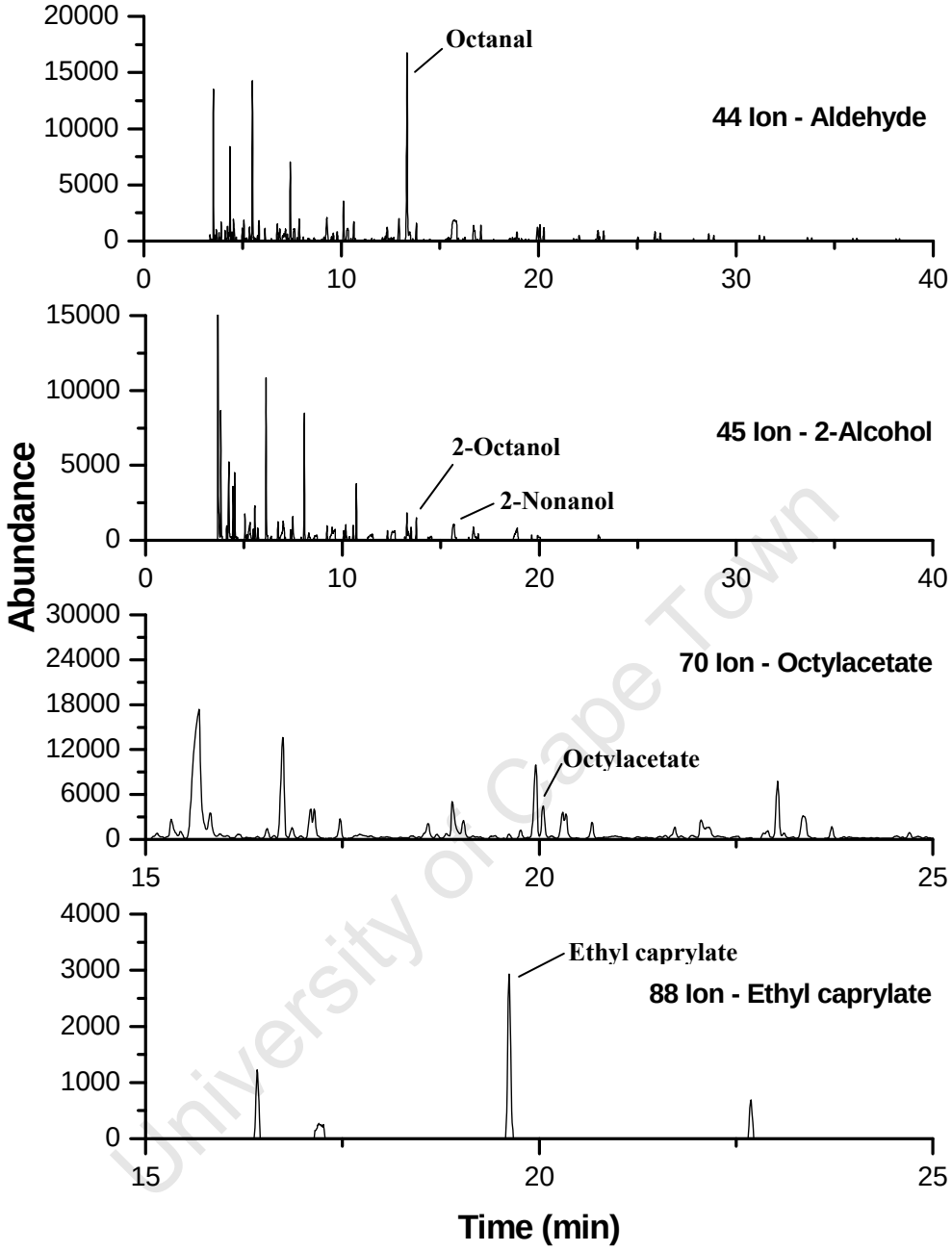

Figure L.14 The corresponding extracted ion chromatograms including that of the aldehydes of 50 wt% Cu catalyst with octanal co-feeding after 96 hours TOL during Fischer-Tropsch synthesis in a Berty reactor for ions m/z=31 (1-alcohols), m/z=45 (2-alcohols), m/z=70 (octylacetate) and m/z=88 (ethyl caprylate)

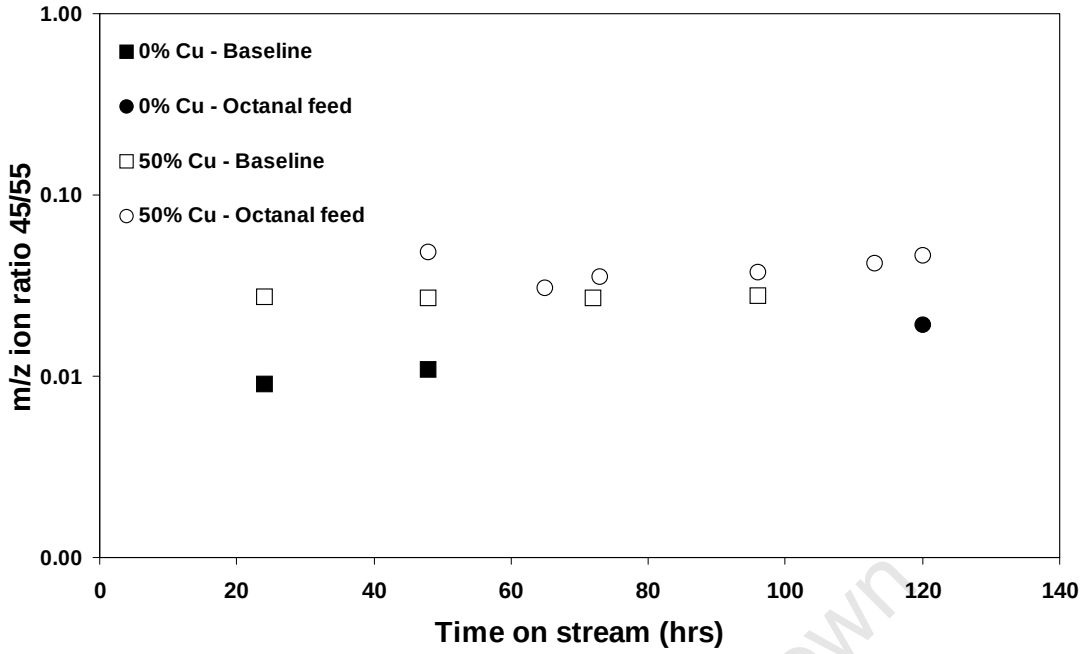

Figure L.15 Ion m/z for 2-octanol (45/55) in product oil for 0 and 50 wt% Cu catalysts for both baseline and octanal co-feeding experiments

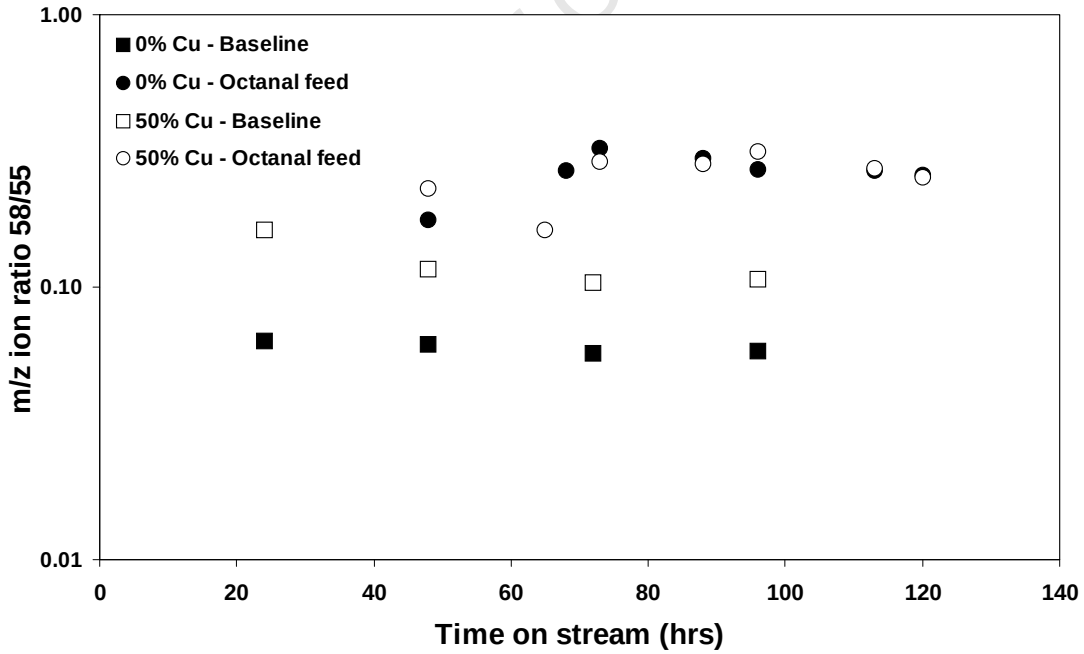

Figure L.16 Ion m/z for nonan-2-one (58/55) in product oil for 0 and 50 wt% Cu catalysts for both baseline and octanal co-feeding experiments

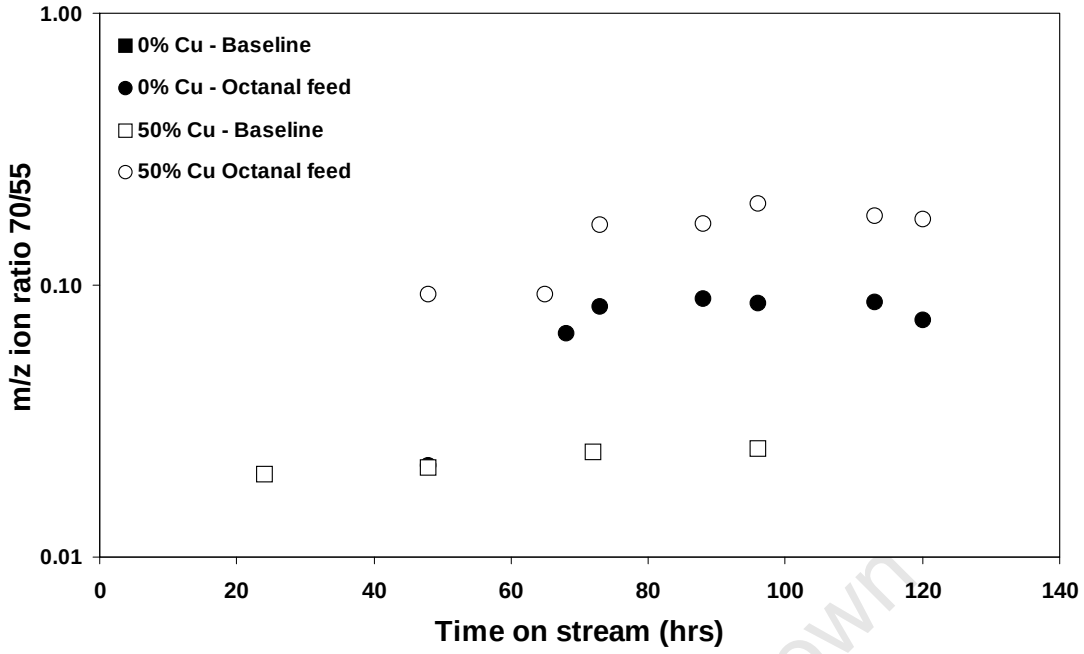

Figure L.17 Ion m/z for octylacetate (70/55) in product oil for 0 and 50 wt% Cu catalysts for both baseline and octanal co-feeding experiments

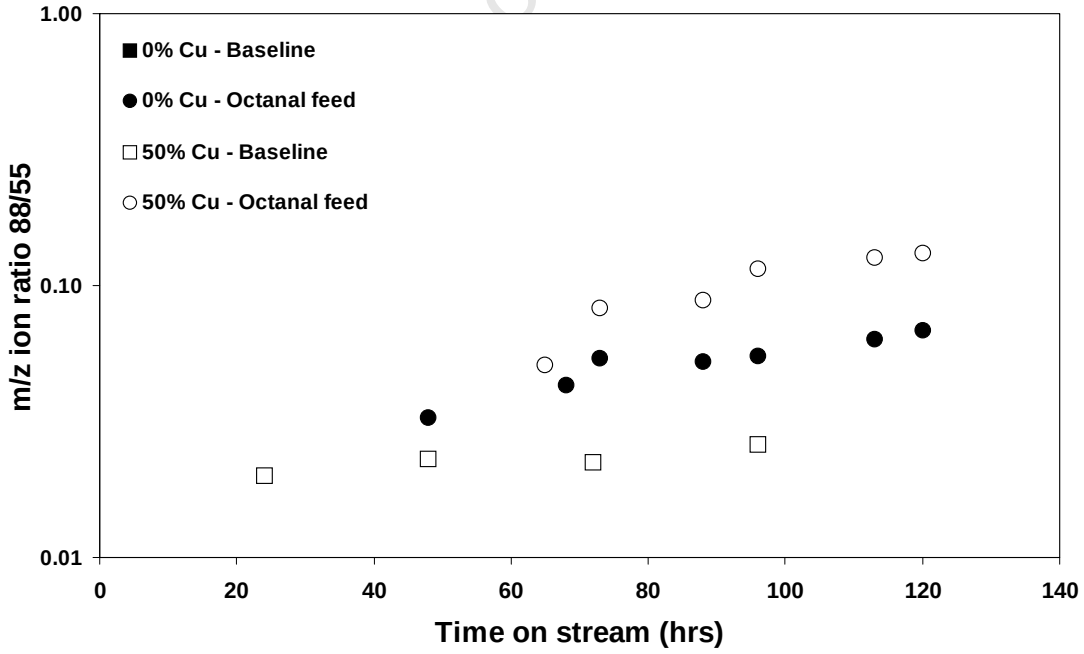

Figure L.18 Ion m/z for ethyl caprylate (88/55) in product oil for 0 and 50 wt% Cu catalysts for both baseline and octanal co-feeding experiments

L.4 Thermodynamics

Table L.4 Equilibrium ratios of C_8 oxygenates in product oil with octanal co-feeding during Fischer-Tropsch synthesis in a Berty reactor for the 0 wt% Cu catalyst using the TIC m/z ion specific areas

Reaction and ratio		**Product ratios**					
		48h	68h	73h	88h	96h	120h
Octanoic acid + H_2 ⇔ Octan-2-one + H_2O	Eq[a]	1199	1055	967	1163	1656	2116
Octan-2-one/ Octanoic acid	Obs[b]	-	-	0.10	0.16	0.18	0.29
1-Octanol ⇔ Octan-2-one + H_2	Eq	38.2	39.0	39.3	38.4	37.0	36.2
Octan-2-one/1-Octanol	Obs	0.13	0.01	0.01	0.02	0.02	0.06
Octanal ⇔ Octan-2-one	Eq	415	415	415	415	415	415
Octan-2-one/ Octanal	Obs	0.26	0.02	0.02	0.03	0.05	0.18
1-Octanol + H_2O ⇔ Octanoic acid +2H_2	Eq	0.032	0.037	0.041	0.033	0.022	0.017
Octanoic acid/1-Octanol	Obs	-	-	0.13	0.10	0.14	0.21
Octanal + H_2O ⇔ Octanoic acid + H_2	Eq	0.35	0.39	0.43	0.36	0.25	0.20
Octanoic acid/ Octanal	Obs	-	-	0.17	0.16	0.26	0.64
Octanal + H_2 ⇔ 1-Octanol	Eq	10.9	10.6	10.6	10.8	11.20	11.4
1-Octanol /Octanal	Obs	1.96	1.20	1.30	1.64	1.92	2.97
Octanoic acid + CO + 2H_2 ⇔ Nonan-2-one + 2H_2O	Eq	205213	147834	120444	177607	370585	603625
Nonan-2-one / Octanoic acid	Obs	-	-	0.18	0.29	0.27	0.33
1-Octanol + CO + H_2 ⇔ Nonan-2-one + H_2O	Eq	45812	37492	33327	40876	59875	76337
Nonan-2-one /1-Octanol	Obs	0.14	0.02	0.02	0.03	0.04	0.07
Octanal + CO + 2H_2 ⇔ Nonan-2-one + H_2O	Eq	497255	398861	351716	441875	670669	873821
Nonan-2-one / Octanal	Obs	0.27	0.03	0.03	0.05	0.07	0.21

[a] Eq: Expected ratio at equilibrium

[b] Obs: Observed product ratios

Table L.5 Equilibrium ratios of C_8 oxygenates in product oil with octanal co-feeding during Fischer-Tropsch synthesis in a Berty reactor for the 50 wt% Cu catalyst using the TIC m/z ion specific areas

Reaction and ratio		**Product ratios**					
		48h	65h	73h	88h	96h	120h
Octanoic acid + H_2 ⇔ Octan-2-one + H_2O	Eq[a]	1156	2176	1627	694	798	1038
Octan-2-one/ Octanoic acid	Obs[b]	0.33	0.10	0.08	0.09	0.09	0.14
1-Octanol ⇔ Octan-2-one + H_2	Eq	39.3	39.3	38.5	43.8	43.4	41.0
Octan-2-one/1-Octanol	Obs	0.007	0.005	0.003	0.003	0.003	0.007
Octanal ⇔ Octan-2-one	Eq	415	415	415	415	415	415
Octan-2-one/ Octanal	Obs	0.07	0.04	0.02	0.02	0.02	0.09
1-Octanol + H_2O ⇔ Octanoic acid +2H_2	Eq	0.034	0.018	0.024	0.063	0.054	0.040
Octanoic acid/1-Octanol	Obs	0.02	0.05	0.03	0.03	0.03	0.05
Octanal + H_2O ⇔ Octanoic acid + H_2	Eq	0.36	0.19	0.25	0.60	0.52	0.40
Octanoic acid/ Octanal	Obs	0.22	0.37	0.22	0.24	0.26	0.63
Octanal + H_2 ⇔ 1-Octanol	Eq	10.6	10.6	10.8	9.48	9.56	10.1
1-Octanol /Octanal	Obs	9.69	7.63	6.46	8.63	9.30	13.48
Octanoic acid + CO + 2H_2 ⇔ Nonan-2-one + 2H_2O	Eq	250533	959026	487893	49764	93318	176818
Nonan-2-one / Octanoic acid	Obs	0.87	0.13	0.16	0.21	0.21	0.22
1-Octanol + CO + H_2 ⇔ Nonan-2-one + H_2O	Eq	57971	117958	80260	19181	31285	45583
Nonan-2-one /1-Octanol	Obs	0.02	0.01	0.01	0.01	0.01	0.01
Octanal + CO + 2H_2 ⇔ Nonan-2-one + H_2O	Eq	611743	1246075	863880	181739	299051	460961
Nonan-2-one / Octanal	Obs	0.19	0.05	0.04	0.05	0.06	0.14

[a] Eq: Expected ratio at equilibrium

[b] Obs: Observed product ratios

Appendix M

Co-feeding: Octan-2-one

M.1 Run details

Table M.1 Catalyst loadings and time on-stream conversions for octan-2-one co-feeding

	0% Cu	50% Cu
Mass catalyst loaded (g)	2.3998	4.7998
Time on line (hours)	24	24
CO conversion (TCD)	85.7	80.4
Carbon conversion (TCD)	39.2	33.7
Time on line (hours)	48	48
CO conversion (TCD)	87.0	81.5
Carbon conversion (TCD)	40.7	33.6
Time on line (hours)	72	72
CO conversion (TCD)	87.7	82.0
Carbon conversion (TCD)	41.8	29.4
Time on line (hours)	77	92
CO conversion (TCD)	87.8	82.1
Carbon conversion (TCD)	41.3	32.0
Time on line (hours)	93	96
CO conversion (TCD)	88.0	83.4
Carbon conversion (TCD)	40.8	37.1
Time on line (hours)	117	
CO conversion (TCD)	88.8	
Carbon conversion (TCD)	45.3	

M.2 GC-FID results

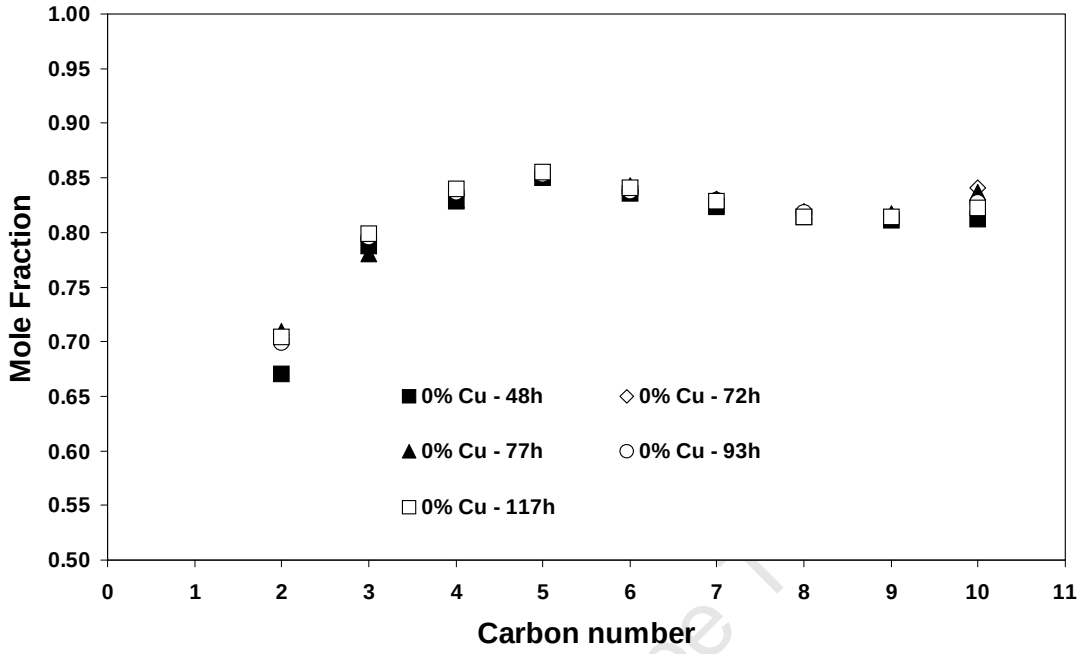

Figure M.1 Mole fraction of linear olefins in linear hydrocarbon product on the 0 wt% Cu catalyst for octan-2-one co-feeding

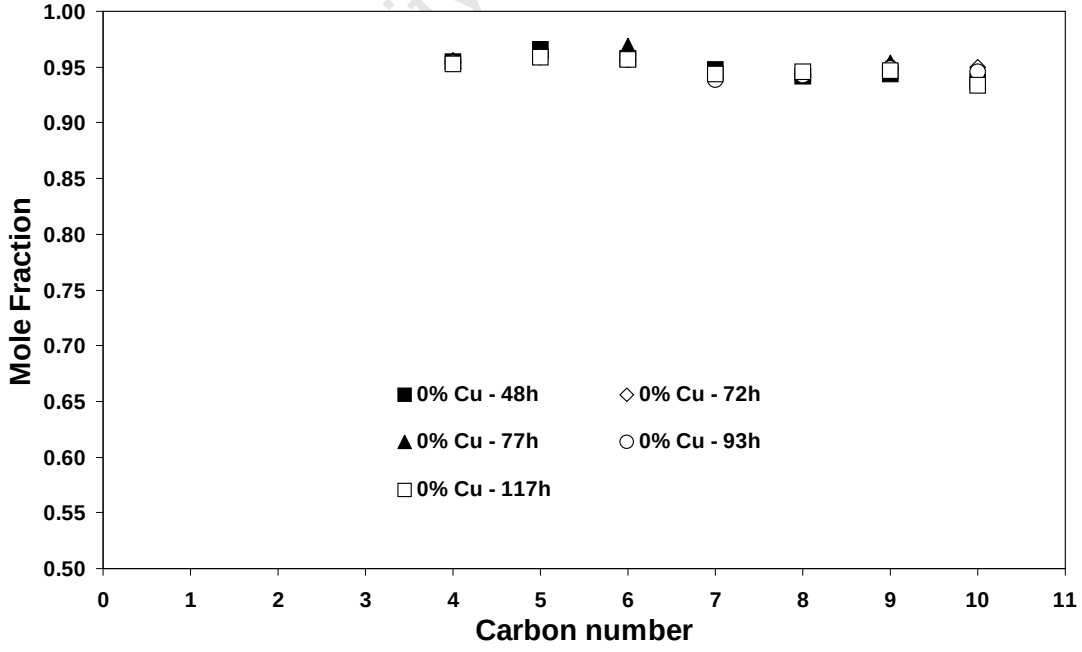

Figure M.2 Mole fraction of α–olefins in linear olefins on the 0 wt% Cu catalyst for octan-2-one co-feeding

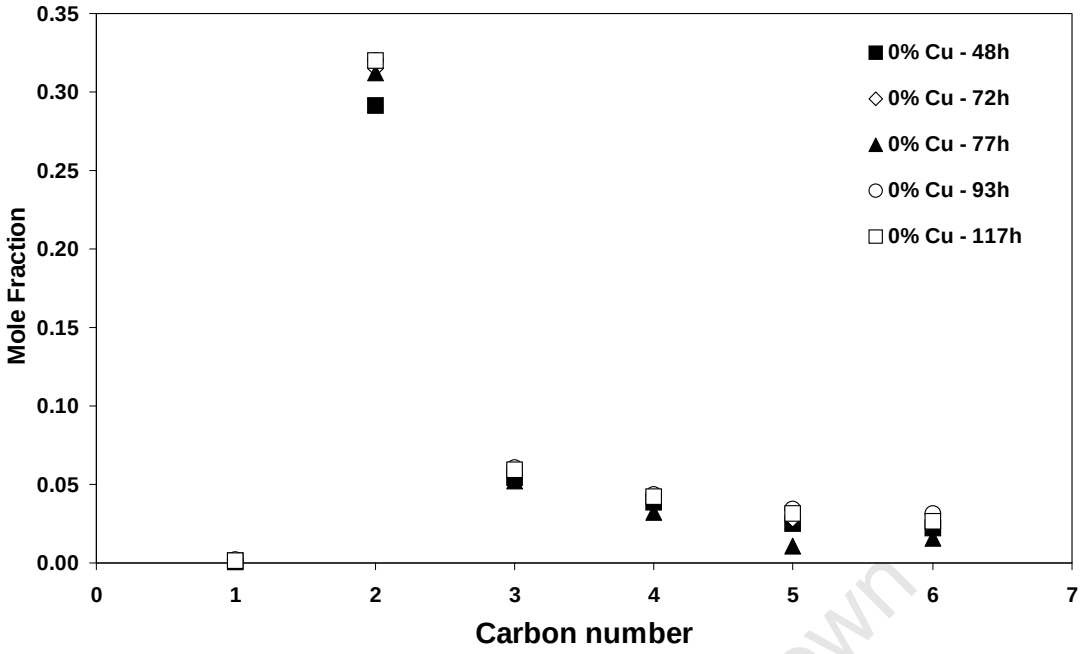

Figure M.3 Mole fraction of alcohols in linear product (excluding aldehydes and ketones) on the 0 wt% Cu catalyst for octan-2-one co-feeding

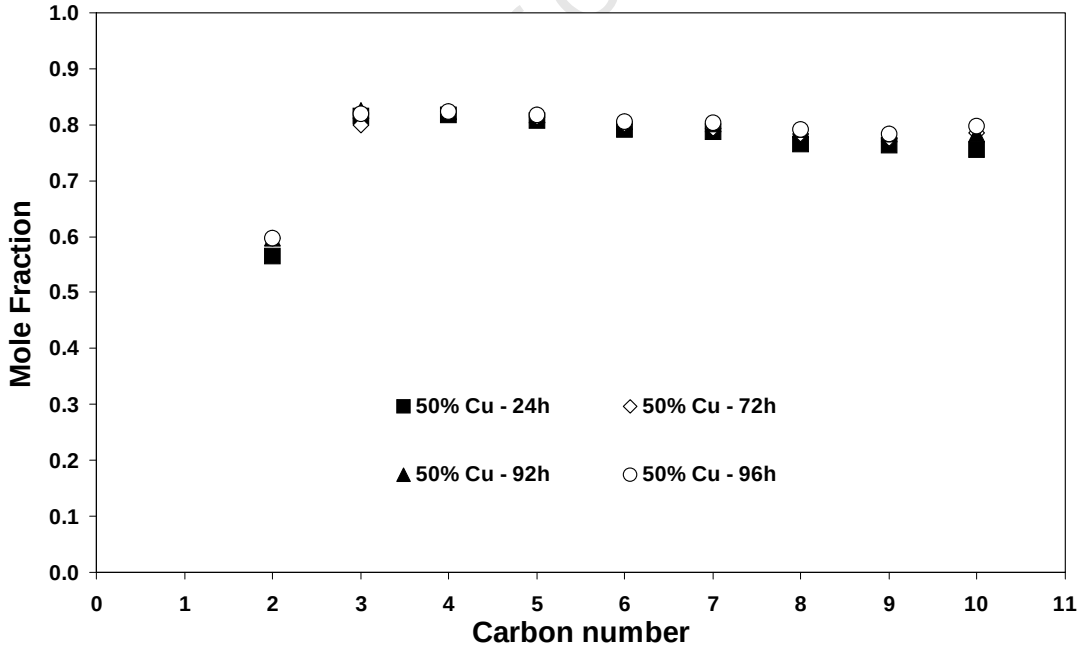

Figure M.4 Mole fraction of linear olefins in linear hydrocarbon product on the 50 wt% Cu catalyst for octan-2-one co-feeding

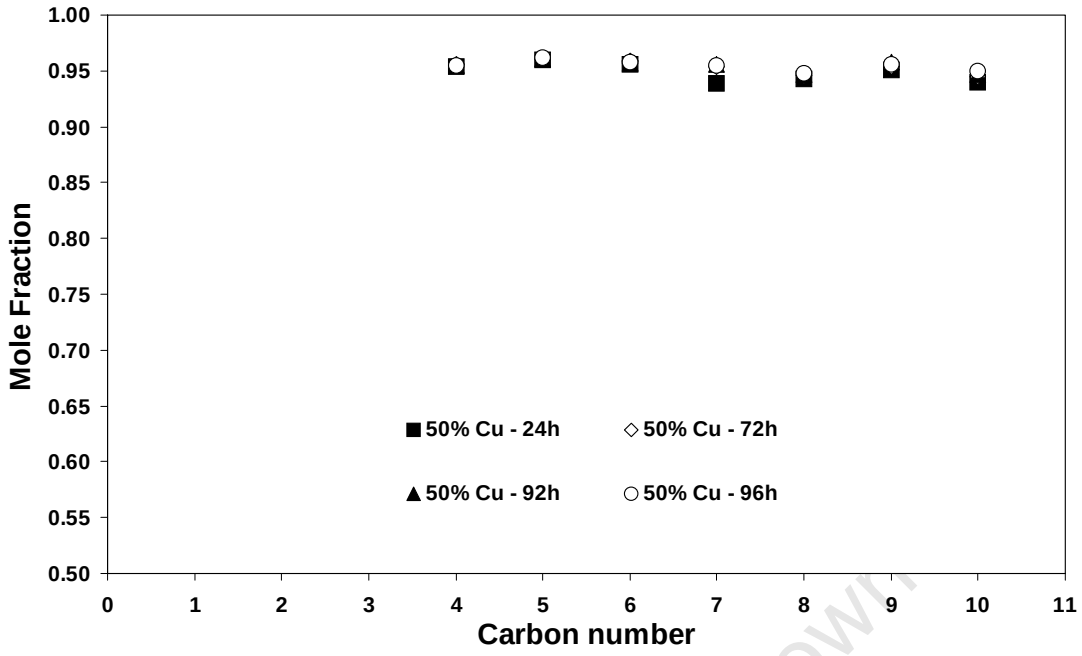

Figure M.5 Mole fraction of α−olefins in linear olefins on the 50 wt% Cu catalyst for octan-2-one co-feeding

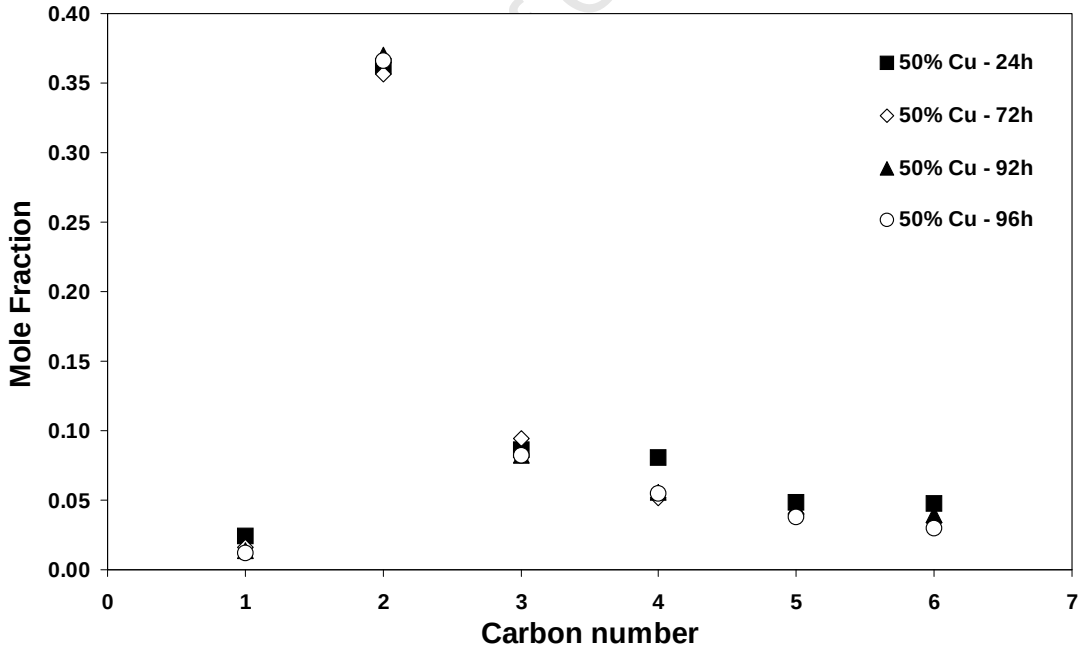

Figure M.6 Mole fraction of alcohols in linear product (excluding aldehydes and ketones) on the 50 wt% Cu catalyst for octan-2-one co-feeding

M.3 GC-MS results

As the major product of the octan-2-one co-feeding was 2-octanol and this was not quantified a feeding molar balance could not be conducted.

Table M.2 Molar flow rates (in µmol/min) of octanol, octanal, octan-2-one, octanoic acid, nonan-2-one, heptane + heptane, octane + octene, and nonane + nonene for octan-2-one co-feeding

				0 wt% Cu Octan-2-one feeding			
TOL	48	53	72	77	93	117	126
Feeding	no		Octan-2-one			no	no
Octanol	0.101	0.123	0.101	0.118	0.109	0.120	0.114
Octanal	0.038	n/a [a]	n/a [a]	n/a [a]	n/a [a]	n/a [a]	0.043
Octan-2-one	0.010	0.067	11.412	6.892	4.730	1.537	0.558
Octanoic acid	0.017	0.021	0.011	0.016	0.012	0.015	0.015
Nonan-2-one	0.008	0.009	0.009	0.010	0.009	0.012	0.012
Heptane + Heptene	4.76	-	4.93	4.81	4.82	4.84	-
Octane + Octene	3.08	-	3.15	3.06	2.98	3.02	-
Nonane + Nonene	1.99	-	1.99	1.94	1.86	1.86	-
				50 wt% Cu Octan-2-one feeding			
TOL	48	56	72	92	96		
Feeding	no		Octan-2-one				
Octanol	0.075	0.106	0.030	0.040	0.076		
Octanal	0.005	n/a [a]	n/a [a]	n/a [a]	0.003		
Octan-2-one	0.002	0.005	3.494	1.893	1.425		
Octanoic acid	0.002	0.004	n/a [b]	0.001	0.002		
Nonan-2-one	0.001	0.001	n/a [b]	n/a [b]	0.001		
Heptane + Heptene	2.68	-	2.85	2.88	2.83		
Octane + Octene	1.80	-	1.89	1.92	1.84		
Nonane + Nonene	1.20	-	1.28	1.29	1.19		

[a] Octanal peak (m/z=44) overlaps with 2-octanol (m/z=45) peak and not isolatable

[b] Peak too small to be quantified

Table M.3 Iso-n ratio of 2-Methyl branched C_9 olefins and paraffins

			0 wt% Cu Octan-2-one feeding				
TOL	48	53	72	77	93	117	126
Feeding	no		Octan-2-one			no	
Iso-n rato	0.12	-	0.16	0.17	0.12	0.14	-
			50 wt% Cu Octan-2-one feeding				
TOL	48	56	72	92	96		
Feeding	no		Octan-2-one				
Iso-n rato	0.09	-	0.11	0.10	0.11		

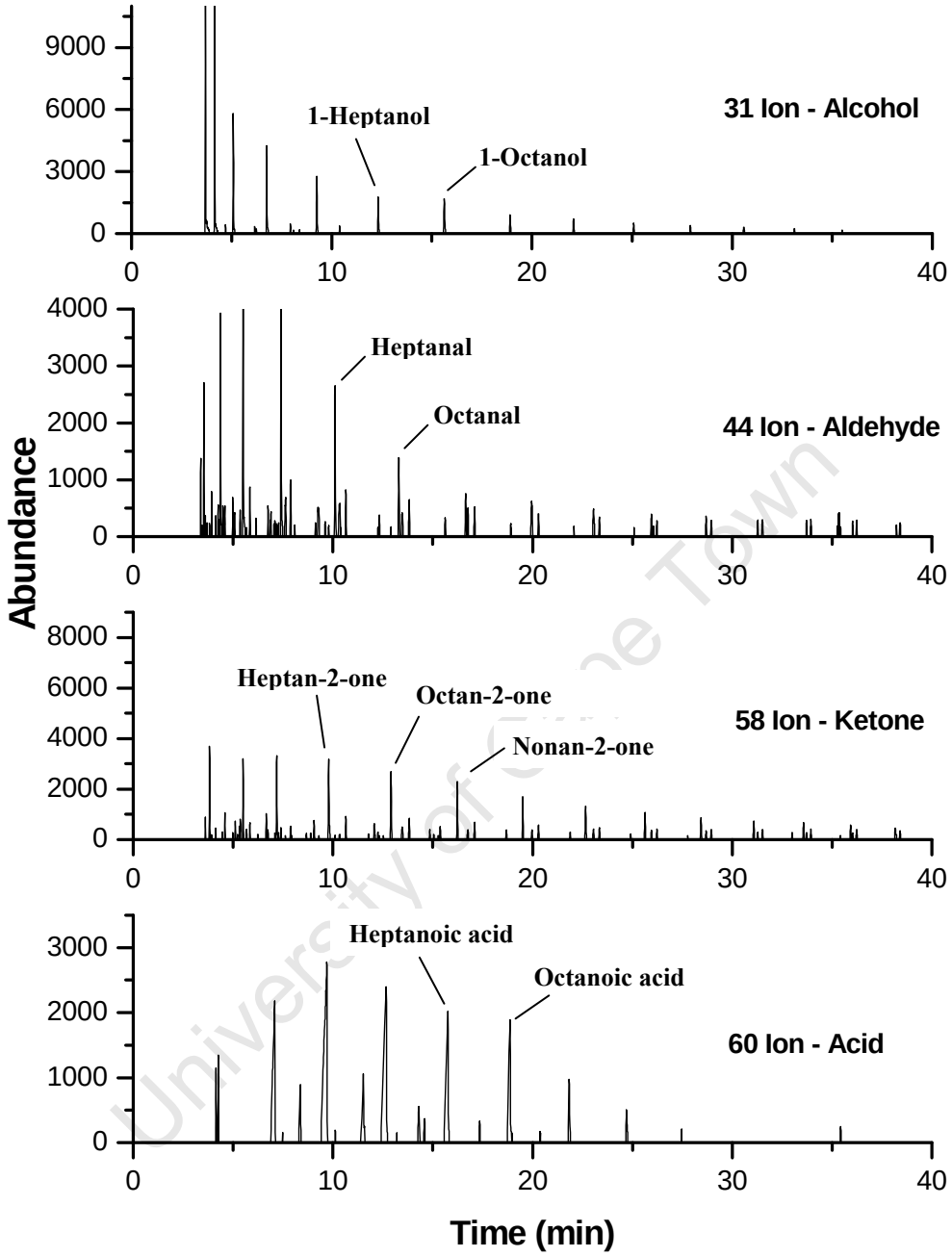

Figure M.7 Extracted ion chromatograms of 0 wt% Cu catalyst with octan-2-one co-feeding after 48 hours TOL during Fischer-Tropsch synthesis in a Berty reactor for ions m/z=31 (alcohols), m/z=44 (aldehydes), m/z=58 (ketones) and m/z=60 (acids)

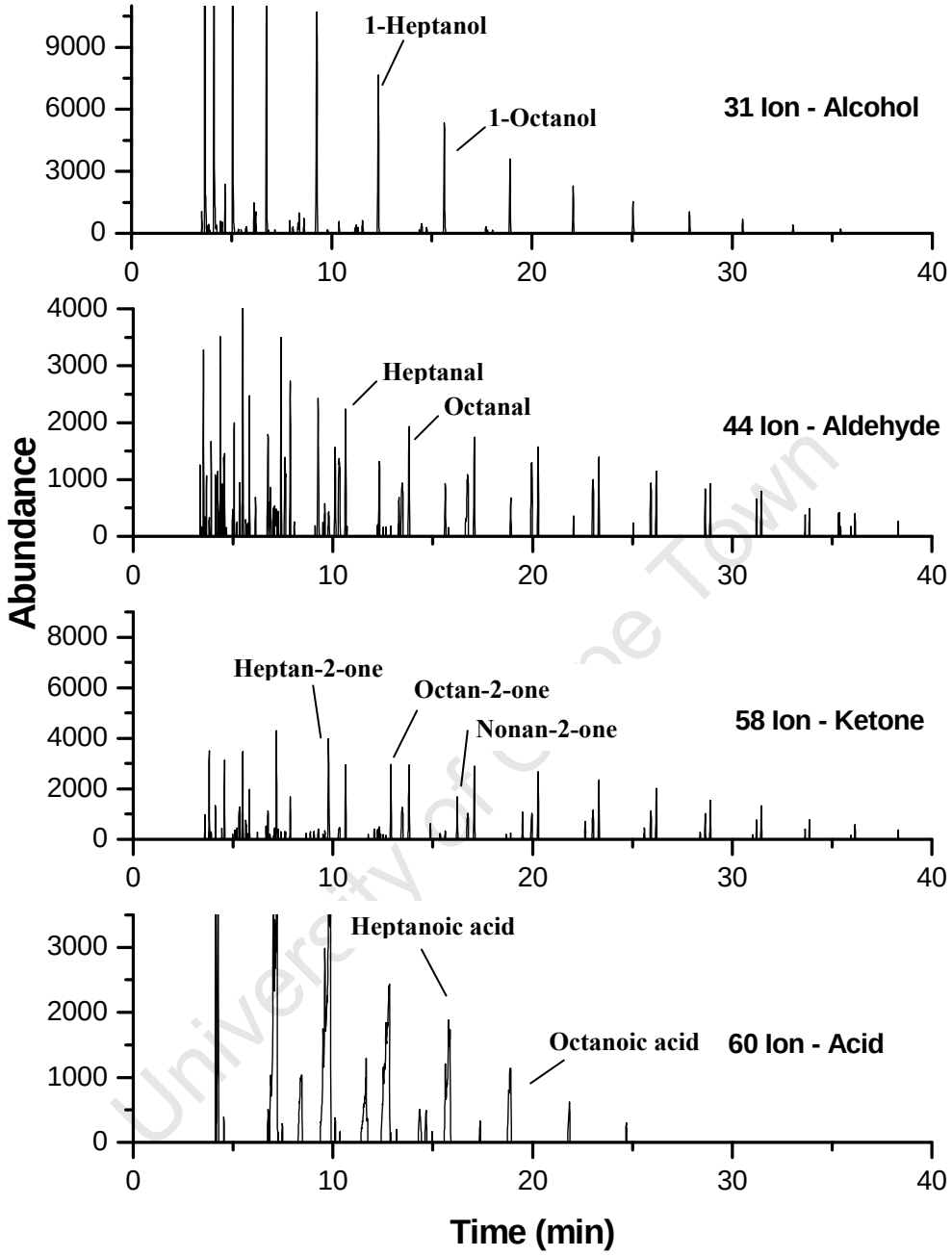

Figure M.8 Extracted ion chromatograms of 50 wt% Cu catalyst with octan-2-one co-feeding after 48 hours TOL during Fischer-Tropsch synthesis in a Berty reactor for ions m/z=31 (alcohols), m/z=44 (aldehydes), m/z=58 (ketones) and m/z=60 (acids)

Table M.4 Ratio of extracted ion (m/z) areas of 1-heptanol (m/z=31), heptanal (m/z=44), heptanoic acid (m/z=60) over decene (m/z=55) during octan-2-one co-feeding

	0 wt% Cu Octan-2-one feeding						
TOL	48	53	72	77	93	117	126
Feeding	no	Octan-2-one				no	no
$\frac{\text{Area 1-Heptanol}}{\text{Area Decene}}$	0.068	0.067	0.063	0.061	0.060	0.075	0.081
$\frac{\text{Area Heptanal}}{\text{Area Decene}}$	0.086	0.082	0.080	0.071	0.078	0.087	0.092
$\frac{\text{Area Heptanoic acid}}{\text{Area Decene}}$	0.201	0.231	0.179	0.217	0.192	0.241	0.276
	50 wt% Cu Octan-2-one feeding						
TOL	48	56	72	92	96		
Feeding	no	Octan-2-one					
$\frac{\text{Area 1-Heptanol}}{\text{Area Decene}}$	0.113	0.131	0.036	0.045	0.089		
$\frac{\text{Area Heptanal}}{\text{Area Decene}}$	0.019	0.023	0.011	0.012	0.015		
$\frac{\text{Area Heptanoic acid}}{\text{Area Decene}}$	0.102	0.135	0.050	0.055	0.094		

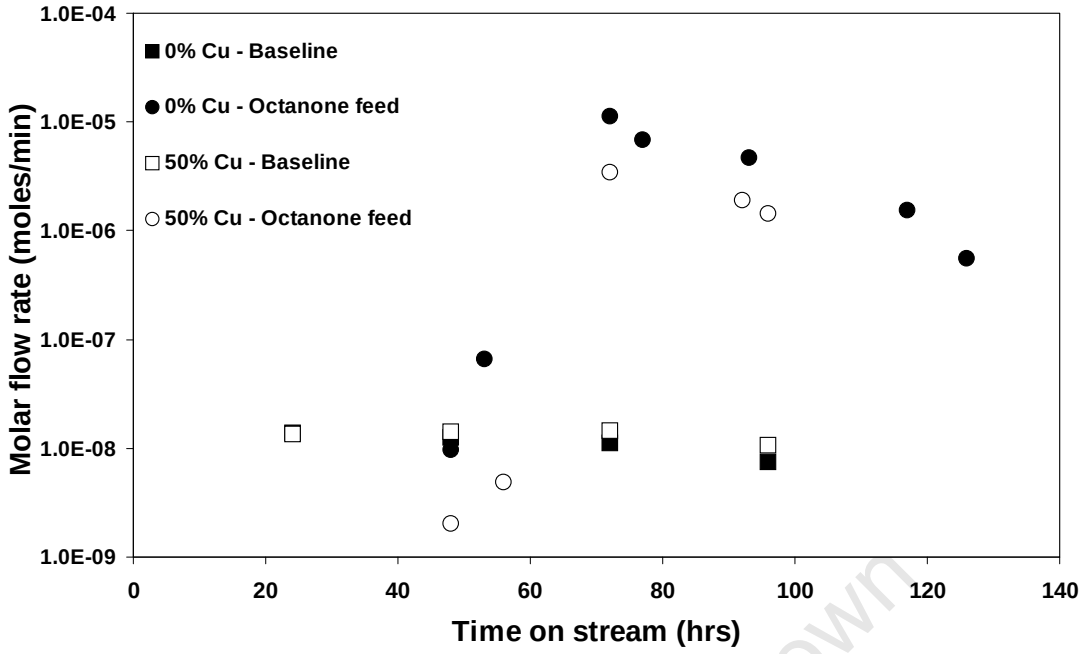

Figure M.9 Octan-2-one flow rate in product oil for 0 and 50 wt% Cu catalysts for both baseline and octan-2-one co-feeding experiments

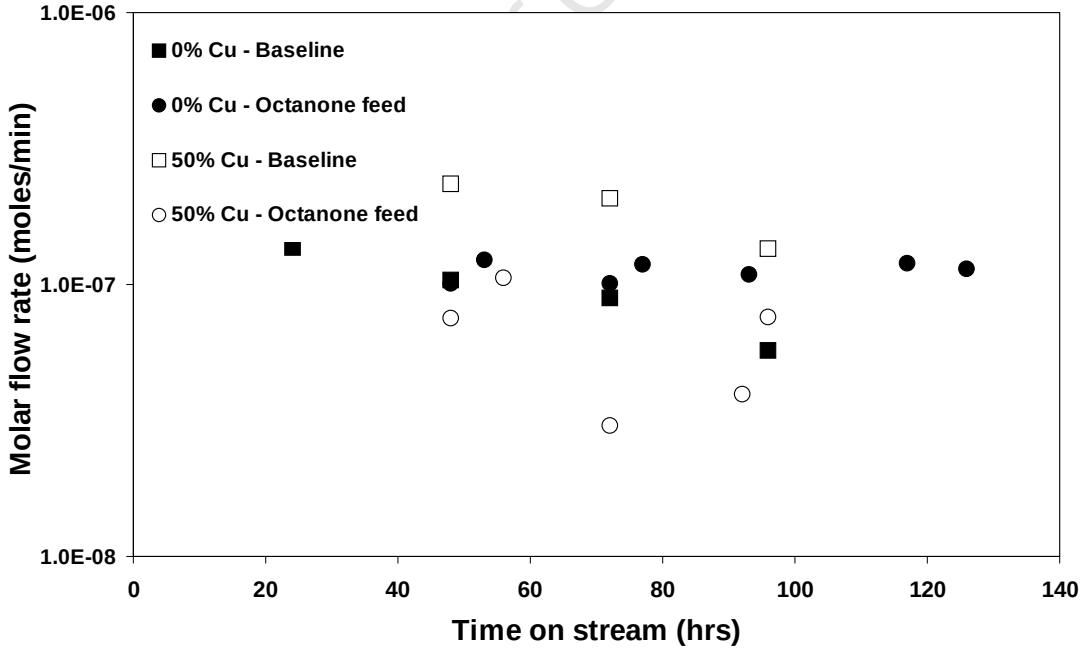

Figure M.10 1-Octanol flow rate in product oil for 0 and 50 wt% Cu catalysts for both baseline and octan-2-one co-feeding experiments

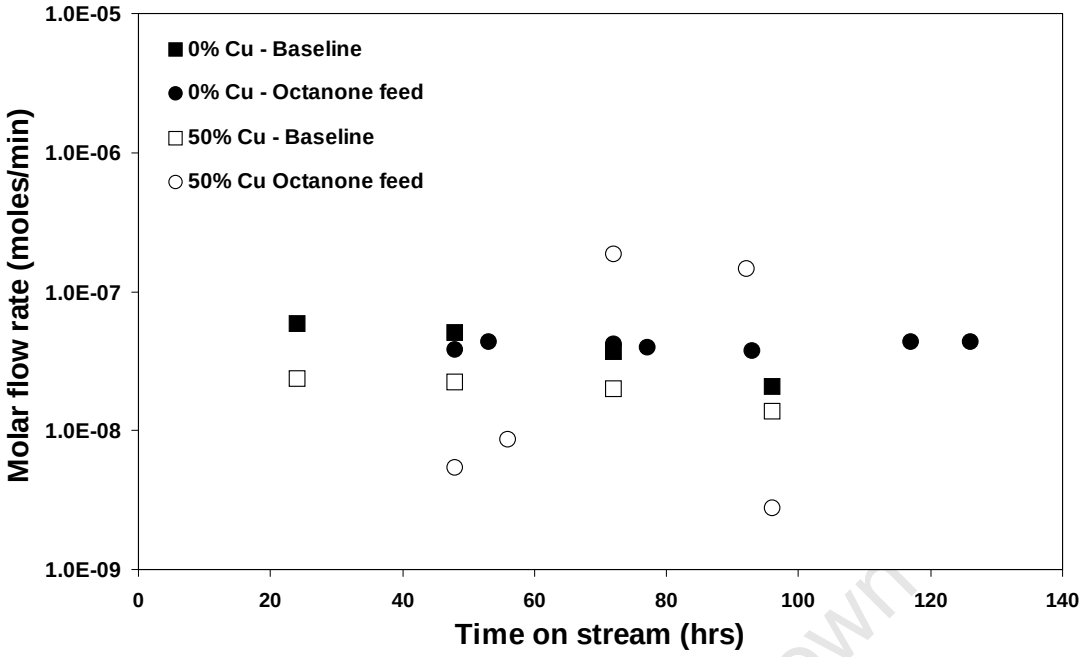

Figure M.12 Octanal flow rate in product oil for 0 and 50 wt% Cu catalysts for both baseline and octan-2-one co-feeding experiments

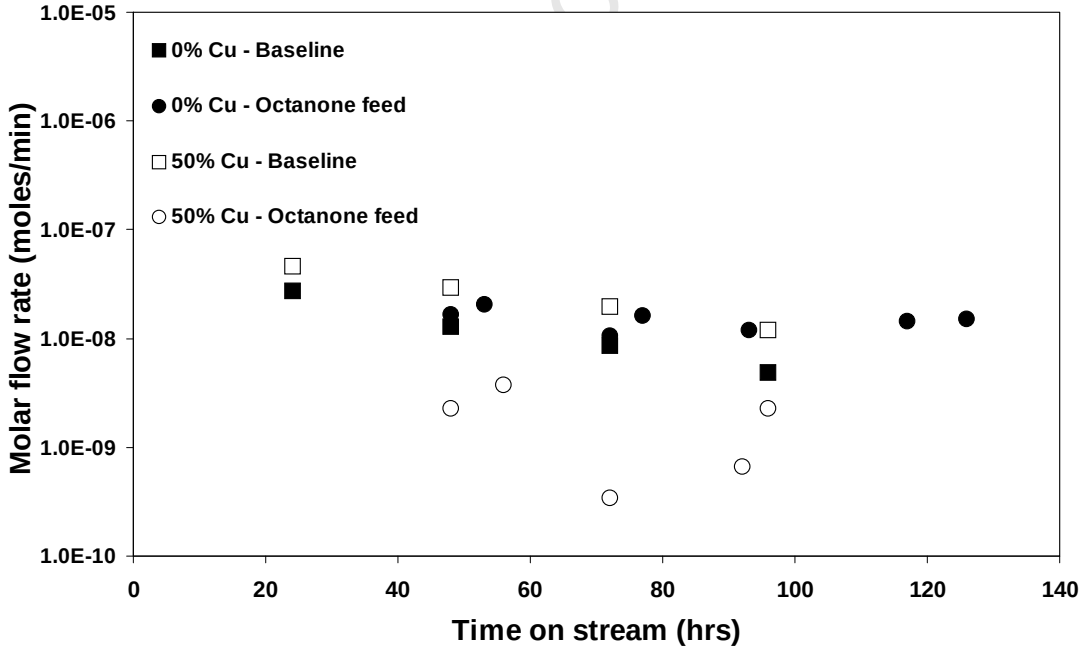

Figure M.13 Octanoic acid flow rate in product oil for 0 and 50 wt% Cu catalysts for both baseline and octan-2-one co-feeding experiments

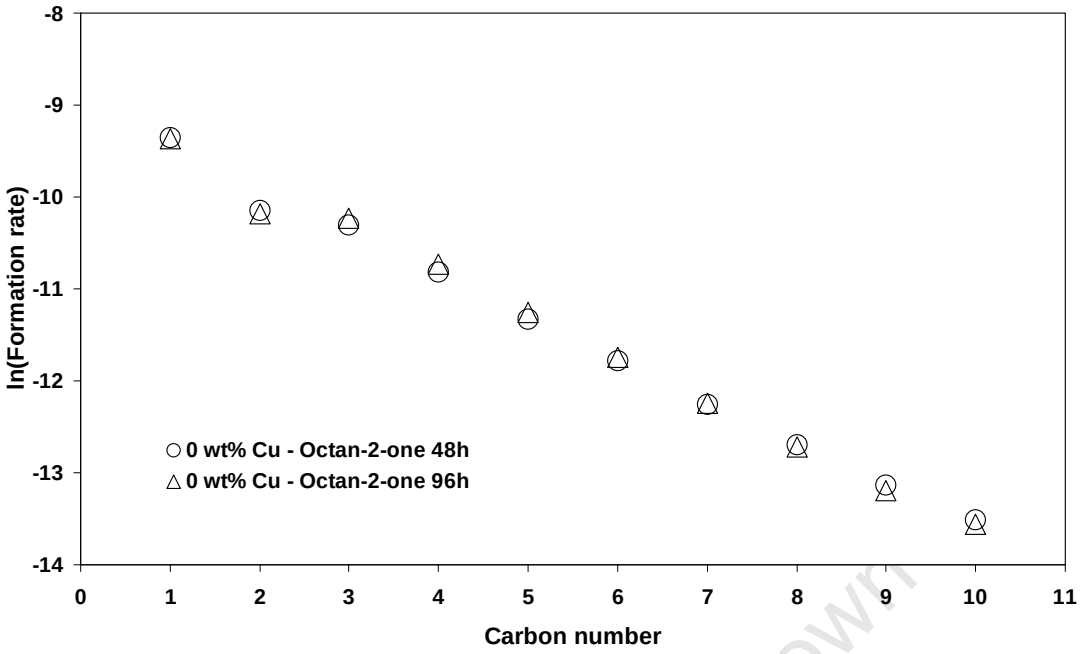

Figure M.14 ASF plot of natural log of formation rates of linear hydrocarbons verse carbon number for 48 and 96 hours with the 0 wt% Cu catalyst during octan-2-one co-feeding

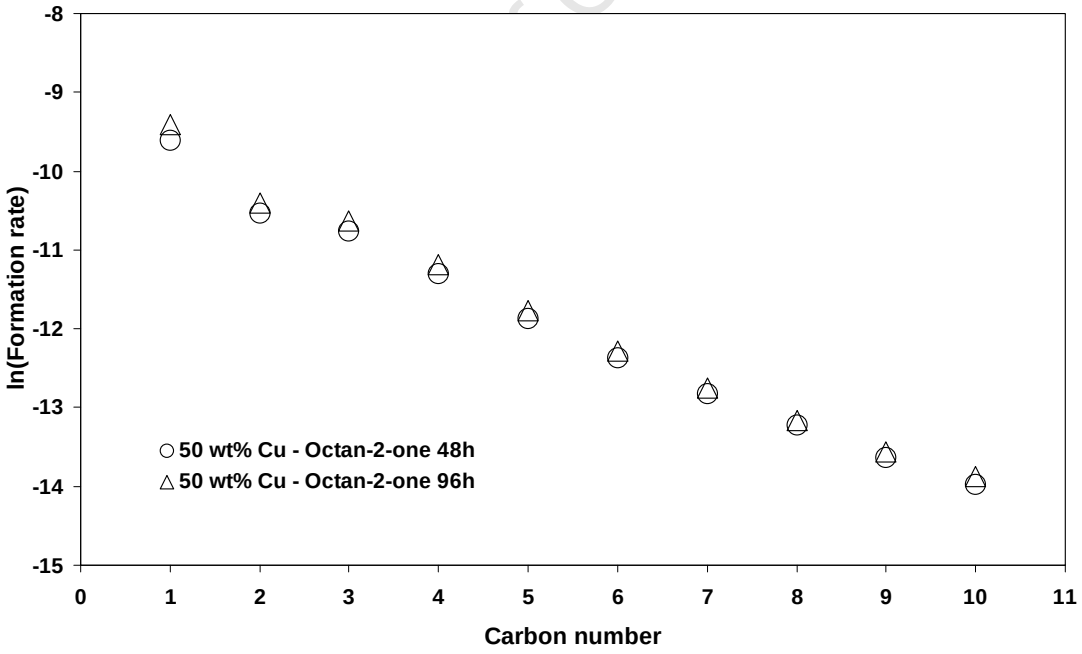

Figure M.15 ASF plot of natural log of formation rates of linear hydrocarbons verse carbon number for 48 and 96 hours with the 50 wt% Cu catalyst during octan-2-one co-feeding

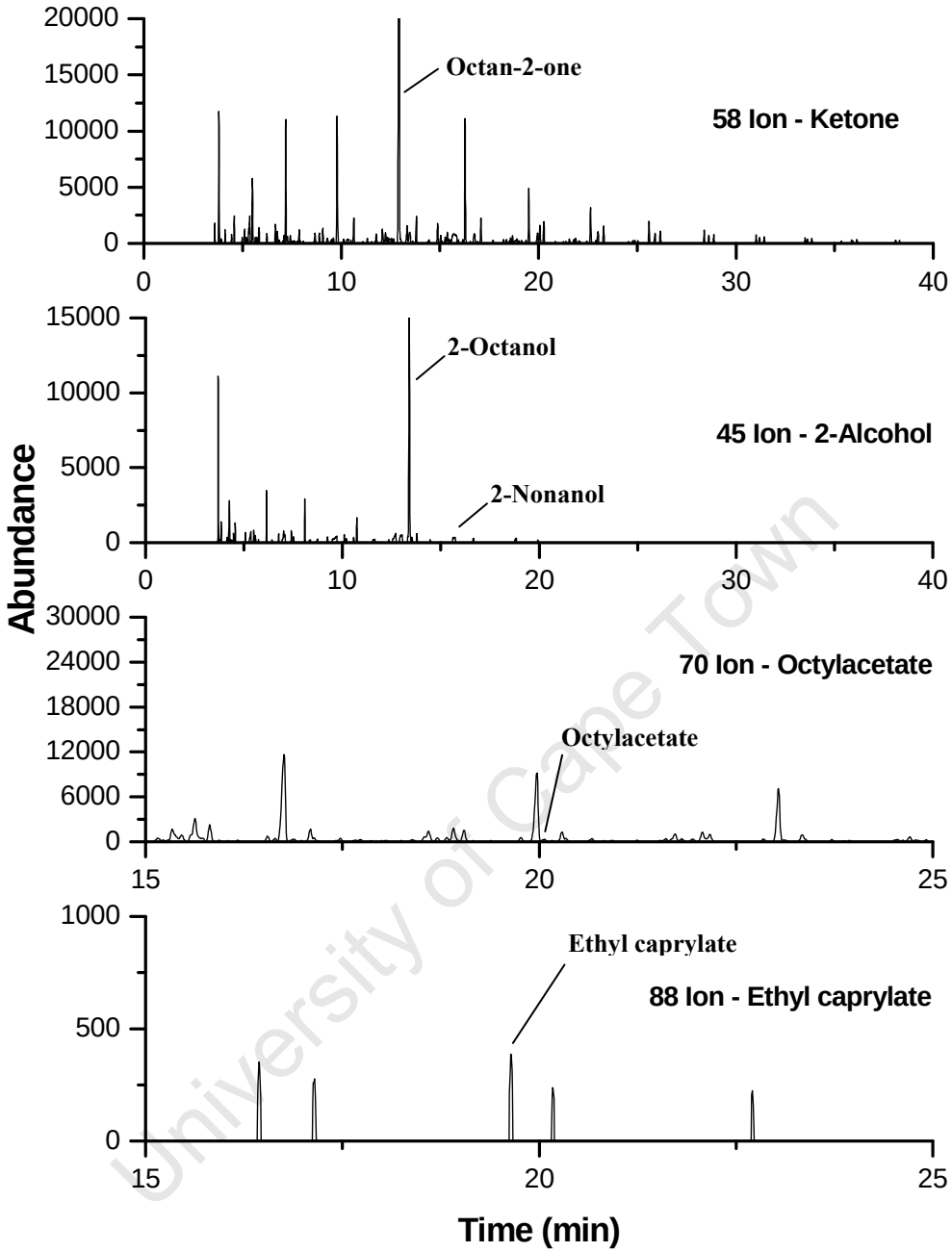

Figure M.16 The corresponding extracted ion chromatograms including that of the methyl-ketones of 0 wt% Cu catalyst with octan-2-one co-feeding after 96 hours TOL during Fischer-Tropsch synthesis in a Berty reactor for ions m/z=31 (1-alcohols), m/z=45 (2-alcohols), m/z=70 (octylacetate) and m/z=88 (ethyl caprylate)

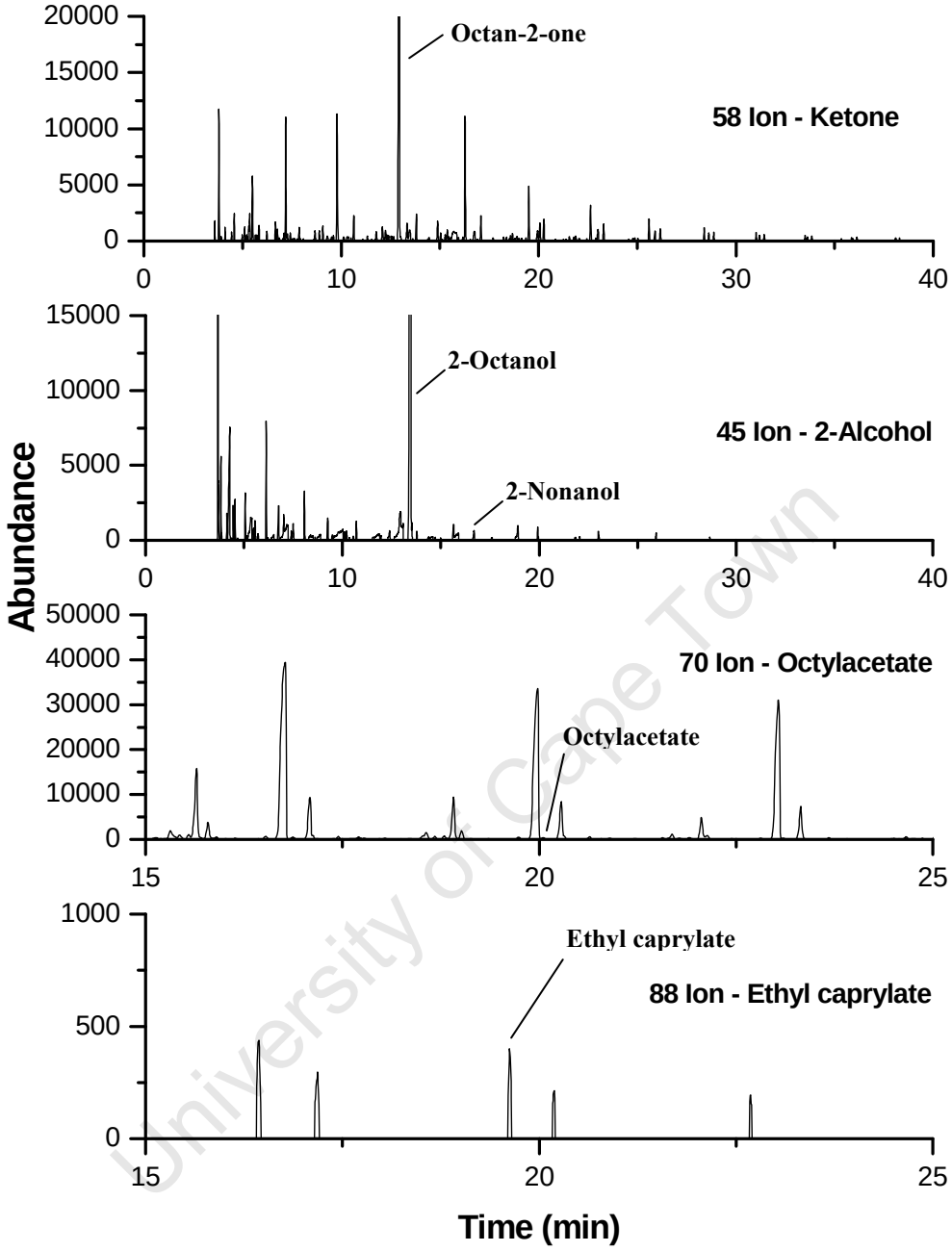

Figure M.17 The corresponding extracted ion chromatograms including that of the methyl-ketones of 50 wt% Cu catalyst with octan-2-one co-feeding after 96 hours TOL during Fischer-Tropsch synthesis in a Berty reactor for ions m/z=31 (1-alcohols), m/z=45 (2-alcohols), m/z=70 (octylacetate) and m/z=88 (ethyl caprylate)

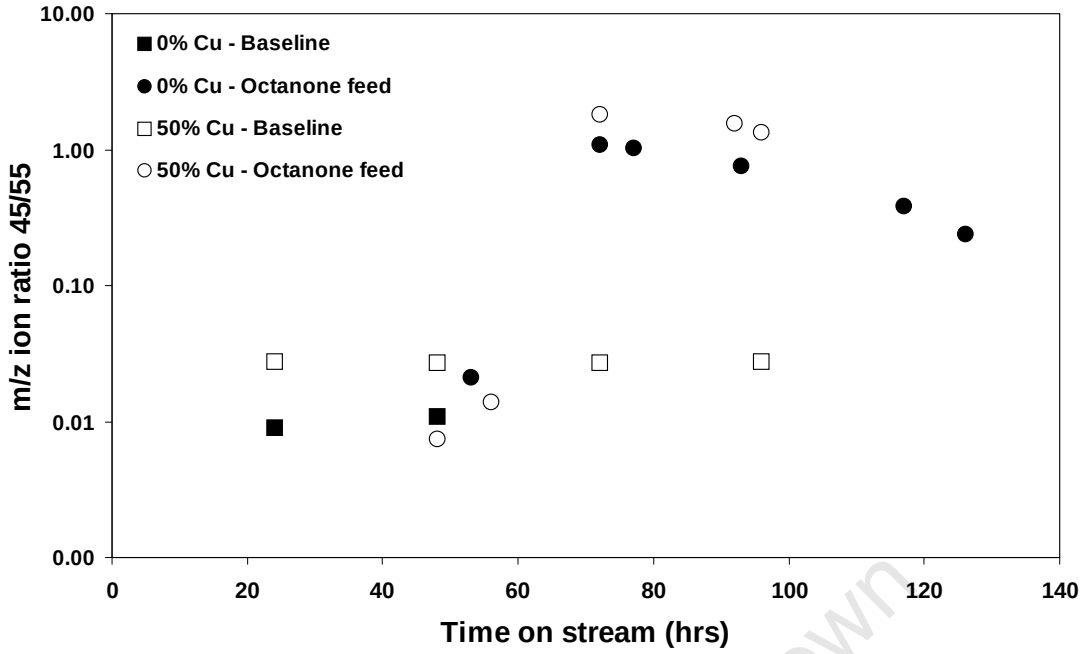

Figure M.18 Ion m/z for 2-octanol (45/55) in product oil for 0 and 50 wt% Cu catalysts for both baseline and octan-2-one co-feeding experiments

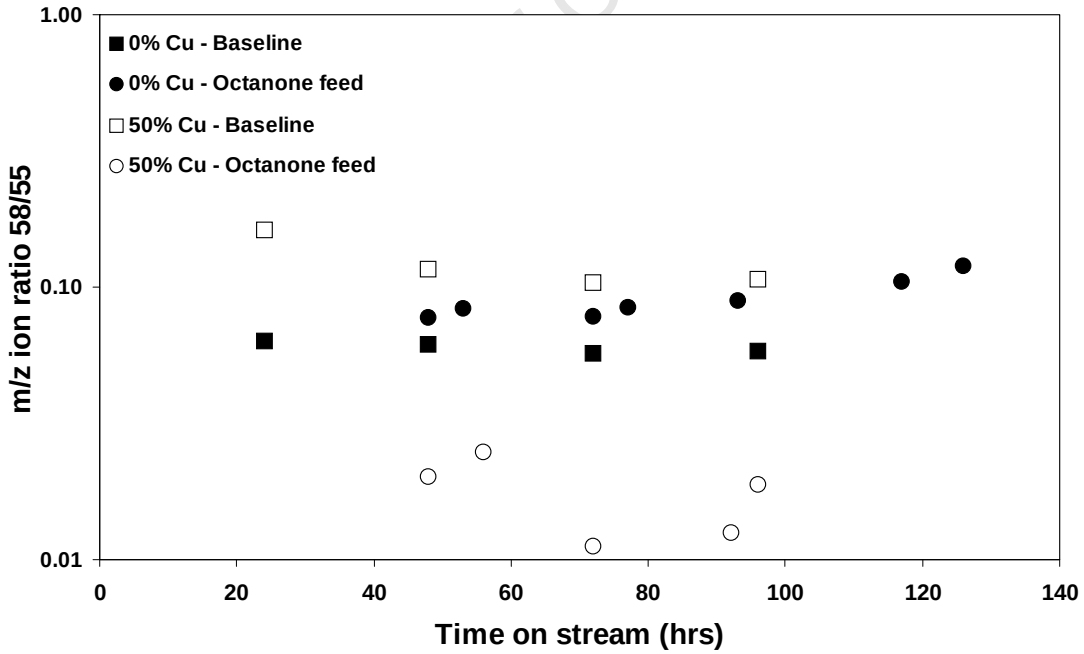

Figure M.19 Ion m/z for nonan-2-one (58/55) in product oil for 0 and 50 wt% Cu catalysts for both baseline and octan-2-one co-feeding experiments

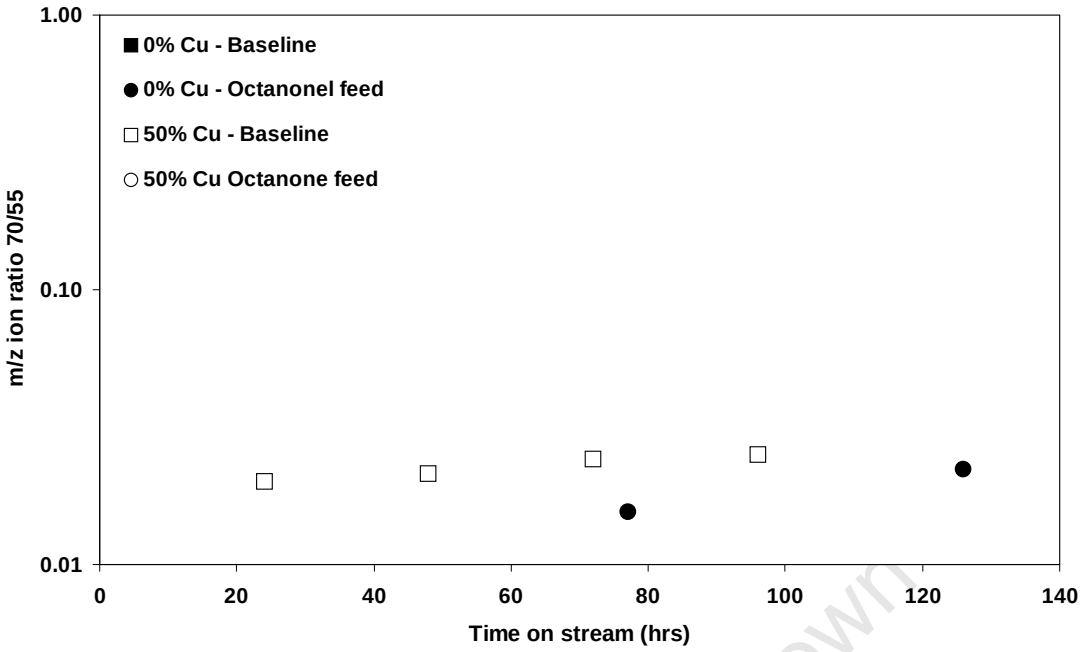

Figure M.20 Ion m/z for octylacetate (70/55) in product oil for 0 and 50 wt% Cu catalysts for both baseline and octan-2-one co-feeding experiments

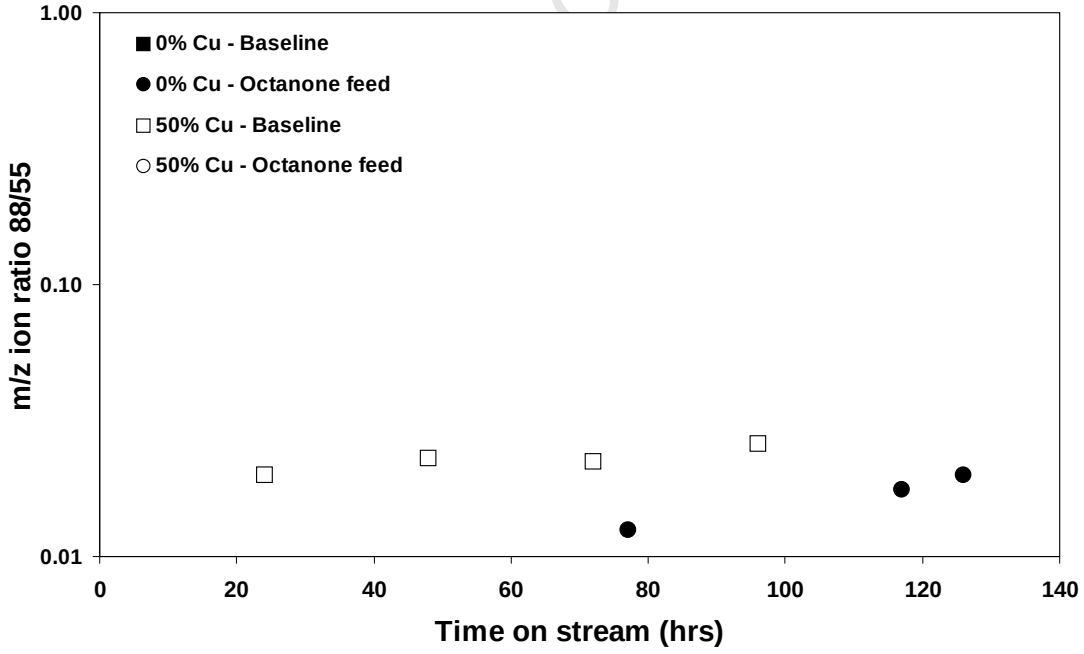

Figure M.21 Ion m/z for ethyl caprylate (88/55) in product oil for 0 and 50 wt% Cu catalysts for both baseline and octan-2-one co-feeding experiments

(Note: All cases where data points are not shown are due to zero values where the peaks were too small to identify correctly. Zero values cannot be shown in logarithmic scales)

M.4 Thermodynamics

Table M 5 Equilibrium ratios of C_8 oxygenates in product oil with octan-2-one co-feeding during Fischer-Tropsch synthesis in a Berty reactor for the 0 wt% Cu catalyst using the TIC m/z ion specific areas

Reaction and ratio		**Product ratios**				
		48h	72h	77h	93h	117h
Octanoic acid + H_2 ⇔ Octan-2-one + H_2O	Eq[a]	979	921	948	967	708
Octan-2-one/ Octanoic acid	Obs[b]	0.59	1061	424	393	106
1-Octanol ⇔ Octan-2-one + H_2	Eq	38.7	39.1	38.9	39.0	40.9
Octan-2-one/1-Octanol	Obs	0.10	113	58.4	43.4	12.8
Octanal ⇔ Octan-2-one	Eq	415	415	415	415	415
Octan-2-one/ Octanal	Obs	0.26	270	173	126	35.0
1-Octanol + H_2O ⇔ Octanoic acid +2H_2	Eq	0.039	0.042	0.041	0.040	0.058
Octanoic acid/1-Octanol	Obs	0.16	0.11	0.14	0.11	0.12
Octanal + H_2O ⇔ Octanoic acid + H_2	Eq	0.42	0.45	0.44	0.43	0.59
Octanoic acid/ Octanal	Obs	0.43	0.25	0.41	0.32	0.33
Octanal + H_2 ⇔ 1-Octanol	Eq	10.7	10.6	10.7	10.6	10.15
1-Octanol /Octanal	Obs	2.64	2.40	2.97	2.90	2.73
Octanoic acid + CO + 2H_2 ⇔ Nonan-2-one + 2H_2O	Eq	134573	112638	119705	123272	64310
Nonan-2-one / Octanoic acid	Obs	0.48	0.87	0.61	0.76	0.81
1-Octanol + CO + H_2 ⇔ Nonan-2-one + H_2O	Eq	36795	32735	33774	34119	24294
Nonan-2-one /1-Octanol	Obs	0.08	0.09	0.08	0.08	0.10
Octanal + CO + 2H_2 ⇔ Nonan-2-one + H_2O	Eq	394856	347448	360085	363157	246658
Nonan-2-one / Octanal	Obs	0.21	0.22	0.25	0.24	0.27

[a] Eq: Expected ratio at equilibrium

[b] Obs: Observed product ratios

Table M.6 Equilibrium ratios of C_8 oxygenates in product oil with octan-2-one co-feeding during Fischer-Tropsch synthesis in a Berty reactor for the 50 wt% Cu catalyst using the TIC m/z ion specific areas

Reaction and ratio		**Product ratios**			
		48h	72h	92h	96h
Octanoic acid + H_2 ⇔ Octan-2-one + H_2O	Eq[a]		3971	1801	1096
Octan-2-one/ Octanoic acid	Obs[b]	0.89	10316	2873	621
1-Octanol ⇔ Octan-2-one + H_2	Eq		35.5	37.4	39.1
Octan-2-one/1-Octanol	Obs	0.03	115	47.8	18.8
Octanal ⇔ Octan-2-one	Eq		415	415	415
Octan-2-one/ Octanal	Obs	0.37	18.6	13.0	508
1-Octanol + H_2O ⇔ Octanoic acid +2H_2	Eq		0.009	0.021	0.036
Octanoic acid/1-Octanol	Obs	0.03	0.01	0.02	0.03
Octanal + H_2O ⇔ Octanoic acid + H_2	Eq		0.10	0.23	0.38
Octanoic acid/ Octanal	Obs	0.42	0.002	0.005	0.82
Octanal + H_2 ⇔ 1-Octanol	Eq		11.7	11.1	10.6
1-Octanol /Octanal	Obs	13.8	0.16	0.27	27.0
Octanoic acid + CO + 2H_2 ⇔ Nonan-2-one + 2H_2O	Eq		3264134	618632	217998
Nonan-2-one / Octanoic acid	Obs	0.45	1.25	0.75	0.39
1-Octanol + CO + H_2 ⇔ Nonan-2-one + H_2O	Eq		219927	91926	53244
Nonan-2-one /1-Octanol	Obs	0.01	0.01	0.01	0.01
Octanal + CO + 2H_2 ⇔ Nonan-2-one + H_2O	Eq		2566179	1019682	564211
Nonan-2-one / Octanal	Obs	0.19	0.002	0.003	0.32

[a] Eq: Expected ratio at equilibrium

[b] Obs: Observed product ratios

Appendix N

Co-feeding: Octanoic acid

N.1 Run details

Table N.1 Catalyst loadings and time on-stream conversions for octanoic acid co-feeding

	0% Cu	50% Cu
Mass catalyst loaded (g)	2.4007	4.8000
Time on line (hours)	24	24
CO conversion (TCD)	85.1	80.7
Carbon conversion (TCD)	38.0	34.8
Time on line (hours)	48	48
CO conversion (TCD)	86.7	81.6
Carbon conversion (TCD)	39.9	35.7
Time on line (hours)	72	72
CO conversion (TCD)	86.8	82.4
Carbon conversion (TCD)	38.8	34.9
Time on line (hours)	80	89
CO conversion (TCD)	87.6	84.0
Carbon conversion (TCD)	41.5	37.2
Time on line (hours)	96	96
CO conversion (TCD)	87.4	84.0
Carbon conversion (TCD)	37.0	37.3
Time on line (hours)	120	113
CO conversion (TCD)	90.0	84.4
Carbon conversion (TCD)	48.5	37.9
Time on line (hours)		123
CO conversion (TCD)		89.1
Carbon conversion (TCD)		44.2

N.2 GC-FID results

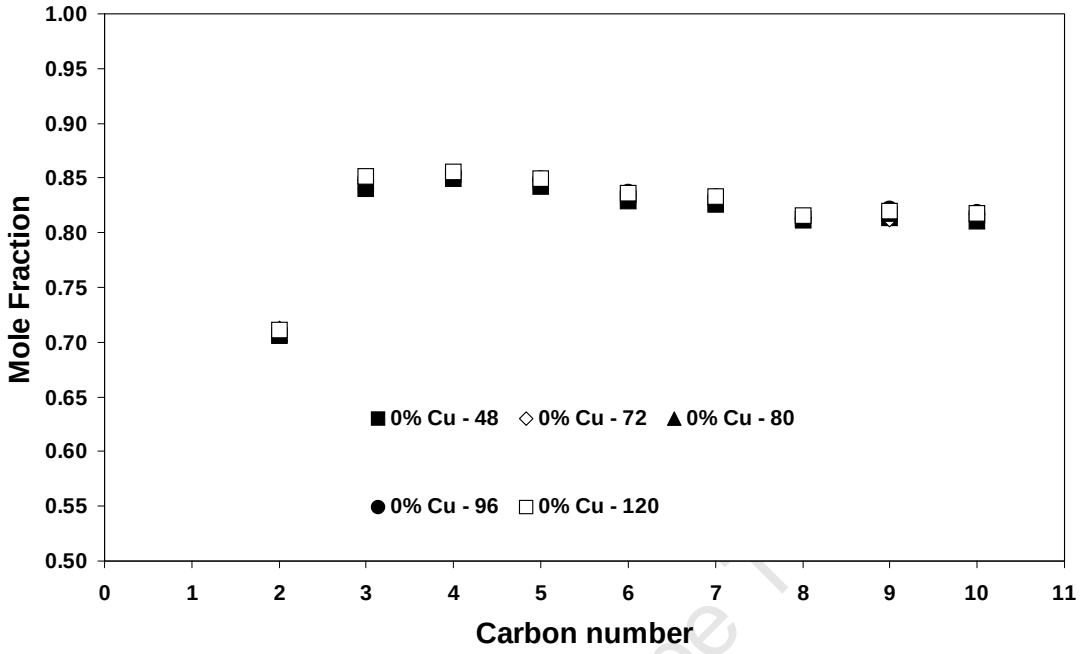

Figure N.1 Mole fraction of linear olefins in linear hydrocarbon product on the 0 wt% Cu catalyst for octanoic acid co-feeding

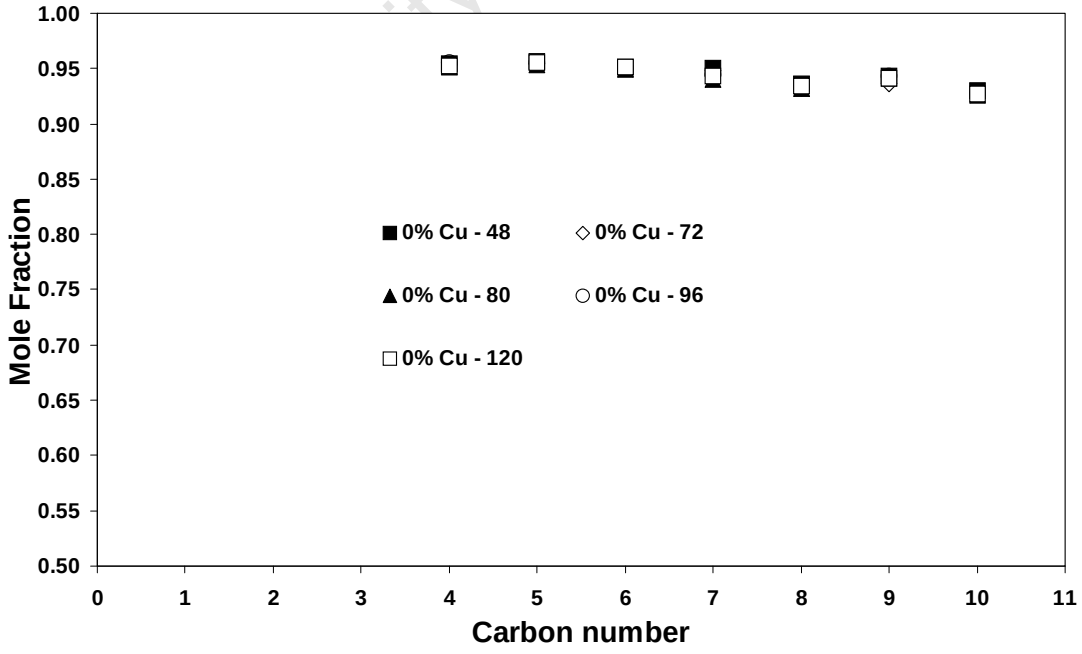

Figure N.2 Mole fraction of α–olefins in linear olefins on the 0 wt% Cu catalyst for octanoic acid co-feeding

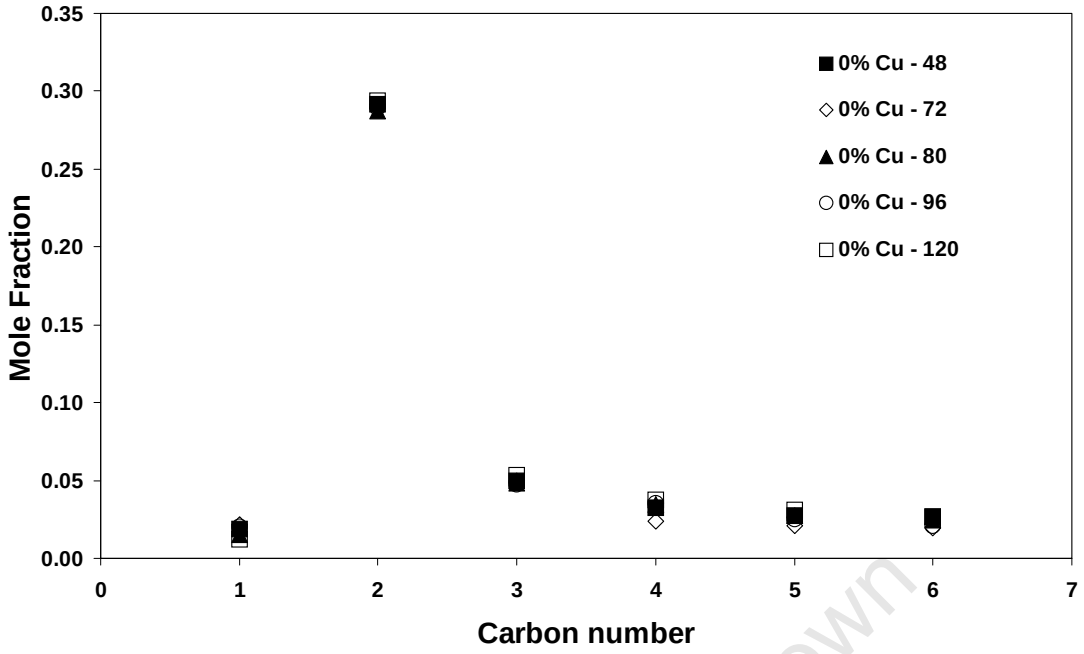

Figure N.3 Mole fraction of alcohols in linear product (excluding aldehydes and ketones) on the 0 wt% Cu catalyst for octanoic acid co-feeding

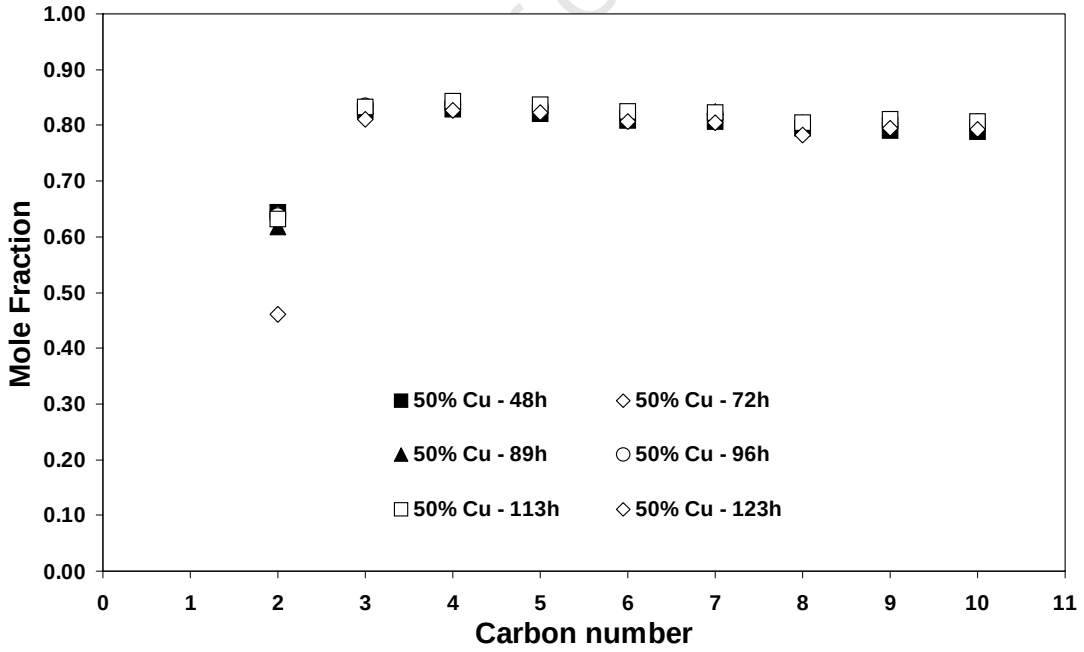

Figure N.4 Mole fraction of linear olefins in linear hydrocarbon product on the 50 wt% Cu catalyst for octanoic acid co-feeding

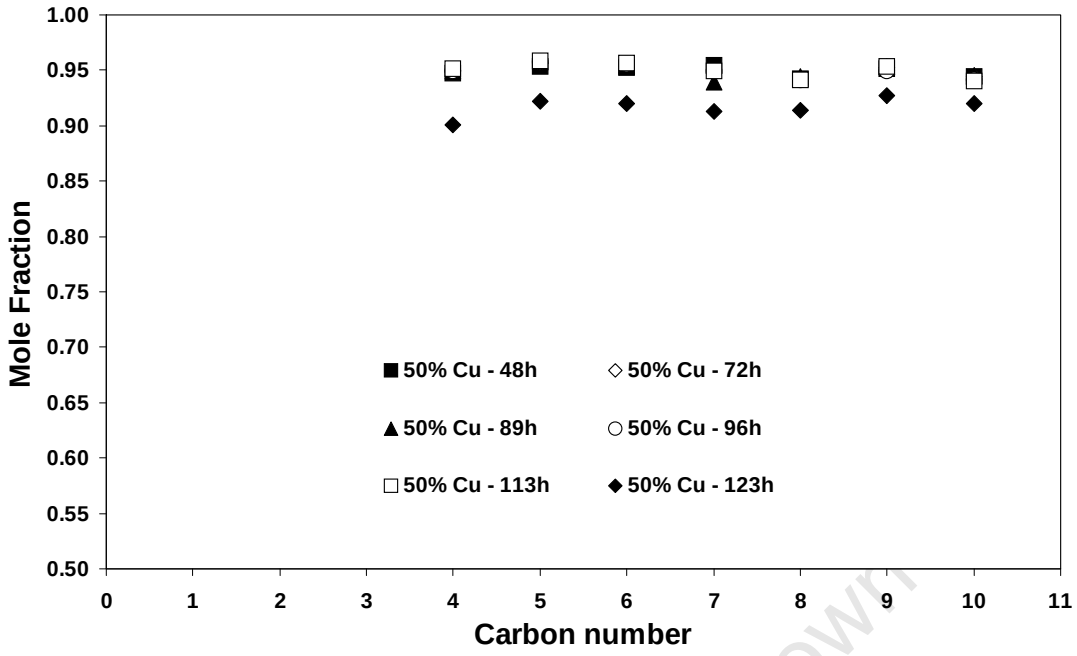

Figure N.5 Mole fraction of α–olefins in linear olefins on the 50 wt% Cu catalyst for octanoic acid co-feeding

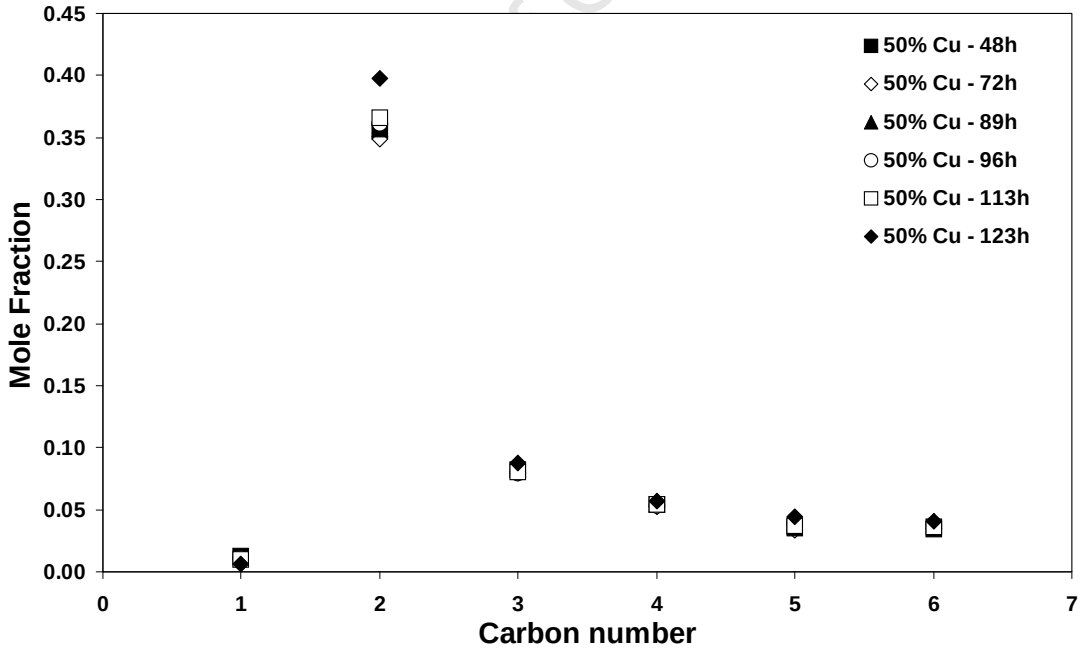

Figure N.6 Mole fraction of alcohols in linear product (excluding aldehydes and ketones) on the 50 wt% Cu catalyst for octanoic acid co-feeding

N.3 GC-MS results

TableN.2 Molar balance of octanoic acid fed to C_8 oxygenate products for both 0 and 50 wt% Cu catalysts.

0 wt% Cu catalyst			
Octanoic acid co-feeding			
Time on-stream of analysis (hrs)	72	80	96
Feed rate (µmoles/min)	0.073	0.153	0.212
Average feed rate (µmoles/min)		0.113	0.183
Exit 1-octanol (µmoles/min)		1.509	1.731
Exit Octanal (µmoles/min)		0.750	0.792
Exit Octan-2-one (µmoles/min)		0.049	0.058
Exit Octanoic acid (µmoles/min)		0.871	1.153
C8 Balance closure (less baseline flows)		2011.0%	1718.7%
50 wt% Cu catalyst			
Octanoic acid co-feeding			
Time on-stream of analysis (hrs)	72	89	96
Feed rate (µmoles/min)	-[a]	-[a]	-[a]
Average feed rate (µmoles/min)		-[a]	-[a]
Exit 1-octanol (µmoles/min)		1.355	1.239
Exit Octanal (µmoles/min)		0.152	0.121
Exit Octan-2-one (µmoles/min)		0.025	0.024
Exit Octanoic acid (µmoles/min)		0.610	0.598
C8 Balance closure (less baseline flows)		-[a]	-[a]

[a] No feed analysis possible due to loss of acid in ampoule sampling

Table N.3 Molar flow rates (in µmol/min) of octanol, octanal, octan-2-one, octanoic acid and nonan-2-one for octanoic acid co-feeding

				0 wt% Cu Octanoic acid feeding			
TOL	48	56	72	80	96	103	120
Feeding	no			Octanoic acid		no	no
Octanol	0.050	0.076	0.798	1.509	1.731	2.043	1.250
Octanal	0.026	0.039	0.406	0.750	0.792	0.839	0.529
Octan-2-one	0.010	0.013	0.047	0.034	0.023	0.020	0.018
Octanoic acid	0.008	0.018	0.382	0.871	1.153	1.542	1.013
Nonan-2-one	0.008	0.000	0.032	0.049	0.058	0.067	0.053
Heptane + Heptene	3.81	-	3.84	3.95	4.06	-	4.03
Octane + Octene	2.51	-	2.51	2.61	2.62	-	2.55
Nonane + Nonene	1.64	-	1.68	1.74	1.69	-	1.55
				50 wt% Cu Octanoic acid feeding			
TOL	48	65	72	89	96	113	123
Feeding	no			Octanoic acid		no	no
Octanol	0.113	0.410	1.424	1.355	1.239	0.836	0.788
Octanal	0.009	0.054	0.159	0.152	0.121	0.085	0.050
Octan-2-one	0.007	0.014	0.021	0.019	0.017	0.013	0.011
Octanoic acid	0.022	0.028	0.949	0.610	0.598	0.368	0.460
Nonan-2-one	0.009	0.013	0.023	0.025	0.024	0.021	0.018
Heptane + Heptene	2.93	-	3.17	3.36	3.41	3.38	2.93
Octane + Octene	2.01	-	2.15	2.23	2.26	2.18	2.01
Nonane + Nonene	1.38	-	1.47	1.47	1.51	1.38	1.38

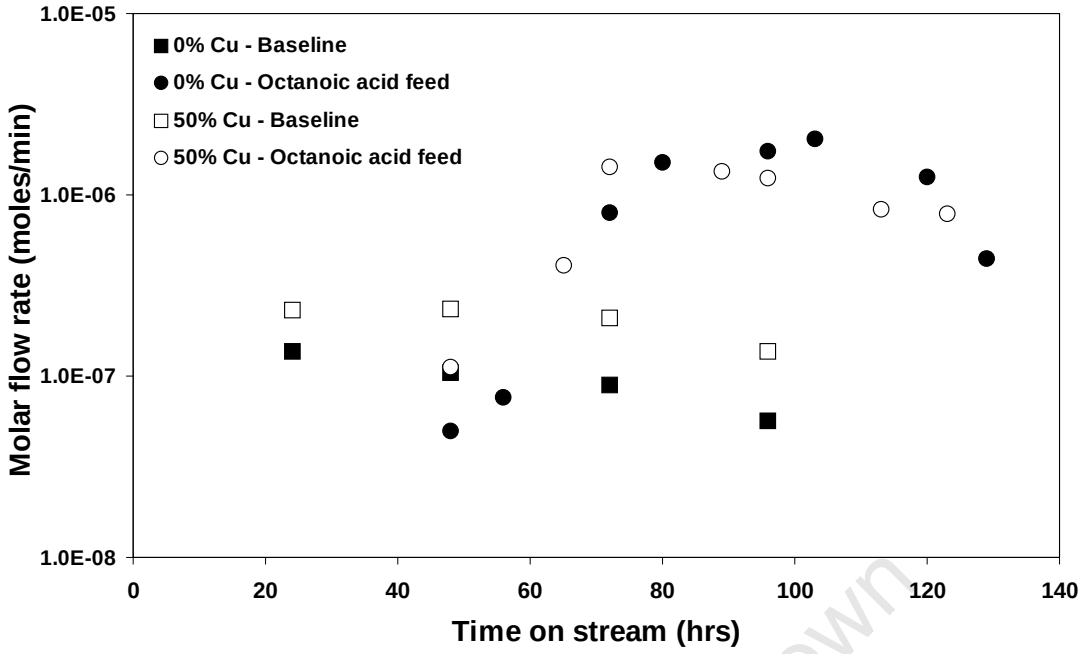

Figure N.7 1-Octanol flow rate in product oil for 0 and 50 wt% Cu catalysts for both baseline and octanoic acid co-feeding experiments

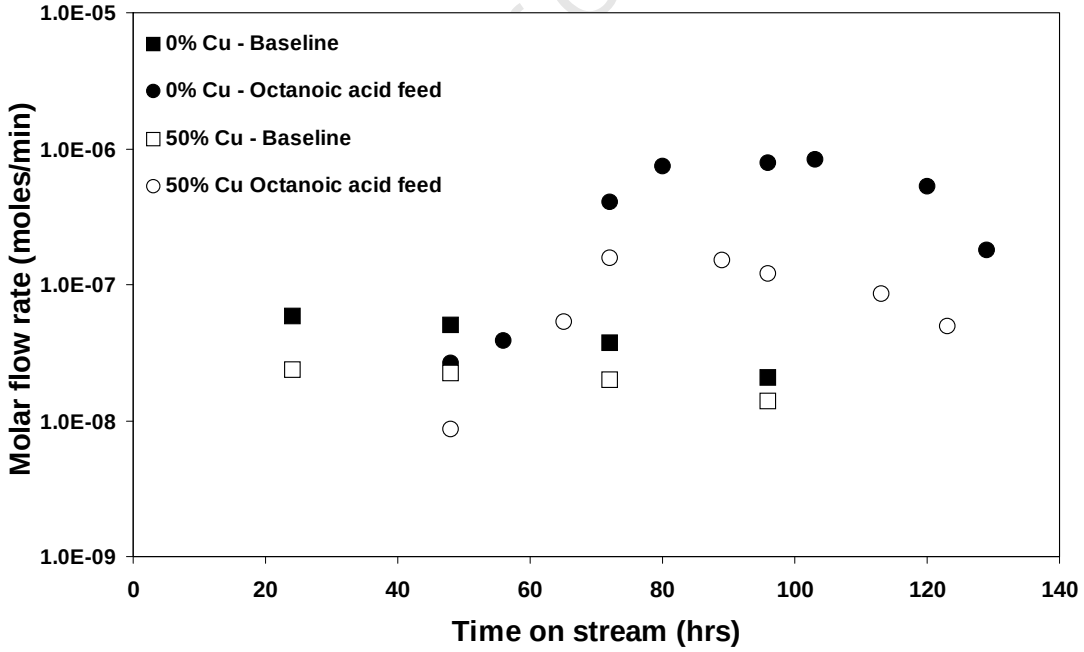

Figure N.8 Octanal flow rate in product oil for 0 and 50 wt% Cu catalysts for both baseline and octanoic acid co-feeding experiments

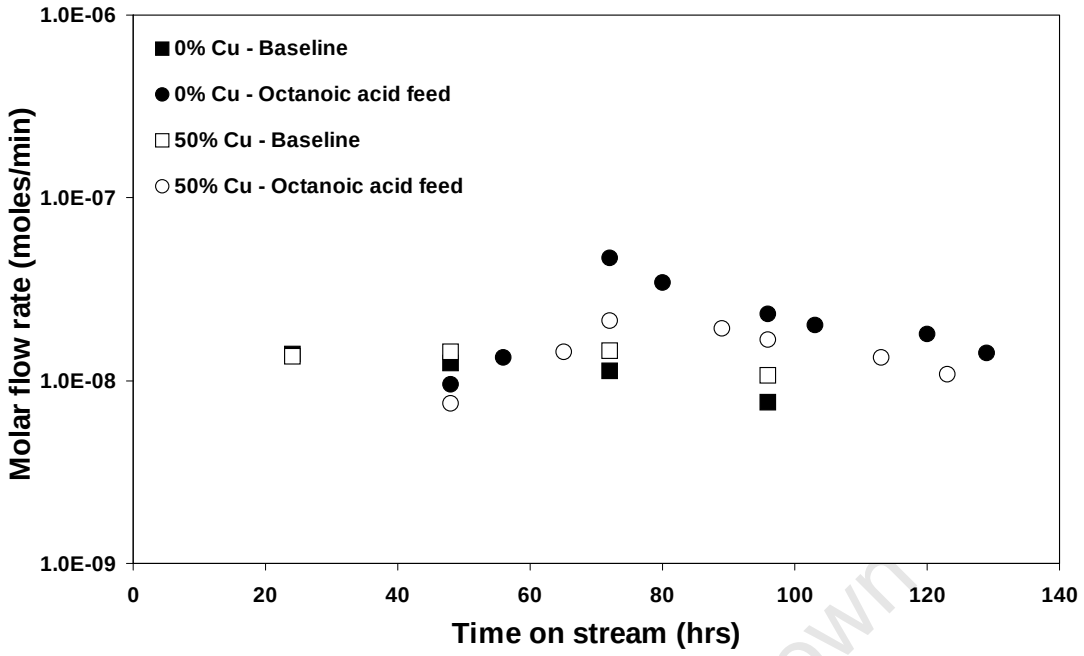

Figure N.9 Octan-2-one flow rate in product oil for 0 and 50 wt% Cu catalysts for both baseline and octanoic acid co-feeding experiments

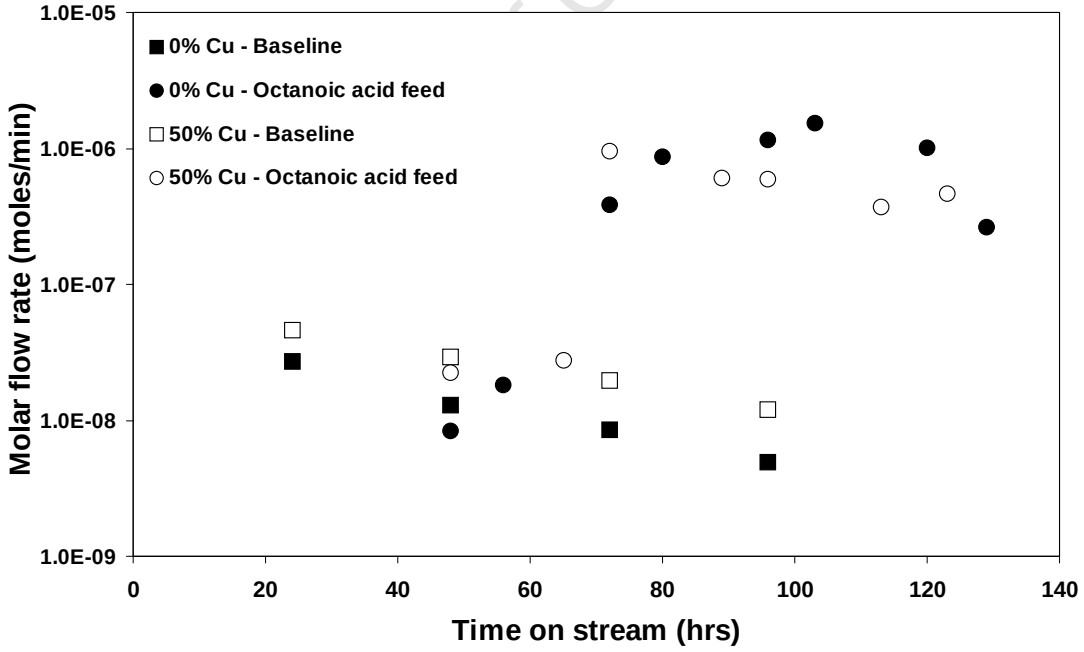

Figure N.10 Octanoic acid flow rate in product oil for 0 and 50 wt% Cu catalysts for both baseline and octanoic acid co-feeding experiments

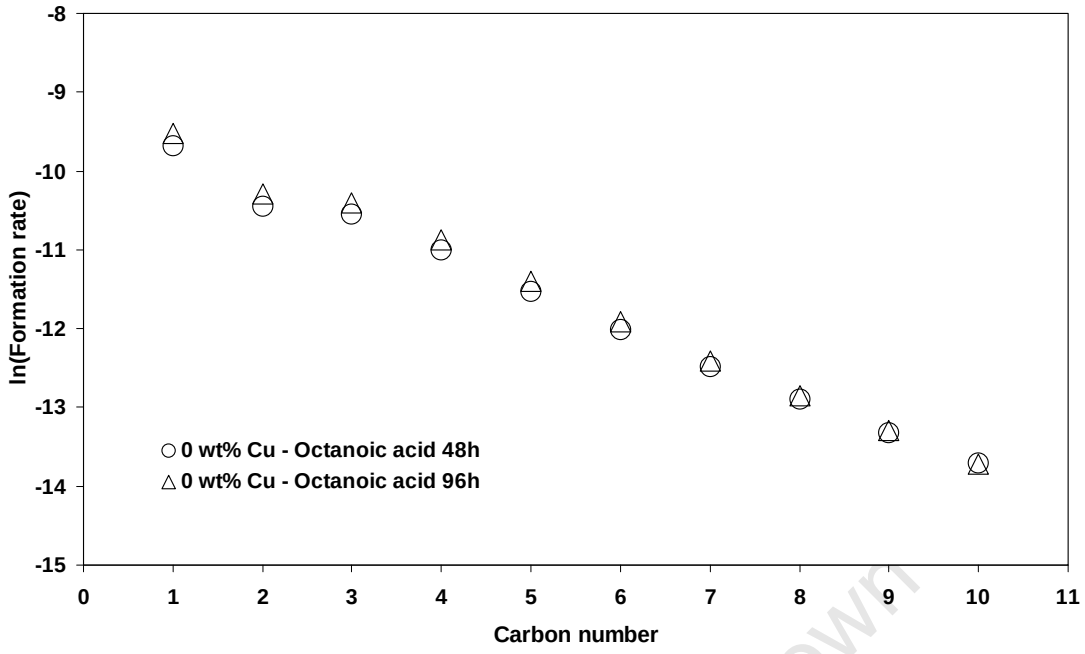

Figure N.11 ASF plot of natural log of formation rates of linear hydrocarbons verse carbon number for 48 and 96 hours with the 0 wt% Cu catalyst during octanoic acid co-feeding

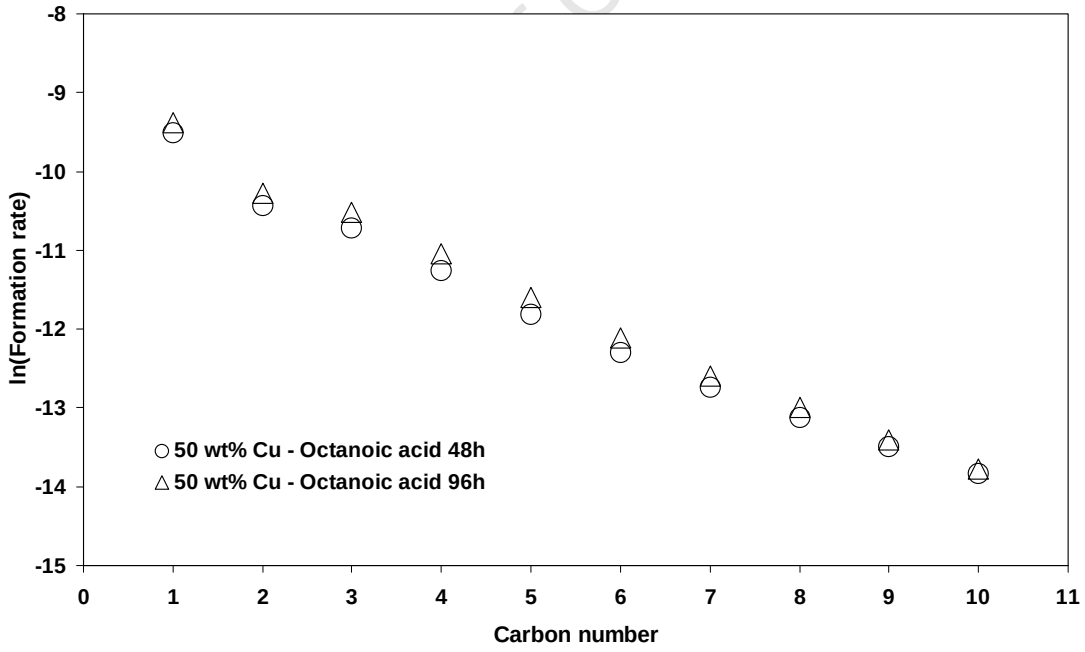

Figure N.12 ASF plot of natural log of formation rates of linear hydrocarbons verse carbon number for 48 and 96 hours with the 50 wt% Cu catalyst during octanoic acid co-feeding

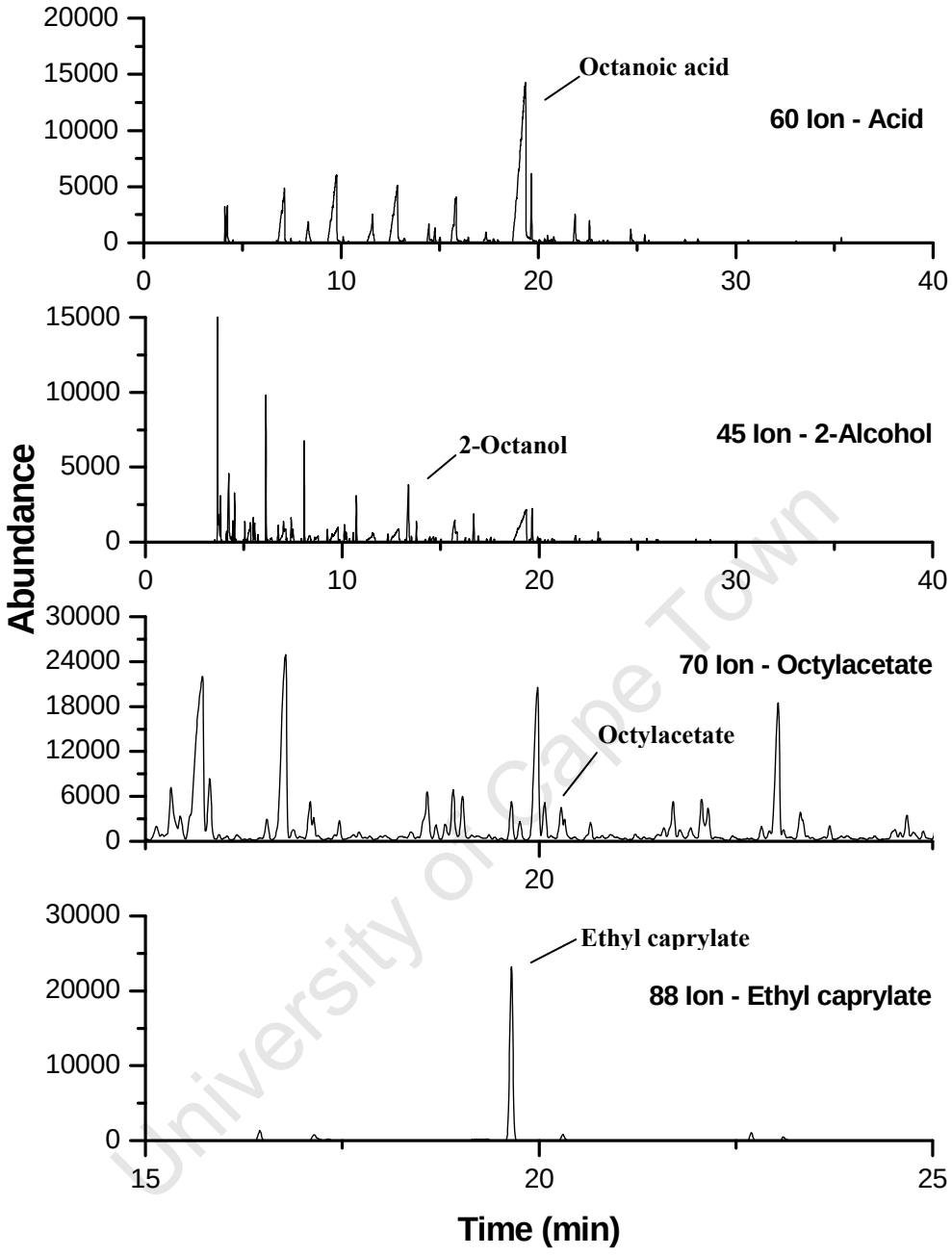

Figure N.13 The corresponding extracted ion chromatograms including that of the carboxylic acids of 0 wt% Cu catalyst with octanoic acid co-feeding after 96 hours TOL during Fischer-Tropsch synthesis in a Berty reactor for ions m/z=31 (1-alcohols), m/z=45 (2-alcohols), m/z=70 (octylacetate) and m/z=88 (ethyl caprylate)

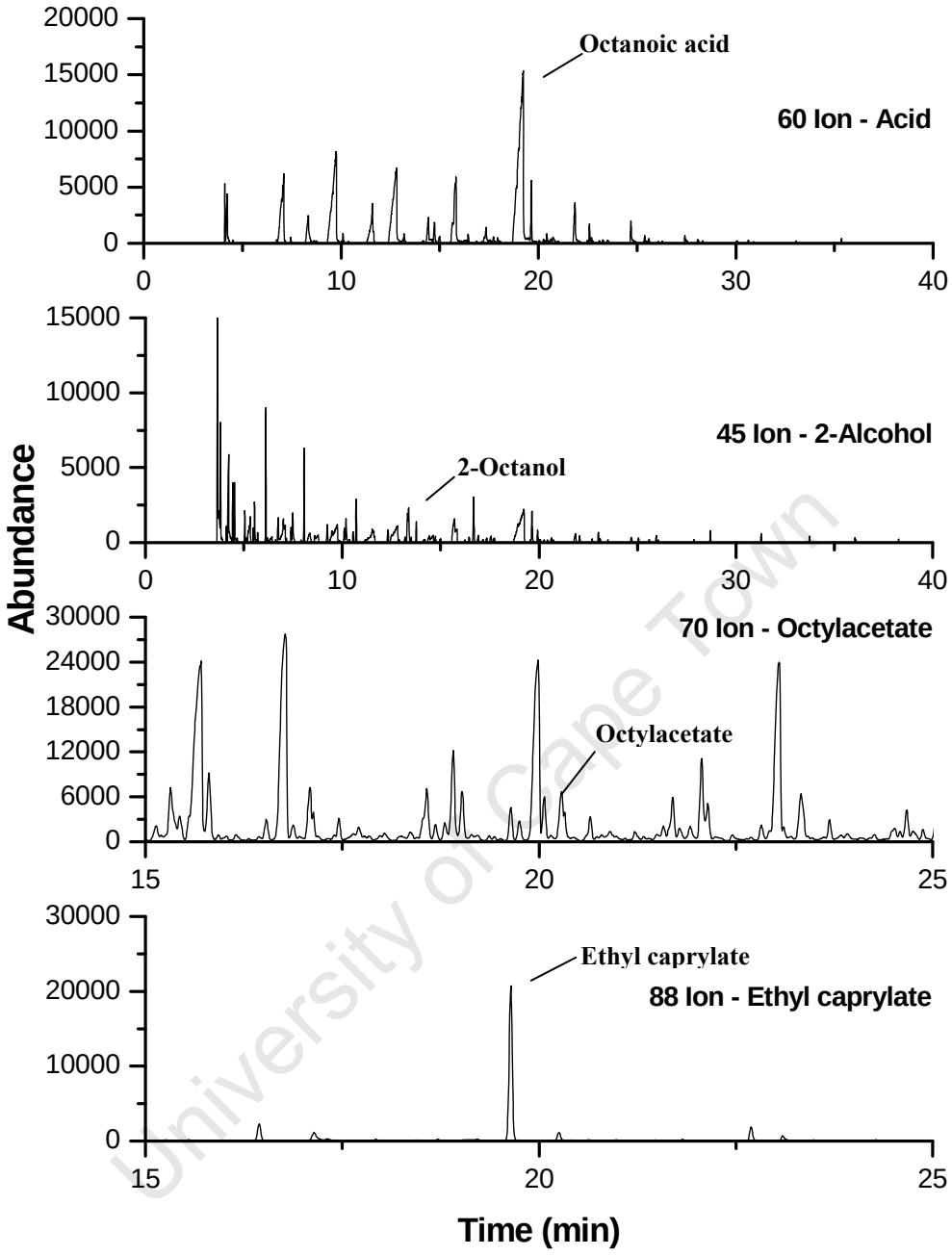

Figure N.14 The corresponding extracted ion chromatograms including that of the carboxylic acids of 50 wt% Cu catalyst with octanoic acid co-feeding after 96 hours TOL during Fischer-Tropsch synthesis in a Berty reactor for ions m/z=31 (1-alcohols), m/z=45 (2-alcohols), m/z=70 (octylacetate) and m/z=88 (ethyl caprylate)

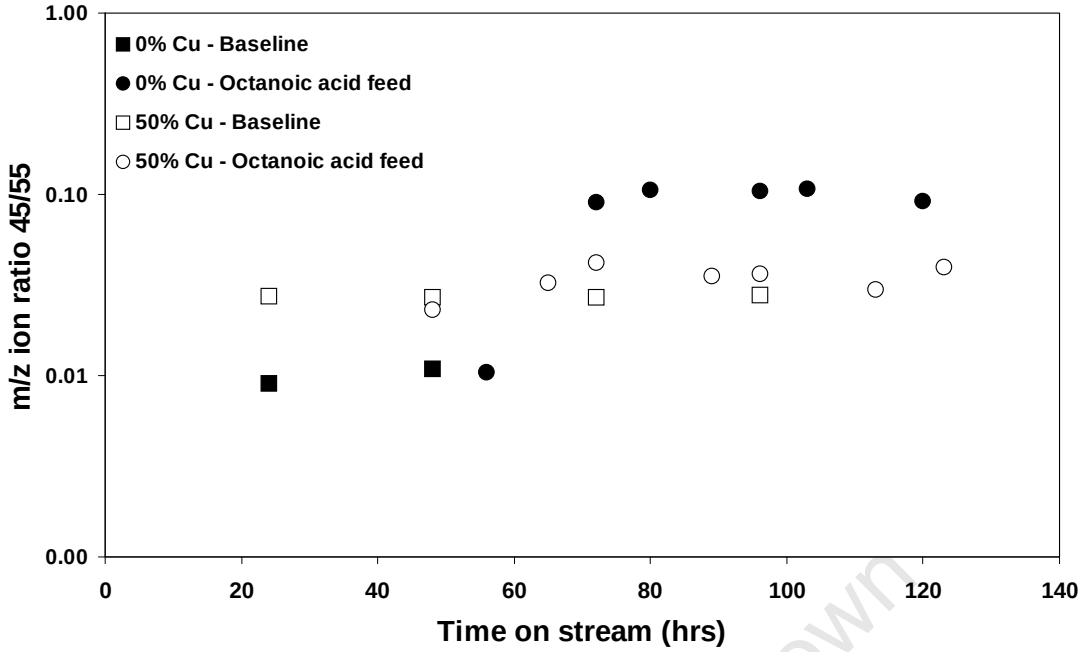

Figure N.15 Ion m/z for 2-octanol (45/55) in product oil for 0 and 50 wt% Cu catalysts for both baseline and octanoic acid co-feeding experiments

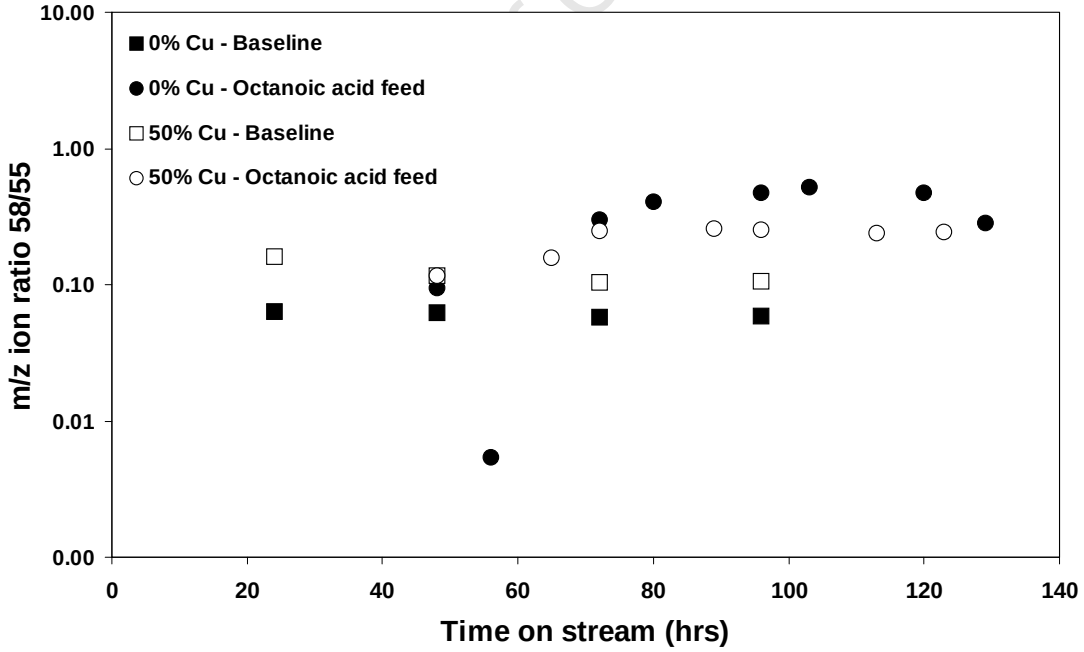

Figure N.16 Ion m/z for nonan-2-one (58/55) in product oil for 0 and 50 wt% Cu catalysts for both baseline and octanoic acid co-feeding experiments

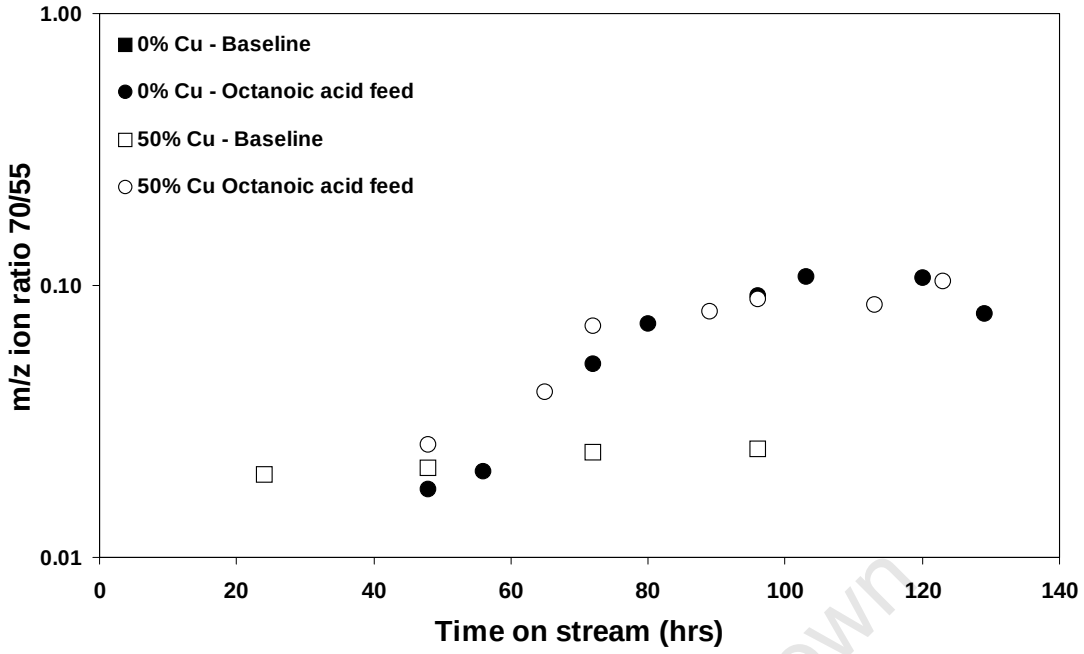

Figure N.17 Ion m/z for octylacetate (70/55) in product oil for 0 and 50 wt% Cu catalysts for both baseline and octanoic acid co-feeding experiments

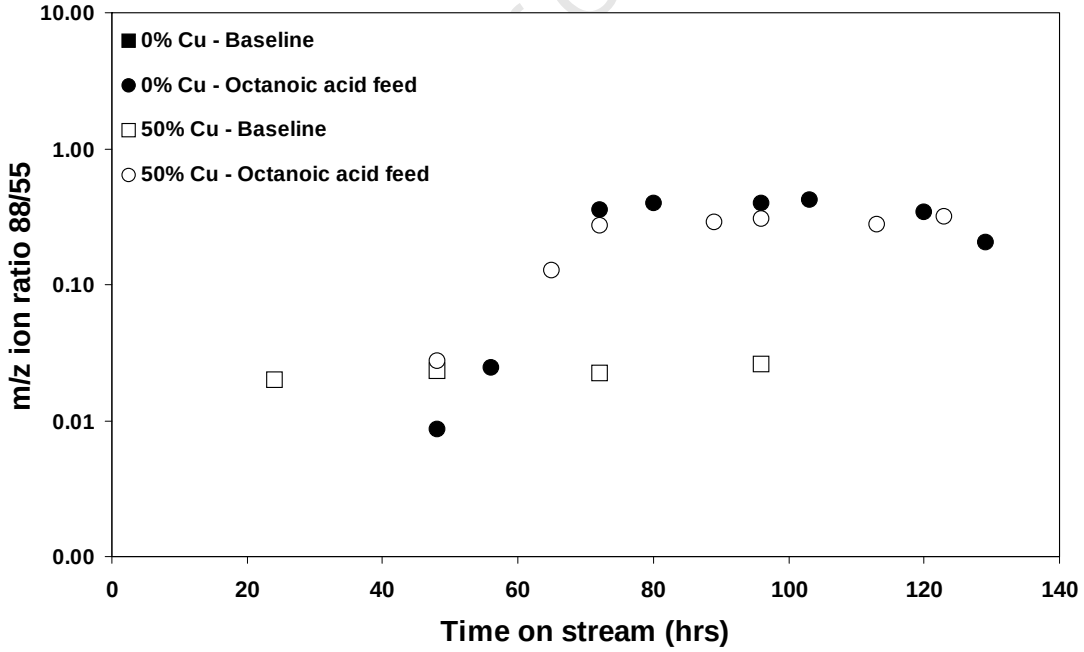

Figure N.18 Ion m/z for ethyl caprylate (88/55) in product oil for 0 and 50 wt% Cu catalysts for both baseline and octanoic acid co-feeding experiments

N.4 Thermodynamics

Table N.4 Equilibrium ratios of C_8 oxygenates in product oil with octanoic acid co-feeding during Fischer-Tropsch synthesis in a Berty reactor for the 0 wt% Cu catalyst using the TIC m/z ion specific areas

Reaction and ratio		Product ratios				
		48h	72h	80h	96h	120h
Octanoic acid + H_2 ⇔ Octan-2-one + H_2O	Eq[a]	928	1010	827	1178	541
Octan-2-one/ Octanoic acid	Obs[b]	1.13	0.12	0.04	0.02	0.02
1-Octanol ⇔ Octan-2-one + H_2	Eq	39.6	39.5	40.5	39.1	43.7
Octan-2-one/1-Octanol	Obs	0.19	0.06	0.02	0.01	0.01
Octanal ⇔ Octan-2-one	Eq	415	415	415	415	415
Octan-2-one/ Octanal	Obs	0.36	0.12	0.05	0.03	0.03
1-Octanol + H_2O ⇔ Octanoic acid +2H_2	Eq	0.043	0.039	0.049	0.033	0.081
Octanoic acid/1-Octanol	Obs	0.17	0.48	0.58	0.67	0.81
Octanal + H_2O ⇔ Octanoic acid + H_2	Eq	0.45	0.41	0.50	0.35	0.77
Octanoic acid/ Octanal	Obs	0.32	0.94	1.16	1.45	1.92
Octanal + H_2 ⇔ 1-Octanol	Eq	10.5	10.5	10.2	10.6	9.50
1-Octanol /Octanal	Obs	1.89	1.97	2.01	2.18	2.36
Octanoic acid + CO + 2H_2 ⇔ Nonan-2-one + 2H_2O	Eq	131823	155345	98221	200569	35801
Nonan-2-one / Octanoic acid	Obs	0.98	0.08	0.06	0.05	0.05
1-Octanol + CO + H_2 ⇔ Nonan-2-one + H_2O	Eq	38013	41163	31792	45572	17715
Nonan-2-one /1-Octanol	Obs	0.17	0.04	0.03	0.03	0.04
Octanal + CO + 2H_2 ⇔ Nonan-2-one + H_2O	Eq	397702	432374	325593	483248	168323
Nonan-2-one / Octanal	Obs	0.31	0.08	0.06	0.07	0.10

[a] Eq: Expected ratio at equilibrium

[b] Obs: Observed product ratios

Table N.5 Equilibrium ratios of C_8 oxygenates in product oil with octanoic acid co-feeding during Fischer-Tropsch synthesis in a Berty reactor for the 50 wt% Cu catalyst using the TIC m/z ion specific areas

Reaction and ratio		**Product ratios**					
		48h	72h	89h	96h	113h	123h
Octanoic acid + H_2 ⇔ Octan-2-one + H_2O	Eq[a]	1218	1338	1171	1088	1079	703
Octan-2-one/ Octanoic acid	Obs[b]	0.33	0.02	0.03	0.03	0.04	0.02
1-Octanol ⇔ Octan-2-one + H_2	Eq	38.3	38.2	38.7	39.3	39.1	42.3
Octan-2-one/1-Octanol	Obs	0.07	0.01	0.01	0.01	0.02	0.01
Octanal ⇔ Octan-2-one	Eq	415	415	415	415	415	415
Octan-2-one/ Octanal	Obs	0.86	0.13	0.13	0.14	0.16	0.22
1-Octanol + H_2O ⇔ Octanoic acid +2H_2	Eq	0.031	0.029	0.033	0.036	0.036	0.060
Octanoic acid/1-Octanol	Obs	0.20	0.67	0.45	0.48	0.44	0.58
Octanal + H_2O ⇔ Octanoic acid + H_2	Eq	0.34	0.31	0.35	0.38	0.38	0.59
Octanoic acid/ Octanal	Obs	2.59	5.99	4.00	4.93	4.31	9.28
Octanal + H_2 ⇔ 1-Octanol	Eq	10.8	10.8	10.7	10.5	10.6	9.79
1-Octanol /Octanal	Obs	13.0	8.98	8.88	10.2	9.80	15.9
Octanoic acid + CO + 2H_2 ⇔ Nonan-2-one + 2H_2O	Eq	293773	342008	244086	209733	199955	62497
Nonan-2-one / Octanoic acid	Obs	0.40	0.02	0.04	0.04	0.06	0.04
1-Octanol + CO + H_2 ⇔ Nonan-2-one + H_2O	Eq	64517	68374	55793	51576	49607	23787
Nonan-2-one /1-Octanol	Obs	0.08	0.02	0.02	0.02	0.02	0.02
Octanal + CO + 2H_2 ⇔ Nonan-2-one + H_2O	Eq	698930	741830	598716	543786	526166	232979
Nonan-2-one / Octanal	Obs	1.05	0.15	0.16	0.20	0.24	0.37

[a] Eq: Expected ratio at equilibrium

[b] Obs: Observed product ratios

"When you wake up in the morning, Pooh,"
said Piglet at last,
"what's the first thing you say to yourself?"

"What's for breakfast?" said Pooh.
"what do you say, Piglet?"

"I say, I wonder what's going to happen exciting *today*?" said Piglet

Pooh nodded thoughtfully.

"It's the same thing," he said.

-A.A. Milne
Winnie-the-Pooh